FATIGUE CRACK PROPAGATION IN A LOW ALLOY STEEL UNDER COMPLEX LOAD SEQUENCES

Thesis submitted for the degree of

Doctor of Philosophy

in the

University of Edinburgh

by

E.H.R. Wade

March, 1975.

University of Edinburgh,
Department of Mechanical Engineering,
King's Buildings,
Mayfield Road,
Edinburgh EH9 3JL.

DECLARATION

I declare that this thesis has been composed entirely by myself and that the work described is my own. All references to the work of other workers have been duely acknowledged.

Signed

(E.H.R. Wade)

ABSTRACT

This thesis describes the author's investigation of fatigue crack propagation in Q1(N) steel plate. The material is a readily welded, Ni-Cr-Mo, low alloy steel whose principal application is in pressure vessel construction. Extensive fatigue tests have been conducted on 35mm thick CKS type specimens. An automated ultrasonic device has been used to determine crack growth rates resulting from both simple and complex loading sequences. All crack propagation results have been correlated against the prevailing stress intensity conditions.

Equilibrium crack growth rates have been determined for constant amplitude loading. For values of the stress ratio, R, in excess of 0.3 growth rates were found to be independent of the applied mean stress intensity. The original Paris equation of the form, $da/dN = C\Delta K^m$, was applicable to the data over a limited range only; an empirical polynomial has been derived to provide more accurate predictions of the equilibrium crack growth rates. For values of R below 0.3 crack closure effects cause growth retardation under constant amplitude loading.

Crack growth resulting from complex load sequences has been experimentally investigated. The influence of dynamic "overloads" and changes in the applied mean stress intensity have been individually investigated. More complex tests have been conducted under both 3 and 8 level block loading. Under no circumstances did the measured growth rates exceed the values predicted on the basis of a summation of the equilibrium damage rates. The reduced growth rates associated with complex load sequences are attributed to crack closure effects caused by residual stresses at the crack tip. It is argued that "in service" damage rates will be determined by the precise load sequence and the component geometry.

Fatigue crack growth in Q1(N) was found to occur by striation forming mechanisms under all loading conditions; the alloy exhibited no tendency to fail by "brittle" mechanisms. Surfaces produced during fracture toughness tests were consistent with this trend. It is concluded that, relative to traditional structural steels, Q1(N) has no tendency to exhibit accelerated fatigue damage.

CONTENTS

NOTATION

A	constant; area
a	crack length
B	specimen thickness
C	constant; compliance
C_r	crack growth retardation parameter
E	elastic modulus
G	strain energy release rate
H	specimen height
K	stress intensity
K_c	critical stress intensity (fracture toughness)
K_I, K_{II}, K_{III}	stress intensity for modes, I, II, III deformation
K_{max}, K_{min}	maximum, minimum K during load cycle
K_{op}	value of K at which "crack opening" occurs
$\overline{K}$	mean stress intensity
K_R	$\overline{K} + \Delta K_{rms}$
ΔK	dynamic stress intensity range
ΔK_{rms}	rms value of ΔK
$\Delta K_H, \Delta K_L$	high, low values of ΔK in two load level test
ΔK_p	maximum dynamic stress intensity range in block load sequence
l	crack length from notch tip in CKS sample
m, m_1	exponents for growth rate expressions
m_w	shaping exponent for Wheeler retardation model
m'	monotonic strain hardening exponent
m''	cyclic strain hardening exponent
N	number of fatigue cycles
N_d	growth delay as number of cycles
K_Q, P_Q	Critical values of K and P obtained from fracture toughness tests. Subscript Q denotes that validity criteria have not been applied.

N_L	fatigue life as number of cycles
n_g, n_n	gross, net crack growth delay as number of cycles
n_H, n_L	number of high, low load cycles in two load level test
n_o	number of cycles to initiate a fatigue crack
n_p	fatigue life after initiation, i.e. propagation only
P	load
P_s	load demand signal at servo amplifier input
R	stress ratio, $\sigma_{min}/\sigma_{max}$; stress intensity ratio, K_{min}/K_{max}
R_Y	radius of monotonic yield zone at crack tip
R_{YD}	radius of dynamic (reversed) yield zone at crack tip
r	distance, spherical coordinates
t	layer thickness in ultrasonic transfer
U	Elber's crack growth retardation parameter
u	acoustic velocity
W	principle dimension of CKS sample
x,y,z	orthogonal coordinates
α	crack growth retardation parameter
θ	angle
λ	acoustic wave length
ν	Poisson's ratio
ρ	density
σ	stress
$\sigma_x, \sigma_y, \sigma_z$	stresses in the coordinate directions x,y,z
σ_{max}, σ_{min}	maximum and minimum stress during load cycle
σ_{YS}	yield stress under monotonic loading
σ_{net}	net section stress in uniformly loaded, uncracked ligament
$\bar{\sigma}$	mean stress
$\Delta\sigma$	dynamic stress range
$\Delta\sigma_H, \Delta\sigma_L$	high and low dynamic stress ranges in two level test

CHAPTER 1

INTRODUCTION

In 1971 The Naval Construction Research Establishment, Dunfermline placed a research contract with The Mechanical Engineering Department of the University of Edinburgh. A Research Associate (the author) was employed to investigate the effect of complex load sequences on the rate of fatigue crack propagation in Q1(N) steel plate. Q1 is the British made equivalent of a steel developed in the U.S.A. and referred to there as HY-80. The material used in this work has been manufactured and inspected to British Naval specification and is therefore designated Q1(N). The HY alloys are classed as medium to high strength steels having both good toughness and good weldability. The weldability was designed into the materials by the simultaneous development of the parent plate compositions and suitable welding procedures. The tensile strength and ductility of welded joints in Q1 exceed the minimum specifications for the parent plate material. The impact properties of the joints are also satisfactory for naval construction. However for certain applications, e.g. pressure hulls, low cycle, high load fatigue conditions are encountered and represent the principal threat to structural integrity. If welded Q1 structures are to be subjected to such conditions the designer must be fully aware of the fatigue properties of both the parent plate and the welded joints.

There are two factors to be considered regarding the fatigue resistance of these materials. In general the fatigue resistance of medium strength steels improves as the tensile strength is raised.

Steels, such as Q1, which have a tempered martensite structure are found to have among the highest endurance ratios.* However these ratios are determined from unnotched specimens; the situation for notched material is less encouraging. The endurance limit of severely notched specimens remains relatively constant as the tensile strength is increased, hence the endurance ratio is decreased. Thus Q1 structures, if notched, may prove to be less resistant to fatigue damage than simple consideration of their tensile properties might suggest. The second consideration is that a welded structure will always contain small defects which act as notches. Admiralty inspection procedures are very stringent, involving detailed ultrasonic examination of all critical welds. But multipass welds on heavy sections are extremely difficult to inspect; thus defects, sufficient to cause fatigue initiation, have to be expected in the joints of large welded structures. To the pressure hull designer the danger of a fatigue failure originating from a welded joint is well recognised. His problem, with the adoption of the relatively new HY steels for naval construction, is to have confidence that the design criteria evolved from the use of lower strength steels still provide, or can be modified to provide, the correct balance between strength under static loading conditions and under fatigue conditions. It was against this general background that the program of work reported in this thesis was evolved.

From the outset it was intended to study crack propagation; it was assumed that crack initiation in a real structure was effectively unavoidable as a consequence of the "defect" content. It is a matter of observation that cracks initiate and start to propagate in welded joints and their associated heat affected zones. It was therefore logical that the original aims of the author's contract included the

---

*Endurance ratio: (Fatigue limit)/(Tensile strength)

study of crack propagation in both parent plate material and welded joints. It was envisaged that the parent plate studies would provide a data base to which the more complex crack propagation characteristics of the welded joints could be related. However, it became apparent at an early stage that, if complex load sequences were to be considered, the study of parent plate material would be a major undertaking in its own right and investigation of crack propagation in welded joints would have to be postponed. This thesis is therefore concerned with crack propagation in Q1 parent plate under a variety of loading conditions.

The principal impediment to practical fatigue design is our inability to relate simplified laboratory test data to realistic service conditions. The evolution of fracture mechanics has significantly advanced our understanding of the stress distributions associated with fatigue cracks. This has made possible the unification of data from different sources under a common set of parameters. The extension of fracture mechanics analyses to components and structures is not generally practical. Even for simple components the costs are considerable; for more complicated situations, e.g. welded plate structures, uncertainties with regard to their loading, shape and structural uniformity make the analyses extremely costly and highly conjectoral. Even given suitable design parameters for structural analysis, there remains the problem of our poor understanding of fatigue damage accumulation under the varying loads experienced in a service environment. Traditional design techniques rely on simple fatigue data usually gained from rotating bending tests. At the other end of the scale the aircraft industry has for some time indulged in full scale testing of airframes under simulated service load conditions. This approach is exceptional and totally impractical for the majority of structures. There is therefore an increasing interest in laboratory

fatigue testing of simple samples or single components under simulated service load conditions. Laboratory test sequences are evolved from records of "in service" loads. In general it is impractical to exactly duplicate the service loads in the laboratory; some simplification of the service record being required to suit the testing facilities available. In so "condensing" service load histories it is important that the researcher is acutely aware of the relative significance of the various load sequences whose effect he aims to simulate. The principal aim of this work has therefore been to examine the effect of individual loading parameters on the rate of fatigue damage accumulation. Crack growth rates have also been investigated under block loading conditions which constitute a first step towards full service load simulations.

This thesis is principally concerned with the influence of complex load sequences on crack propagation rates. However a major undertaking during the early stages of the work was the development of a satisfactory system for continuously measuring the length of a growing fatigue crack. An automated, ultrasonic device was developed by the author to monitor crack length and control the load applied to the sample such that the crack tip stress intensity was maintained constant. Although the development of this device was critical to the subsequent crack propagation studies it was essentially a separate problem. It was felt that the continuity of this thesis would benefit from having the details of the crack monitor excluded from the main text; therefore a self contained appendix has been included to deal with this important aspect of the work. The main text, which deals with the crack propagation studies, is presented according to conventional format, starting with a review of published literature.

CHAPTER 2

LITERATURE REVIEW

2.1 General Background

2.1.1 Preamble

Fatigue may be concisely defined as: the phenomenon whereby a crack develops and extends in a material under alternating stress conditions whose magnitude is less than the initial static strength of the structure.

The traditional concepts of fatigue are being rapidly restated in the modern terminology of fracture mechanics. However, many of the pre-fracture mechanics concepts remain valid and traditional determinations of the relative fatigue resistance of different materials are still an essential aid to design engineers. Many excellent reviews of the traditional approach to fatigue have been published, amongst these the books by Forrest [1] and Yokobori [2] are well known. An introduction to the application of fracture mechanics in fatigue is provided by Barnby [3], more detailed information is available from Knott [4]. Liebowitz [5] has edited a comprehensive multi-volume review of fracture. The extensive series of ASTM Special Technical Publications provides a comprehensive record of work that is currently being undertaken in fatigue research. Despite the revolution in thinking, that has been caused by the development of fracture mechanics, fatigue failure in metals is still considered to be a three stage process involving:

1) Crack initiation, usually at the component's surface.

2) Propagation of the crack on a macro-scale.

3) Final fast failure by "static" mechanisms.

The differences between these stages are considered below.

2.1.2 Crack initiation

The distinction between stages 1 and 2 is readily made in simple laboratory situations, though it may be less clear in complex components. Crack initiation results from dislocation movement on slip planes in grains lying at the material's surface. The exact mechanism of initiation is not understood. However it is apparent that even when the nominal stress remains less than the materials elastic limit some irreversible plastic deformation occurs at certain surface sites. Even in nominally smooth samples thin folds of material are raised from the surface; these "extrusions" are associated with "intrusions" or micro-cracks. Because the process is associated with dislocation movement on slip bands the micro-cracks grow in a shear mode, i.e. at 45^{o} to the dominating principal stress. As the crack extends it is observed to undergo a re-orientation such that it lies normal to the principal stress. This rotation which represents the change from stage 1 (initiation) to stage 2 (propagation) will usually occur when the micro-crack encounters an obstacle to slip such as a grain boundary [6]. In many practical cases crack initiation occurs at a "feature" that acts as a notch or stress raiser. Machine marks, corrosion damage or metallurgical inhomogeneites are typical "notches" that will accelerate crack initiation by creating a local stress concentration. It is not the author's intention to review the metallurgy of crack initiation, readers who seek further information are referred to reference [7].

2.1.3 Crack propagation

Stage II crack growth commences when the initiated micro-crack grows out of its slip band. From this moment the crack will follow the path of least resistance. Transgranular crack growth is normal though under certain circumstances the crack may follow slip bands [8] or lines of weakness caused by such features as grain boundaries [9,10] and quench bands [11]. Furthermore a crack may deviate under the influence of a localised internal stress field [12]. On a fracture surface the region of stage II propagation is readily distinguished by its characteristic markings. Typically the surface is smooth compared with the region of final fast failure and exhibits the "beach" and "river" markings described in elementary text books of metallurgy. At high magnifications the fracture surface is often seen to be striated normal to the direction of crack growth. The clarity of these features depends on both the material and the load history experienced. Many workers have confirmed that these markings correspond to the cycle by cycle growth of the crack [13]; their spacings can be used as a quantitative measure of crack growth rates. Cracks propagating in thin sheet components may rotate to lie in a plane at 45° to the principal stress. The morphology of the fracture surface changes; the striations being replaced by a dimpled appearance. These features have not proved satisfactory for quantitative measurement of crack growth rates.

2.1.4 Final "static" failure

Final rapid failure of the structure occurs when the crack has weakened it to the point that its static strength is insufficient to support the maximum load experienced. The moment of failure and the nature of the fracture surface that results will vary according to the loading conditions and the material properties. There are three factors to be considered.

1) The material has experienced cyclic loading and therefore may have hardened or softened according to its bulk cyclic properties.

2) The component is very severely notched by the stage II fatigue crack.

3) The applied strain rates under fatigue loading may vary greatly from one situation to another.

The result of these effects may be to produce a final fracture whose appearance is not typical of "static" failure in the same material. From the point of view of structural integrity this final stage of failure is not of fundamental importance. Given that a crack can initiate and propagate continuously under service conditions final failure is inevitable.

This thesis is entirely concerned with stage II propagation and specifically the effect that complex load sequences have on crack growth rates. The understanding and analysis of crack growth mechanisms have been greatly advanced by the use of fracture mechanics concepts. A brief outline of this method of analysis is therefore given in the next section.

2.2 Basic Fracture Mechanics

2.2.1 Analysis of the elastic stress field at a crack tip

Griffith's famous equation [14] presented the concept of the energy balance that controls brittle crack propagation. Orowan [15] appreciated that in metallic materials the plastic deformation occurring at the tip of an advancing crack would dominate the surface energy requirements considered by Griffith. Consideration of a cracked sample loaded under fixed grip conditions shows that if kinetic energy changes are negligible the rate of energy absorption by the

crack growth process is equal to the rate of change of elastic energy in the material [16]. This latter parameter was designated "the strain energy release rate" (G) by Irwin [17]. He showed [18] that G could be related to the specimen compliance (C) by

$$G = \tfrac{1}{2} P^2 (dC/da). \tag{2.1}$$

Using the coordinates shown in Figure 2.1, he derived expressions for the stresses in the vicinity of a crack tip contained in a two dimensional sheet of isotropic elastic material. For a remote load applied in the y direction he obtained:

$$\sigma_x = \frac{K}{\sqrt{(2\pi r)}} \cos\frac{\theta}{2}\left(1 - \sin\frac{\theta}{2}\sin\frac{3\theta}{2}\right) \tag{2.2}$$

$$\sigma_y = \frac{K}{\sqrt{(2\pi r)}} \cos\frac{\theta}{2}\left(1 + \sin\frac{\theta}{2}\sin\frac{3\theta}{2}\right) \tag{2.3}$$

$$\tau_{xy} = \frac{K}{\sqrt{(2\pi r)}} \sin\frac{\theta}{2}\cos\frac{\theta}{2}\cos\frac{3\theta}{2}\,. \tag{2.4}$$

The parameter K is seen to occur in each expression. Furthermore for any given location (θ and r constant) the three stress terms are seen to be proportional to K. Thus this parameter, which is termed the "stress intensity factor", affords a convenient quantitative characterisation of the crack tip stress field. Its unconventional units of $MNm^{-3/2}$ serve to emphasise that it does not detail a physical reality such as stress or strain but instead represents the overall intensity of the crack tip stress field. The above analysis applies to the "opening" mode of crack loading, otherwise referred to as "mode I". Figure 2.2 shows the designation of the three modes that are required to provide a general description of a loaded crack. Mode I is the most important in practical failure considerations, the other

modes are however important in the development of our understanding of crack tip deformations.

Bueckner [19] has demonstrated that the energy available for crack extension is equal to the strain energy difference of the stress fields before and after the extension occurs. Thus Irwin was able to relate his evaluation of the elastic stress field to the strain energy release rate (G). He showed that for plane stress conditions the relationship was:

$$K^2 = EG. \tag{2.5}$$

Under plane strain conditions the relationship is modified by the existing through thickness constraint. Expression 2.5 becomes:

$$K^2 = EG/(1 - \nu^2). \tag{2.6}$$

Irwin had originally suggested that G_c, the strain energy release rate at the onset of crack extension, would be a material property dependent only on specimen geometry. Direct determination of G_c requires a measurement of specimen compliance which is not altogether simple. However K, whilst directly related to G, has the advantage that its determination is a normal stress analysis problem involving the applied stress and the component geometry. Thus there should be a critical value of K, K_c, associated with the onset of crack extension in an elastic medium which is more readily measured in practice than is the equivalent value of G_c. A survey of the various methods of calculating stress intensity factors is beyond the scope of this review. It is sufficient to note that an increasing number of analytical solutions are becoming available. These solutions are particularly

applicable to relatively simple, symmetrically loaded crack configurations. Laboratory testpieces and structural components present more complicated stress fields for which the stress intensity factors are usually computed numerically by use of recursive finite element techniques. An extensive survey of K determinations is given by Paris and Sih [20]; alternatively Kenny and Campbell [16] provide a brief summary with many references to original work.

It should be emphasised that the analysis outlined in this section is only applicable to isotropic materials under purely elastic loading conditions. It has already been stated that in metallic materials, plastic deformation will be the dominant energy "sink" of the fracture process. It is pertinent therefore to consider how the linear elastic fracture mechanics concepts can be applied to realistic situations involving crack tip plasticity.

2.2.2 Consideration of crack tip plasticity

The three stresses evaluated by Irwin's analysis of the opening mode are shown schematically in Figure 2.3(a). Under conditions of plane stress ($\sigma_z = 0$) the material at the crack tip will yield when $\sigma_y = \sigma_{YS}$ and for a perfectly elastic/plastic material this is the maximum stress obtainable. Thus in practice a redistribution of the stress field occurs as indicated by the broken line in Figure 2.3(b). The displacement of the stress field in the x direction results from the requirement of the unyielded and yielded solutions to have the same load bearing capability. Under conditions of plane strain, i.e. in thicker sections, constraint in the z direction results in the value of σ_y required to cause yielding being

$$\sigma_y = \sigma_{YS} + \sigma_z \quad \text{(Tresca criterion).} \tag{2.7}$$

This condition is shown in Figure 2.3(c). The plastic zone is reduced to about 1/3 of the plane stress size. More detailed analysis of the size and shape of the plastic zone resulting from Mode I deformation is hindered by the lack of an analytical model for these conditions. However, Irwin [21] has suggested that as a first approximation the zone be considered circular in the x/y plane. On the basis of the approach already discussed he gives the radius of the yielded region (R_Y) as:

$$R_Y = \frac{1}{2\pi} \left(\frac{K_I}{\sigma_{YS}}\right)^2 \tag{2.8}$$

for plane stress conditions and

$$R_Y = \frac{1}{5.6\pi} \left(\frac{K_I}{\sigma_{YS}}\right)^2 \tag{2.9}$$

for plane strain. A much more detailed consideration has been presented by Rice [22]. He considered mode III deformation for which an analytical model is available. Although this mode is of little practical importance from the point of view of crack growth it is considered [23] that the gross features of crack tip plasticity will be similar for modes I and III. The detailed conclusions drawn from the analysis of mode III loading are beyond the scope of this review, however, it is worth noting that the simplified approach presented above is not invalidated. It is concluded that mode I loading of a cracked component results in a plastically yielded zone at the crack tip. This is shown schematically in Figure 2.4. The foregoing discussion has been concerned with static loading conditions; the same approach is broadly applicable to fatigue conditions subject to certain modifications.

2.2.3 Crack tip plasticity under fatigue loading conditions

The fracture mechanics approach to crack tip plasticity under cyclic loading conditions has been expounded by Rice [22]. The analysis is based on the principles of plastic superposition developed for special cases by Hult and McClintock [24] and Rice [25]. The principal conclusion is that the plastic deformation exists in two forms. Firstly there is the monotonic yield zone resulting from the peak of the first load cycle; this has the form discussed above. Secondly there is the influence of load reversal to be considered. Unloading or load reversal is equivalent to the superimposition of a negative load, which, according to the purely elastic theory already discussed, results in the creation of an infinite negative crack tip stress. (Plastic blunting effects are necessarily ignored.) Thus reversed plastic flow is initiated at the crack tip. However, under the conditions of cyclic loading the stress required to produce reversed yielding is twice the monotonic yield stress. Hence the extent of the reversed plastic zone is obtained by substituting $2\sigma_{YS}$ for σ_{YS} in equations 2.8 and 2.9. For both plane stress and plane strain conditions the zone is found to be $\frac{1}{4}$ the size of that resulting from monotonic loading over the same stress intensity range. Figure 2.5(c) shows a schematic representation of the monotonic and cyclic plastic zones existing at the crack tip under fatigue loading conditions.

Irwin's stress intensity parameter was originally derived for purely linear elastic materials. The above sections have discussed modifications required to accommodate small scale crack tip plasticity. The stress distribution outside the plastic zone is assumed to be physically displaced but otherwise undisturbed by the occurrence of yielding at the crack tip. Rice [22] has considered the validity of

this assumption. For a remotely stressed crack opening under mode III deformation he compared the crack tip plastic zone sizes obtained from exact computations with those obtained from the modified stress intensity analysis. For monotonic loading he found the stress intensity approach remained accurate so long as the net section stress was less than $0.40\sigma_{YS}$. Under fatigue conditions it is the size of the reversed plastic zone that is critical, thus as a consequence of its smaller size, the limit on the net section stress is raised to $0.8\sigma_{YS}$. These values do not represent precise limits to the range over which the stress intensity parameter is applicable, nor are equivalent values available for the practically important mode I deformation. However as the features of modes I and III are considered to be broadly similar it is concluded that the stress intensity approach is applicable to fatigue crack propagation in materials for which fracture toughness determinations are invalidated by excessive crack tip plasticity. In practice stress intensity is found to correlate well with measured rates of fatigue crack growth for a wide range of materials. Consequently, in the absence of a more suitable parameter, it has been widely adopted for the formulation of crack propagation "laws". The more important equations are reviewed in the next section.

2.3 Suggested Laws of Fatigue Crack Propagation

A recent review [26] of suggested laws of fatigue crack propagation lists 33 separate expressions for the crack growth rate, da/dN. These laws are developed from many different approaches and in many cases are found to have considerable similarities. The earlier suggestions were extensively reviewed by Paris and Erdogan [27]. They made a critical study of the laws of Head [28], Frost and Dugdale [29], Liu [30], McEvily and Illg [31] and Paris et al [32]. Their conclusion was that only the last two of the mentioned laws were

applicable over a wide range of data. Furthermore they demonstrated the equivalence of the stress parameter used by McEvily and Illg to the stress intensity approach of Paris et al. Referring to Figure 2.6, which details the stress intensity parameters used for constant amplitude loading, the generalised form of the equation proposed by these workers is

$$\frac{da}{dN} = C(\Delta K)^m \qquad (2.10)$$

where ΔK is the dynamic stress intensity range and m is a material parameter. McClintock [33] has outlined alternative theoretical approaches to the determination of the exponent m. Attempts have been made to formulate crack propagation laws from specific material properties. Weertman's [34,35] proposal embodied brittle fracture considerations, McEvily and Johnston [36] incorporated monotonic tensile properties to predict a "universal" crack growth curve and Tomkins [37] has used the mechanical properties determined from cyclic stress-strain measurements. From the practical point of view these theoretically based derivations impose artificial constraints on the mechanisms considered. The fatigue process itself has no respect for these limitations, thus equations derived for specific mechanisms tend not to have a general practical applicability.

It should be emphasised that the stress intensity approach has no exact physical basis. Strictly speaking it is applicable only to conditions of small scale yielding, i.e. the crack tip plastic zone is small with respect to the component and crack dimensions. Furthermore, plastic zone corrections, when used, are based on the monotonic yield strength which may not be applicable for cyclic stress conditions. However, as has already been stated, the majority of recent equations proposed have embodied the stress intensity approach. The success of the general Paris equation (equation 2.10) is well

demonstrated by the extensive presentation of data by Frost, Pook and Denton [38]. They have reanalysed earlier work in terms of the Paris equation. Their results, for more than 15 materials, indicate that for dynamic loading about a constant mean stress intensity the exponent m in equation 2.10 remains constant over a considerable range of crack growth rate. It is clear from the data of Frost et al that, whilst ΔK is the dominating parameter, secondary effects such as the applied mean stress must also be considered if growth rates are to be accurately expressed. Most of the more recent "laws" listed by Hoeppner and Krupp [26] acknowledge the primary influence of dynamic stress range but also attempt to accommodate some of the secondary effects (e.g. mean stress, frequency, strain hardening) which are known to affect crack growth rates. Notable for the attention it has received is the proposal of Forman et al [39] which includes the effect of mean stress intensity by use of the stress ratio parameter, R. Foreman's equation is

$$\frac{da}{dN} = \frac{C(\Delta K)^m}{(1-R)K_c - \Delta K} \qquad (2.11)$$

where R is given by

$$R = K_{min}/K_{max} \qquad (2.12)$$

Dover and Hibberd [40] have found propagation rates in Q1(N) steel sensitive to the applied mean stress under a variety of random loading conditions. They have not tested their data against equation 2.11, but have instead proposed a simpler expression which does not involve a fracture toughness value. They proposed

$$\frac{da}{dN} = C\Delta K_{rms}^{\ m} K_R^{\ m_1} . \qquad (2.13)$$

Experimental results indicated that different values of both m and m_1 were required for crack rates above and below 10^{-2} μm/cycle.

Recently the general trend has been to utilize fracture mechanics parameters in the formulation of growth rate laws. The nature of the stress intensity function is such that equations which embody it do not relate to physical crack growth mechanisms, the proposed equations being empirical in nature. It is therefore desirable to use the simplest satisfactory expression; for this reason the majority of workers adopt the original expression of Paris et al [32], (equation 2.10), as the basis of growth rate "laws". This expression can readily be modified to include secondary effects such as mean stress. Fracture mechanics provides a convenient and satisfactory framework for the formulation of empirical expressions that fit a limited amount of experimental data. If expressions are to be widely applicable they will require to be more closely related to the actual mechanisms of crack growth. The extreme difficulty of achieving this condition is apparent from the review of growth mechanisms that follows.

2.4 Crack Growth Mechanisms

2.4.1 Preamble

The difficulties of studying the mechanisms of fatigue crack propagation are well known. The very nature of the process makes access to the crack tip impossible. Furthermore in metals the conditions at the tip are subject to inherent inhomogeneities such as grain size, grain orientation and the presence of second phase material. To further frustrate the experimentalists there is the problem of fracture surface attrition destroying potentially interesting evidence during subsequent load cycles. There is no doubt that the process of fatigue crack growth is extremely complex, involving a

variety of different micro-mechanisms. This fact, together with the problems of experimental observation, has resulted in our knowledge of the failure processes being largely conjectoral. Given these restrictions it is not surprising that the majority of work has been concerned with aluminium alloys. In these alloys cracks propagating under pure "opening mode" conditions reveal a regularly marked fracture surface. In other materials, particularly steels, the striations are observed to be less regular and often completely absent. Before considering the mechanisms that have been proposed as a direct result of striation analysis it is important to emphasise that, whilst these features provide clues to the mechanisms that created them they are not invariably associated with crack propagation. McMillan and Hertzberg [41] have shown the difference in appearance of fracture surfaces produced under pure mode I and mixed mode conditions. During the course of propagation cracks are prone to rotate from a plane normal to the principal stress to one inclined to it. In thin materials the inclined (plane stress) configuration may prevail throughout. In thicker materials it is found that the point at which the rotation occurs is determined by the specimen geometry and loading conditions. The limited attention given to the mechanisms of cracks propagating under mixed mode conditions is largely a result of the failure of the fracture surface to provide quantitative information. Hertzberg [42] investigated the "elongated dimples" found on slant fracture surfaces but was unable to correlate them with the measured macro-growth rate. The author's experimental work has all been concerned with plane strain type fractures which lie normal to the principal imposed stress; propagation under these conditions will now be considered.

2.4.2 Mechanisms of mode I growth

The extensive interest in fracture surface striations stems from the observation by Forsyth and Ryder [13] that each applied load cycle results in the formation of a single striation. Thus the striation spacings can be used to estimate local crack growth rates. Recently this technique has been extensively used to study growth rates under complex load sequences, an aspect that will be considered in the next section. The same authors suggested [43] that striations could be explained by a two stage process involving debonding of second phase material ahead of the crack tip followed by ductile necking of the intervening ligament. This early suggestion would seem to conflict with the observed variation of striation spacing with the applied stress. Laird [44] has given extensive consideration to the way in which striations are produced. Precise matching of fracture surfaces indicates that the way in which they "fit" together varies, he has observed both "peak to peak" and "peak to valley" matching. He proposed a mechanism involving plastic "blunting" of the crack on the tensile stroke and resharpening to form twin "notches" during the compressive phase. The "notches" are later seen as striations. Schijve [45] considers that in 2024-T3 aluminium material the compressive, or unloading phase, results in the resharpening of a single notch at the crack tip. In both models the crack growth is considered to occur during the period of increasing load. This is in accordance with the observations of McMillan and Pelloux [46]. A suggested correlation between striation spacing and dislocation subgrain size has been discounted by the work of Klesnil and Lukáš [47]. Alternative dislocation models for crack tip deformation have been proposed by Tomkins and Briggs [48] and Spitzig et al [49]. These models like those of Laird [44] and Schijve [50] suggest dislocation movement on shear planes inclined at 45° to the crack growth direction. It is

probable that the severe plastic deformations occurring at the crack tip require these and other dislocation mechanisms to be operative. Our knowledge of the crack tip conditions is insufficiently complete to validate the proposal of detailed dislocation models. Plumbridge [51] notes the generality of the plastic blunting approach, he considers that the complexity of observed striation morphologies indicates that no single mechanism is dominant in the crack growth process. Furthermore striations have been extensively observed on the fatigue fracture surface of polymeric materials [51] indicating that crystallographic processes are not required for their formation. Steels in general exhibit more broken fracture surfaces which are not so readily analysed. Koterazawa et al [52] have recently studied the fracture surface of a carbon steel and performed precision matching tests of the separated material. They conclude that the growth mechanism as evidenced by the fracture surface is probably a "plastic blunting" mechanism of the type discussed above.

The above represents the general concensus regarding crack propagation mechanisms under mode I crack opening conditions. It is important to recognise the limitations of these concepts. It is probable that the prevailing growth mechanisms change according to the loading conditions and perhaps the crack growth rate. For example there is a critical dynamic stress intensity level below which a crack will not extend [38]. It has been suggested [53] that this limit is associated with propagation at the rate of one lattice spacing per cycle. Regardless of the accuracy of this explanation one would not expect the growth mechanisms operative under these conditions to be accurately described by the generalised models developed for higher growth rates.

2.4.3 Mechanisms producing accelerated growth rates

The various crack growth rate laws proposed have embodied a variety of suggested crack tip failure mechanisms, some of which were mentioned in the previous section. A growth rate equation, stated in terms of the stress intensity parameter, results in a value of the exponent m (equations 2.10 and 2.11) which typifies the operative failure mechanism. Predicted values of m lie between 2 and 4 [51]; many experimentally determined values agree well with these predictions. However, values up to seven and in exceptional cases up to 10 [54] have been reported. These high values imply that crack tip failure is occurring by faster mechanisms than those envisaged by the theoretical models. Ritchie [54] has demonstrated the existence of brittle fracture modes in steel. He consideres these result in high m values and increased sensitivity to mean stress effects. High strength alloys are particularly prone to exhibit high m values, there remains considerable scope for elucidating the mechanisms responsible.

The tendency for cracks propagating under mode I conditions to rotate into an inclined plane has already been mentioned. Subsequent crack tip deformation is a combination of modes I and II. Fractographic studies [44] indicate that the failure mechanism differs significantly from the conditions that produce striations under pure mode I deformation. Further evidence of a change of mechanism is provided by the higher m values determined for inclined crack configurations [38]. Propagation under these mixed mode conditions is less well understood than that which occurs under pure opening mode deformation. As the experimental work reported in later chapters is concerned with pure mode I conditions the mechanisms of mixed mode growth will not be further considered.

2.4.4 The influence of crack tip environment

So far no mention has been made of the effects of environment on crack propagation mechanisms. Aggressive conditions are well known to accelerate crack growth rates. Fractographic evidence [41] indicates that environmental conditions can significantly affect the propagation mechanism operative at the crack tip. This thesis is solely concerned with propagation under prevailing laboratory conditions of temperature and humidity. Traditionally such conditions have not been regarded as "corrosive" and are used as the reference conditions against which crack rates measured in more hostile environments are compared. However, it is known that for certain materials [1, 51] growth rates are reduced if tests are performed in vacuo. It is important to distinguish between accelerated cracking due to electrochemical removal or embrittlement of material at the crack tip and the mechanisms by which growth rates are reduced in vacuo. It is suggested that this latter effect is due to "rewelding" of material that has already been parted by purely mechanical action. Forrest [1] quotes results that indicate steel is little affected by the change from ambient conditions to in vacuo testing. Plumbridge [51], on the other hand, draws attention to work that indicates water vapour has a critical effect on propagation mechanisms in steel. Traditionally ambient conditions have been regarded as satisfactory for crack growth studies.
If chemical action at the crack tip was a parameter of major importance one would expect the growth rate to be sensitive to the testing frequency, this is generally not found to be the case for low frequency testing of steels [1]. It is particularly significant that Q1(N) material has been found insensitive to frequency effects [55]. With regard to the present author's work the limitations of tests performed in the prevailing laboratory atmosphere are acknowledged but it was considered that any environmental influence in growth rates would be

secondary to the consequences of the complex load sequences to be investigated.

2.5 Crack Growth Under Complex Load Sequences

2.5.1 Preamble

For large welded structures fatigue crack initiation is recognised to be highly accelerated due to the unavoidable imperfections of the welded joints. Thus the structure's life is primarily determined by the crack propagation stage of fatigue failure. The principal obstacles to predicting crack propagation rates and hence component lives are:

1) Uncertainty concerning the location of the most critical crack.

2) Stress analysis of the cracked region requires knowledge of the crack path, the mode of displacement and material effects arising from features such as welded joints.

3) A poor understanding of load history effects. By this is meant the influence of prior loading conditions on subsequent crack growth rates.

In simple situations, e.g. laboratory tests, the first two of the above problems can be eliminated. The problem of accounting for load history effects continues to make accurate growth rate predictions impossible. It is to the elucidation of these load interaction effects that the experimental work in this thesis is directed. The aspects of load interaction that have been experimentally investigated are reviewed in the following sections.

2.5.2 The influence of static mean stress

Empirical assessments of the influence of mean stress in determining the fatigue life of unnotched samples were made by Goodman,

Gerber and Soderberg. Forrest [1] presents these essentially similar approaches. All three were agreed that the application of a tensile mean stress resulted in a reduced fatigue life. Forman et al [39] have reconsidered the matter and have used the current stress intensity terminology to formulate an expression for crack growth rate that embodies a mean stress intensity parameter. They suggest that when the maximum stress intensity of a fatigue cycle approaches the fracture toughness (K_c) of the material the crack growth rate will become infinite, i.e.

$$K_{max} \xrightarrow{\lim} K_c \ , \ \frac{da}{dN} \longrightarrow \infty . \qquad (2.14)$$

The Forman growth rate expression, which has already been stated as equation 2.11, is

$$\frac{da}{dN} = \frac{C(\Delta K)^m}{(1-R)K_c - \Delta K} \ , \qquad \begin{matrix}(2.11)\\(\text{restated})\end{matrix}$$

where R is the stress intensity ratio given by

$$R = K_{min}/K_{max} \ . \qquad \begin{matrix}(2.12)\\(\text{restated})\end{matrix}$$

This expression was originally "validated" by comparison with experimental growth rates determinated in thin sheets of aluminium alloys. Pearson [56] investigated crack growth rates in six aluminium alloys and found the Forman relation to be applicable only after modification. He proposed

$$\frac{da}{dN} = \frac{C(\Delta K)^m}{[(1-R)K_c - \Delta K]^{\frac{1}{2}}} \ . \qquad (2.15)$$

He found this expression fitted the original data of Forman et al as accurately as the original expression. He notes the sensitivity of both equations 2.11 and 2.15 to the incorporated value of K_c and

suggests that the original proposal of Forman was found satisfactory as a result of the very high K_c values associated with his thin sheet material. Confirmation of the general trend of crack growth acceleration with increasing mean stress in aluminium alloys has been forthcoming from several other workers [38, 57, 58, 59].

The effect of mean stress on crack propagation in steels is not so readily generalised. Early work by Frost [60] indicated that steels were relatively insensitive to the applied mean stress. In contrast there is the work of Evans et al [61] who found their data for the effect of mean stress in rail steels was well fitted by the original Forman expression. Fedderson et al [62] have detected a small mean stress effect in D6AC steel tested in dry air. Dover and Hibberd [40] have found 7mm thick plates of Q1(N) are sensitive to increasing stress ratios under random loading conditions.

The physical explanation of the way in which the static mean stress influences crack growth rates is not complete. Considerable attention has been given to the concept of crack closure. Rice [22] has shown that fracture mechanics does not predict physical closure under zero to tension loading. Experimental evidence presented by Elber [63] indicates that closure does in fact occur under these conditions. This viewpoint is supported by Sih and Wei [64] who have used both strain gauge and electro-potential techniques to detect physical closure. It is argued that crack closure eliminates the crack tip stress singularity and thus reduces the effective dynamic stress intensity range with a consequent reduction in the crack growth rate. Elber [65] developed an expression for the effective stress intensity range that was based on measurements of macro-closure effects. Sih and Wei considered it unrealistic to relate crack tip conditions to the measurable gross closure effects. Despite its empirical nature Elber's approach is important in that it attempts to predict the quantitative influence of a crack growth retardation

mechanism. A quantitative statement of Elber's model is presented in section 2.7.7.

An alternative view of the mean stress effect is presented by Ritchie and Knott [66] who investigated crack propagation in EN30A steel. Different heat treatments were used to produce two batches of material having the same yield strength but in one case the alloy was "brittle" at the test temperature, in the other case it was unembrittled. The rate of crack propagation in the embrittled material was found to be accelerated by the application of a tensile mean stress; in the unembrittled state the crack growth rate was insensitive to this parameter. "Brittle" fracture facets were observed on the surface of the sensitive material, these were absent from the fracture surfaces of unembrittled material. The conclusion was that these "monotonic fracture modes" were responsible for the mean stress sensitivity of the embrittled steel. Knott [67] goes further in suggesting that similar, but less pronounced effects, could account for the observed mean stress sensitivity of other steels. Unlike crack closure this model cannot readily be treated quantitatively; none the less the concept of alternative failure mechanisms is important.

2.5.3 The effect of changes in mean stress

The above section has considered the influence of a steady mean stress applied to a crack propagating under constant dynamic stress conditions. Clearly an appreciation of the influence of a change in mean stress is required if load history effects are to be understood. Discontinuous changes in mean stress are particularly apparent in "block loading" tests, in random tests the effect exists but is obscured by the irregularity of the load sequence. Dowling [68] has considered possible analyses of service load records with a view to performing a damage summation. He considers load sequences on a

cycle by cycle basis. Under these conditions the mean stress is seen to be constantly changing and may therefore be significant in influencing the overall damage rate.

Very few studies have been made of the effect of changes in mean stress in isolation from other loading parameters. Many studies of block loading and dynamic overloads have involved changes in the applied mean stress levels but not independently of the other variables. The author is only aware of two studies that have isolated mean stress changes from other effects. Both utilized type 2024 aluminium alloy. Dowling [68] used the load sequence shown in Figure 2.7. The overall crack rate was reduced as $\Delta(\bar{\sigma})$ increased. McMillan and Pelloux [46] used similar block loading sequences for their fractographic study of the same alloy. They interpreted their fractographs to show that crack extension occurred only on the tension stroke of the load cycle, showing how exaggerated growth resulted from the first cycle after an increase in mean stress had occurred. They also demonstrated that crack growth under constant dynamic load conditions temporarily ceased if a sufficient mean stress reduction occurred.

The very limited number of practical investigations of crack propagation following changes in mean stress is surprising. Steels in particular have been completely ignored. In contrast the effect of dynamic overloads on subsequent crack growth rates has been extensively researched. In many senses dynamic overloads and changes in mean stress can be regarded as having a similar influence on crack tip processes. Thus the concepts invoked to explain the influence of overload conditions may also be applied to sequences involving changes of mean stress. The sections that follow review experimental studies of dynamic overload sequences.

2.5.4 Crack growth retardation following tensile overload

Figure 2.8 shows the most commonly investigated overload sequences. Referring to the figure it is seen that type (a) and (b) sequences only involve a change of the dynamic stress intensity range whilst types (c) and (d) also involve a change of mean stress during the overload period. Type (c) sequences, involving a single overload cycle have received the most attention. Experimental techniques have varied considerably, some workers have applied an overload sequence only once in a sample's life, others have favoured periodic repetition of the basic low-high-low sequence. Most of the published work has been performed on aluminium alloys, steels have received less attention.

Consider first the crack propagation occurring under the low dynamic stress intensity conditions after a type (c) overload. Experimental observations indicate that overloads below a critical value do not affect subsequent propagation [69]. For the titanium alloy investigated, a type (c) sequence was employed and the critical overload values lay between 120 and 150% of ΔK_L. Higher tensile overloads result in subsequent crack growth retardation [69, 70, 71, 72] and in extreme cases crack arrest [72]. Figure 2.9 shows two reported retardation effects, curve I represents the "crack length/no. of cycles" record in the absence of overload conditions. Curve II shows a minimum growth rate immediately following removal of the overload as reported by [52, 70, 73, 74]. Curve III shows "delayed retardation" as reported by [73, 75, 76]. For 7075-T6511 aluminium alloy Corbly and Packman [75] reported delays of about 100 cycles before the minimum growth rate occurred.

A number of mechanisms have been advanced to account for the observed retardation effects of overload cycles. These have been discussed by Schijve [77] and Jones [69]. Extensive consideration

has been given to the concept of crack closure. Fracture mechanics indicates that a tensile overload results in an extension of the crack tip plastic zone. On returning to the low stress conditions this non-equilibrium zone causes a compressive stress to be superimposed on the crack tip region. For purely dynamic overloads fracture mechanics do not predict crack closure, however Elber's work [63, 65] suggests that macro-closure occurs more readily. Furthermore the compressive stress field resulting from a tensile overload favours localised crack tip closure. Elber considers that the maximum compressive stress occurs at a point ahead of the crack's position at the moment that the overload is removed. The minimum crack growth rate therefore occurs after the crack has extended into the overload plastic zone. Thus the observed phenomenon of delayed retardation may be explained. Plastic zone interaction effects, similar to that detailed above, have been adopted by other workers as the basis of quantitative retardation expressions. The expressions which are presented in sections 2.7.5 and 2.7.6, are empirical in nature and therefore are not associated with a specific growth delay mechanism. It is nonethe less clear that the crack tip stress conditions existing after the application of an overload sequence are principally responsible for the observed growth retardation.

An alternative retardation mechanism involves the concept of "plastic blunting" of the crack tip. A crack extension mechanism such as that proposed by Laird [44] or Schijve [45] is considered. The crack tip is opened and "blunted" on the tensile stroke and resharpened on the compressive stroke. Growth retardation by "blunting" is suggested to occur as a result of the tensile stroke of an overload sequence. The growth rate would be minimised immediately after the overload condition was removed. Such a mechanism would be consistent with the instantaneous retardation of curve II in Figure 2.9.

Jones [69] has considered the possibility of growth retardation being due to strain hardening in Ti-6%Al-4%V alloy. By determining crack growth rates in samples subjected to different levels of pre-strain he discounts strain hardening as the cause of retardation.

An interesting complication of the retardation behaviour is the occurrence of accelerated crack growth immediately following an overload. Schijve [77] has observed this effect in type 2024-T3 aluminium alloy subjected to a type (b) sequence, (Figure 2.8). He suggests that a complex crack tip stress field is created in which the tensile and compressive phases of the overload create opposed stress fields. Figure 2.10 shows how the overall crack growth pattern is thought to be related to the crack tip stress condition. Accelerated growth has not been observed following type (c) overload conditions, this is consistent with the proposed mechanism as no zone of tensile residual stress would exist after this load sequence.

2.5.5 Application of multiple overloads

A further important aspect of crack growth retardation concerns the number of overload peaks (n_H) applied. There are three approaches to investigating this parameter. Figure 2.11 distinguishes the three retardation parameters that are used. The minimum gradient of the growth curve represents the point of maximum retardation. The interval n_g represents the gross delay after the removal of the overload condition. The interval n_n represents the net delay to crack extension when the damage due to the overload is considered. The existence of these different approaches complicates comparisons of results from different sources. Corbly and Packman [75] investigated the effect of multiple overloads on 7075-T6511 aluminium alloy using a type (c) load regime. They investigated both the initial and the minimum growth rates after the overload by measuring striation spacings.

Their results are summarised in Figure 2.12. It can be seen that retardation increases with the number of overload cycles applied. Hudson and Raju [74] used the same materials for their study but presented the retardation in terms of the net delay n_n,(Figure 2.11). The delay was found to increase with the number of overload cycles applied for values of n_H below 20. Above this value the measured delay was relatively constant; this is supported by the observations of Corbly and Packman. Porter [78] applied repeated overloads to 7075-T6 aluminium and to a Ti-6%Al alloy. He varied the number of overload cycles (n_H) whilst maintaining the interval between overload blocks constant at 50 cycles. Single overload cycles resulted in the greatest net delay in crack growth. Clearly the propagation resulting from the overload cycles had a very significant effect on the overall average growth rate. For both materials sequences of more than 15 overload cycles resulted in the average growth rate exceeding the rate prevailing in the absence of any overload effects. Porter's results for 7075-T6 aluminium are shown in Figure 2.13. Similar work was done by Rice and Stephens [76] on 12%Mn steel. They used single overload cycles but varied the interval between repetitions from 1000 to 20,000 cycles. Overloads equal to 120, 150, 175 and 200% of ΔK_L were employed in a type (c) sequence. Crack growth retardation was observed for all these overload conditions.

2.5.6 Propagation during overload phase

Complete consideration of a tensile overload involves determination of the crack propagation rate at the high stress level. Some of the above mentioned workers have considered this implicitly by reporting net delay periods. As only a few overload cycles are applied growth rate determinations are usually performed by striation interval measurements. McMillan and Pelloux [46] used this technique

in their work on aluminium. They found the first overload cycle resulted in exaggerated growth which rapidly stabilised to the expected "equilibrium"rate. This finding is supported by other workers [52,76] who investigated the effect of type (c) overloads on steel. Trebules et al [79] found the overload growth rate could be "accelerated" for up to 350 cycles. These investigations involved mean stress changes, the situation is less clear if purely dynamic overloads are considered. The results of Koterazawa et al [52] indicate that in the absence of mean stress changes the overload cycles result in initially accelerated growth rate which rapidly decreases to the "equilibrium" rate. Thus, under these conditions, the net damage resulting from the overload will be little influenced by accelerated growth rates at the high stress level; retardation effects that follow the overload are expected to dominate the overall damage rate. However, if specimen life or component life considerations are involved then it is important to realise that the application of an overload to a cracked structure may result in immediate static failure in situations where continued support of the low load level was possible.

2.5.7 Compressive overloads and accelerated growth

Discussion so far has only considered tensile overloads. Figure 2.8(d) shows a compressive sequence that has been investigated by Rice and Stephens [76]. They found a single compressive cycle could reduce their specimen life by up to 23%. Further insight into the effect of compressive overloads has been gained by consideration of the two purely dynamic overload routines, Figure 2.8(a) and (b). It is found that the reversal of sequence has a significant effect on crack growth rate. Porter [78], Schijve [80] and McMillan and Hertzberg [41] have all observed the effect. Porter showed that both sequences

resulted in retardation relative to the no overload condition. The type (a) sequence resulted in significantly greater retardation. McMillan and Hertzberg found that the damage due to the overload cycle was approximately the same for both load sequences but that propagation was initially accelerated after the type (b) sequence. Schijve considered more complex load sequences in which the overloads were of either type (a) or type (b); as with the other workers type (b) was found to result in a significantly shorter specimen life. In the case of the type (d) overload, which imposes an entirely compressive cycle, it is considered that tensile residual stresses are created which increase the effective stress intensity of subsequent cycles. Crack growth acceleration therefore occurs. For the purely dynamic overloads it is considered that the two halves of the cycle have a self cancelling effect so that both retardation and acceleration effects are reduced. Figure 2.10 shows Schijve's suggestion for the crack tip stress condition after a type (b) overload. The effect of the compressive half cycle is thought to be reduced as a result of crack closure effects. Thus for both type (a) and type (b) sequences the residual effect of the tensile half cycle dominates the crack tip stress condition sufficiently to cause growth retardation in both cases.

Clearly the details of crack growth during and after dynamic overloads are extremely complex. Currently a considerable qualitative understanding of the principal effects exists. Quantitative predictions remain very inadequate. The aim of quantitative theories is to predict crack growth rates under service load conditions, therefore, before considering the quantitative cumulative damage models some of the experimental observations concerning more complex load sequences will be reviewed.

2.6 Crack Growth Under Programmed Loading Conditions

2.6.1 Preamble

Consideration has so far been limited to the influence of individual loading parameters and crack growth rates have been considered on a cycle by cycle basis. Of more practical importance are the growth rates associated with service load conditions. A great deal of attention has been given to propagation rates under simulated service load sequences with a view to:

1) identification of particularly damaging aspects of service load spectra;

2) evolution of suitable test sequences which hopefully should by simpler and less time consuming than full service load simulations;

3) identification of shortcomings in existing laboratory test routines.

The majority of the investigations have been associated with the aerospace industry and therefore aluminium alloys have been the principal materials used. A most comprehensive survey of results has been presented by Schijve [77]. The majority of load regimes investigated can be placed in one of the following catagories.

a) Full service load simulations.

b) "Spectrum" loading based on service load data.

c) Block loading sequences based on service load data.

The difference between these catagories is clear from Figure 2.14. Full service load simulations provide the "base line" data against which damage occurring under simplified load sequences is compared. Schijve [77] quotes his own work to show that the degree to which the service load is truly simulated can have a considerable effect on specimen life. Jacoby [81] also draws attention to the significant difference in damage rates that results from small changes in the applied service load simulation. In general attempts to simplify or

shorten the test sequence result in conservative life predictions when compared with a full cycle by cycle service load simulation. However, interest in simplified and accelerated tests stems from their practical and economic advantages.

2.6.2 Service and spectrum loading

Random or spectrum loading sequences have been extensively investigated. In many cases these represent an accurate service load simulation though in others a considerable simplification is involved. Published results indicate that crack growth rates are sensitive to the manner in which the load sequence is generated. Naumann [82] showed that in 7075-T6 aluminium the specimen life increased in the following order.

1) Random sequence of complete load cycles.
2) Random sequence of half cycles, alternatively positive and negative.
3) Random sequence of half cycles, no restrictions.

Furthermore the effect of band width is not entirely clear. The results of Hillberry [83] using 2024-T3 aluminium and Bussa [84] using a low carbon steel indicate that specimen life is reduced under wider band loading spectra. However such variations in loading conditions necessarily involve a hypothesis for damage summation. Hoddinott [85] has shown that randomisation of a narrow band sequence does not reduce the fatigue life of mild steel.

Work by Jacoby [86], Schijve [87] and others has indicated that overloads in complex loading sequences have qualitatively the same influence on specimen life as during the simplified sequences previously discussed. Briefly: tensile overloads increase life, compressive overloads reduce life. This straight forward extension of simple test results has been brought into question by the work of Watson et al [88]

who have investigated overloads applied under conditions of strain control. They found a reduction in the life of their mild steel specimens resulted when purely dynamic overloads were included in a full service load simulation. They reported that both crack initiation and, to a lesser extent, crack propagation were accelerated by the inclusion of overload cycles.

2.6.3 Block loading

Block loading sequences offer a simple and cheap approach to complex load fatigue tests. The method of evolving a block load regime, as originally described by Gassner [89], is shown in Figure 2.15. The load levels are determined from the service load history in the manner shown, no such process is available to determine the sequence of block application. The test sequence is known to have a potentially significant influence on the rate of crack growth. Schijve [80] has reported an extensive series of tests on precracked sheets of 2024-T3 aluminium. A pronounced effect of both load sequence and block length was observed. His results are summarised in Figure 2.16. Barsom [90] applied similar load sequences to ASTM A514-B steel and found that the growth rates were sequence independent when analysed on the basis of ΔK_{rms}. Barsom used "smoothed" load sequences that resulted in fewer load discontinuities than occur in traditional block tests of the type used by Schijve. Hardrath et al [91,92] have also investigated the way in which block order influences crack growth rates. The sequences employed are shown in Figure 2.16b, for both alloys tested the specimen life increased in the order:

low-high, "irregular", low-high-low, high-low.

These results are shown in Figure 2.17.

Steels have been subjected to similar tests by Kawamoto et al [93] and Tedford et al [94], both groups report no significant sensitivity to sequence effects. Tedford considered two further points. He modelled the same service load spectrum with 4,8 and 16 level block regimes. Specimen lives determined under 8 and 16 level tests were equal, the 4 level test resulted in a longer life. This supports the original proposition of Gassner [89] that considered eight-levels to be sufficient. Truncation effects were considered for both extremes of the load spectrum. The lowest three load levels in the 8 block program were found to have no effect on specimen life, thus a considerable time saving could be effected by using only the highest levels for certain tests. This would not seem to be a general conclusion as the authors quote conflicting references for and against the importance of low load cycles. In contrast truncation of high loads was found to have a critical influence on specimen life. Inclusion of 1 cycle in 2000 was found to be significant at the highest loads.

Clearly block load tests must be fully researched before being applied to any given problem. Steels would appear to be less sensitive to the influences of sequence but care is required to model the load spectrum accurately, particularly at the highest load levels. More generally the last three sections demonstrate the extreme complexity of predicting crack growth rates, or component lives in any multi-load level test. The final section of this review considers the more commonly quoted attempts to formulate quantitative cumulative damage expressions.

2.7 Quantitative Cumulative Damage Predictions

2.7.1 The Palmgren-Miner rule

This, the most simple and most obvious of cumulative damage predictions, was independently evolved by several workers prior to 1945. The concept first proposed by Palmgren [95] and independently restated by Miner [96] is simply summarised as follows.

1) Under constant dynamic loading conditions n_i cycles applied will consume a fraction of the component's total fatigue life given by n_i/N_i where N_i is the life to failure under the imposed conditions.

2) Under complex loading conditions failure occurs when the sum of these fractions is equal to unity.

$$\text{i.e.} \quad \sum \frac{n_i}{N_i} = 1 \qquad (2.16)$$

This rule is also referred to as the "linear damage rule" as a consequence of Miner's assumption that the damage occurring in a constant amplitude test is linearly dependent on the number of cycles applied. This aspect was originally disputed [97] though Schijve [98] has subsequently argued that linear damage is implicit in the proposed summation of equation 2.16. The principal weaknesses of the proposed analysis are:

1) No distinction is made between crack initiation and crack propagation. The rate of damage is assumed to be unaffected by the change in growth mode.

2) Failure is considered to occur at the same damage "level" or crack length irrespective of the applied load.

3) No load interaction effects are accounted for.

Not withstanding these limitations the Palmgren-Miner rule has been extensively used principally as a consequence of its simplicity.

Attempts have been made to mitigate some of the above deficiencies notably by separate consideration of crack initiation and crack propagation.

2.7.2 The damage summation of Corten and Dolan

Corten and Dolan [99] evolved a similar approach to that of Palmgren and Miner the principal differences being:

1) Distinction between crack nucleation and propagation.
2) Recognition of the non-linearity of the rate of crack advance per cycle during a specimen's life.

The number of cycles required to nucleate a crack was defined by a complicated expression that required experimental determination of several constants. Subsequent propagation of the crack was assumed to occur on a cycle by cycle basis, but account was taken of the increased rate of propagation at high crack lengths. The difference between the Palmgren-Miner and Corten-Dolan summations is shown in Figure 2.18. The Corten-Dolan method of prediction suffers from complexity which makes it unsuitable as a design tool and, like the suggestion of Palmgren and Miner, it is unable to account for load sequence effects. A simplified two stage damage summation has been considered by Manson et al [100].

2.7.3 The double linear damage rule of Manson et al

Manson et al [100] have formulated an empirical expression for assessing the damage occurring during a simple two load level test. The load sequence considered is shown in Figure 2.19(a); the order of application of $\Delta\sigma_1$ and $\Delta\sigma_2$ may be reversed. The period of crack initiation is empirically distinguished from crack propagation.

Damage occurring in these two phases is summed separately on a linear basis. The conditions are given in Figure 2.19(b). The proponents of this summation found that their technique gave equal or better life predictions than the original Palmgren-Miner rule for the simple load sequences considered. Figure 2.19(a) compares the two approaches. It is seen that for a high/low load sequence the Manson model predicts a longer life at the second stress level. This, and the reverse effect for low/high sequences, is in keeping with experimental observation. There is no reason why this model should not be extended to deal with multi-level tests, its accuracy under such conditions is untested. The principal drawbacks of the law are its assumption of linear damage and its inability to deal fully with load interaction effects. The complexity of the required summation is sufficient to prevent its adoption as a design "tool" until it is shown to have a general superiority to the Palmgren-Miner rule.

2.7.4 The linear cumulative growth approach

This approach to damage analysis is an obvious combination of the Palmgren-Miner rule with more modern, fracture mechanics, crack growth considerations. Engle [101] has evolved a computer program for linear growth summations, however the approach has been independently adopted by many workers including the present author. The basic precepts of the technique are:

1) Crack nucleation is not considered.

2) Propagation is considered on a cycle by cycle basis to be a function of stress intensity or a similar parameter.

e.g. $$\frac{da}{dN} = f(K) \qquad (2.17)$$

Data is obtained from equilibrium growth rate measurements.

given by

3) The crack length is a simple summation of the damage accruing in each load cycle i.e.

$$a_n = a_o + \sum_{i=1}^{n} f(K) \qquad (2.18)$$

4) A specimen failure condition is not included, it could however be written in, if life predictions were required.

This approach considers crack propagation only and therefore represents a simplification of the previously reviewed "life" predictions. The potential advantages of a cycle by cycle incremental law are apparent, the principal limitation is an inability to deal with load interaction effects which result in propagation rates differing significantly from the predicted steady state rates.

2.7.5 The Wheeler growth retardation model

Three models will now be considered that attempt to treat load interaction effects. They are all specifically concerned with the retardation effects which are observed to result from the application of tensile overloads. The models are all developments of the cumulative linear growth approach, each tries to account for growth retardation by manipulation of the basic growth rate expression which was given as equation 2.10.

Wheeler [102] proposes the incorporation of a retardation parameter in the "stress intensity/growth rate" expression. He modifies the expression

$$\frac{da}{dN} = C(\Delta K)^m \qquad \begin{matrix}(2.10)\\(\text{restated})\end{matrix}$$

to become

$$\frac{da}{dN} = C_r C(\Delta K)^m \qquad (2.19)$$

where C_r is the retardation parameter which may take values between zero and unity. Wheeler suggests retarded growth is due to plastic zone interaction effects. He proposes that retardation occurs so long as the equilibrium crack tip plastic zone is "inside" the greatest prior plastic zone. This is shown schematically in Figure 2.20(a); the zone shapes are, of course, not true physical representations. Referring to Figure 2.20(a) Wheeler's proposal for the retardation parameter is

$$C_r = \left(\frac{2R_Y}{a_p - a}\right)^{m_w} \quad ; \qquad (2.20)$$

m_w is a shaping exponent that has to be determined by experiment. Typical values of the retardation parameter are shown in Figure 2.20(b). From equation 2.20 and Figure 2.20(b) the crack growth rate is seen to be a minimum immediately following the overload.

2.7.6 The FDL model

Willenborg et al [103], working at the US Air Force Flight Dynamics Laboratory (FDL), have proposed a model similar to that of Wheeler. They too calculate the plastic zone size resulting from the overload conditions and like Wheeler suggest that growth is retarded until the equilibrium zone "touches" the overload zone. Figure 2.21(a) shows the situation in which some crack propagation has occurred at the low load (σ_L) conditions since the overload (σ_H) ceased. Willenborg et al evaluate the equivalent overload (σ'_H) at each crack length that would result in the same separation of the plastic zone boundaries. They postulate that both maximum and minimum stress levels are reduced by the amount σ_r which is given by:

$$\sigma_r = (\sigma'_H - \sigma_L) \quad (2.21)$$

Hence the effective maximum and minimum stress levels are given by:

$$(\sigma_{max})_{eff} = ((\sigma_L)_{max} - \sigma_r) \quad (2.22)$$

$$(\sigma_{min})_{eff} = ((\sigma_L)_{min} - \sigma_r) \quad (2.23)$$

Negative "effective" values are set to zero and an "equivalent" stress intensity value calculated.

$$(\Delta K)_{eff} \propto [(\sigma_{max})_{eff} - (\sigma_{min})_{eff}] \quad (2.24)$$

The retardation predicted by this model is dependent on the exponent m used in equation 2.10. Figure 2.21 (c) shows the general form of the prediction; complete crack arrest is seen to occur if $\sigma_H > 2\sigma_L$ and like the Wheeler model maximum retardation occurs immediately after the overload is removed.

2.7.7 The Elber crack closure model

The concept of crack closure advanced by Elber [63,65] has already been discussed in Sections 2.5.2 and 2.5.4. The importance of the model is that unlike those in the two previous sections it does not necessarily predict maximum retardation immediately after the overload condition. Elber proposed

$$\frac{da}{dN} = C(\Delta K_{eff})^m = C(U\Delta K)^m \quad (2.25)$$

where U is given by

$$U = \frac{K_{max} - K_{op}}{K_{max} - K_{min}} \quad (2.26)$$

K_{op} is the stress intensity required to "open" the crack tip. Elber argues that the crack tip stress singularity is eliminated by crack closure, thus damage only occurs for that part of the load cycle for which the crack is open. From his experimental work on 2024-T3 aluminium Elber proposes

$$U = (0.5 + 0.4R) \text{ where } 0.1 < R < 0.7 \qquad (2.27)$$

Using this expression Elber successfully accounted for growth rates in 2024-T3 aluminium alloy under variable amplitude loading conditions. Sih and Wei [64] have also measured loading conditions under which macro-closure effects were detectable. They conclude that the closure expression proposed by Elber (equation 2.27) should not be regarded as generally applicable.

The attractiveness of the crack closure model is apparent from the frequency with which it is invoked to provide a qualitative explanation of growth retardation. A satisfactory quantitative model will require a great deal of further development.

2.7.8 Damage predictions - "the state of the art"

The last three damage summation techniques considered have all been developed specifically to deal with the occurrence of crack growth retardation following tensile overload conditions. Even given this limitation they are unsatisfactory for the following reasons.

1) No change in delay is predicted for multiple overloads as compared with single overload cycles.

2) Small overloads are experimentally observed to result in no measurable delay, the models predict some delay for all overload levels.

3) Delayed retardation, observed in pracice, is not accounted for by the Wheeler and FDL models.

From a more general standpoint these damage summations have not been developed to deal with the more complex loading conditions that a component is subjected to in service. Thus while the Wheeler, FDL and Elber models are of interest to the research worker their more general application to design is not possible. In practice the designer is left with variations of the Palmgren-Miner rule as the only numerical means of assessing cumulative damage behaviour. This restriction is clearly unsatisfactory as the linear damage rule is known to be grossly inaccurate. Schijve [77] has attempted to set out the logical and safe way to go about predicting component lives. He considers extensive test programmes are necessary to provide guide lines for designers. The aim is at all times to design on the basis of "interpolation" between known results rather than risk "extrapolation" to untested conditions. Numerical cumulative damage predictions remain a hope for the future.

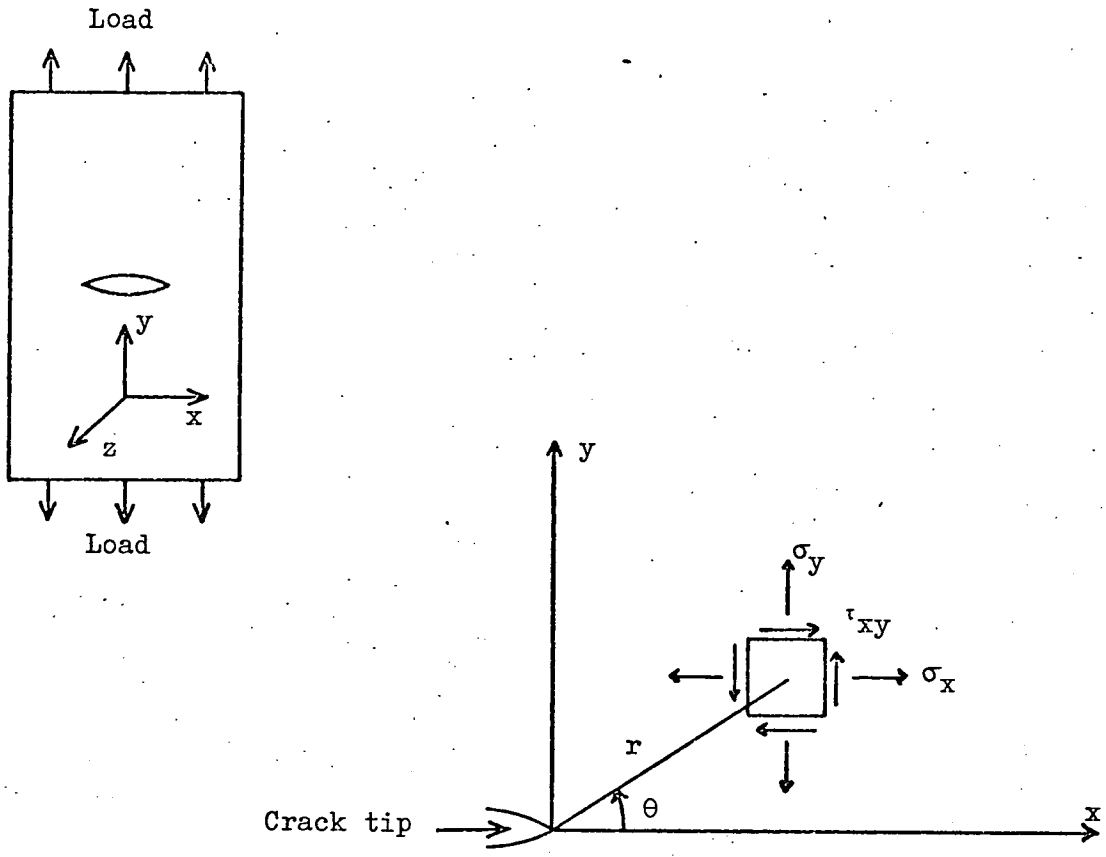

Figure 2.1 Coordinate system for description of crack tip stress field.

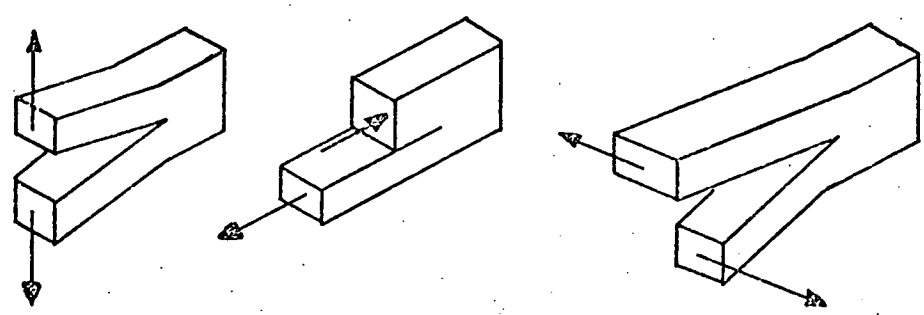

Mode I "Opening"

Mode II "Shear"

Mode III "Anti-plane Shear"

Arrows indicate the direction of load application.

Figure 2.2 Standard designation of crack opening modes.

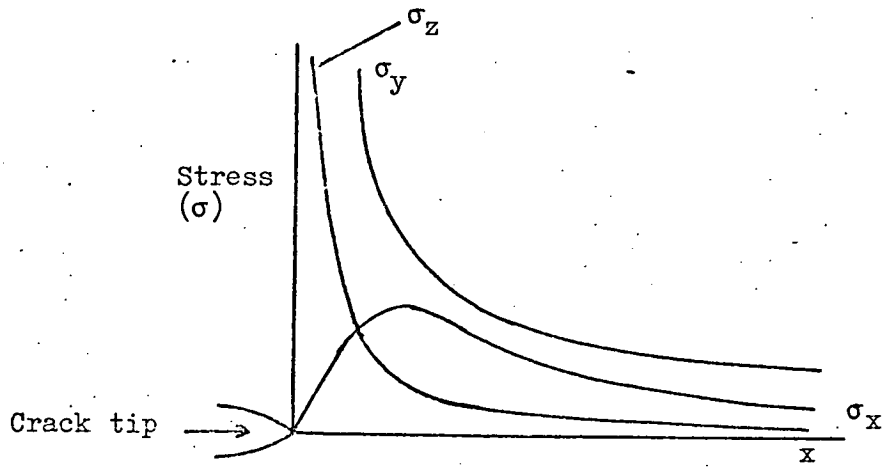

a) Principal crack tip stresses. Linear elastic solution. [3]

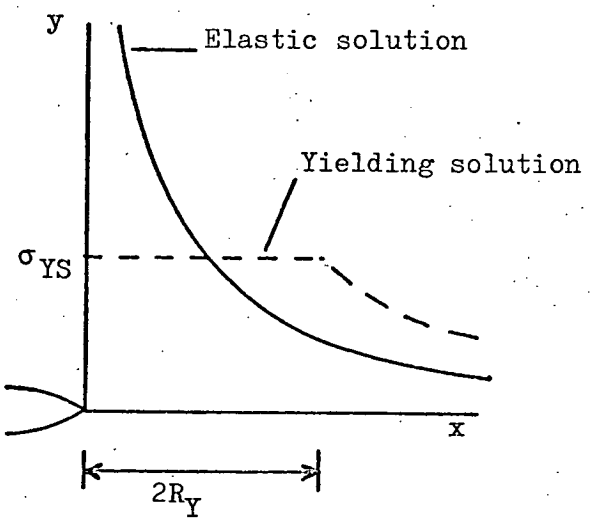

b)

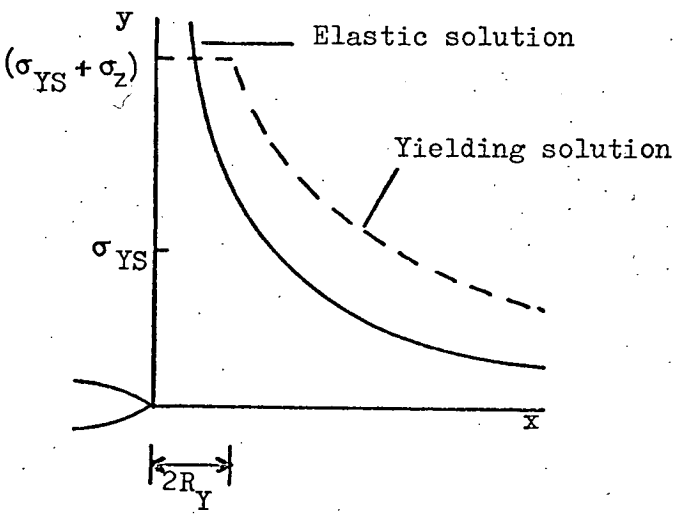

c)

b and c) Modification to linear elastic solution for σ_y required to accommodate crack tip yielding.

b) Plane stress, c) Plane strain.

Figure 2.3 Linear elastic and elastic-plastic crack tip stress solutions. Schematic only.

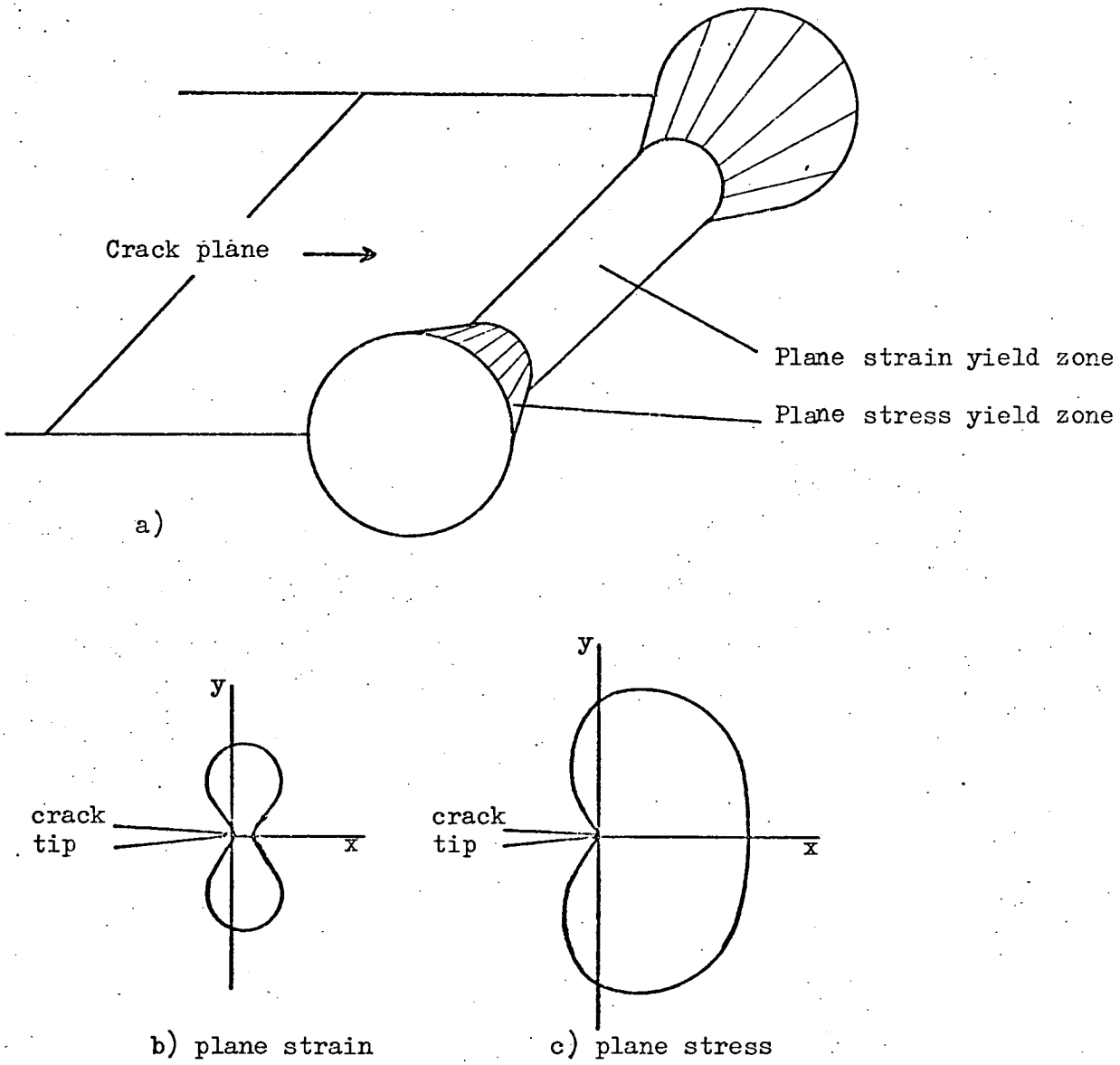

Figure 2.4 Crack tip plastic zone configurations.

a) Circular approximation proposed by Irwin [21].
This is found to be similar to the actual mode III yield boundary.

b and c) Yield boundaries calculated by McClintock and Irwin [23] for Mode I deformation.

b) plane strain, c) plane stress.

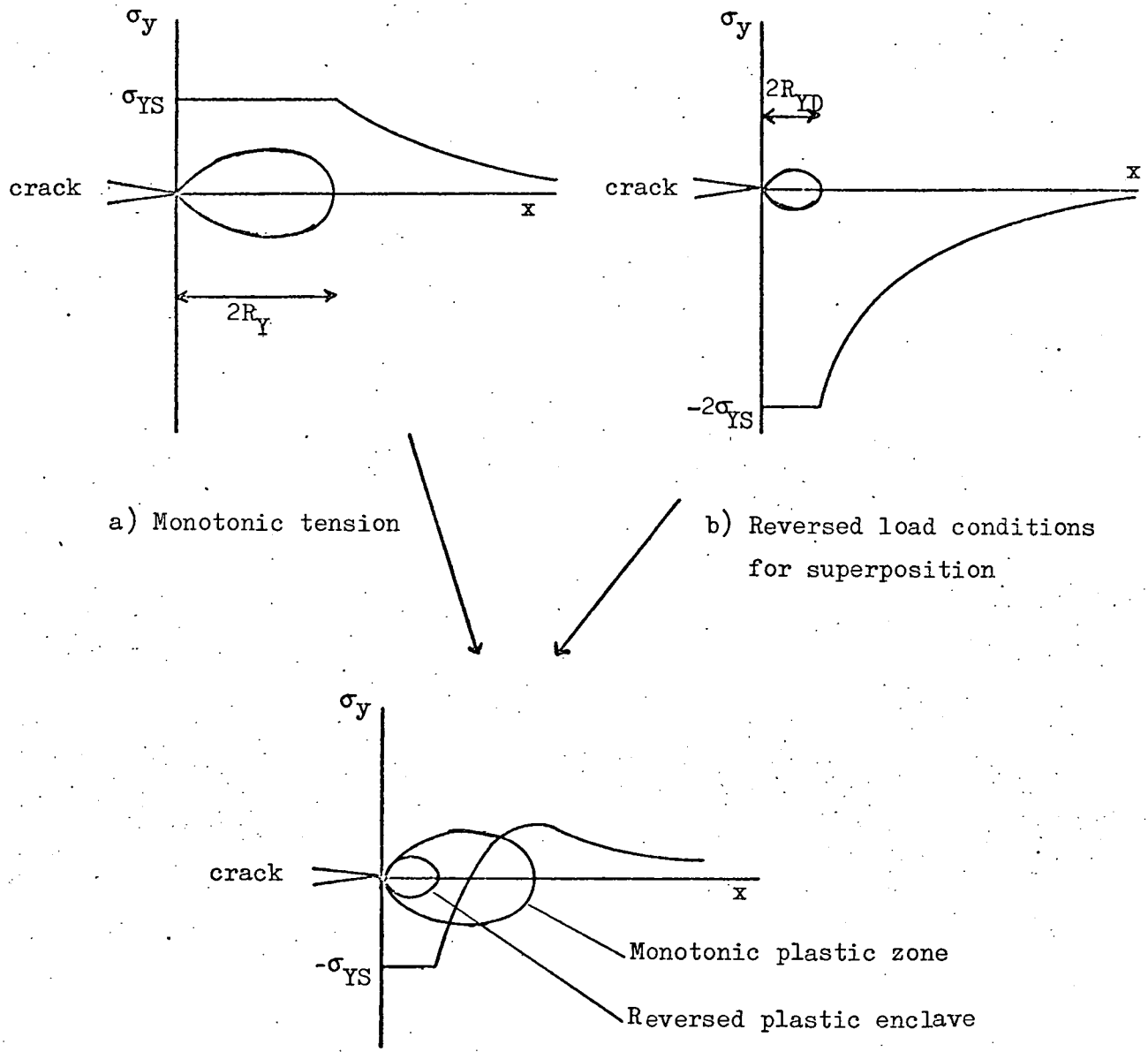

Figure 2.5 Crack tip plastic zone formation under conditions of load reversal. (After Rice [22]).

a) Monotonic yielding under tensile conditions.

b) Reversed yielding in compression, yield occurs at $-2\sigma_{YS}$.

c) Superposition of (a) and (b). Shows plastic zone boundaries and σ_y distribution after load reversal.

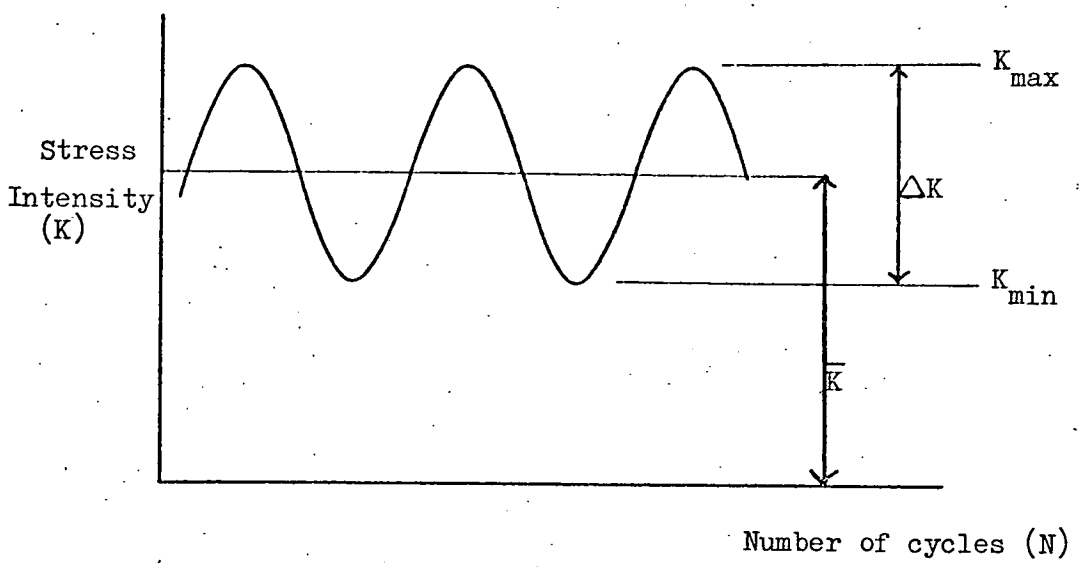

Figure 2.6 Stress intensity parameters for a constant load amplitude test.
Stress ratio = $R = K_{min}/K_{max}$.

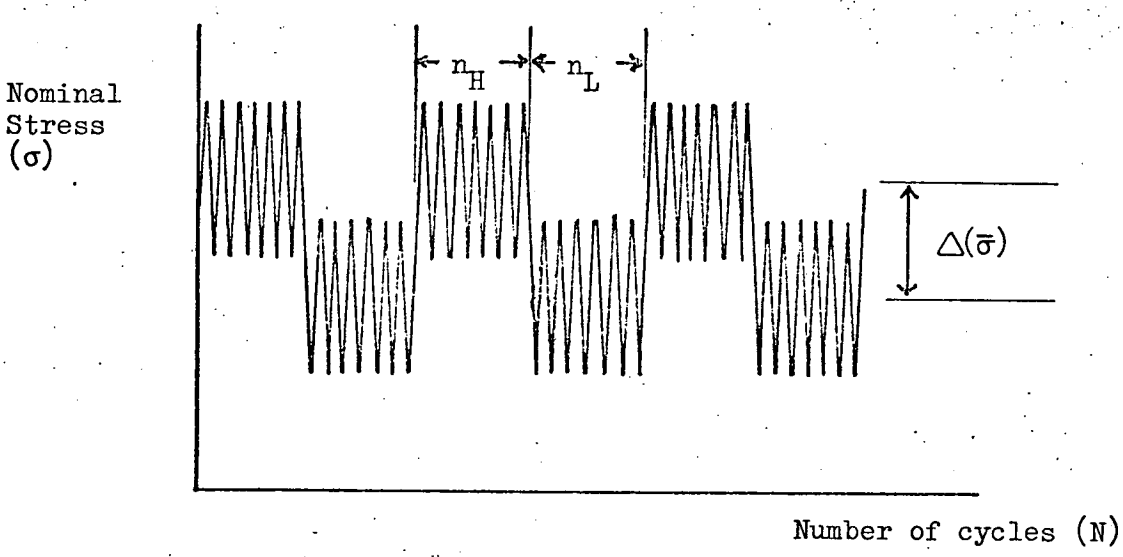

Figure 2.7 Load sequence employed by Dowling [68] to investigate the effect of mean stress changes, $\Delta(\bar{\sigma})$. ($n_H = n_L = 22$ cycles).

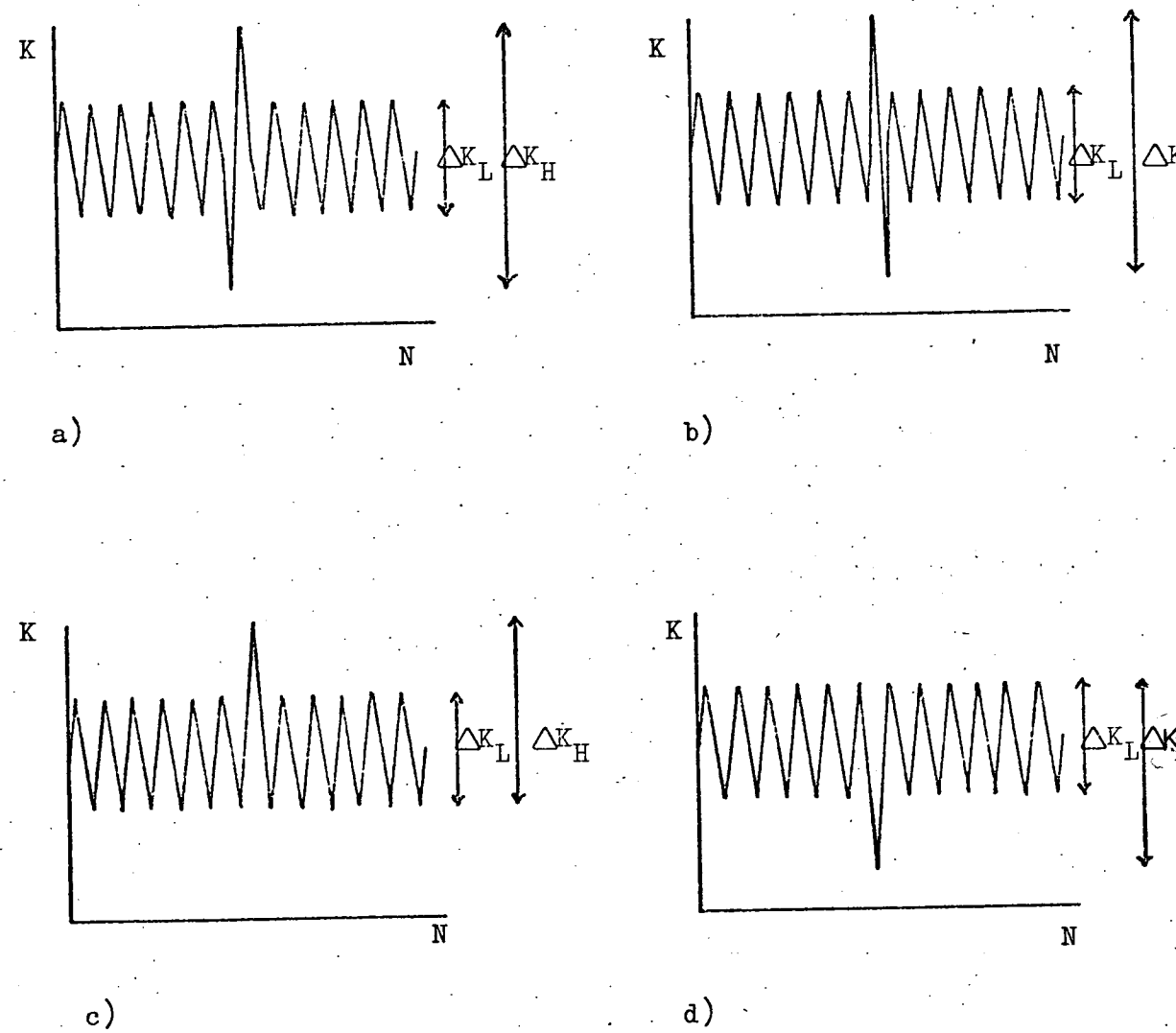

Figure 2.8 Four dynamic overload sequences that have been experimentally investigated.

a) Purely dynamic overload, negative start.

b) Purely dynamic overload, positive start.

c) Combined dynamic and static overload, tensile.

d) Combined dynamic and static overload, compressive.

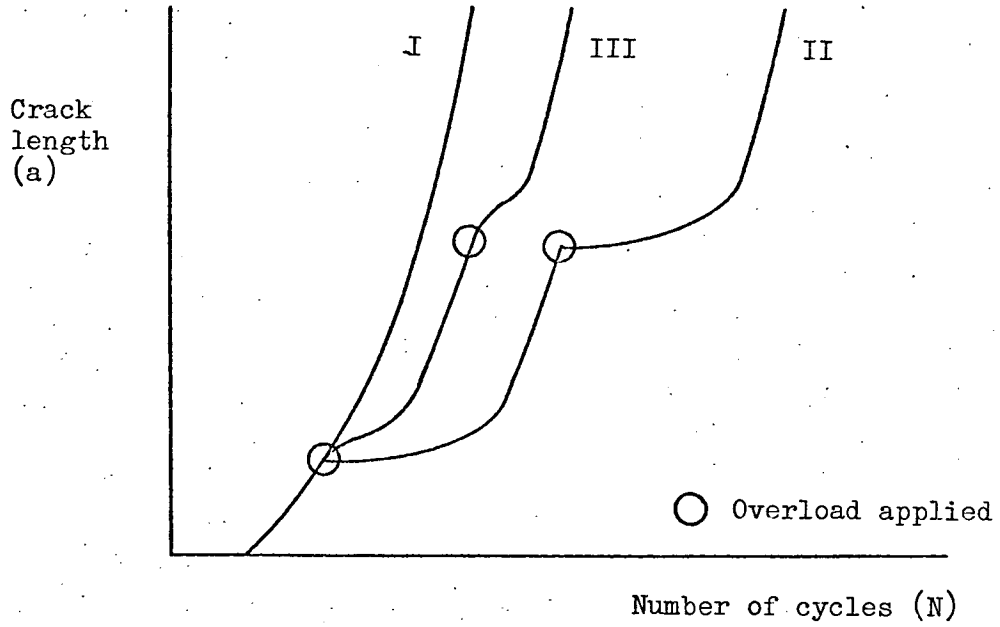

Figure 2.9 Schematic crack growth records for different overload conditions (After Schijve [77])

I: No overload conditions.

II: Combined dynamic and static overload, as per Figure 2.8(c).

III: Purely dynamic overload, as per Figure 2.8(b).

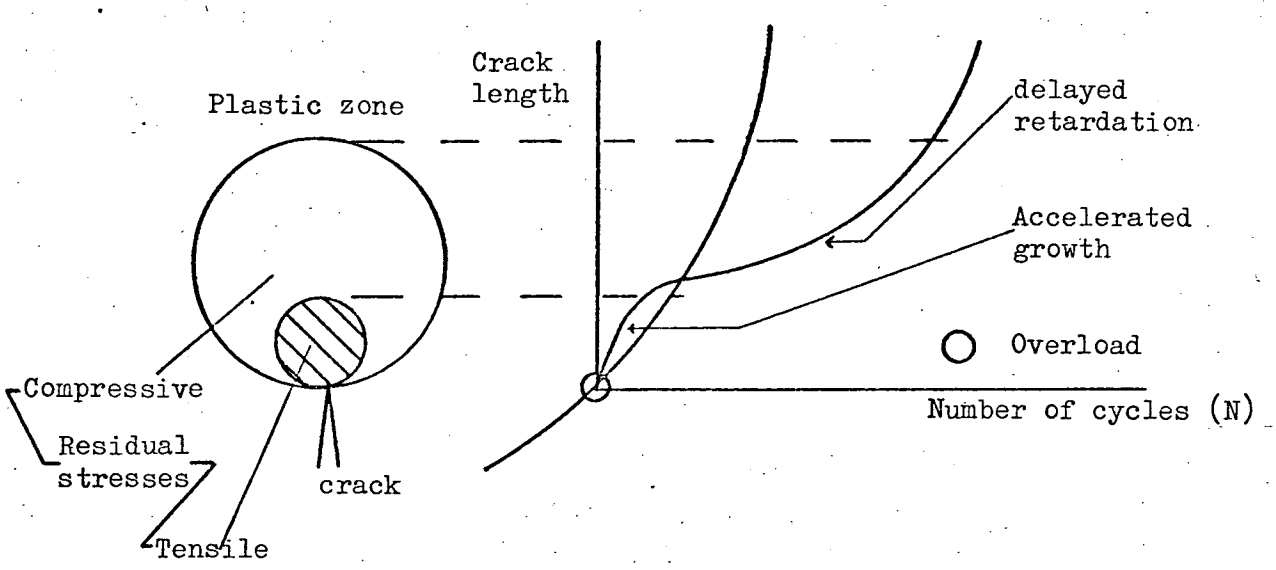

Figure 2.10 A suggested mechanism for accelerated growth following a dynamic overload. Overload sequence (b), Figure 2.8. (After Schijve [77]).

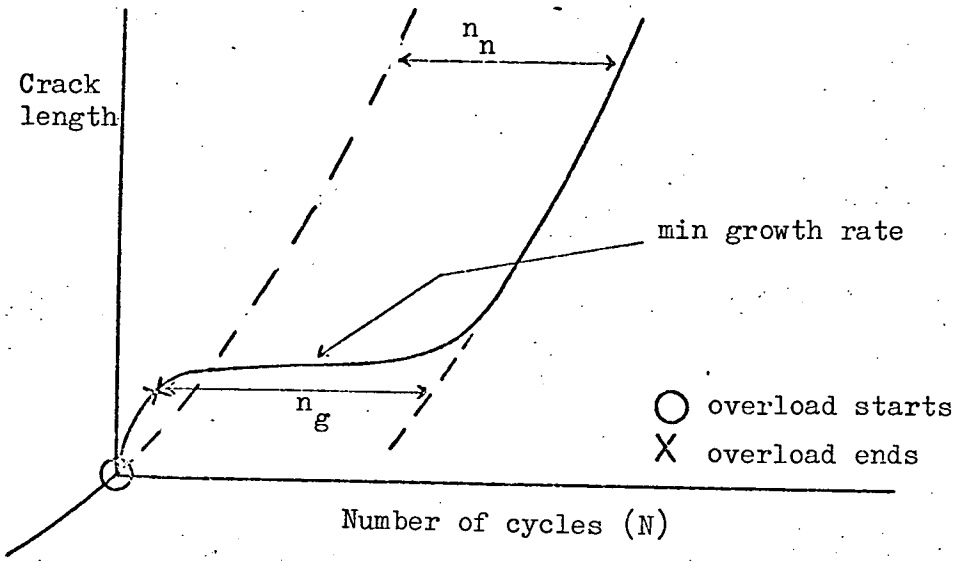

Figure 2.11 Different parameters for quantifying overload induced delays. n_g = gross delay after overload.
n_n = net delay to overall crack growth.

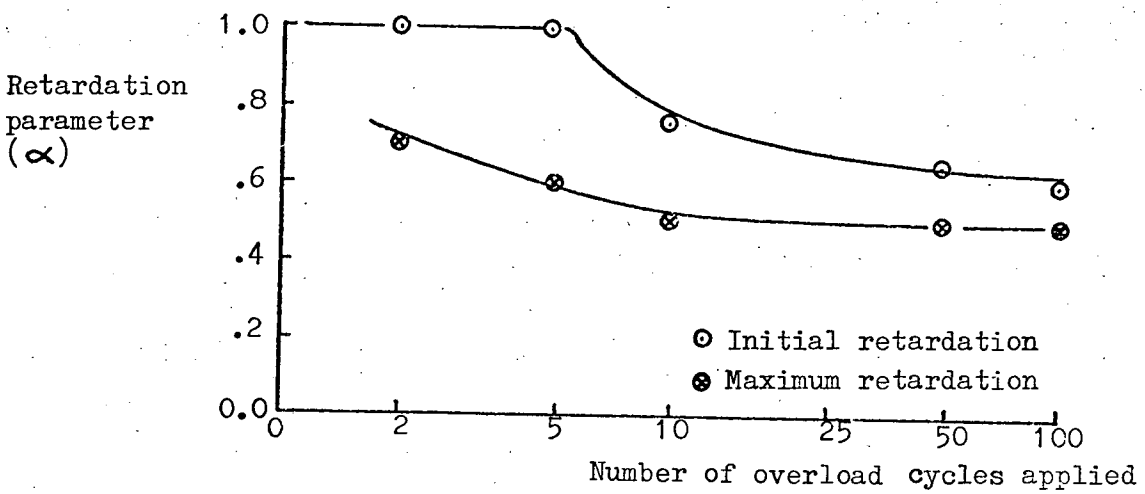

Figure 2.12 Crack growth retardation reported by Corbley and Packman [75] for type 7075-T6511 aluminium. Growth retardation as a function of number of overload cycles applied. Type (c) overload, Figure 2.8.

$\Delta K_H = 22\ MNm^{-3/2}$ $\Delta K_L = 16.5\ MNm^{-3/2}$ $\alpha = \frac{da/dN\ (retarded)}{da/dN\ (const.\ amplitude)}$

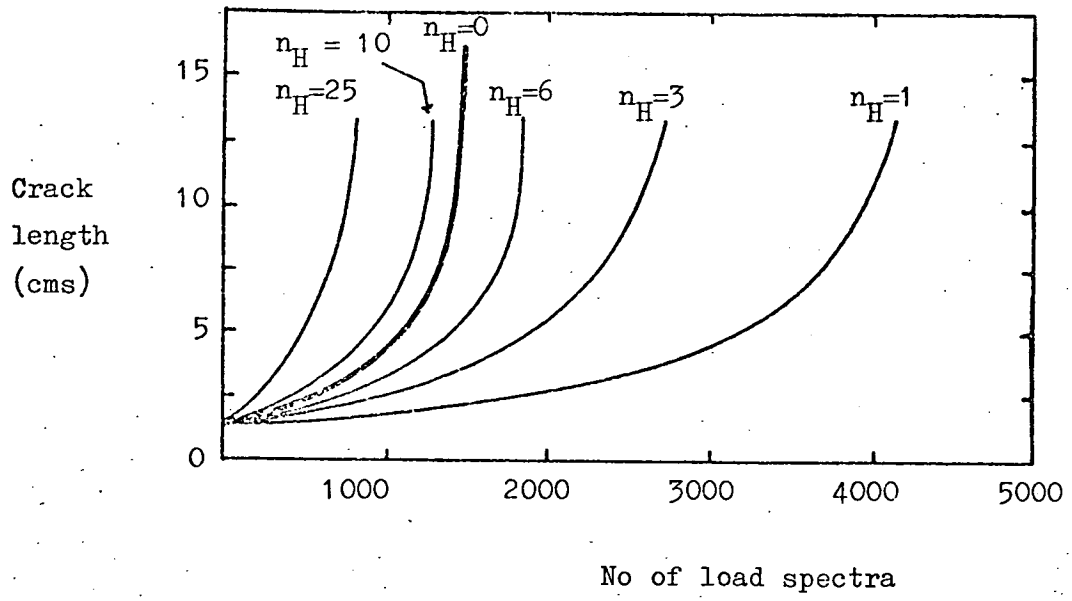

a) Crack growth rate results. One spectrum = $50 + n_H$ cycles, see (b) below.

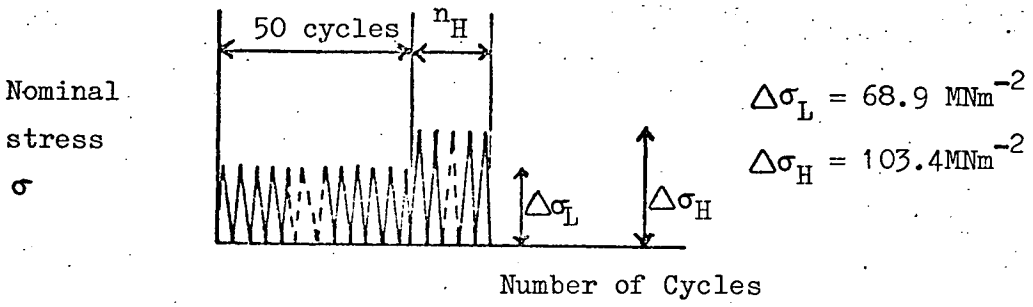

b) Load spectrum

Figure 2.13 The influence of multiple overloads on the crack growth rate in 7075-T6 aluminium. Results from Porter [78].

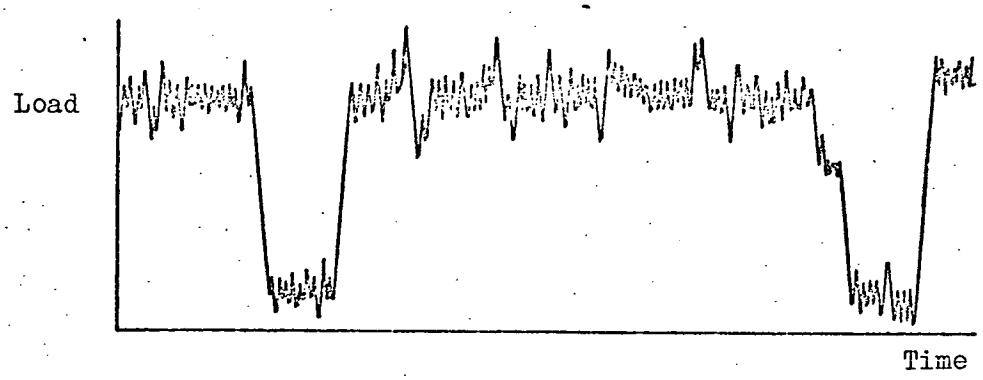

a) Typical aircraft flight load simulation including ground-air-ground cycles. Gust sequences, flight duration, etc. may be randomised or repeated.

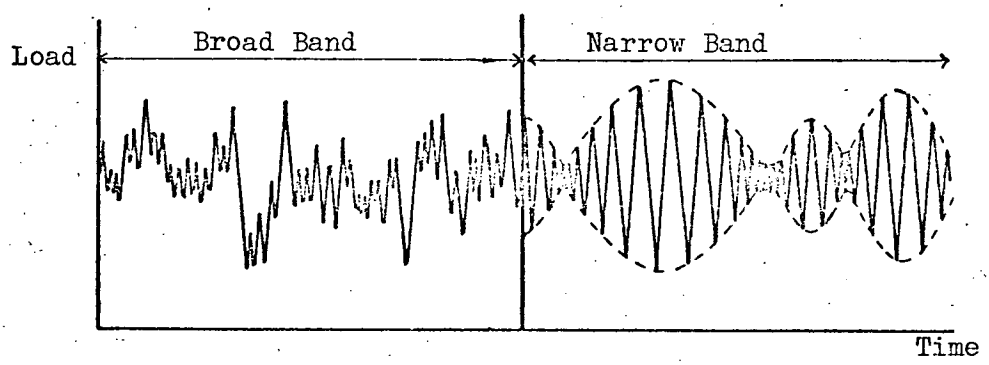

b) Alternative spectrum loading sequences having identical load/frequency distributions.

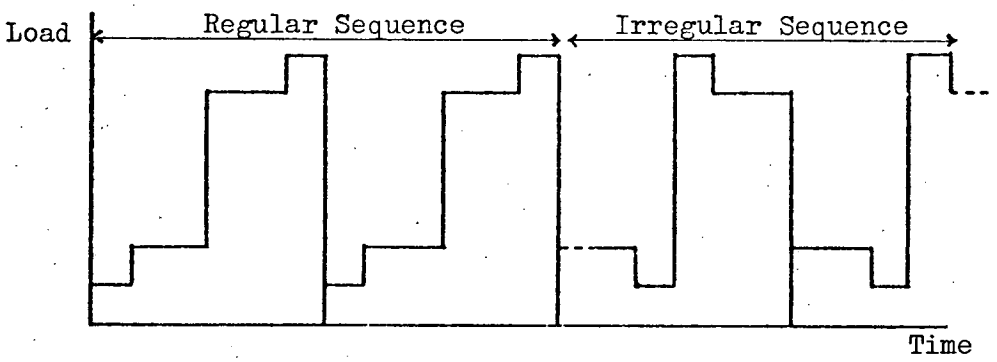

c) Block load routines. The regularity of the load sequence may be varied.

Figure 2.14 Distinction between the principal types of loading sequence employed in complex load fatigue testing.

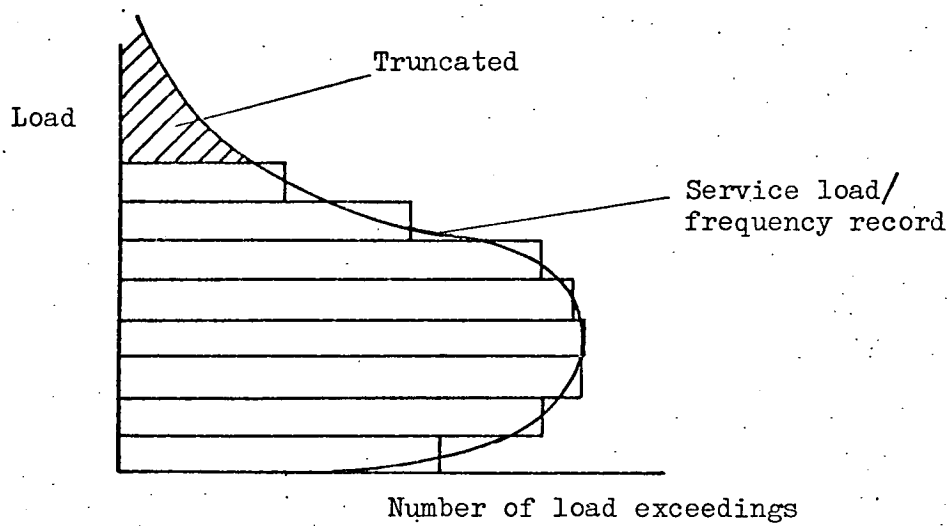

Figure 2.15 Formulation of a typical "Gassner" block load sequence from service load data. The truncated part of the service load record is not included in the block sequence.

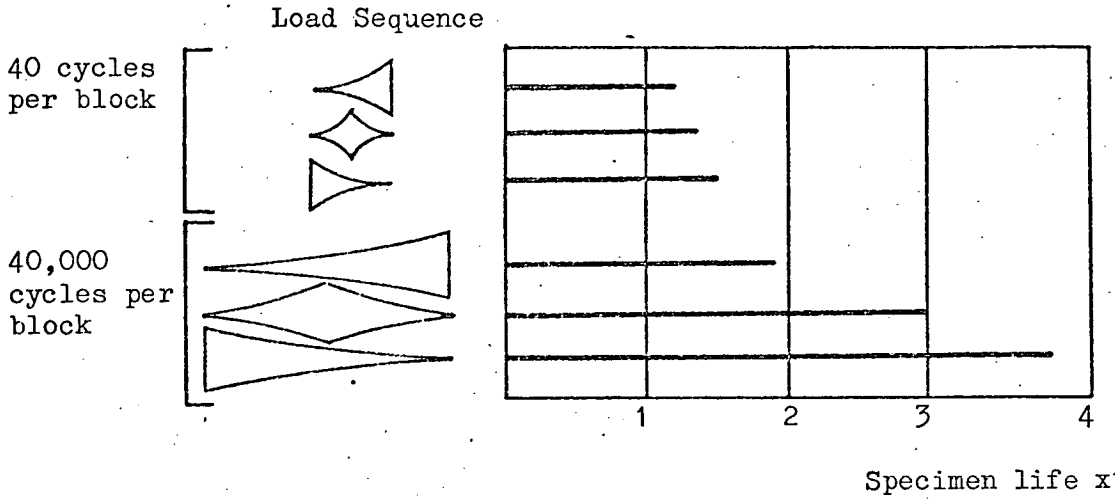

a) Specimen life determinations using 7 level load sequences.

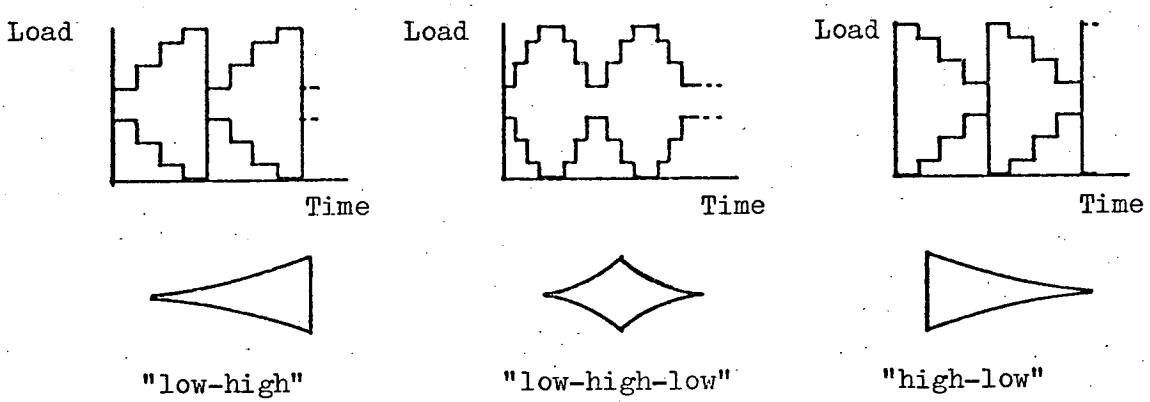

b) Convention for description of block load sequences.
Top: 4 level test sequence; middle: symbolic notation;
bottom: verbal description.

Figure 2.16 The influence of block length and load sequence on specimen life in 2024-T3 aluminium alloy. (From Schijve [80]).

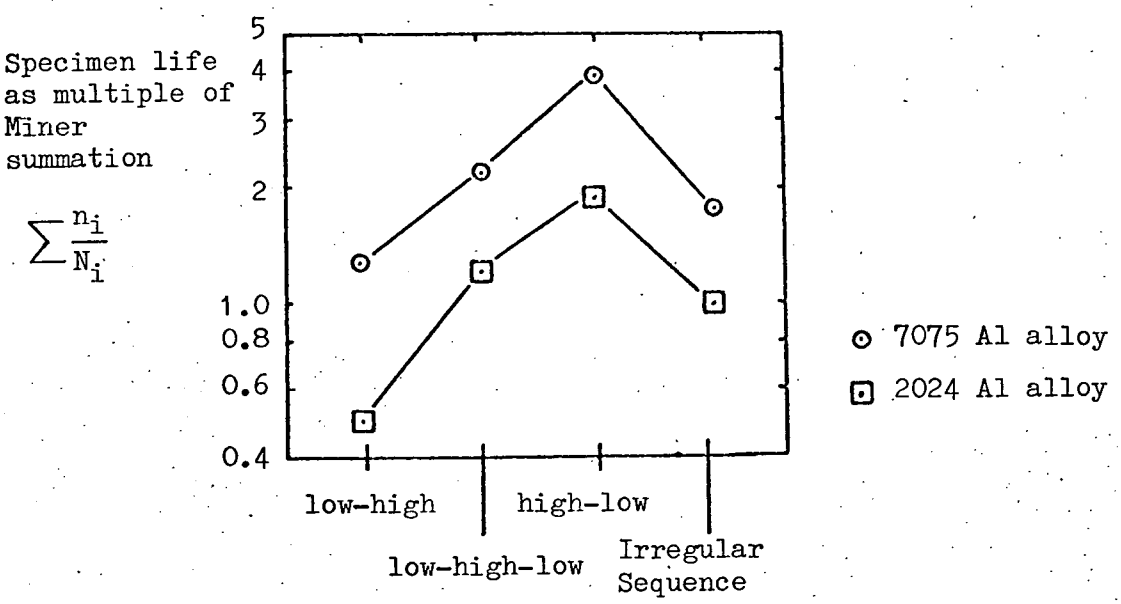

Load sequences as per Figure 2.16(b)

Figure 2.17 Influence of block load sequence on specimen life for two aluminium alloys under tensile mean stress conditions. (From Hardrath et al [91,92]).

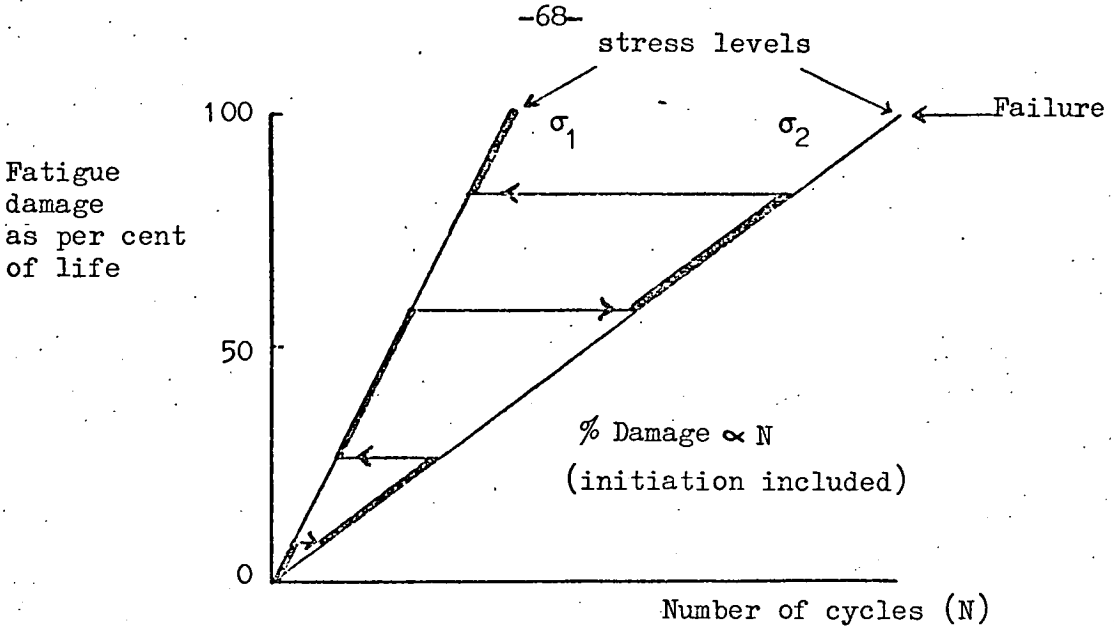

a) Palmgren-Miner linear damage summation for two stress level test.

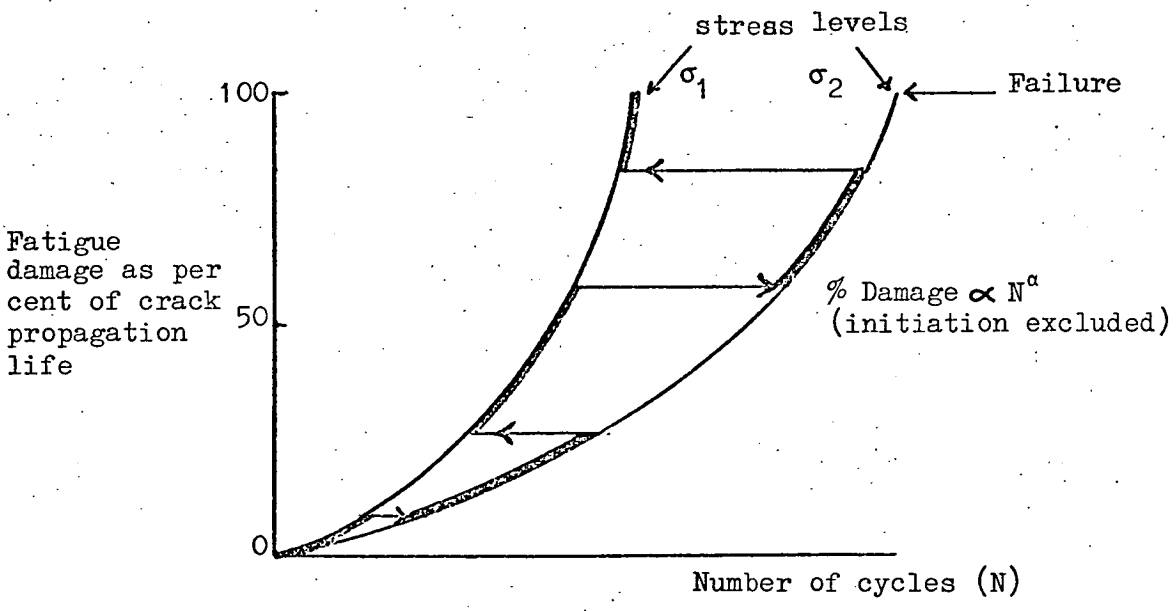

b) Non-linear damage summation of Corten and Dolan for a two stress level test. Intervals for crack nucleation are separately evaluated and added to the propagation life.

Figure 2.18 The Palmgren-Miner [95,96] and Corten and Dolan [99] damage summations compared.

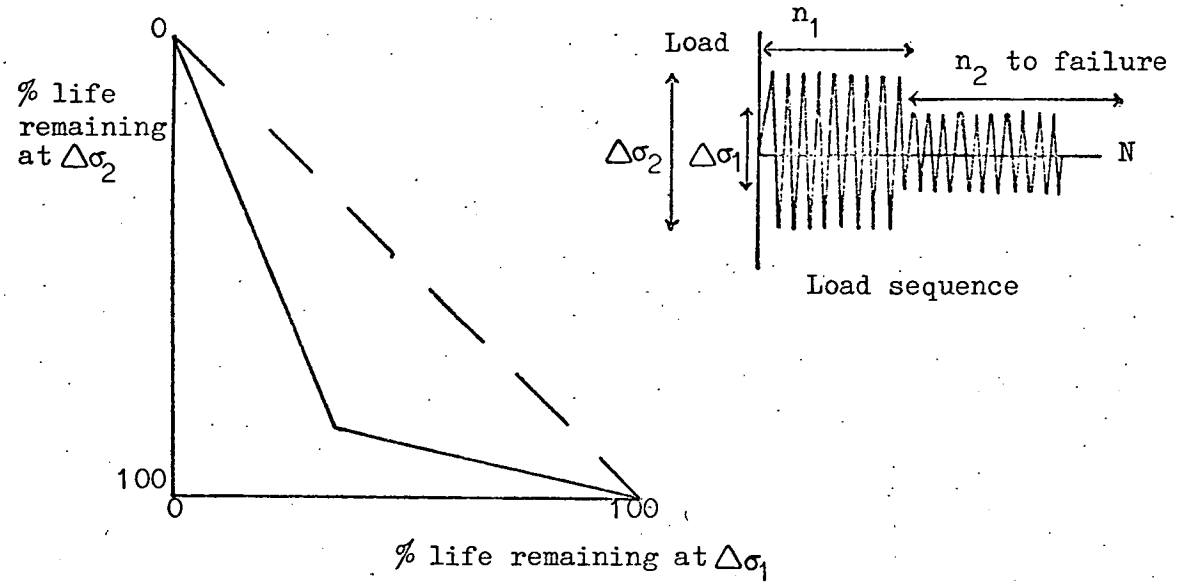

a) Life Predictions: ———— Double linear damage law, nucleation separately evaluated.

— — — Palmgren-Miner rule, nucleation and propagation not considered separately.

b) Empirical Conditions

For initiation $\sum \frac{n}{n_o} = 1$

if $n_L > 730$ cycles $n_o = n_L - 14n_L^{0.6}$

$n_L < 730$ cycles $n_o = 0$

For propagation $\sum \frac{n}{n_p} = 1$

if $n_L > 730$ cycles $n_p = 14n_L^{0.6}$

$n_L < 730$ cycles $n_p = n_L$

Figure 2.19 Comparison of Palmgren-Miner rule with double linear damage law of Manson et al [100] for a simple two level load sequence.

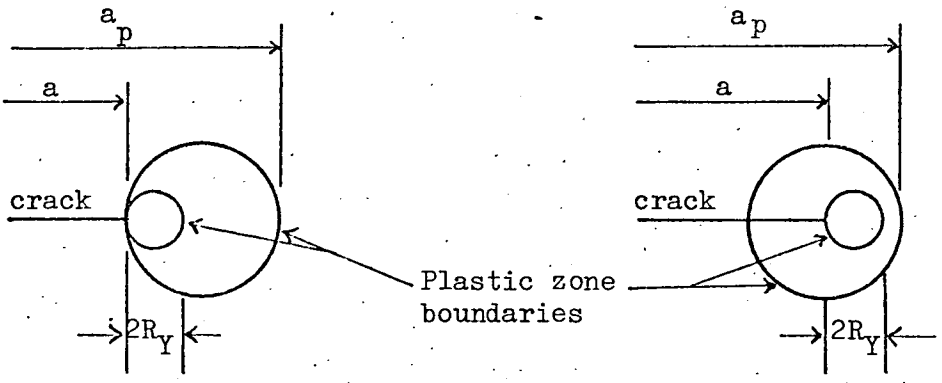

$$\frac{da}{dN} = C_r C(\Delta K)^m \qquad C_r = \left(\frac{2R_Y}{a_p - a}\right)^{m_w}$$

a) Evaluation of retardation parameter by considering plastic zone sizes and positions. The outer zone is created by the prior overload condition. Schematic only.

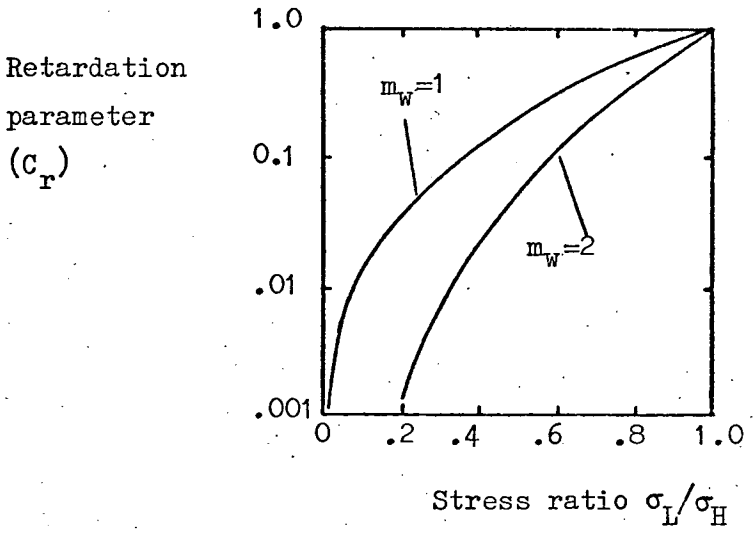

b) Retardation predicted for two different values of m_w. For D-6AC steel m_w was evaluated as 1.3.

Figure 2.20 Wheeler [102] crack growth retardation model.

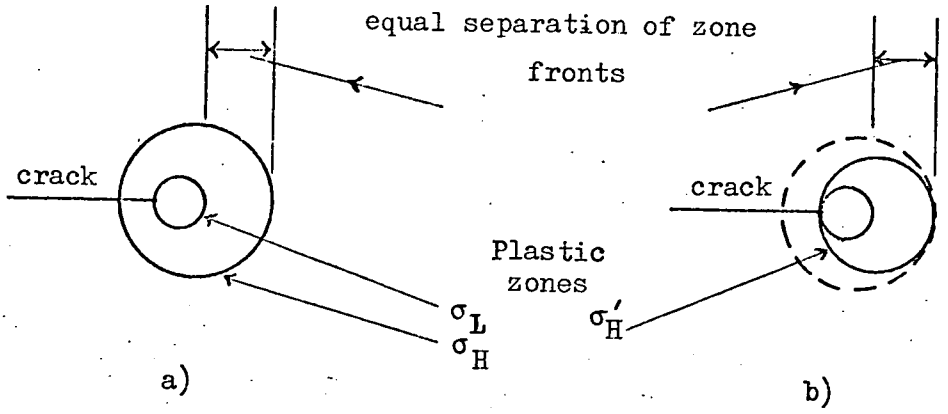

a) Physical condition for which retardation is to be evaluated. Some crack growth has occurred since the overload condition was removed. The equilibrium plastic zone at σ_L is contained by the overload (σ_H) plastic zone.

b) The FDL model calculates the value of σ'_H whose application would produce the same separation of the plastic zone boundaries.

$$\frac{da}{dN} = C(\Delta K_{eff})^m = C_r C(\Delta K)^m$$

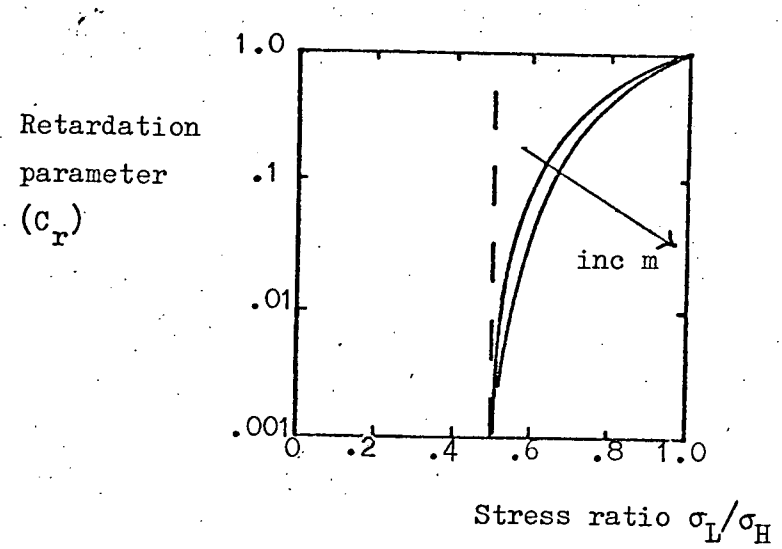

c) Predicted retardation immediately following the removal of the overload conditions. C_r from equation 2.19.

Figure 2.21 FDL crack growth retardation model [103].

CHAPTER 3

EXPERIMENTAL FACILITIES AND PROCEDURES

3.1 Material

Q1(N) is a nickel-chromium-molybdenium, low alloy, structural steel manufactured to British Naval specifications. The material is also commercially available as a pressure vessel grade alloy supplied to ASTM specification A543-65 [104]. The properties of Q1(N) are derived from a quench and temper heat treatment. For 35mm plate of the type used in this work the treatment specified by the ASTM standard is:

1) Quench by water spray or immersion from the fully austenitic condition, (temperature not specified).

2) Temper for a minimum of 1.5 hours at a temperature in excess of 593°C.

Treated correctly the as quenched microstructure should comprise a minimum of 80% martensite at the plate mid thickness [105]. Q1(N) is subjected to the following additional processes:

1) The liquid metal is vacuum degassed prior to casting.

2) The plates are "cross rolled" to limit mechanical anisotropy.

3) Each "as rolled" plate is subjected to a full ultrasonic inspection.

All the material used in this work has been taken from a single plate held by NCRE at Rosyth. The material was manufactured by The Conset Iron Company Ltd., the prequench soaking temperature was 930°C, tempering was conducted at 640°C for 1.5 hours. The chemical

composition, as determined by the manufacturers, is given in Table 3.1; the ASTM specification is given for comparison. Basic mechanical properties have been determined by NCRE. Their results are given in Table 3.2 and Figure 3.2.

It is seen from Table 3.1 that the molybdenum level of the plate is significantly below the specified level. This may account for the slightly low ultimate strength reported, as molybdenum not only increases hardenability during quenching but also reduces the rate of softening during tempering. However, comparison of the reported strengths with those specified by ASTM is complicated by the different test piece geometries used. The results indicate a minimum of anisotropy in Q1 though it should be noted that only two of the three principal directions were investigated. The monotonic load/extension and the cyclic stress/strain characteristics of the material, as determined by the author, are presented in Chapter 4. Representative microstructures are included in Chapter 5.

3.2 Fatigue Test Facility

The only fatigue test facility available to the author was a converted 600kN Mohr and Frederhauf universal test frame. In its original state this equipment was hydraulically operated but was not equipped for fatigue loading. The necessary cyclic capability was achieved by replacement of the original low capacity hydraulic pump with a 52kW unit capable of delivering 90 litres per minute at a pressure of $3.4 MNm^{-2}$. A closed loop servo system was created by the installation of a Moog spool valve controlled by electronics purchased from RDP Ltd. This conversion had been planned and the necessary equipment purchased prior to the author's arrival in Edinburgh; the author was required to complete the modifications and commission the

various units. A general view of the test frame is shown in Figure 3.3, details of the hydraulic circuit are given in Figure 3.4. The problems encountered on the hydraulic side were typical of a new installation of this type. Considerable attention had to be given to the details of pipe work, noise control and operational safety. The circuit shown in Figure 3.4 has performed satisfactorily for the last two years.

The control electronics were purchased as an integrated system comprising:

Signal Generator: An 8 block digital programmer which could also be used for simple constant amplitude tests.

Transducer Amplifiers: 3 channel facility.

Servo Amplifier: Compatible with the transducer amplifiers for closed loop drive of the Moog spool valve.

Monitoring Equipment: Digital voltmeter, switching units, input/output facilities and internal calibration system.

The control system is shown schematically in Figure 3.5. The Department did not have a load cell capable of withstanding the fatigue loading conditions that were to be used. For this reason the load feed-back signal for the servo amplifier was obtained from measurements of the oil pressure in the hydraulic actuator. This is the same system as that used in the original Mohr and Federhauf equipment. A pressure transducer was installed on the main body of the jack, its distance from the Moog was minimised. Static load calibrations were performed against the original Mohr and Frederhauf load display which was calibrated to $\pm \frac{1}{2}\%$ by the makers' agents at the start of the project. The RDP digital load readout was shown to be accurately linear when checked against the Mohr and Frederhauf display. Thus under static conditions an accuracy of 1% on load valves could be assumed.

Dynamic loading conditions highlighted the overriding problem of the system. The Mohr and Frederhauf actuator was only actively driven in one direction, no reversed load capability existed. The consequence of this was that all test sequences had to be either entirely compressive or entirely tensile, furthermore the jack had to be returned to its "zero position" under the combined influences of its own weight and the load borne by the sample. An uneven effect resulted in which the upward, "driven", stroke of the jack was potentially very much faster than the return stroke. Thus testing frequencies were not limited by the load control "loop", but by the slow return of the jack. In practice it was found that testing of the CKS sample was limited to 2Hz.

The original design of the Mohr and Frederhauf hydraulic jack posed certain safety problems. The actuator piston had no physical overtravel "stop"; only a mechanically operated switch, linked to the hydraulic pump, prevented the piston from rising out of its bore. Under these circumstances a Moog valve malfunction could have resulted in a disastrous separation of the piston from the test frame. For this reason a 19mm ($\frac{3}{4}$inch) bore solenoid valve was installed in the hydraulic pressure line to provide a second "cut off" in case of emergency. The overall safety sequence therefore was a follows:

1) Electronic "overtravel" detector. Set to limit cross head travel between 0 and 100mm.
   Action: closed Moog valve;
   switched off hydraulic pump.

2) Overtravel switch (mechanical). Activated at crosshead displacements of 300mm.
   Action: closed Moog valve;
   closed solenoid valve;
   switched off hydraulic pump.

Additional safety circuits were incorporated to close down the pump in the event of:

1) Overheating of the hydraulic oil;

2) A pipe burst condition resulting in pressure loss;

3) Insufficient oil being present in the reservoir.

The numerous malfunctions of the equipment that have been experienced during its three years service have been satisfactorily contained by the above safety circuits.

3.3 Fatigue Sample Selection

The factors to be considered in the selection of a fatigue sample could conveniently be divided into two categories. The fundamental considerations were independent of the nature of the test facility to be used, but the factors influencing the final sample selection were principally influenced by the physical constraints imposed by the Mohr and Frederhauf test frame. The most important factors are listed below.

Test Facility Independent

1) It was required to measure crack propagation rates independently of initiation and specimen life.

2) A fracture mechanics analysis for the crack tip stress intensity conditions was required.

3) A specimen was required in which the crack would propagate under pure mode I opening conditions. It was particularly intended to avoid inclined fractures opening under mixed mode conditions.

4) In order to maximise the rate of data collection it was desired to minimise the growth increment over which da/dN could be determined. The sample was required to permit accurate crack length measurement, preferably by an automated device.

5) It was desired to test full thickness plate material so as to accommodate any variations in properties that might exist across the short transverse section.

Test Facility Dependent

6) The unidirectional hydraulic actuator imposed tension/tension or compression/compression conditions. No reversed load capability existed.

7) The sample was required to support the maximum possible load at high crack lengths so as to optimise the "return" force on the actuator. Low "return" forces would have resulted in impractically low test frequencies.

8) The Mohr and Frederhauf tension facility was at ground level, the compressive facility used the upper side of the cross head 2m above ground level. Operator access to the compressive facility was therefore unsatisfactory.

9) Wherever the sample was positioned good access to the crack was required for optical measurement of the crack length.

10) The automated crack monitoring system adopted influenced the possible sample dimensions.

11) Samples could not be lifted into position by crane. Gross weight had therefore to be limited.

A "Compact Fracture Toughness Specimen", (CKS), was considered to provide the best compromise to the many requirements listed above. Figure 3.6 details the dimensions which were finally specified. Referring to the figure the thickness, B, was limited by the nominal plate thickness to 35mm. It was anticipated that this thickness would not be sufficient to provide true "plain strain" conditions according to the criterion embodied in the Proposed British Standard on Fracture Toughness Testing [106]. For practical reasons it was

decided that, provided a flat, "plane strain" type fracture prevailed during testing, this thickness limit could be accepted. Preliminary tests indicated that this condition was satisfied over a range of crack growth rates.

Thickness apart, the CKS sample requires the specification of one dimension only, the remainder are related on a proportional basis. The standard test piece dimensions are given in the British Standard Proposal [106]. The basic dimension is the net width, (W), which was fixed at 254mm (10in). Walker and May [107] have published a stress intensity analysis for this sample which is applicable to cracks whose lengths are between $a/W = 0.3$ and $a/W = 0.7$. A 254mm sample therefore contains a 101mm (4in) length over which the crack tip stress intensity may be evaluated. To take maximum advantage of this region the machined notch was limited to 127mm (5in). Fatigue precracking then extended the crack 12.7mm to the point at which $a/W = 0.3$. The precracking routine is separately described in section 3.5.2.

An automated, ultrasonic fatigue crack growth monitor was developed for use with the CKS sample. The details of this device are given in Appendix 1. Specially designed loading links were required to accommodate the specimen and the crack monitor installation in the Mohr and Frederhauf test frame. The design of these items is considered in the next section.

3.4 Specimen Loading Configuration

It is recommended that rigid one piece yokes, pinjointed to the specimen, be used for fracture toughness testing of CKS samples [106]. In this work the large specimen size and the "head room" required by the crack monitor installation precluded the fabrication

of one piece yokes. A double pinjointed configuration was adopted both above and below the specimen. This system had the advantages of easy fabrication, flexibility for assembly and dismantling, and easy specimen alignment during testing. The details of the link system are shown in Figure 3.7. The individual components were machined in the departmental workshop from mild steel plate supplied by NCRE. The four "pins" were commercially case hardened to increase their wear resistance. The whole loading system was required to survive severe fatigue conditions, an attempt was therefore made at the design stage to limit nominal stresses to 77 MNm^{-2} (5t.s.i) at machine loads of 400 kN (40 tons). The dimensions of the Mohr and Frederhauf cross head prevented the topmost member (A in Figure 3.7) satisfying this specification, its nominal peak stress was 168MNm^{-2} (11 t.s.i.) at the same machine load. In retrospect it can be stated that maximum fatigue loads have not exceeded the design limit of 400kN and that there is no apparent fatigue damage of the loading system after approximately 1500 hours of testing.

Considerable care was taken to ensure the correct alignment of the sample relative to the loading links. Spherical seatings were provided both above and below the sample. The bearing surfaces were kept well lubricated to optimise the self aligning properties of the configuration. The alignment of samples was repeatedly checked during testing. Under fatigue loading conditions the effects of pin friction are difficult to predict. Pook [108] has shown that the effect can significantly influence the crack tip stress intensity for single edge notch fracture toughness samples. The author has performed a similar analysis for the CKS sample used in this work. The details are presented in Appendix II and the implications regarding the accuracy of the applied stress intensity are discussed in section 3.5.3.

3.5 Procedure for Crack Growth Rate Determinations

3.5.1 Specimen preparation

CKS specimens machined to the dimensions shown in Figure 3.6 were manufactured by NCRE. A ground surface finish had been specified for all faces; the as received quality showed considerable variation but was generally satisfactory. Particular attention was paid to the sample's top and bottom surfaces as variations in quality could influence the performance of the ultrasonic crack monitor. If the finish on these faces was unsatisfactory they were lightly surface ground. Final preparation consisted of boring and tapping the top surface to receive the crack monitor. Twenty-two, 6mm deep, holes were tapped to 4BA size. Also, for samples on which COD measurements were to be performed, provision was made to mount a standard 25mm Instron extensometer across the end of the notch. The extensometer was mounted on two small plinths, each attached to the sample by a pair of 6BA bolts. The arrangement is shown in Figure 3.8.

Provision for optical measurement of the crack length was made by polishing one, and in some cases both, faces of the specimen along the line of expected growth. This was done manually using a hand held electric drill fitted with a flexible rubber polishing pad. Progressively finer grades of "Emery" paper were used in the dry state. No significant specimen heating occurred. When all the markings produced by surface grinding at NCRE had been removed, final polishing was performed with diamond lapping compounds. The final surface finish, achieved with 1 μm diamond compound, gave excellent visibility of the crack tip. The polished faces were scribed with reference lines using a vernier height gauge on a precision table. These lines, spaced at 10mm intervals, provided reference points from which crack lengths were measured.

Finally, before loading into the test frame, the sample was checked for ultrasonic homogeneity. The crack monitor probe was traversed through its full range whilst the ultrasonic signal was monitored. Of the 15 samples checked it was only necessary to reject one 20mm section of crack path on the grounds of ultrasonic inhomogeneity. On completion of the ultrasonic check the sample was loaded into the Mohr and Frederhauf test frame.

3.5.2 Precracking

The loading of a new sample provided a convenient occassion to check electronic calibrations in the RDP control equipment. A full calibration check of the individual modules was conducted according to the manufacturer's instructions. On the whole stability was excellent and very little adjustment was required. The prepared sample with the crack monitor attached was first loaded into the upper support links only. In this condition the cross head was displaced and an accurate load zero set. The lower loading pin was then engaged and the sample was manually aligned in preparation for fatigue precracking.

The CKS specimen dimensions were such that 12.7mm (0.5ins) of precrack were required before the crack tip stress intensity analysis was applicable. It was found convenient to use an overnight precracking routine in which the load was reduced after successful initiation. The loading conditions are detailed in Table 3.3. The crack monitor was not active during precracking, load shedding was therefore not employed. The nominal stress intensity conditions at completion were $\overline{K} = 66.5 MNm^{-3/2}$, $\Delta K = 26.6 MNm^{-3/2}$. The precracking routine detailed in Table 3.3 was found to be satisfactorily reproducible, the crack length after 18 hours being 14mm $\pm$ 1mm.

3.5.3 Load control considerations

All crack growth tests were conducted under conditions of stress intensity control. In a CKS type specimen the crack tip stress intensity increases as the crack extends. For the sample used in this work the load requirement is given by [107]:

$$P = \frac{K_I \, BW^{\frac{1}{2}}}{Y} \tag{3.1}$$

where the compliance function Y is given by

$$Y = 29.6 \left(\frac{a}{W}\right)^{1/2} - 185.5 \left(\frac{a}{W}\right)^{3/2} + 655.7 \left(\frac{a}{W}\right)^{5/2} - 1017 \left(\frac{a}{W}\right)^{7/2} + 638.9 \left(\frac{a}{W}\right)^{9/2} \tag{3.2}$$

when $$0.3 \leqslant \frac{a}{W} \leqslant 0.7 . \tag{3.3}$$

To maintain constant stress intensity conditions at the tip of a growing crack in such a sample requires continual reduction of the applied load level. It was considered unsatisfactory to perform this task manually as it would have entailed regular operator intervention. The ultrasonic crack monitor was therefore equipped with a load shedding capability which continually modified the load signal to maintain constant stress intensity conditions in accordance with equations 3.1. The means by which this was achieved is described in Appendix 1. This load shedding facility greatly simplified the procedure for setting test loads.

The RDP block programmer was used to provide the load signals for all tests. Eight blocks are available, each with digital facilities for setting:

1) The static load level.
2) The dynamic load range.
3) The test frequency.
4) The number of cycles in each load block.

For constant amplitude tests the individual blocks were set identically and allowed to run sequentially without causing any disturbance to the regularity of the load signal. To achieve a given stress intensity, load levels were set according to equation 3.1 for a crack length of $a/W = 0.3$. Substituting the appropriate value of Y and the specimen dimensions the equation reduces to

$$P = 3.01 \times 10^{-3} . K_I \quad MN \tag{3.4}$$

when K_I is expressed as $MNm^{-3/2}$. Having thus set the block programmer load signal the fatigue crack length was measured optically using a x8 hand held magnifier. The surface crack length could be determined to an accuracy of $\pm$ .05mm. The ultrasonic monitor was allowed to find its equilibrium physical position under the prevailing test conditions and set according to the procedure given in Appendix 1. This process results in the application of the load appropriate to the crack length and the required stress intensity conditions.

The actual load applied to the sample was monitored by means of the hydraulic actuator oil pressure. Readout was provided by a tracking digital voltmeter capable of recording dynamic maxima and minima. Load values were manually recorded and processed using The University's on-line computing facilities. There was initially some uncertainty concerning the validity of using measurements of the oil pressure in the hydraulic actuator to determine dynamic loading conditions. This problem was resolved by observing the COD response of a cracked sample as the test frequency was raised from .1Hz to the normal test frequency of 2Hz. The COD/load relationship remained linear over this range indicating that dynamic effects did not invalidate the assumed equivalence of pressure and load.

It is difficult to place accurate confidence limits on the measured specimen loads. Table 3.4 details the principal sources of error, it is apparent that pin friction effects are the major factor to be considered. The overall accuracy is therefore principally influenced by the operative coefficient of friction. As considerable care was taken to maintain good pin lubrication it is reasonable to suggest that the applied load lies within -4.5% + 1% of the value read from the monitoring equipment.

3.5.4 Measurement of crack growth rates

All crack growth rates reported in Chapter 4 were determined by the ultrasonic crack monitor. The operation of this device is detailed in Appendix 1. A brief outline is included here for the sake of continuity.

The device senses crack extension by normal ultrasonic flaw detection techniques. A mobile probe mounted on top of the sample is advanced with the growing crack to maintain a constant reflected signal intensity. The probe's position is determined to a sensitivity of $\pm$ 12μm by a potentiometer. Experiment has shown that excellent agreement is obtained between probe advance and fatigue crack extension. Output from the position measuring potentiometer was recorded on a Honeywell y/t chart recorder such that 100mm of chart were equivalent to 1.06mm of crack extension. The gradient of the resultant "crack extension/number of fatigue cycles" trace was determined and scaled to yield a crack growth rate value. Appendix 1 should be consulted for further details of the technique.

3.6 Fracture Toughness Tests

The author was advised by NCRE that according to British Standard Proposals [106] valid facture toughness tests could not be made on Q1(N) at room temperature. However it was important to determine the maximum stress intensity appropriate to the planned fatigue tests. For this reason it was decided to perform a series of "non-standard" fracture toughness tests in an attempt to define a critical stress intensity, K_c, for the prevailing conditions. As far as possible the tests were conducted in accordance with the 1968 BISRA "Proposed British Standard for Plane Strain Fracture Toughness Testing" [106]. Sample selection presented the principal problem. The 254mm CKS sample adopted for fatigue testing was suited to fracture toughness determinations but to perform a statistically significant number of tests at a rate of one per sample would have involved excessive consumption of these expensive test pieces. Smaller samples would have been suitable for the tests but could not be considered due to the lack of an alternative precracking facility. It was therefore decided that multiple tests should be performed on a single CKS sample utilising the full stress intensity region analysed by Walker and May [107] in preference to the more restricted recommendation of the BISRA Standard Proposal. The use of a single sample for multiple tests is not "standard" procedure and the author is not familiar with any results determined on this basis. However Brown and Srawley [109] have recognised the possibility of performing multiple tests and indicate that so long as a new fatigue crack is grown between tests the procedure is acceptable.

Instrumentation for these tests was simple. Crack extension was monitored by COD measurements. A 25mm gauge length Instron extensometer was positioned across the machined notch as shown in Figure 3.8. The device was coupled to a transducer amplifier in the RDP

control equipment, this provided a DC output that was compatible with a standard, flat bed x/y plotter. An analogue load output was similarly available. An appropriate load demand signal was provided by a DC voltage ramp generator whose rise time could be controlled to give the specified rate of stress intensity increase required by the BISRA Standard Proposal. Crack lengths were optically measured to an accuracy of $\pm$ 0.05mm before each test. K_c values were determined from the stress intensity/COD record by the use of a 4% offset construction. The full range of post test checks required by the BISRA Standard Proposal were applied, the details of these are reported with the results in Chapter 4.

3.7 Determination of Static and Cyclic Stress/Strain Properties

Both the monotonic and cyclic stress/strain properties of Q1(N) were determined using a 250kN Instron test facility. The instrument was of the screw driven variety. Both kinds of test were performed on identical dumb-bell type specimens. This specimen and its loading grips had been specifically designed for cyclic stress/strain measurements by Dr. G.M.C. Lee. Its dimensions are given in Figure 3.9. The Instron test system is fully integrated, requiring no extra instrumentation for standard tensile tests. The cyclic loading capabilities of the instrument had been modified to provide analogue load and strain outputs. Cyclic stress strain histories could therefore be directly recorded on an x/y plotter. Cyclic properties were determined using an incremental step test of the type proposed by Raske and Morrow [110]*. The Instron control system had been modified to provide automatic load reversal at preset strain limits. However it was necessary to manually reset both limits after each cycle; a very low strain rate was therefore imposed on the tests. It should be noted that the tests were conducted on samples comprising

* The strain sequence used is detailed in Figure 3.10.

a small proportion of the Q1(N) plate cross section. Both the monotonic and cyclic properties reported in sections 4.1.2 and 4.1.3 may therefore differ from the bulk properties of the full thickness plate material used in the fatigue tests.

3.8 Metallography and Fractography

3.8.1 Metallography

Only a small amount of metallography has been undertaken in connection with the crack propagation studies reported in this thesis. Standard preparation facilities comprising mechanical grinding and polishing weels were available in The Department. A Zies "Photomicroscope" has been used. This instrument has a 35mm film camera coupled with an automatic exposure metre. A solution of nitric acid in glycerol was found to be the most satisfactory etch for revealing the microstructure of Q1(N).

Etching solution:	Concentrated nitric acid	4ml
	Glycerol	96ml

3.8.2 Optical fractography

A 35mm "Nikon" camera has been used to record the optical appearance of the fatigue fracture surfaces. The fractographs shown in Chapter 5 were taken using a nominal magnification of x 0.53 on the film, the final size of the prints was obtained by photographic enlargement. The fracture surface relief resulted in the focus being unsatisfactory at magnifications in excess of the above value. Various alternative lighting configurations were investigated, the most satisfactory results were obtained using the system shown in Figure 3.11. This configuration was used for all the optical fractographs presented in Chapter 5.

The large size of the CKS test pieces presented problems regarding the preservation of fracture surfaces. No sufficiently large desiccator facilities were available. This problem was overcome by the use of a surface lacquer to exclude the atmospheric environment. At the completion of testing samples were loaded to cause gross crack opening by failure of the unfatigued ligament. Electrical insulating lacquer, supplied by RS Components Ltd., was applied to both surfaces. The lacquer was readily removed by acetone, or a proprietary solvent, when the surfaces were required for examination.

3.8.3 "Stereoscan" fractography

Limited access was available to a Cambridge Instruments Mark 2A "Stereoscan" scanning electron microscope which was the property of the Institute of Tree Biology. The instrument has recently proved unreliable; an excessive amount of "down time" has been experienced during the available operating periods. This problem has seriously curtailed the scope of the electron fractography undertaken.

Some difficulty was experienced in preparing satisfactory samples for SEM examination. Q1(N) is not readily machined as a consequence of its hardness. The maximum permitted size for specimens was 8mm x 8mm x 4mm high. The preparation procedure was as follows.

1) The cracked samples were yielded to produce gross crack opening. The fracture surfaces were immediately protected with insulating lacquer.

2) A bandsaw was used to separate the two halves of the specimen. One half was retained for optical examination.

3) The fracture surface selected for SEM examination was scribed at 5mm intervals, normal to the direction of crack growth.

4) The 35mm wide fracture surface was divided into three equal "strips" by end milling two channels parallel to the direction of crack growth. (See Figure 3.12) A 6.3mm diameter tool was used to a depth of 4mm.

5) The direction of crack propagation was marked on each area to be examined by placing light centre punch marks adjacent to the relevant scribe lines.

6) A bandsaw was used to separate the fracture surface from the bulk of the sample. The result of this operation is shown in Figure 3.12.

7) The three strips were separated along the milled channels.

8) The areas to be examined were separated from the individual strips by use of a light, hand-held hacksaw.

Considerable care was taken throughout the above procedure to prevent damage occurring to the fracture surface. The small samples obtained were ultrasonically cleaned and examined in the central section well away from the machined boarders. No evidence of physical damage was observed during examination. The results of the scanning electron microscopy are presented in Chapter 5.

Element	ASTM Specification (%)	Q1(N) Plate 5849 (%)
Carbon	0.23 max	0.18
Manganese	0.40 max	0.30
Silicon	0.18-0.37	0.23
Nickel	2.53-3.32	2.44
Chromium	1.44-2.06	1.32
Molybdenum	0.41-0.64	0.35
Phosphorus	0.035 max	0.005
Sulphur	0.04 max	0.01
Titanium		0.007
Vanadium	0.03 max	0.01
Copper		0.06
Iron	Remainder	-
Arsenic		0.017
Antimony		0.002
Lead		0.0005
Tin		0.008
Cobalt		0.013
Aluminium		0.022
Nitrogen		0.007

Table 3.1 Chemical composition. ASTM specification A543-65 and Q1(N) plate 5849.

(Q1(N) analysis by Conset Iron Co. Ltd.)

Sample Origin[1]	Sample Orientation[1]	0.2% Proof Strength MNm^{-2}	U.T.S. MNm^{-2}	Elongation %
1	Longitudinal	605	715	28
2	"	609	723	30
3	"	619	735	29
1	Transverse	615	710	26
2	"	618	727	27
3	"	626	735	27
ASTM Specification[2]		586	723-862	16 min

Notes: 1) See Figure 3.1 for details of sampling locations and orientations.

2) NCRE tests were performed on 14.2mm diameter, round specimens which had a gauge length of 50.8mm. ASTM specification requires tests to be conducted on full thickness rectangular specimens; a 50.8mm gauge length is specified.

Table 3.2 Mechanical properties of Q1(N) Plate 5849 and the requirements of ASTM specification A543-65.

(Tests performed by NCRE)

Time hrs.	Static Load kN	Dynamic Load range kN	Crack length (l) mm
0	200	110	0
4	"	"	1.7
6	"	"	8.0
6	"	80	8.0
18	"	"	14.0

Notes: 1) The above represents the normal procedure, slight variations in detail were affected to suit circumstances.

2) Crack lenghts shown are typical only.

3) Test frequency = 2Hz. Total cycles in 18hrs = 129,600.

4) Stress intensity conditions at a/W = 0.3, l = 12.7 mm: $\overline{K} = 66.5 MNm^{-3/2}$, $\triangle K = 26.6 MNm^{-3/2}$.

Table 3.3 CKS specimen precracking routine.

Source of Error	Magnitude %
1) Static calibration of Mohr and Frederhauf system[1]	± 0.5
2) Static calibration of pressure transducer and RDP Electronics from Mohr and Frederhauf system	± 0.5
3) Loading configuration	
a) Pin friction (μ=0.2)[2]	+ 0 - 4
b) Specimen alignment[3]	± 0
4) Consequences of dynamic operation	
a) Transducer "noise"[4]	± 0
b) Transducer signal[5]	± 0.5

Notes: 1) Performed by makers.

2+3) See Appendix II.

4) Noise became significant when maximum and minimum load values were read. An allowance was made for this effect during analysis, the net effect is therefore insignificant.

5) Deduced from COD/load relationship as frequency increased from "near static" conditions (0.1Hz) to test frequency (2Hz).

Table 3.4 Potential errors in load determinations.

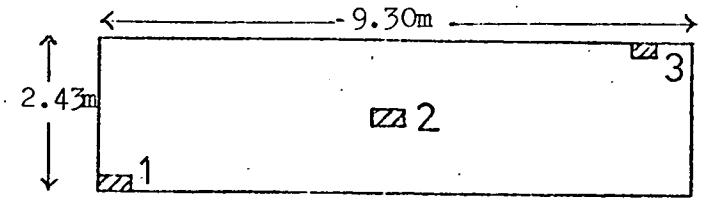

a) Q1(N), Plate 5849. Nominal thickness: 38mm. Location of sampling sites for mechanical tests reported in Table 3.2.

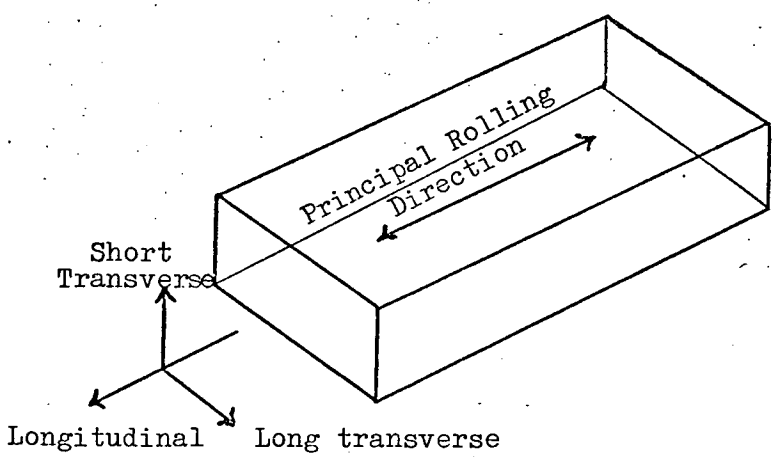

b) Standard designation of plate orientations.

Figure 3.1 Sampling location and orientation of NCRE mechanical test specimens.

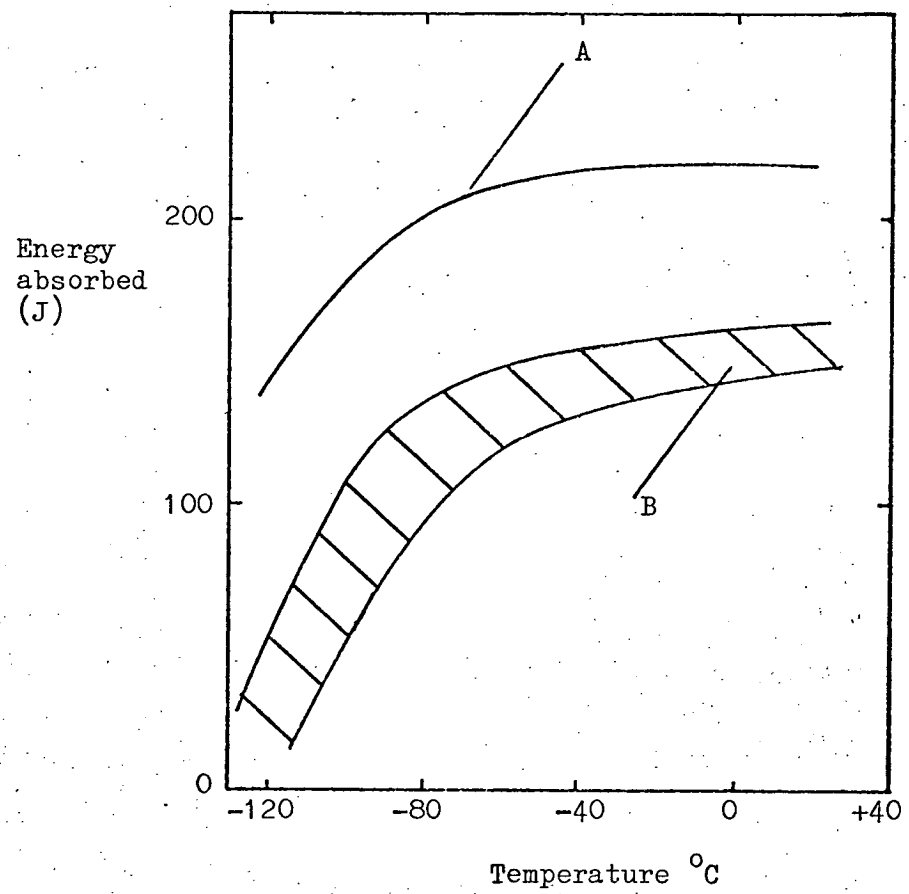

A Longitudinal sample from location 1.

B Long transverse samples. One sample from each test location. All results lie within the scatter band shown.

All tests: zero fracture surface crystallinity above -60°C.

Figure 3.2 Q1(N), Plate 5849.

Charpy impact test results reported by NCRE.

(For test locations and orientations see Figure 3.1).

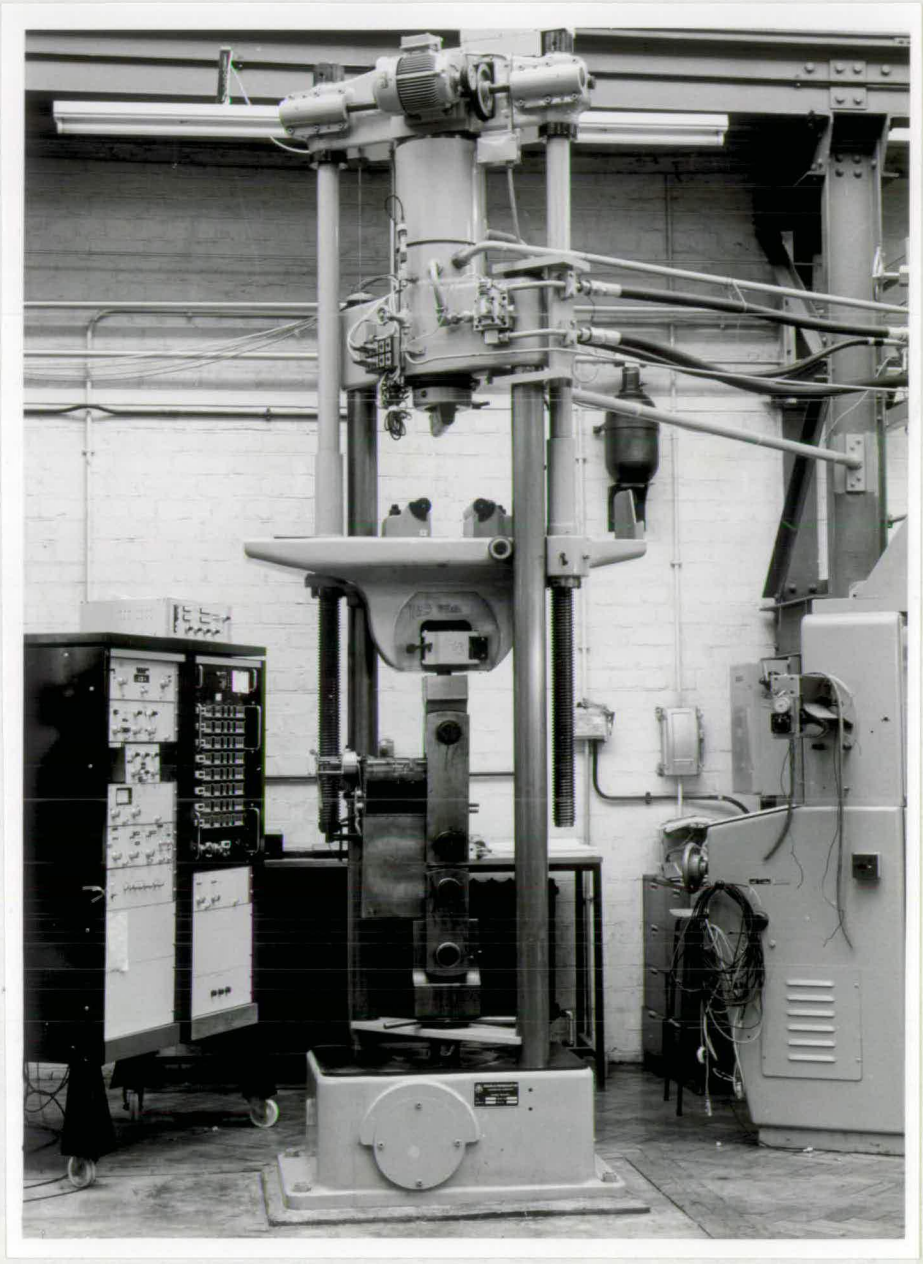

Figure 3.3 General view of fatigue test installation with CKS sample and crack monitor installed.

Magnification: x1/22

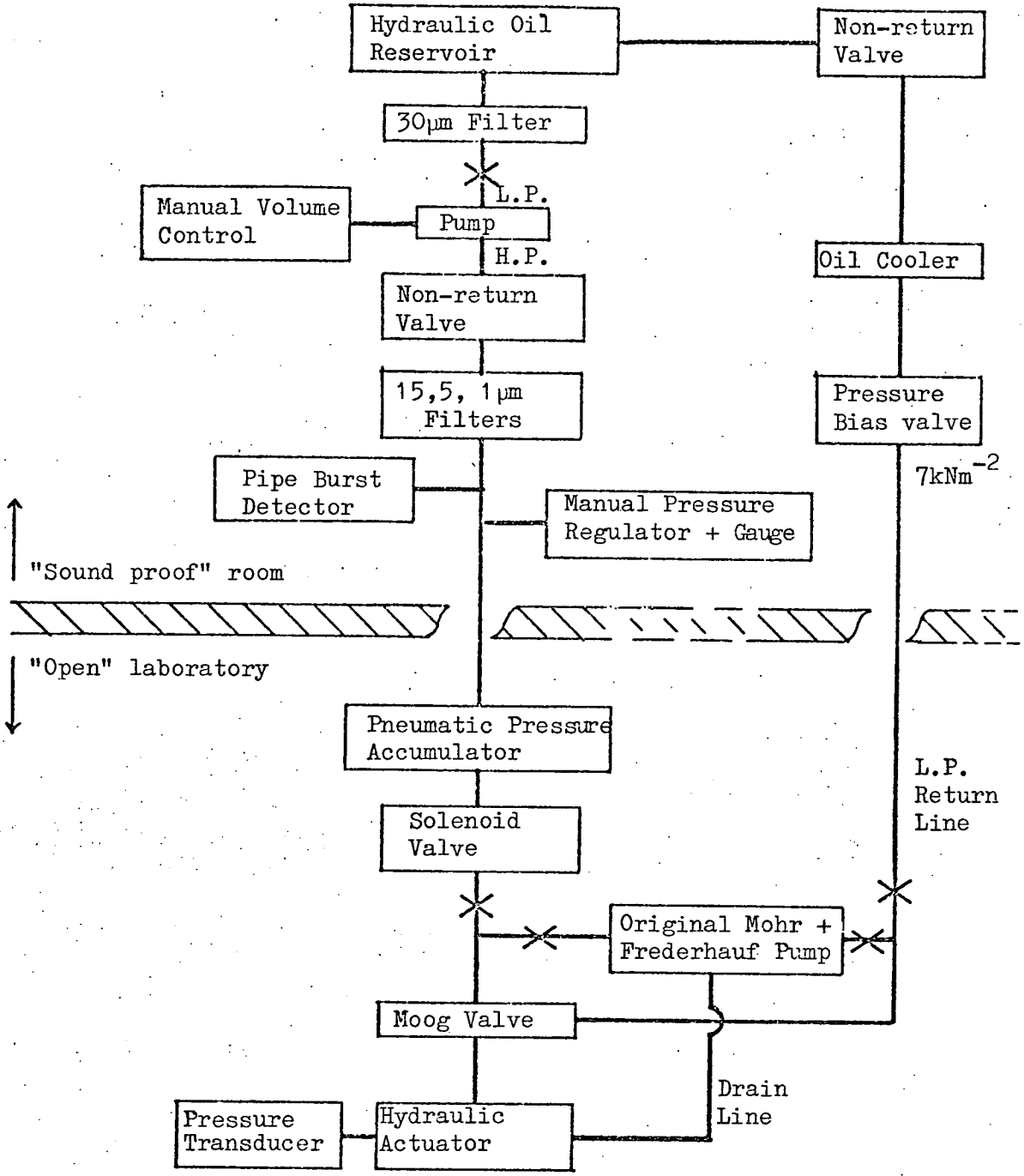

Notes: 1) ✕ Denotes manual on/off valve

2) Pressure bias valve in return line set to maintain a pressure of $7kNm^{-2}$ in the line as a noise prevention measure.

3) L.P. = low pressure, H.P. = high pressure.

Figure 3.4 Hydraulic circuit for fatigue test facility.

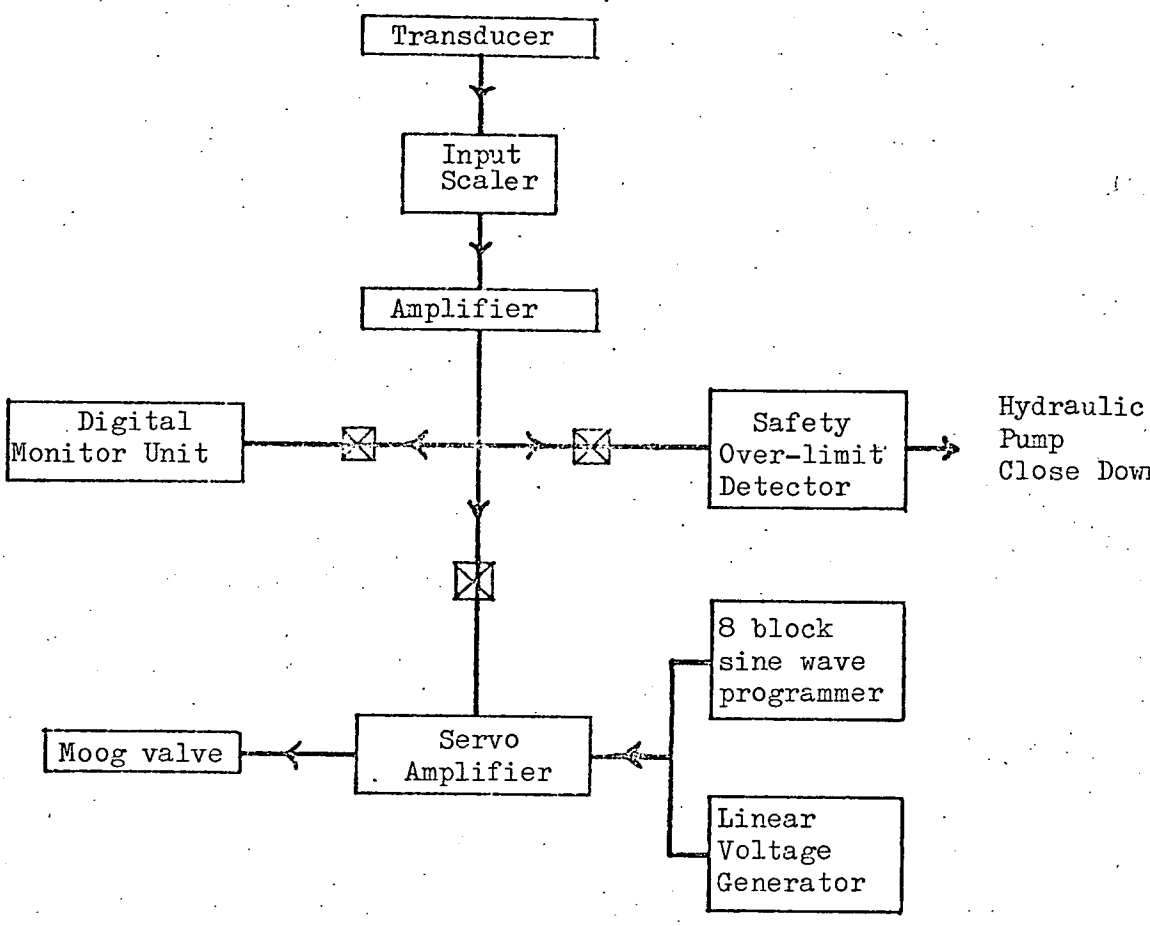

Notes: 1) Three separate transducer amplifier channels were available in practice. Only a single channel is shown for clarity.

2) ⊠ Denotes amplifier output selection capability. Inputs to control modules could be taken from any of the three transducer amplifiers.

Figure 3.5 Control system for fatigue test facility.

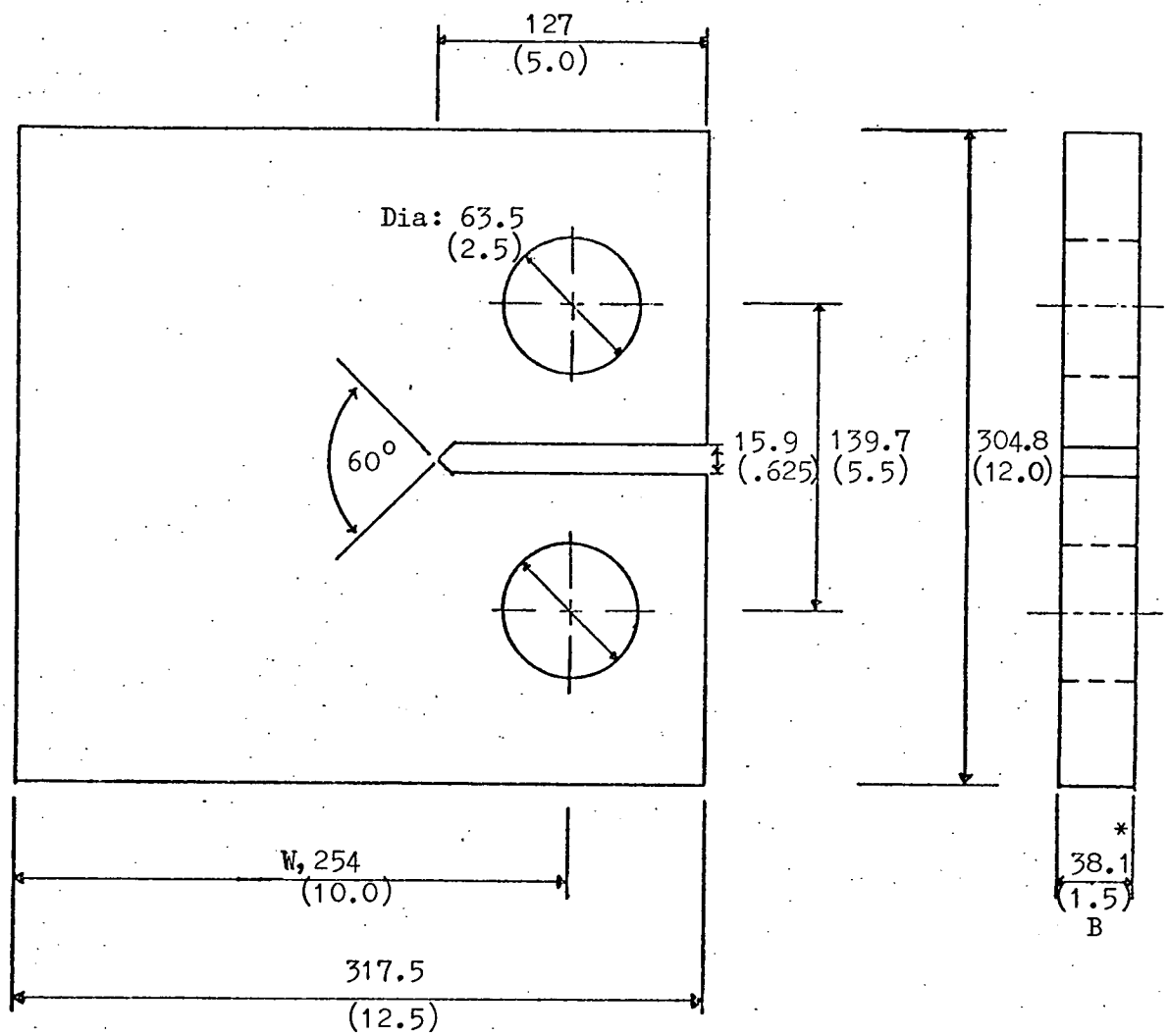

Dimensions in millimetres and (inches).

*Nominal plate thickness, in practice after machining B ≃ 35mm.

Figure 3.6 Dimensions of CKS test piece.

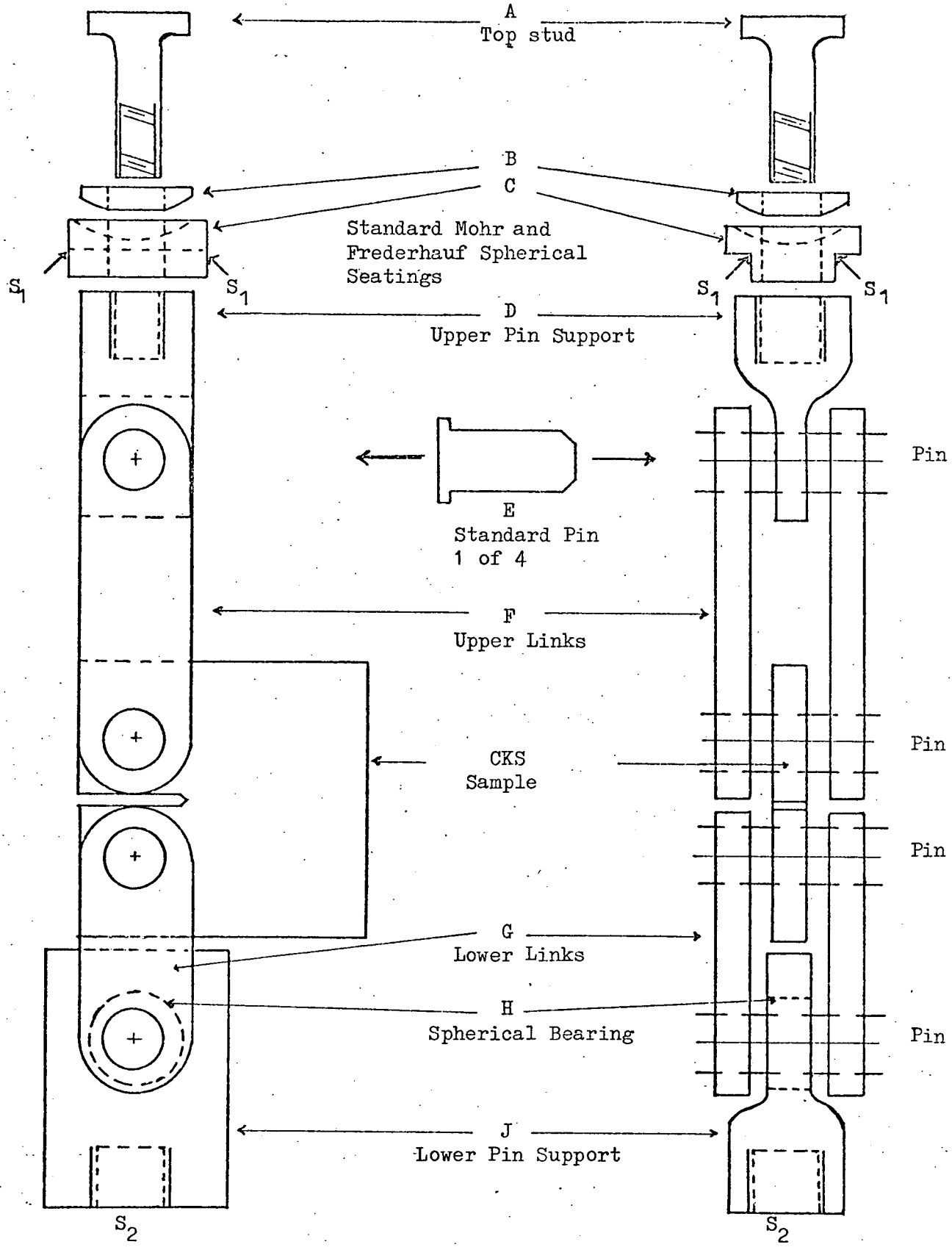

Figure 3.7 Loading configuration for CKS sample scale 1/6.3

The top stud "A" was threaded into "D" after passing through "B" and "C". The assembly is supported at S_1 by the test frame crosshead and at S_2 by a threaded stud in the base of the frame.

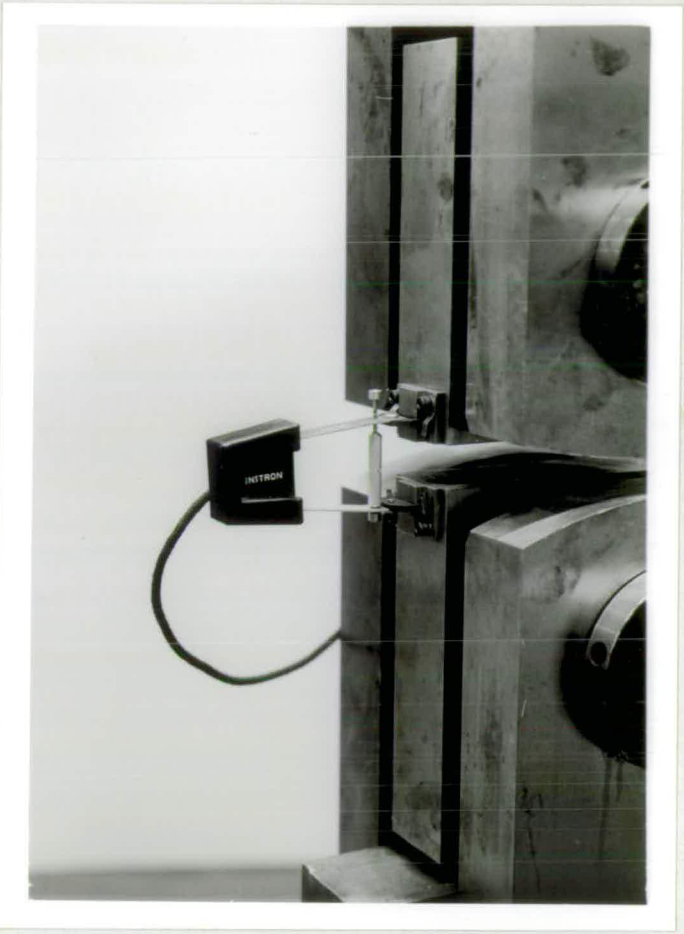

Figure 3.8 Location of "Instron" extensometer for COD measurements.

Magnification: x1/3

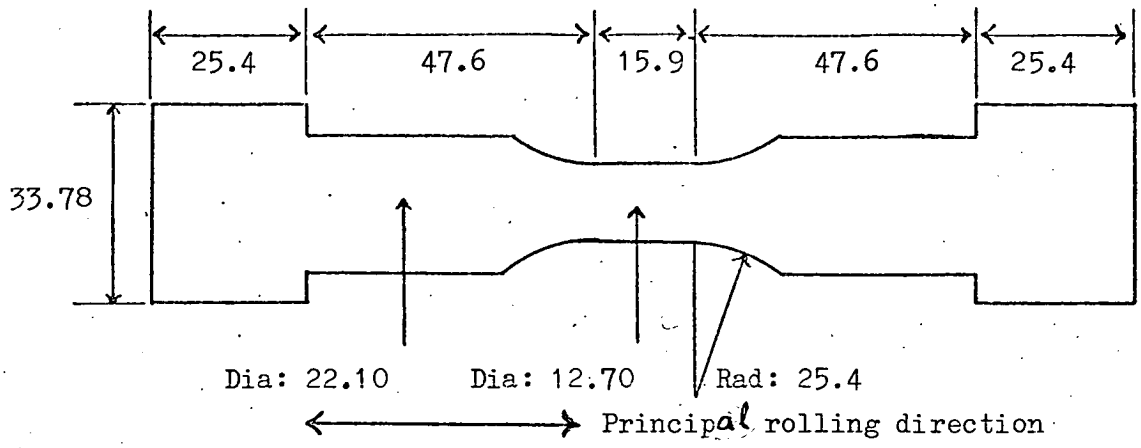

Figure 3.9 Sample for cyclic stress/strain tests.
All dimensions in mm.

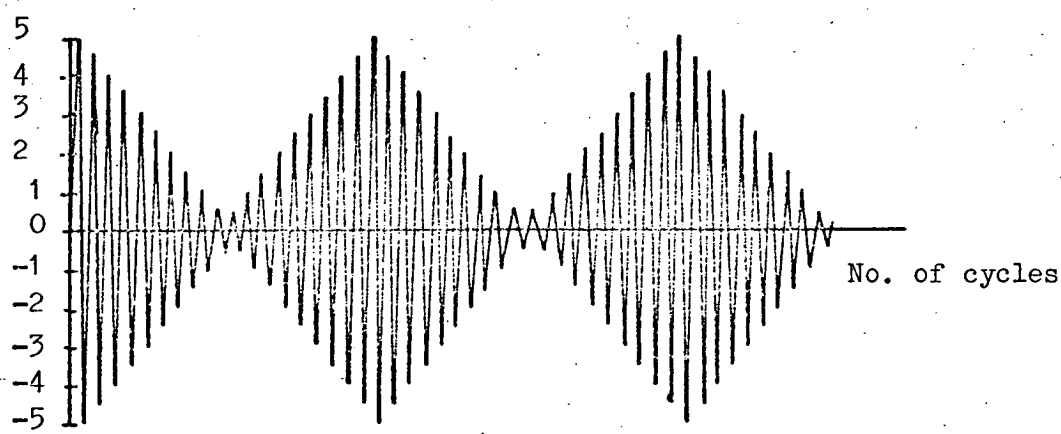

Strain rate : 0.166% per second

"Step" increment: 0.5% strain

Figure 3.10 Strain sequence for incremental step test.

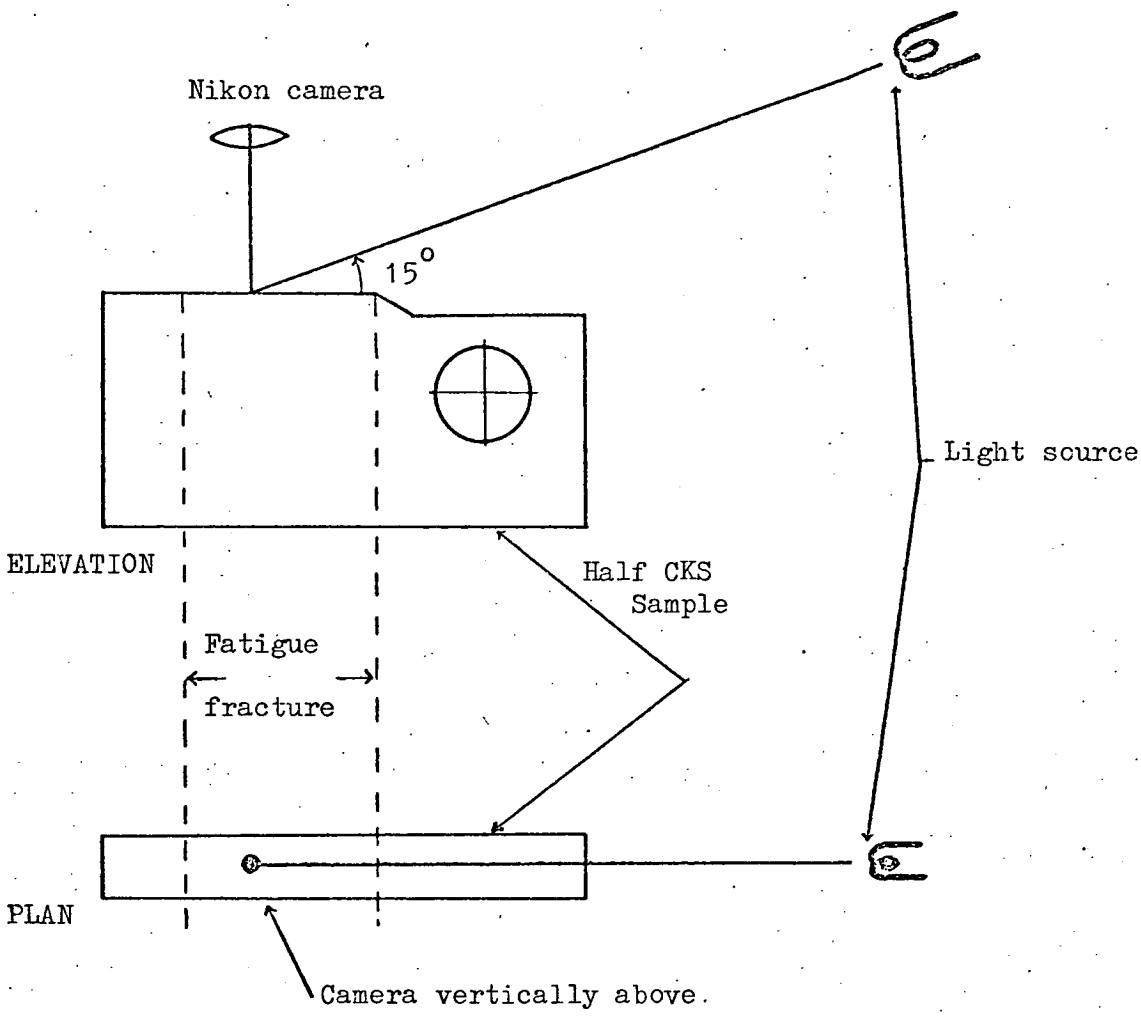

Figure 3.11 Illumination used for macro-fractography.

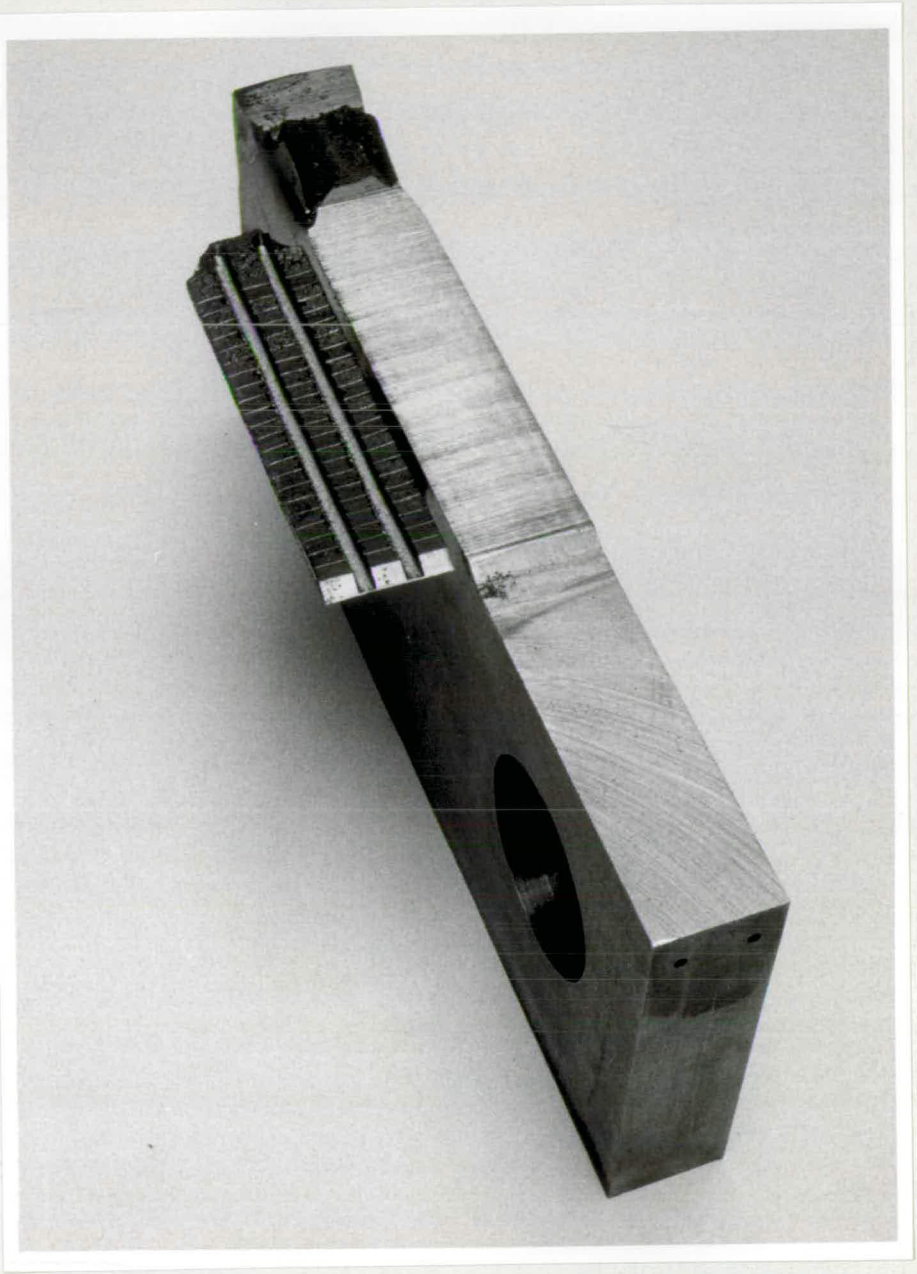

Figure 3.12 Preparation of fracture surface for SEM fractography. The full procedure is described in section 3.8.3.

Magnification: x1/2

CHAPTER 4

MECHANICAL TEST RESULTS

4.1 Basic Material Properties

4.1.1 Through thickness hardness traverses

Vickers hardness measurements were made, across the short traverse section of the original plate, on six CKS samples. Preliminary investigations indicated that the burning operation used to prepare the specimen blanks from the "as rolled" plate had created regions of anomolous hardness at the specimen edges. The hardness impressions were therefore made, after suitable preparation, on the machined face of the notch at a distance of approximately 65mm from the front edge. An indentor pressure of 30kg was used; at 250HV the diagonal measurement of the impression was 0.472mm.

The results of the investigation are shown in Figure 4.1. The individual samples showed no significant variation of hardness across the short transverse section. The average hardness values determined for the six samples were: 242, 244, 245, 245, 246 and 252 HV. In each case the scatter about the average was less than $\pm$ 6HV. In addition to revealing the "through thickness" uniformity of individual samples these results also show that there was no gross variation of properties between the different specimens.

4.1.2 Monotonic stress/strain characteristic

Simple tensile tests were performed on three samples of the type shown in Figure 3.9. The results are reported in Table 4.1; Figure 4.2 shows a typical load/extension record. The extremely high elongation values at failure result from the specimen's small gauge length. The average values of both the yield stress and the ultimate tensile strength determined by the author exceed the NCRE measurements (Table 3.2) by nearly 6%. Given the dimensions of the plate from which the different samples were taken this discrepancy is reasonable.

4.1.3 Cyclic stress/strain characteristic

The cyclic stress/strain properties of Q1(N) were determined using an incremental step test as detailed in section 3.7. No significant variation was detected in the cyclic properties of the three samples tested. Using the strain sequence shown in Figure 3.10 three high-low-high blocks were found sufficient to produce a "stabilised" stress/strain response. The broken line in Figure 4.2 shows a typical deformation "loop" obtained by cycling the material between strain limits of $\pm$ 5%; also shown is the locus of the "loop tips" obtained by cycling over smaller strain ranges. The continuous line in the figure shows the monotonic tensile properties of the material. It is apparent that Q1(N) softens under cyclic loading conditions.

4.1.4 Fracture toughness determinations

Eight fracture toughness tests were performed on a single CKS sample of the dimensions shown in Figure 3.6. The test procedure has been detailed in section 3.6. Table 4.2 presents the results.

Figure 4.3 shows three load/COD test records and the 4% offset construction used to determine the critical load values. The records have been reduced to half their original linear size. From the figure it can be seen that at low crack lengths (test 1) the linearity of the "elastic" section is excellent. Furthermore the zero error due to "gauge settling" was minimal. In subsequent tests, at higher crack lengths, the linear portion of the test record was reduced by more severe zero errors and the onset of crack tip yielding at lower load values. However, on the original full size records, there was always a substantial linear range through which the first analytical construction could be placed with confidence. From Table 4.2 it will be seen that the average K_c value determined from six tests was 146 $MNm^{-3/2}$, the scatter about this value was -6.4% to + 8.2%.

The tests were performed as far as possible, according to the proposed British Standard Fracture Toughness Test Method [106]. For a test to be considered satisfactory 13 criteria must be met. The tests reported above failed to satisfy the following requirements of the proposed standard.

1) Multiple tests were performed on a single sample.

2) Tests were conducted outside the narrow a/W range detailed in the proposed standard.

3) The maximum stress intensity during precracking exceeded the 50% K_Q limit by up to 10%.

4) For a valid plane strain fracture toughness determination the specimen thickness is required to exceeed the factor $2.5(\frac{K_Q}{\sigma_{YS}})^2$. For the K_Q values obtained a thickness of 140mm is required, some four times greater than the available plate thickness.

Clearly the tests reported in this section were not able to produce a valid plane strain fracture toughness value for Q1(N). The intention was to obtain a realistic upper limit of stress intensity values, i.e. K_c, for use during fatigue crack propagation tests. The extent to which the concept of "fracture toughness" is applicable to Q1(N) is discussed in Chapter 6.

4.2 Crack Propagation Tests

4.2.1 The influence of mean stress intensity on equilibrium crack propagation rates

The first aim of this work was to determine the equilibrium fatigue crack propagation rates in Q1(N) under simple constant amplitude loading. The limitations of the hydraulic actuator meant that all fatigue tests had to be conducted with a tensile mean stress applied to the sample. It was not clear from the literature how the crack growth rate would be influenced by this requirement. Thus it was decided to investigate the mean stress parameter before determining the equilibrium $da/dN/\Delta K$ characteristic.

The experiments were formulated in consideration of the K_c value reported in the previous section. The initial intention was to limit the peak stress intensity (K_{max}) to 146 $MNm^{-3/2}$, i.e. K_c. Six dynamic stress intensity ranges were selected for investigation over a range of mean stress intensity values. The results are presented in Figure 4.4. Early results indicated that there was no significant increase in crack growth rate as K_{max} approached K_c. For this reason the limit on K_{max} was relaxed and tests performed at both maximum and mean stress intensities in excess of K_c. The hydraulic actuator and the specimen configuration precluded compressive loading, furthermore in order to maintain alignment of the pin-loaded

sample a minimum load of 10kN was required. Thus the minimum stress intensity (K_{min}) attainable was determined by the prevailing crack length, as at constant load

$$K \propto f(a) . \qquad (4.1)$$

Figure 4.4 indicates that crack growth rates in Q1(N) remain constant over a wide range of tensile mean stress intensity. The practical restrictions of the loading system prevented extension of the experiments to lower mean stresses. No evidence of accelerated growth rates was obtained as either K_{max} or $\overline{K}$ approached K_c.

4.2.2 Equilibrium, constant amplitude, crack growth rates

The insensitivity of crack rates to the applied mean stress intensity, demonstrated in the previous section, makes the presentation of equilibrium growth rate data both meaningful and simple. Figure 4.5 presents constant amplitude crack growth rate data collected from several samples during general testing. The tests were all conducted at a mean stress intensity of 100 $MNm^{-3/2}$. Also shown in Figure 4.5 are crack rates deduced from the investigation of mean stress intensity reported in the previous section. For each value of ΔK investigated an average growth rate has been determined from the linear section of the $da/dN/\overline{K}$ characteristic presented in Figure 4.4. There is seen to be excellent agreement between these values and those obtained from the individual tests conducted at $\overline{K} = 100\ MNm^{-3/2}$.

The data line drawn in Figure 4.5 was determined by a least squares curve fitting procedure. A third order polynomial was found to best fit the experimental results. The polynomial provided a convenient means of "storing" the equilibrium growth rate data for use when predicting damage under complex loading conditions.

If da/dN and ΔK are expressed as μm/cycle and $kNm^{-3/2}$ respectively, the polynomial is:

$$\log\left(\frac{da}{dN}\right) = -150.1 + 88.84\log(\Delta K) - 17.95(\log(\Delta K))^2 + 1.240(\log(\Delta K))^3; \quad (4.2)$$

it is applicable over the range

$$120\ MNm^{-3/2} > \Delta K > 17\ MNm^{-3/2}\ . \quad (4.3)$$

Figure 4.6 compares the data presented in Figure 4.5 with the Q1(N) growth rate scatter band determined by Evans and Taylor [55] at the National Physical Laboratory. These workers also employed CKS type samples loaded under tension/tension conditions. Referring to Figure 3.6 the basic dimensions of their samples were W = 30.5mm and B = 15mm. Despite this considerable difference in specimen size, results from the different sources are in good agreement over most of the ΔK range investigated by the workers at NPL.

4.2.3 The influence of discontinuous changes in mean stress intensity

The work reported in Section 4.2.1 involved discontinuous changes of mean stress intensity between tests. It was apparent that reductions in $\overline{K}$ significantly retarded the subsequent crack growth rate for some period. As changes in mean stress intensity are frequently encountered in complex load sequences it was decided to determine if the associated effects were sufficiently reproducible to

be characterised by experiment. Following an encouraging preliminary investigation tests were performed at three levels of dynamic stress intensity. The load sequence used and the notation adopted are shown in Figure 4.7(a). The tests were conducted as follows.

1) Equilibrium crack growth was established at $\bar{K}$ = 100 $MNm^{-3/2}$ and the required value of ΔK.

2) The mean stress intensity was reduced to the lower level in a single, discontinuous step. The change in $\bar{K}$ is denoted $\Delta(\bar{K})$.

3) Dynamic loading at the lower level continued until the ultrasonic crack monitor indicated that significant further crack growth had occurred.

4) The mean stress intensity was returned to the original value of 100 $MNm^{-3/2}$. A step change was again involved.

5) Growth following the increase in $\bar{K}$ was monitored; when substantial equilibrium growth had occurred a further test could be performed.

The dynamic stress intensity range was constant throughout the above test sequence.

As previously mentioned a reduction in $\bar{K}$ results in a retarded crack growth rate, however quantification of the effect is made difficult by the change in crack front profile that occurs. In all cases a reduction of the mean stress intensity was observed to result in "tunnelling" of the crack tip. Figure 5.4 shows typical examples of the change in crack front profile. Both ultrasonic and optical determinations of crack length following a reduction in $\bar{K}$ indicated that there was a period of zero growth, ultrasonic measurements showed that the crack then started tunnelling at the specimen mid-thickness

whilst no growth was detectable at the surface. On returning the mean stress intensity to the high level rapid growth was observed at the specimen surface whilst no significant acceleration was detected by the ultrasonic crack monitor. From the fracture surfaces (Figures 5.4(a) and (b)) it was apparent that the crack front rapidly returned to its original equilibrium configuration by failure of the unfractured cutaneous ligaments. The different crack front profiles observed during a high-low-high mean stress intensity sequence are shown schematically in Figure 4.8. It is apparent that during the tunnelling phase at the low $\overline{K}$ value it is the crack length at the specimen mid-thickness that controls the crack front position on return to the higher value of $\overline{K}$. In recognition of this fact ultrasonic measurements of crack front position were used to quantify the growth delay associated with a reduction of $\overline{K}$.

Figure 4.9 shows two ultrasonically determined crack growth records following a reduction in mean stress intensity. A nominal growth delay parameter was obtained by determining the duration of the clearly defined "zero growth interval" that followed the reduction in $\overline{K}$. Although this parameter necessarily represents a gross simplification of the actual crack tip mechanism it was found to be satisfactorily reproducible. Figure 4.10 presents the ultrasonically determined delay intervals for three different dynamic stress intensity ranges. The same data is replotted in Figure 4.11 using a logarithmic scale for the delay parameter. It is apparent that for each value of ΔK the data points approximate to a straight line of the form:

$$\log N_d = A + B[\Delta(\overline{K})] \quad . \qquad (4.4)$$

The effect of increasing $\bar{K}$ after tunnelling at the lower mean stress intensity level has already been described above and presented schematically in Figure 4.8. Optical measurements of crack length indicated that dramatically accelerated growth occurred at the sample surface, however no acceleration of the ultrasonically determined growth was detectable. The qualitative conclusion is that if crack length is measured to the most advanced part of the crack front, increases of $\bar{K}$ do not result in an acceleration of the growth rate. No detailed quantitative measurements of the growth following an increase of $\bar{K}$ have been undertaken.

The tests reported in this section were very demanding in terms of both material and time. The changes in crack front profile required extended periods of "recovery" to regain equilibrium conditions. Furthermore the zero growth periods could last for as long as four hours. Data collection under these condition was extremely slow. The tests were therefore discontinued although it was considered that a more extensive investigation was desirable.

4.2.4 The influence of dynamic overloads

The work reported in previous sections has all been conducted under conditions of constant dynamic stress intensity. The interaction of different dynamic loading conditions is obviously central to the problem of cumulative damage. A systematic investigation of simple interactions was therefore undertaken; as in previous sections the intention was to isolate the effects from the influence of other parameters. A frequency of 2Hz and a mean stress intensity ($\bar{K}$) of 100 $MNm^{-3/2}$ was maintained throughout the sequence of tests. A range of dynamic overload conditions (ΔK_H) were applied to a series of three "base" values of ΔK, (ΔK_L). The general stress intensity

sequence and the notation employed are shown in Figure 4.7(b). Figure 4.12 specifies the different overload conditions investigated at each value of ΔK_L. In this extensive sequence of two level tests the average crack growth rate was determined over an interval involving multiple repetition of the overload sequence. Apart from the different dynamic stress intensity levels the other parameters investigated were n_H and n_L, the number of high and low load cycles applied in any sequence. Values of n_L were continuously varied between 1 and 4000, n_H was restrictied to two values: 1 and 20.

The results of these overload tests are presented in Figures 4.13 - 4.27. In each case the average crack growth rate is plotted against the ratio n_L/n_H, this permits a comparison of the data for $n_H = 1$ and $n_H = 20$. Identical axes have been used in all the figures to permit the crack growth rates under different conditions to be compared by simply "overlaying" the relevant graphs. In each figure the continuous line indicates the growth rate predicted on the basis of a linear damage summation. The summation, which is essentially the linear cumulative growth model described in section 2.7.4, is detailed in Appendix 3. The growth rates used in the summation have been taken from Figure 4.5 by means of the polynomial given as equation 4.2. The damage occurring at $\Delta K_H = 150$ MN m$^{-3/2}$ was so severe that growth rates were not investigated for $n_H = 20$.

Figures 4.13 to 4.27 indicate very good agreement between the measured and predicted growth rates. It is particularly notable that at a given ratio of n_L/n_H there is in general no significant difference in the growth rates determined for $n_H = 1$ and $n_H = 20$.

Crack growth rates were not measured for values of n_L in excess of 4,000. However for all load combinations "equilibrium" growth rates were found to have been re-established at the prevailing ΔK_L level by the end of the largest n_L interval investigated. Thus

subsequent data points, unmeasured in this work, can confidently be expected to tend increasingly toward the predicted values as the dominance of the equilibrium growth becomes more pronounced.

4.2.5 Crack growth under three level block loading conditions

Figure 4.28(a) presents the details of an 8 level block load sequence which was of interest to NCRE. The individual load levels were specified as a percentage of the material's yield stress. From this sequence a three level regime was evolved for use in the first block loading tests. It was hoped that this extreme simplification would facilitate the interpretation of damage accumulation under block loading conditions. The details of the derived three level sequence are given in Figure 4.28(b). Stress levels expressed as a percentage of the material yield stress are not directly applicable to a fatigue cracked, fracture toughness type specimen; a conversion to stress intensity values is necessary. To achieve this an arbitrarily selected dynamic stress intensity value (ΔK_p) was made equivalent to the 100% stress level of both the 3 and the 8 block sequences. The value of ΔK for each block was then scaled according to the original percentage stress values. Tests were made at different values of ΔK_p to determine how the maximum stress intensity range influenced the average crack growth rate.

The three level block loading tests performed fall into two categories: a) those with constant mean stress intensity, b) those with constant K_{min}. In each category three different sequences of load application were investigated; these are shown in Figure 4.29. Figure 4.30 presents the experimentally determined average crack growth rates for each load regime. These are indicated both as: average growth per cycle, and as: gross growth per three blocks. Also shown in the figure is the growth rate predicted according to the

linear summation used in the previous section.

Figure 4.30 shows that under all the three level loading conditions used the rate of crack growth increased progressively as the value of ΔK_p was raised. Furthermore the "shapes" of the individual growth rate characteristics all closely follow the form of the predicted growth function. Under conditions of constant mean stress intensity the rate of growth resulting from the "low-high-low" and "high-low" sequences is consistent at approximately 80% of the predicted growth rate. da/dN determinations for the "low-high" regime rise from this level to 100% of the predicted rate at the highest values of ΔK_p investigated. The available data is insufficient to support a definitive statement of the influence of load sequence on crack growth rates under constant $\overline{K}$ conditions.

The 3 load level tests performed at constant K_{min} reveal a clearer trend. Growth rates for all three load sequences were significantly below the values obtained in the constant $\overline{K}$ tests. Furthermore the "low-high" regime was found to cause fatigue damage at a consistently higher rate than the other two sequences investigated. A load sequence effect does appear to be operative under these conditions, but it is again important to recognise the limited nature of the available data.

4.2.6 Crack growth under eight level block loading conditions

The same process used to convert the three level block sequence from percentage stress to stress intensity values was applied to the 8 level NCRE block regime, (figure 4.28(a)). Only a limited number of tests have been completed using 8 level sequences. Figure 4.31 details the three different load regimes that have been investigated. (The equipment available was not capable of producing an eight level low-high-low sequence.) Figure 4.32 presents the measured crack growth rates,

the scale used is the same as that of Figure 4.30. The continuous line in the figure is the growth rate predicted by linear summation of the equilibrium damage rates, (see Appendix 3).

The results follow the same basic pattern as was observed for the three level tests. The general "shapes" of the measured growth rate/ΔK_p functions, for the different loading conditions, closely follow the form of the predicted characteristic. The crack growth rates measured under constant mean stress intensity conditions were approximately 20% below the predicted values, the discrepancy is increased for tests performed under constant K_{min} conditions. There is insufficient data to determine with confidence if loading sequence is significant under the latter conditions. However, it is noticeable that none of the "low-high" data points fall below the "high-low" points. This trend is consistent with the results of the three level tests.

Chronologically the 8 level tests reported in this section came at the end of the author's fatigue investigations. It was apparent that more extensive 8 level tests required considerable modifications to be made to the "load signal generator/servo amplifier" interface. Such improvements were not consistent with the available time scale. This section should therefore be regarded only as a preliminary investigation, not a full survey, of 8 level test sequences.

Sample	Yield Stress MNm^{-2}	UTS MNm^{-2}	Elongation[1] %
T1	645	750	72
T2	634	749	70
T3	658	768	65
Average	646	756	69

Note 1. 10mm gauge length used.

Table 4.1 Monotonic tensile properties determined by the author using the sample shown in Figure 3.9.

Test No	Crack length at test (a/W)	K_c $MNm^{-3/2}$
1	0.30	[Insufficient load]
2	0.35	
3	0.39	138
4	0.43	154
5	0.51	158
6	0.57	148
7	0.62	141
8	0.66	138

Average: 146 + 12 (8.2%) $MNm^{-3/2}$

- 8 (6.4%)

Table 4.2 Fracture toughness test results.

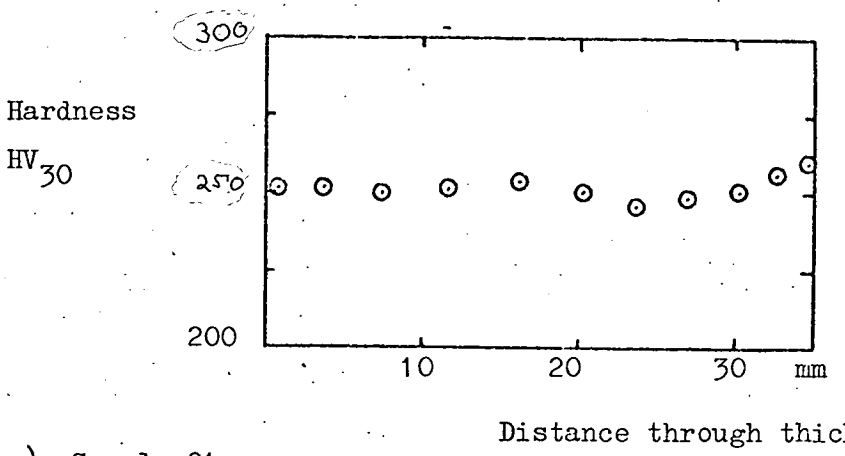

a) Sample 01

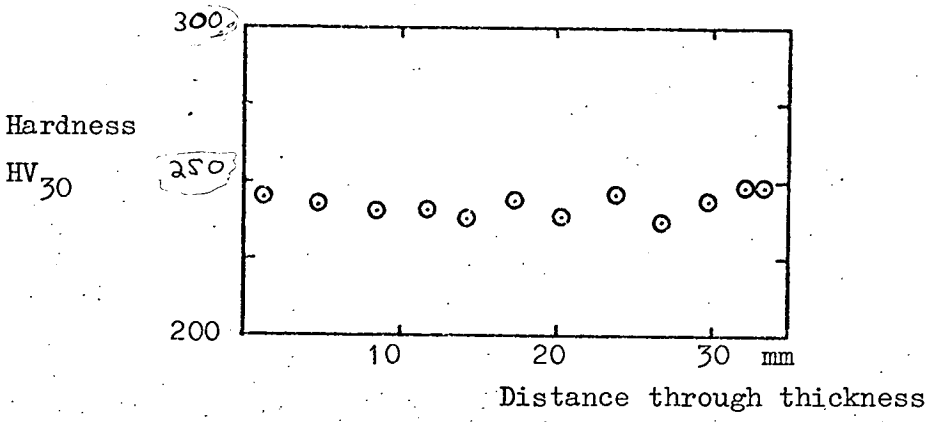

b) Sample 04

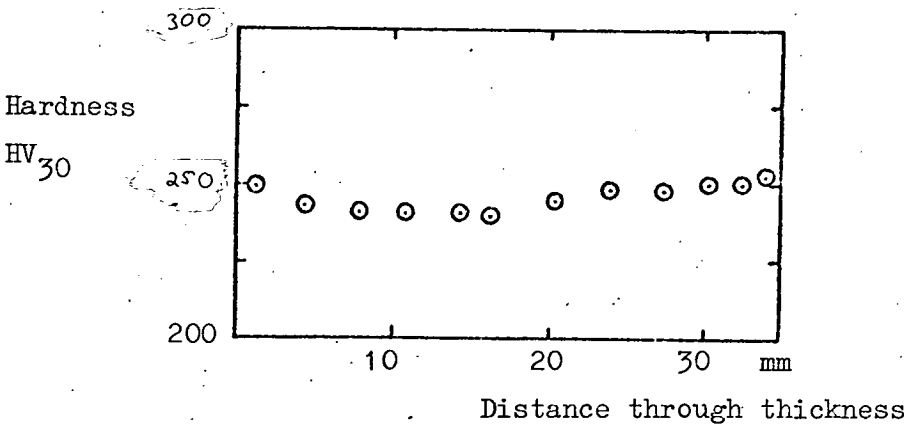

c) Sample 08

Figure 4.1 Hardness determinations across the short transverse section of six CKS samples. See Figure 3.1 for definition of plate orientations.

(Continued on next page)

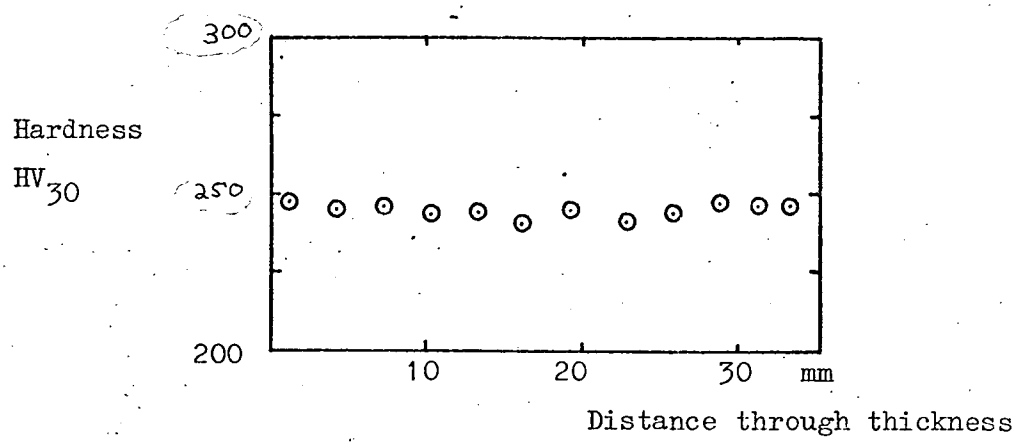

d) Sample 12

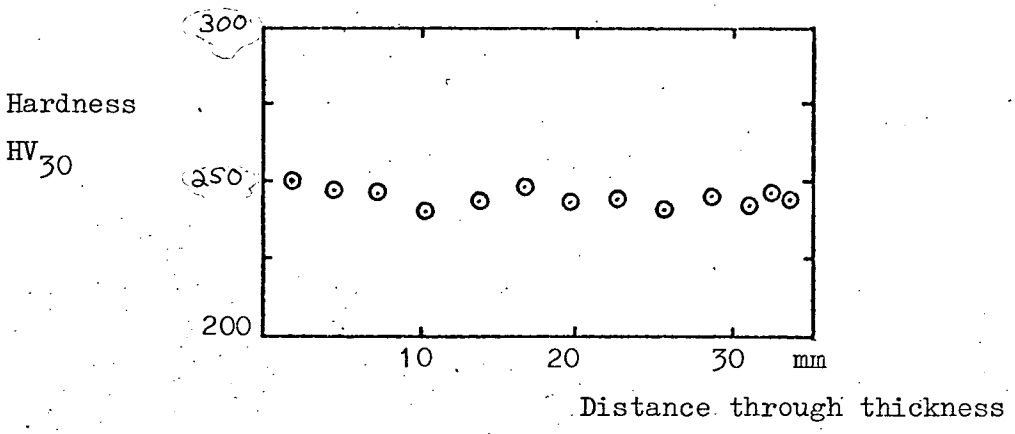

e) Sample 15

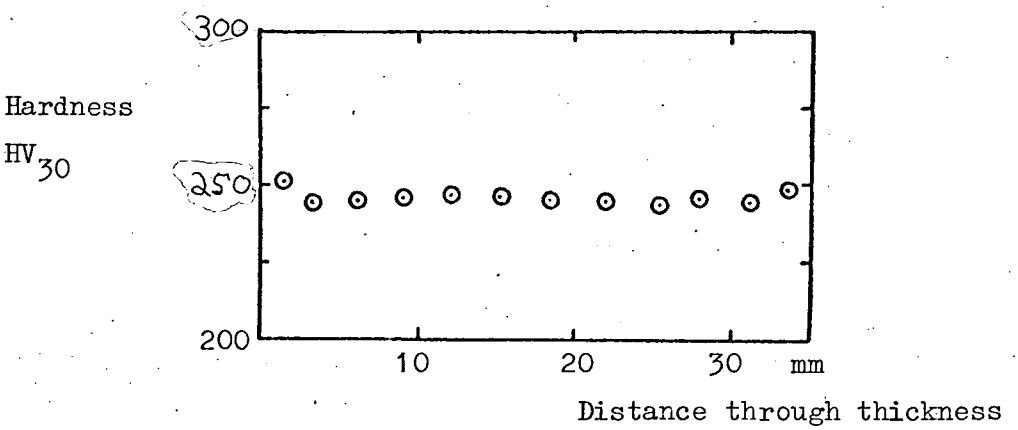

f) Sample 19

Figure 4.1, continued.

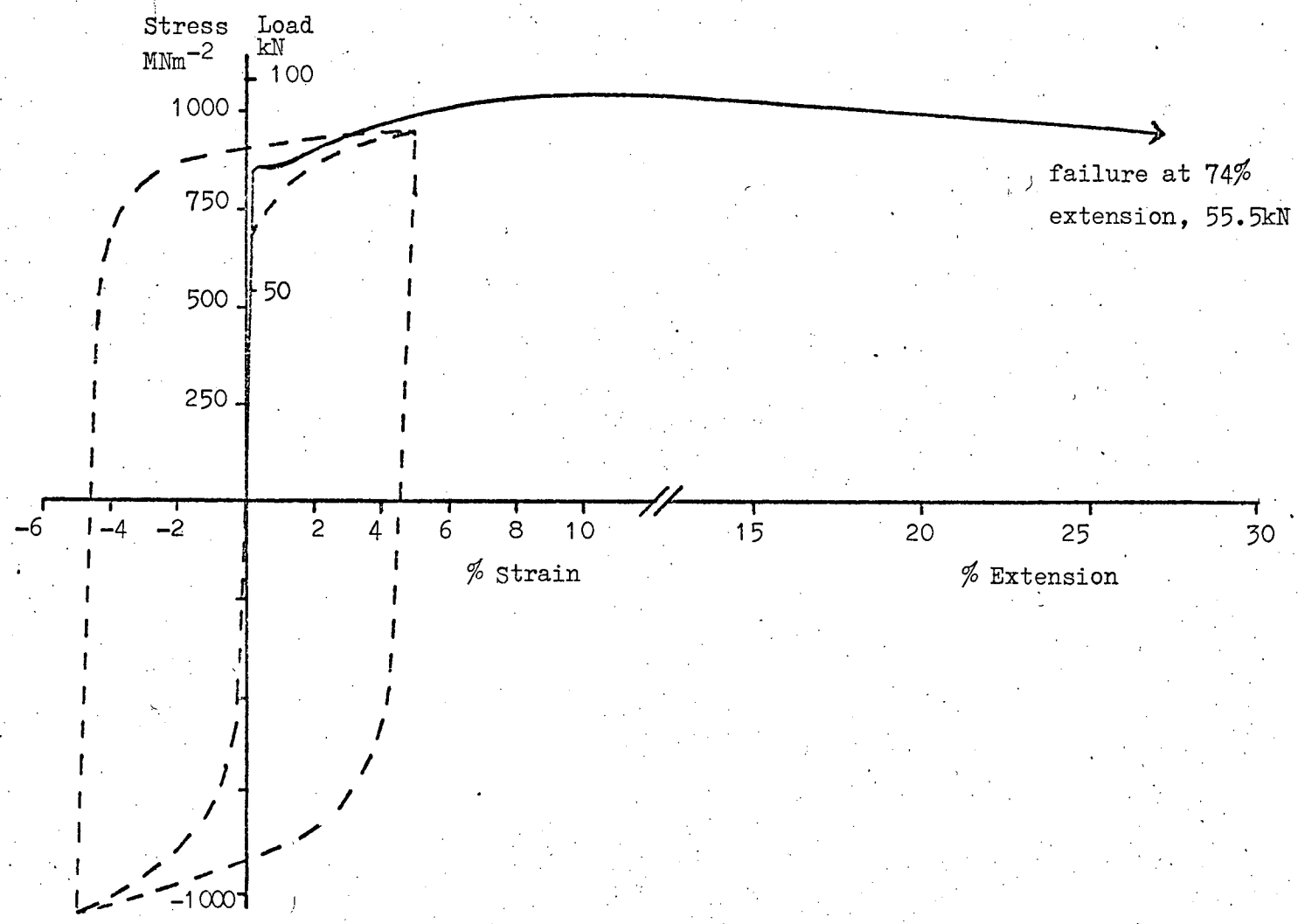

Figure 4.2 Comparison of monotonic and cyclic stress/strain properties of Q1(N).

Solid line: monotonic; broken line: cyclic.

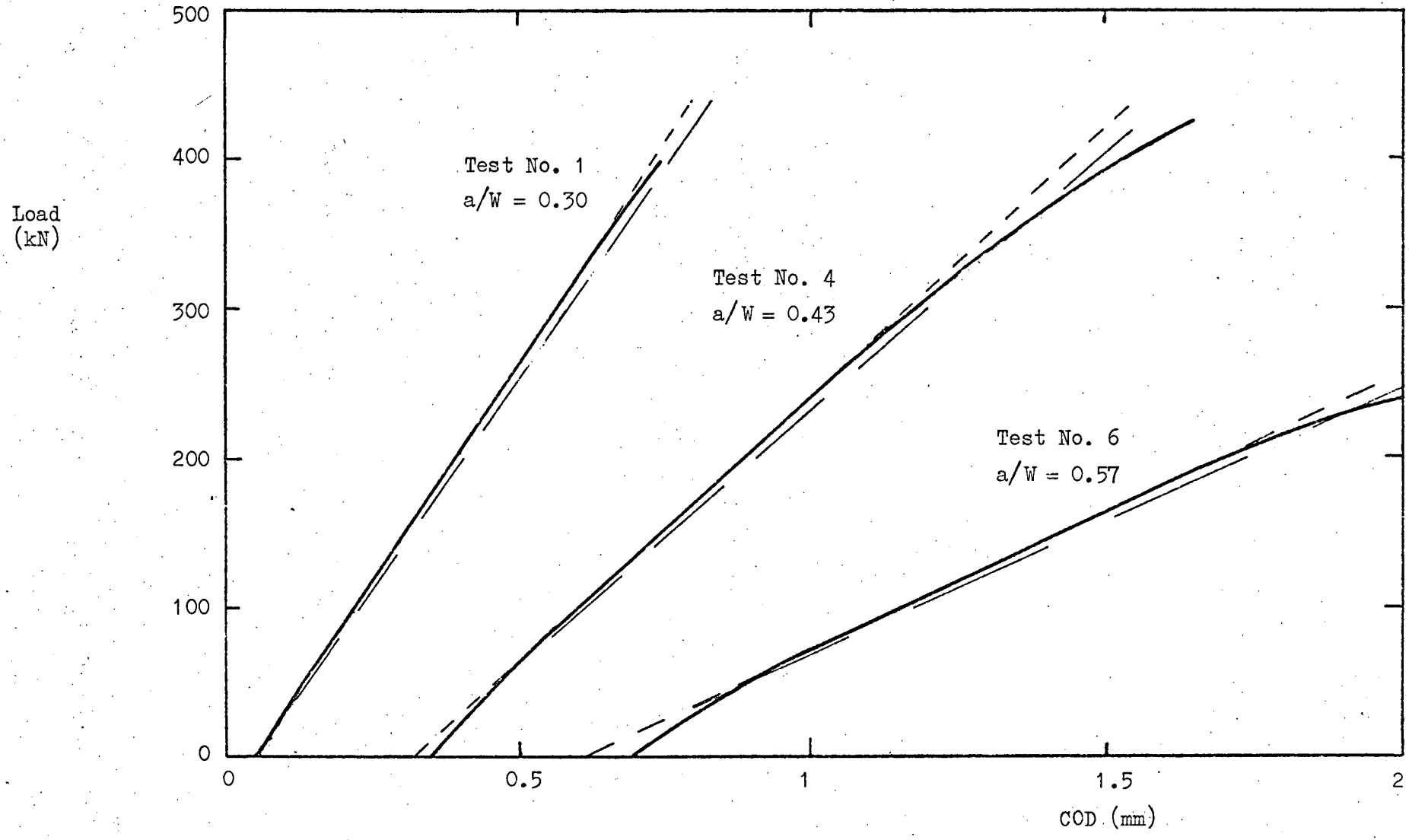

Figure 4.3 Examples of fracture toughness test records. Reproduction at one half original linear size. The broken lines show the 4% offset construction. The test results are given in Table 4.2.

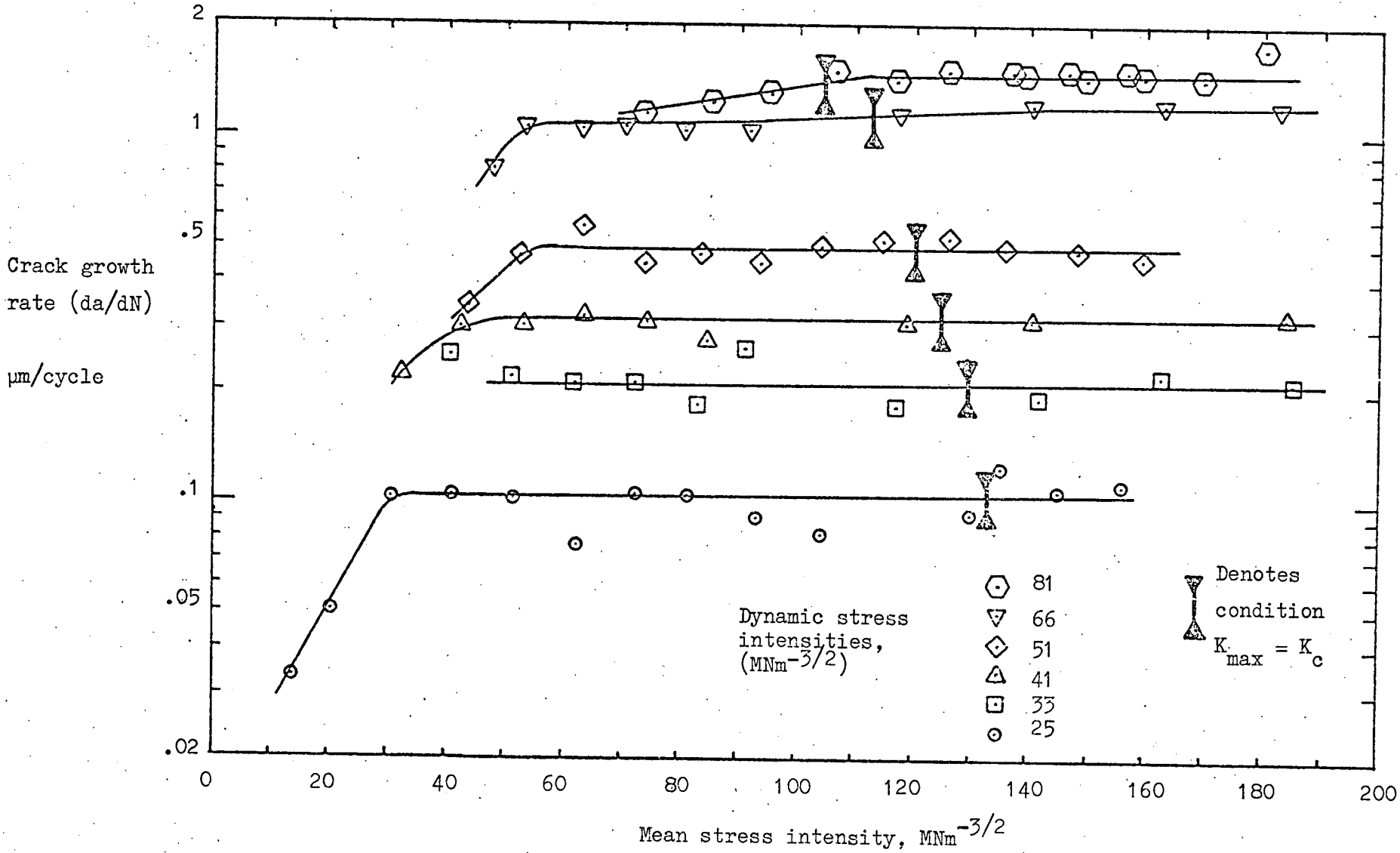

Figure 4.4 The influence of mean stress intensity on equilibrium crack growth rates.

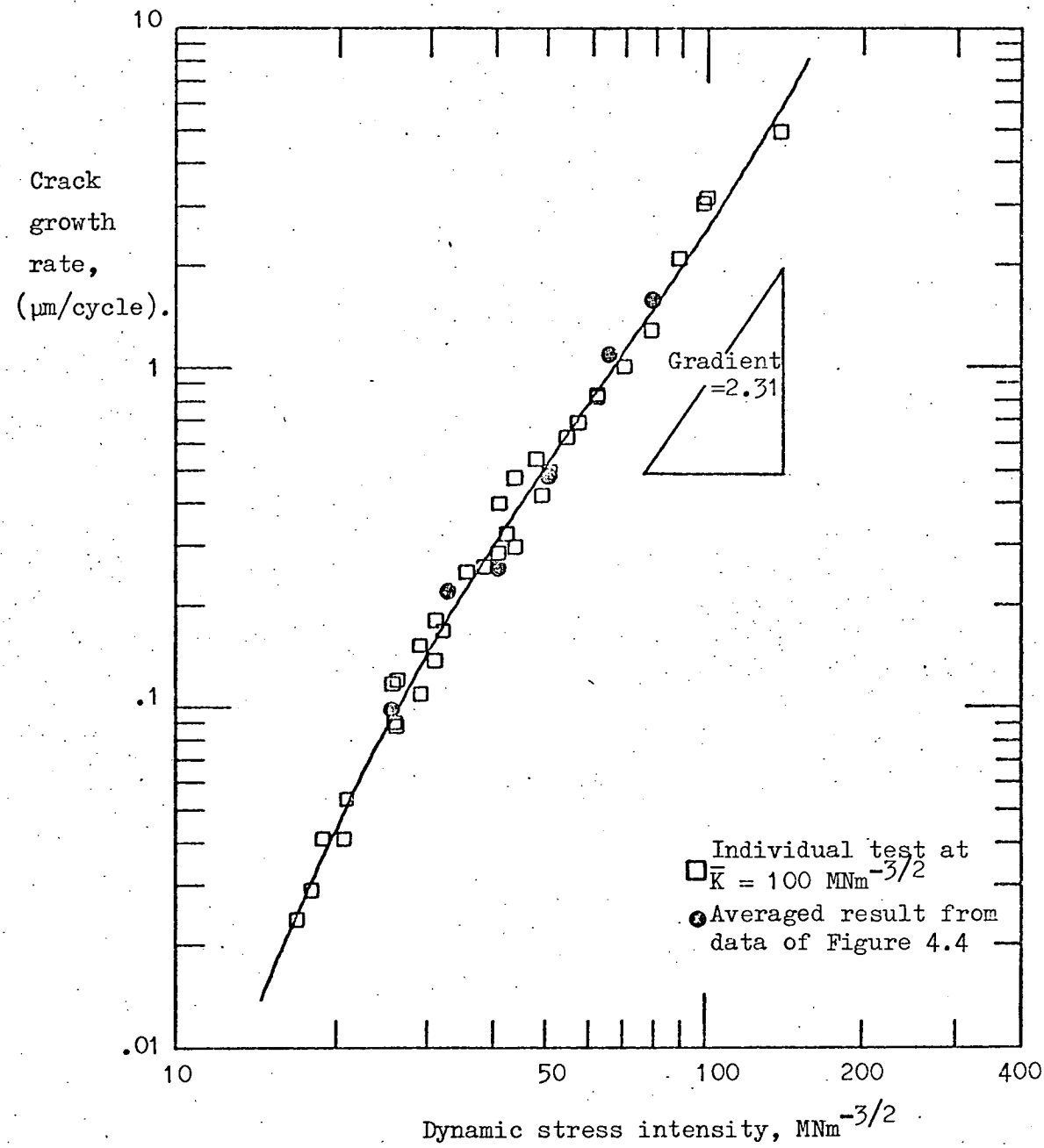

Figure 4.5 Equilibrium fatigue crack growth rates in Q1(N). Tests conducted under constant dynamic stress intensity conditions.

The data line was fitted to the individual results only; the averaged results from Figure 4.4 are shown for comparative purposes.

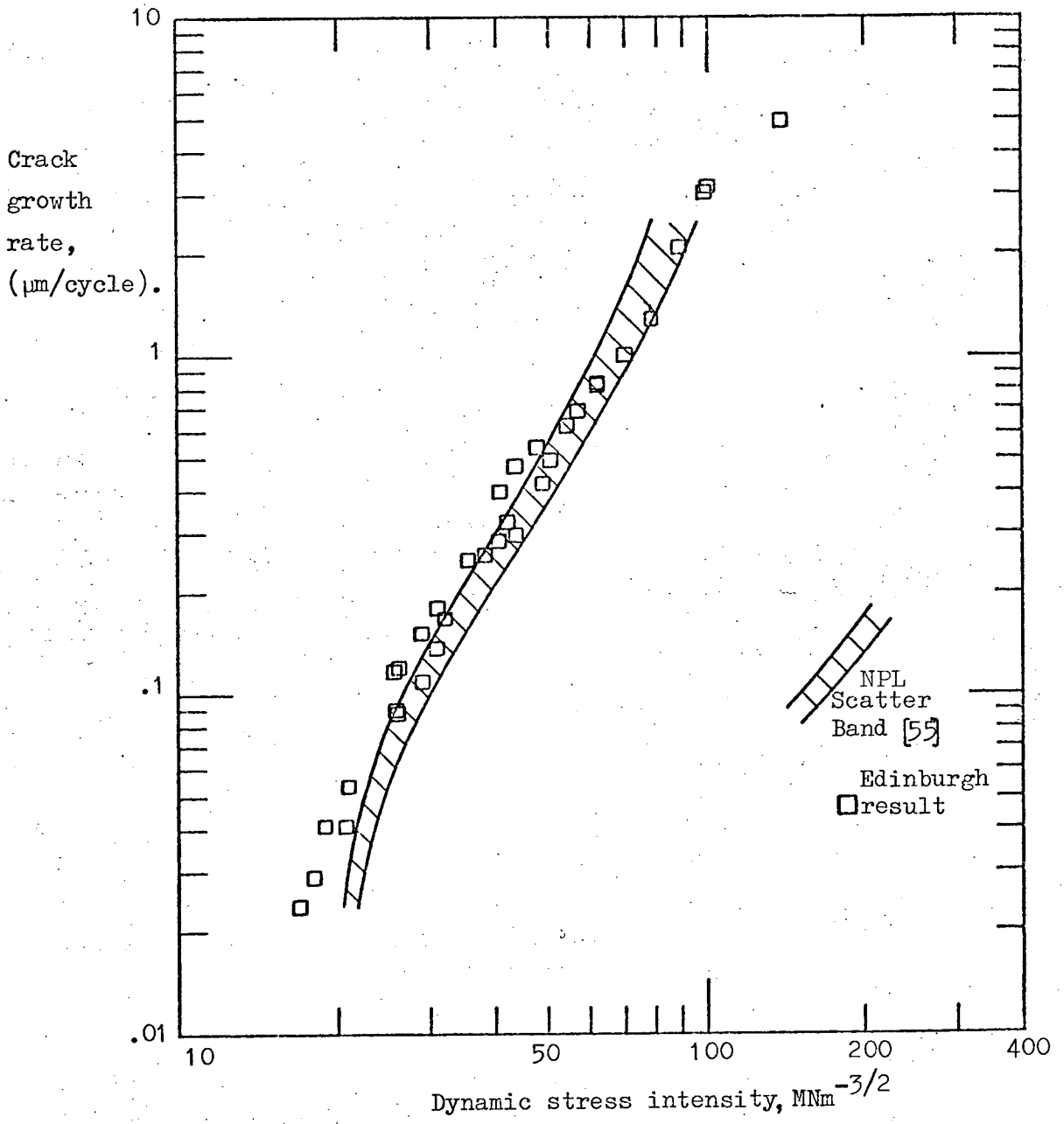

Figure 4.6 A comparison of the equilibrium fatigue crack growth rates determined by the author with those reported by Evans et al [55].

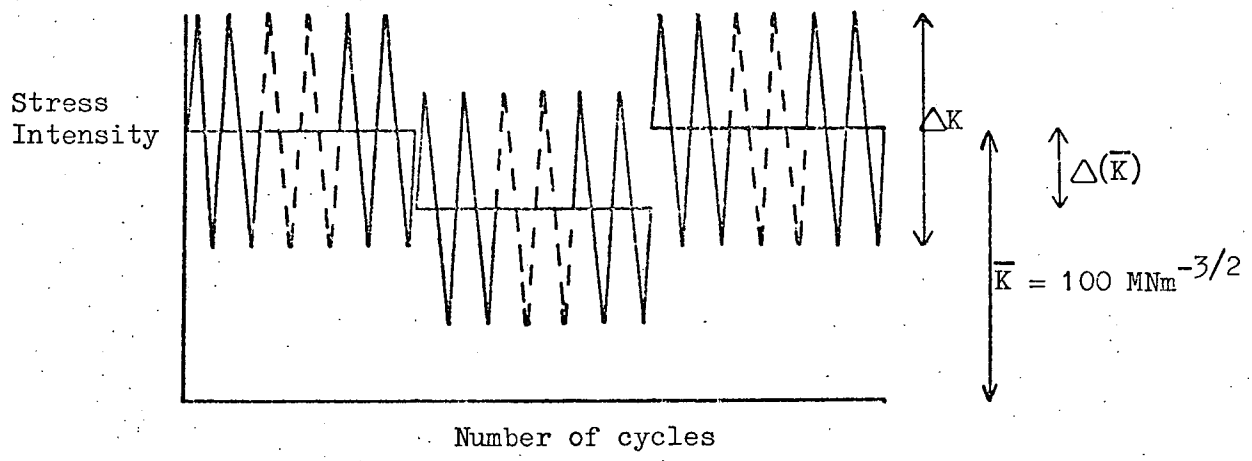

a) Load sequence used to investigate crack growth following discontinuous changes in mean stress intensity.

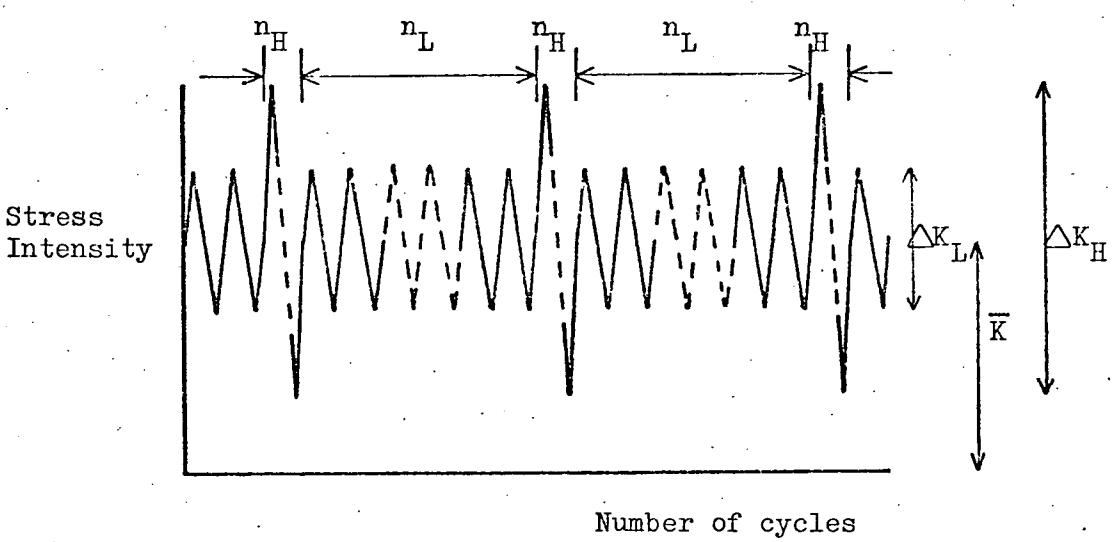

b) Dynamic overload test sequence at constant $\bar{K}$

Figure 4.7 Test load sequences.

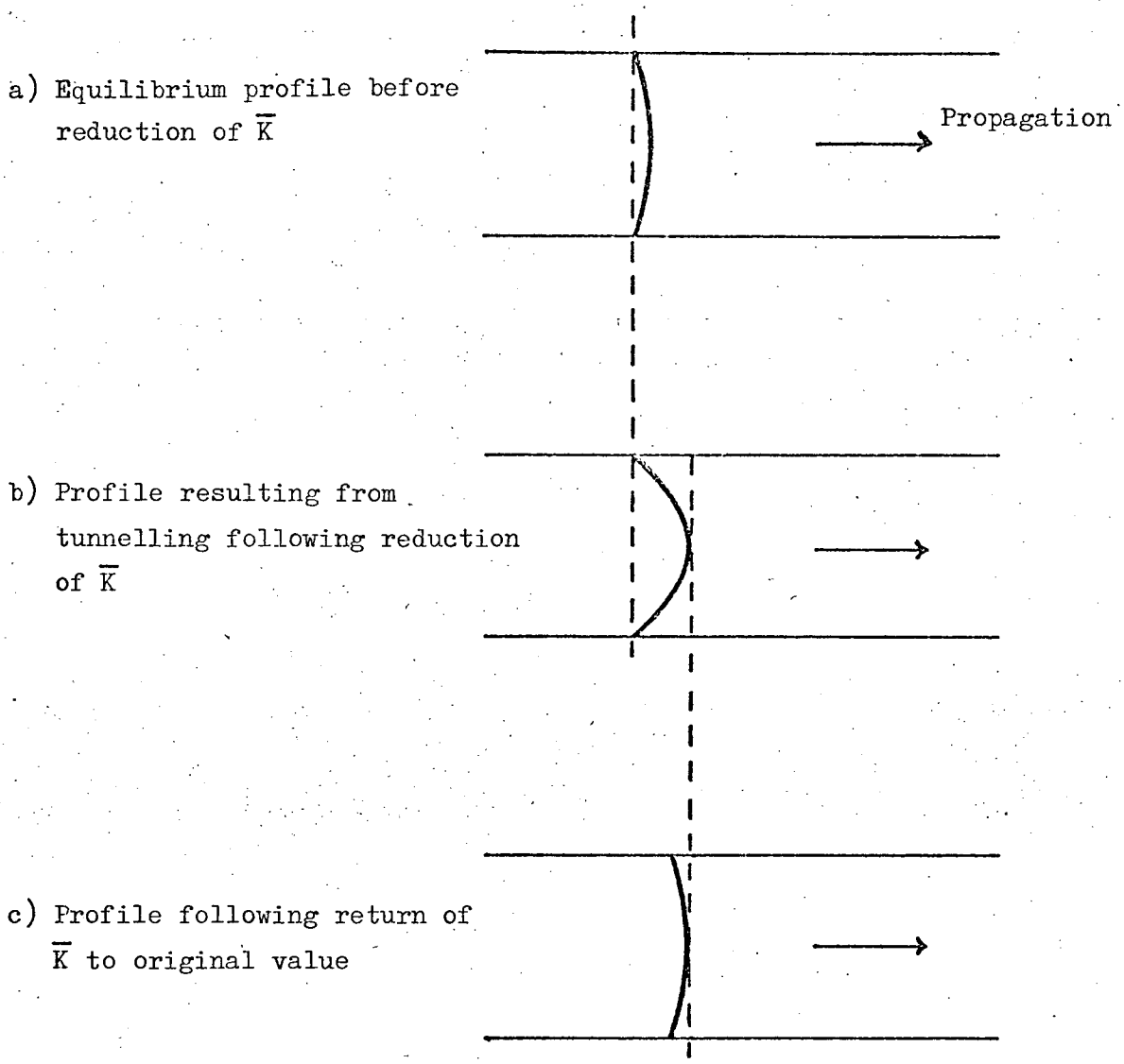

Figure 4.8 Schematic, plan view, of fatigue fracture surface showing the different crack front profiles observed during tests involving changes in mean stress intensity.
See also Figure 5.4.

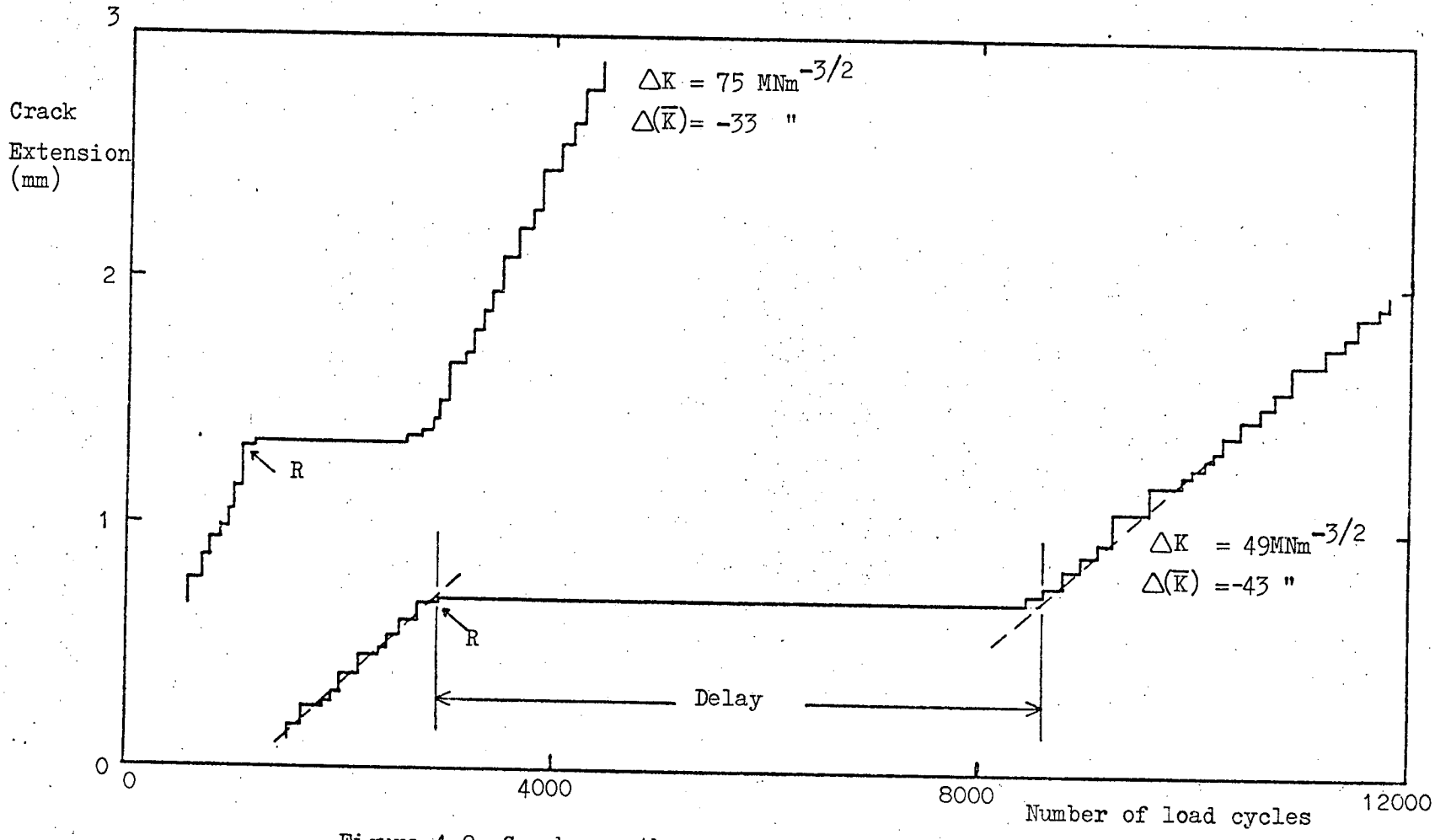

Figure 4.9 Crack growth records for tests involving a reduction of $\overline{K}$. "R" indicates the point of $\overline{K}$ reduction.

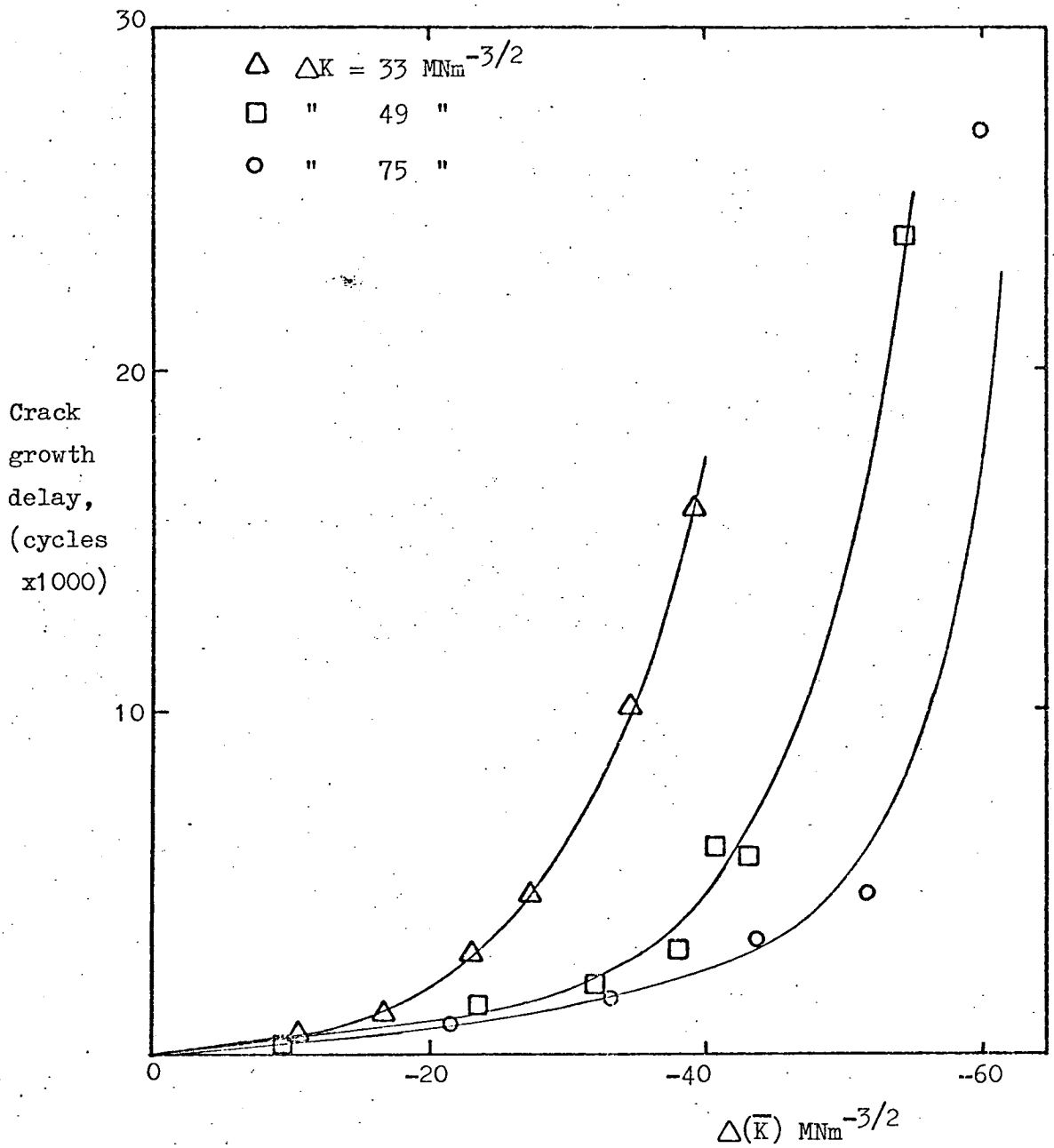

Figure 4.10 Ultrasonically determined delays in crack growth following reductions of $\overline{K}$ at different values of ΔK.

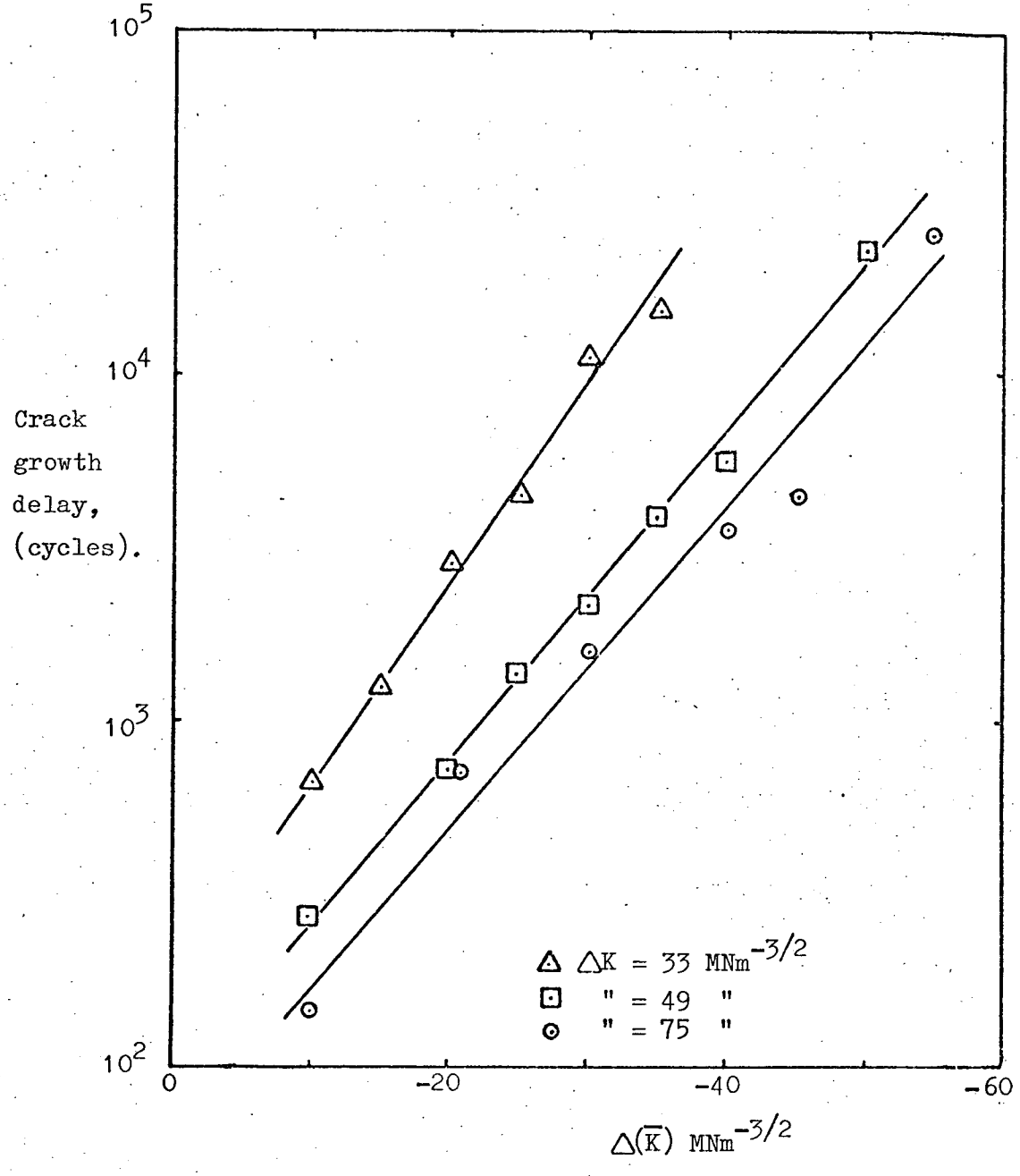

Figure 4.11 Crack growth delay data from Figure 4.10 replotted with a logarithmic ordinate.

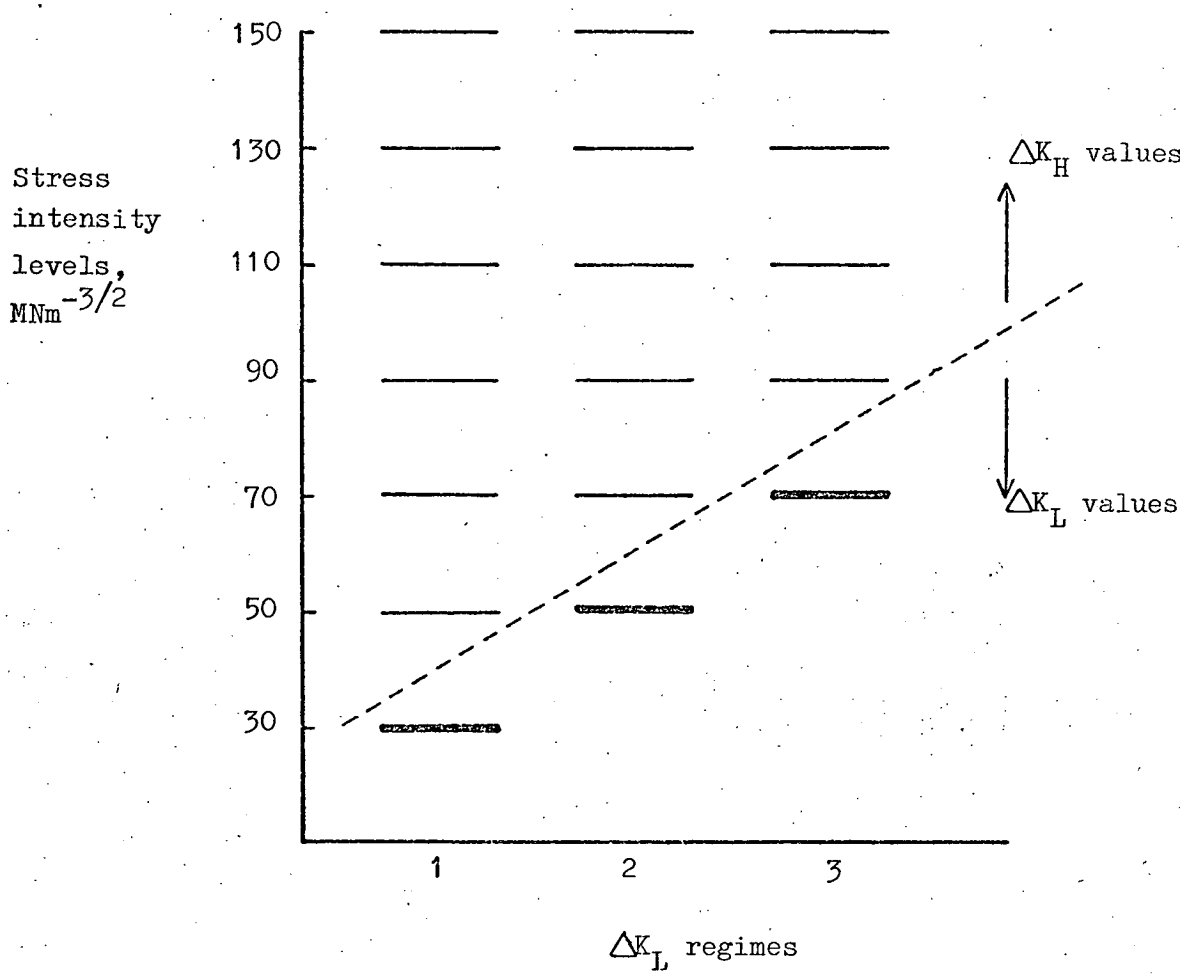

Figure 4.12 Stress intensity combinations used for dynamic overload tests. For the values of ΔK_L shown, overload tests have been performed at each of the ΔK_H values shown in the same column.

See Figure 4.7(b) for general notation.

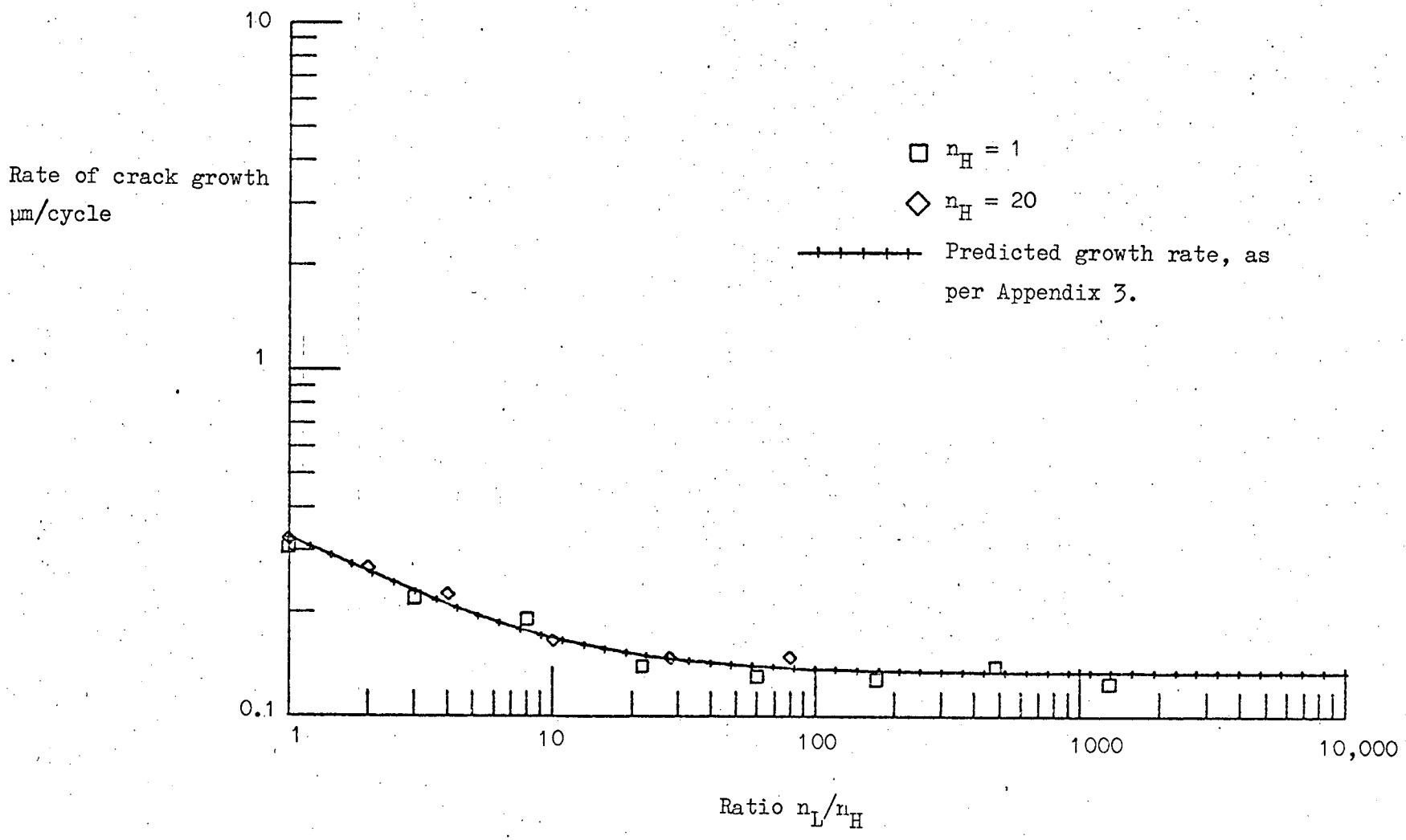

Figure 4.13 Dynamic overload test.

$\overline{K}$ = 100 ΔK = 30 ΔK = 50 MN $m^{-3/2}$

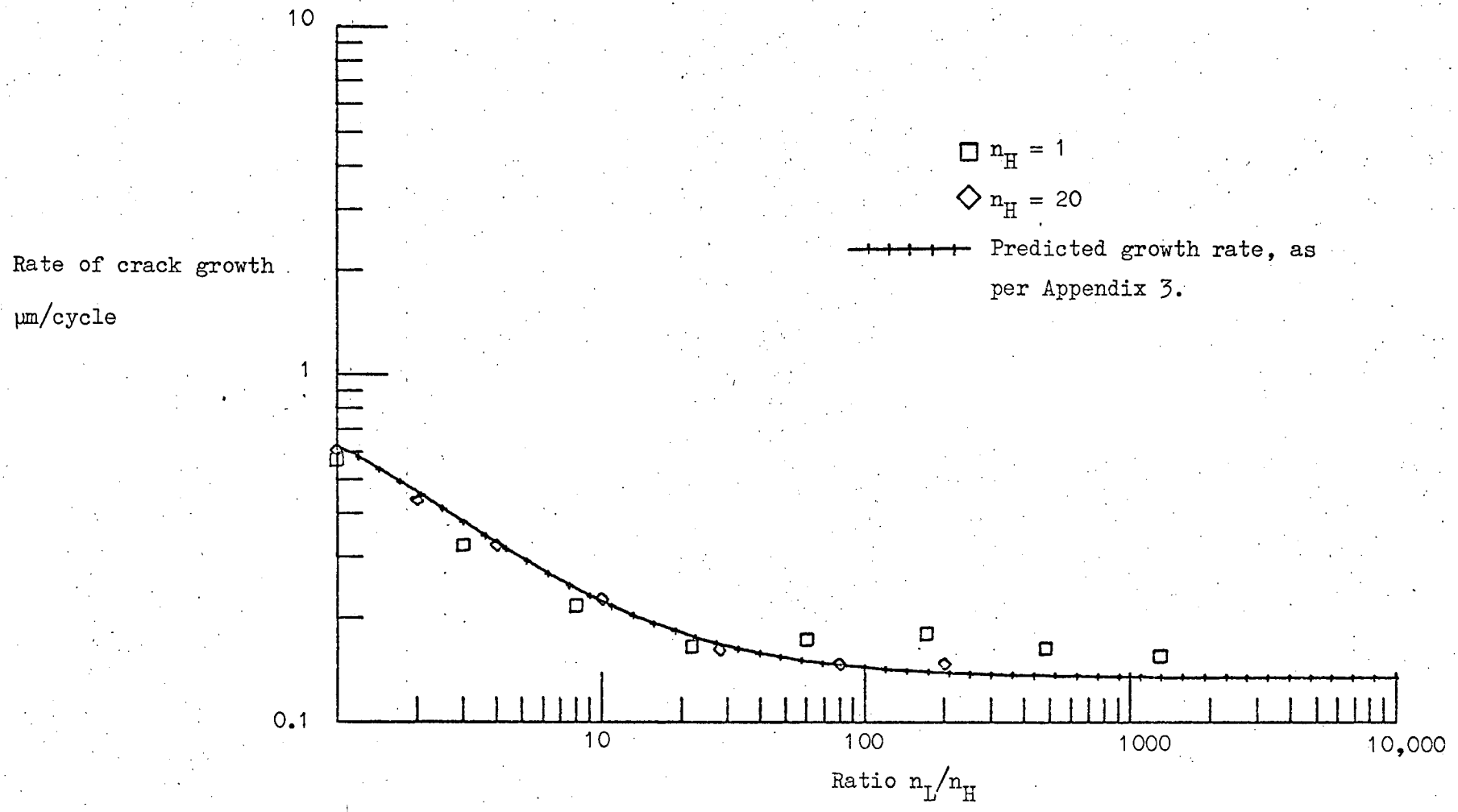

Figure 4.14 Dynamic Overload Test

$\overline{K} = 100, \Delta K_L = 30, \Delta K_H = 70$ $MNm^{-3/2}$

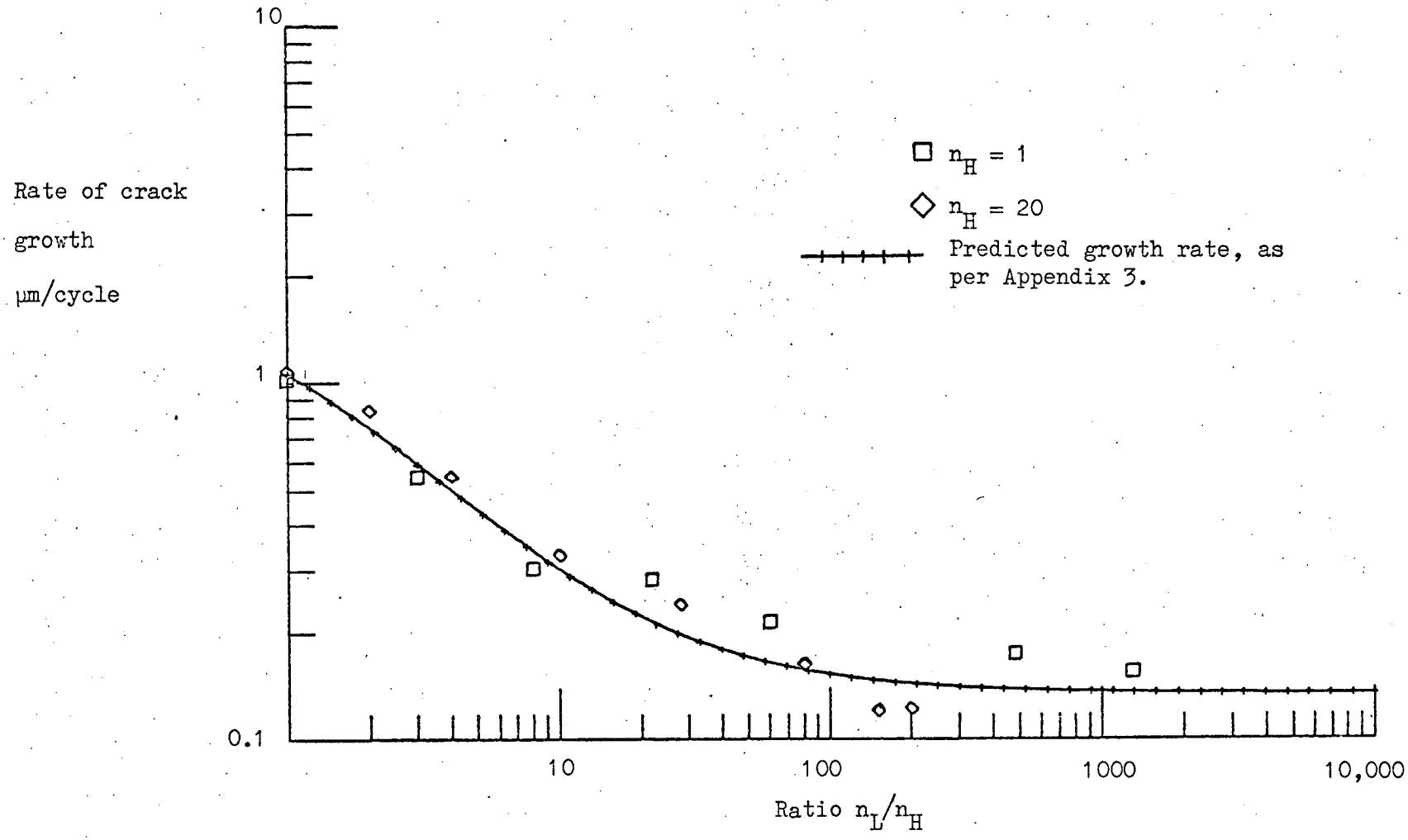

Figure 4.15 Dynamic overload test

$\overline{K} = 100$, $\Delta K_L = 30$, $\Delta K_H = 90$ $MNm^{-3/2}$

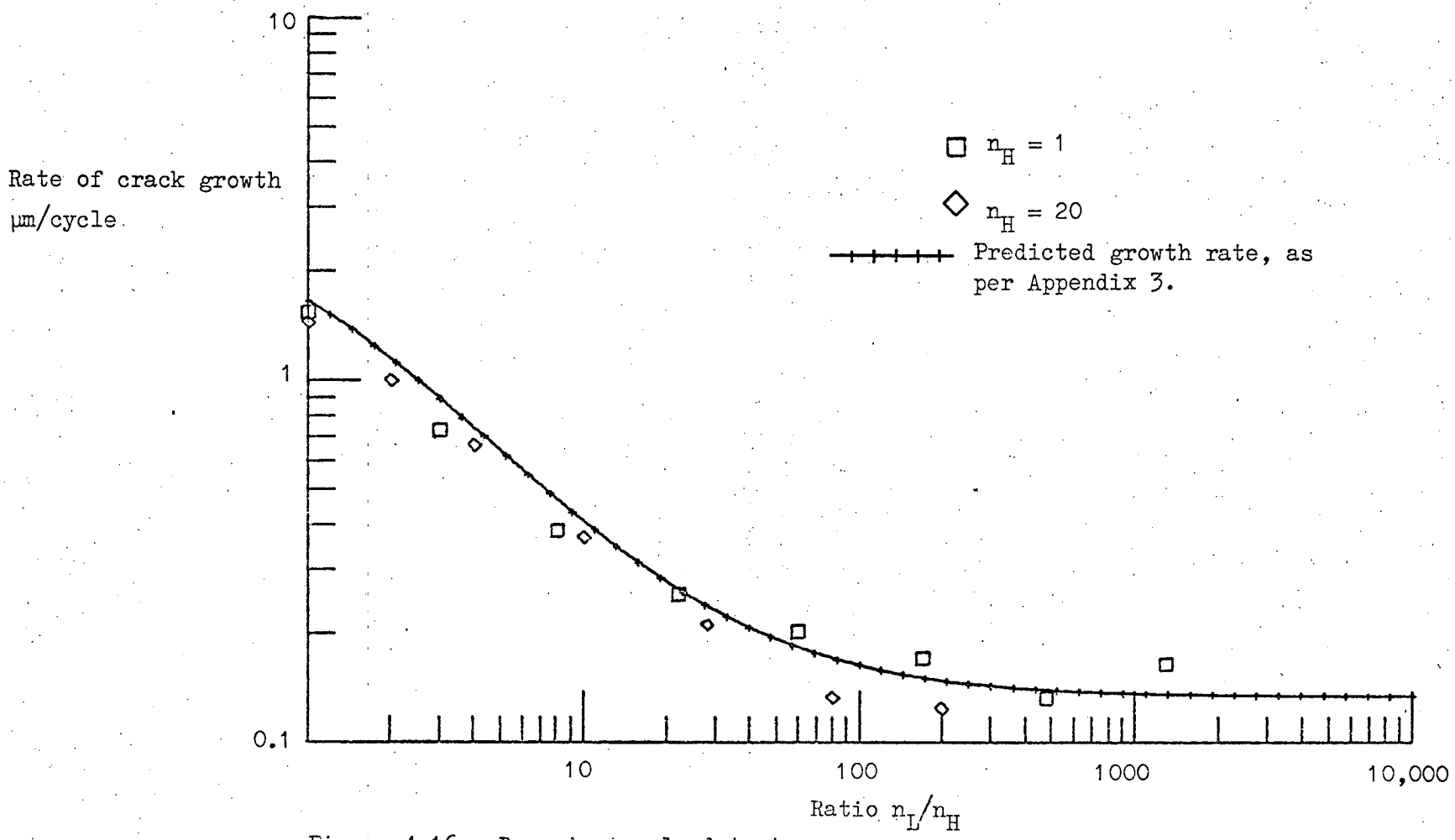

Figure 4.16 Dynamic overload test

$\overline{K} = 100$, $\Delta K_L = 30$ $\Delta K_H = 110$ $MNm^{-3/2}$

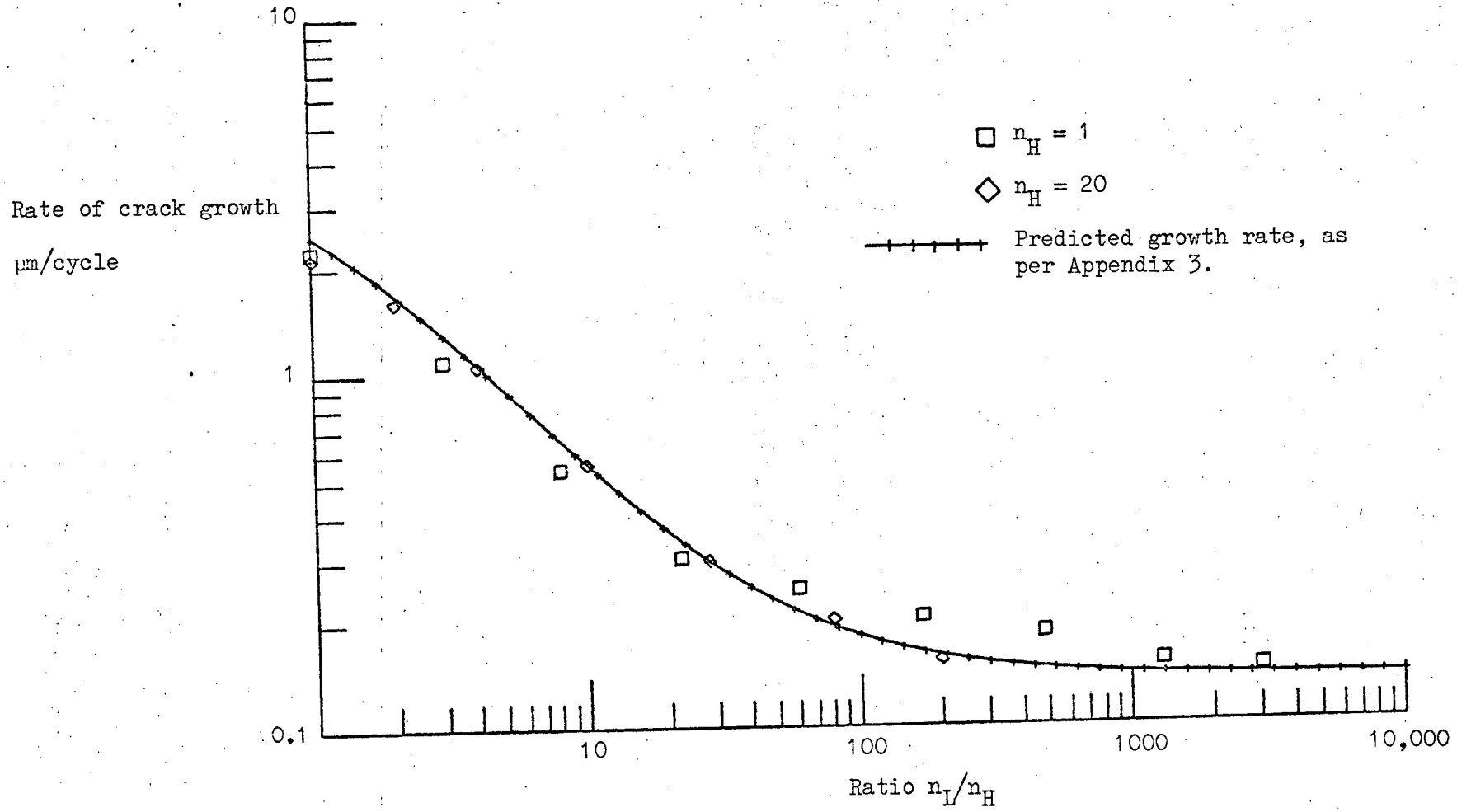

Figure 4.17 Dynamic overload test

$\overline{K} = 100.$ $\Delta K_- = 30.$ $\Delta K_+ = 130$ $MNm^{-3/2}$

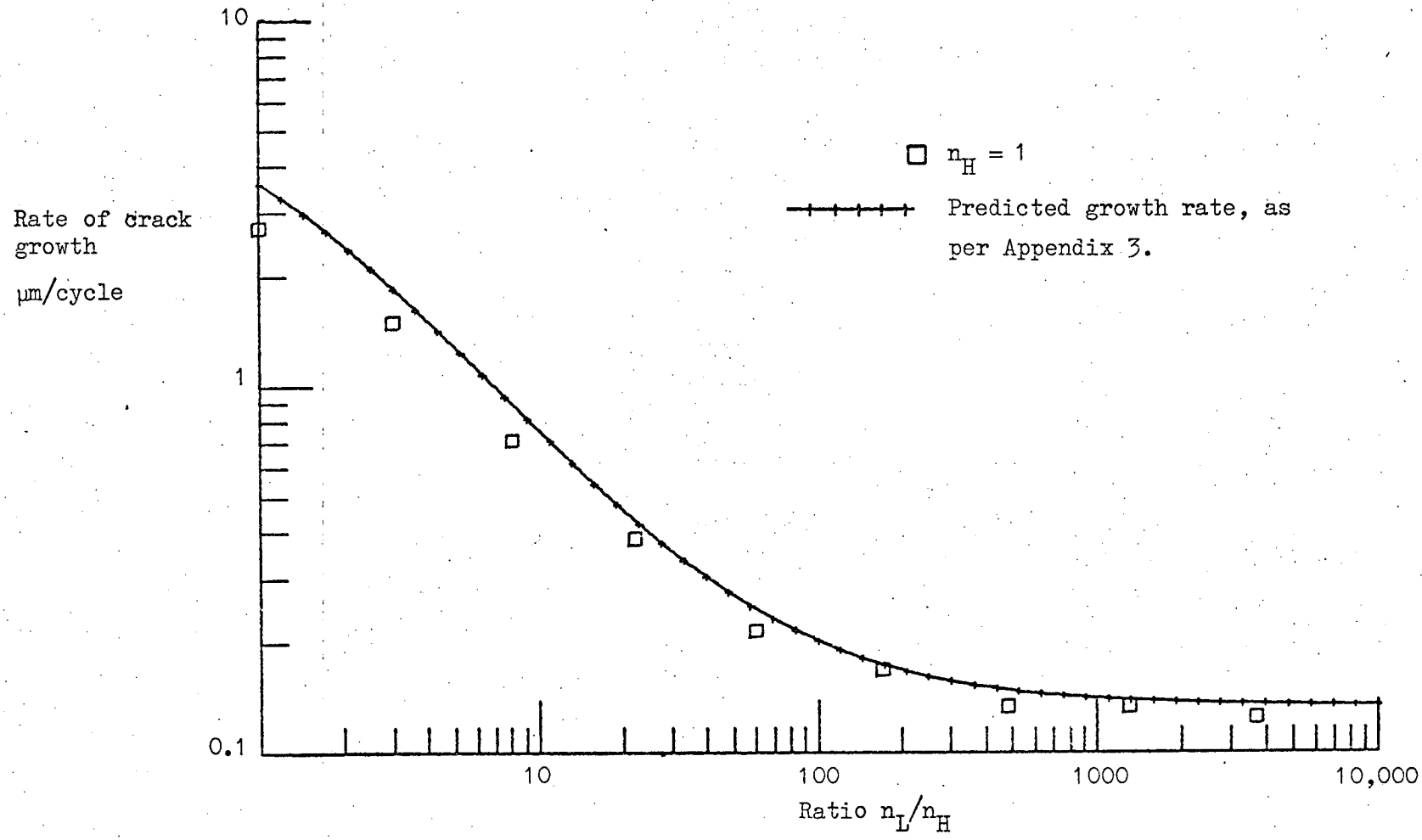

Figure 4.18 Dynamic overload test

$\overline{K} = 100$, $\Delta K_L = 30$, $\Delta K_H = 150$ $MNm^{-3/2}$

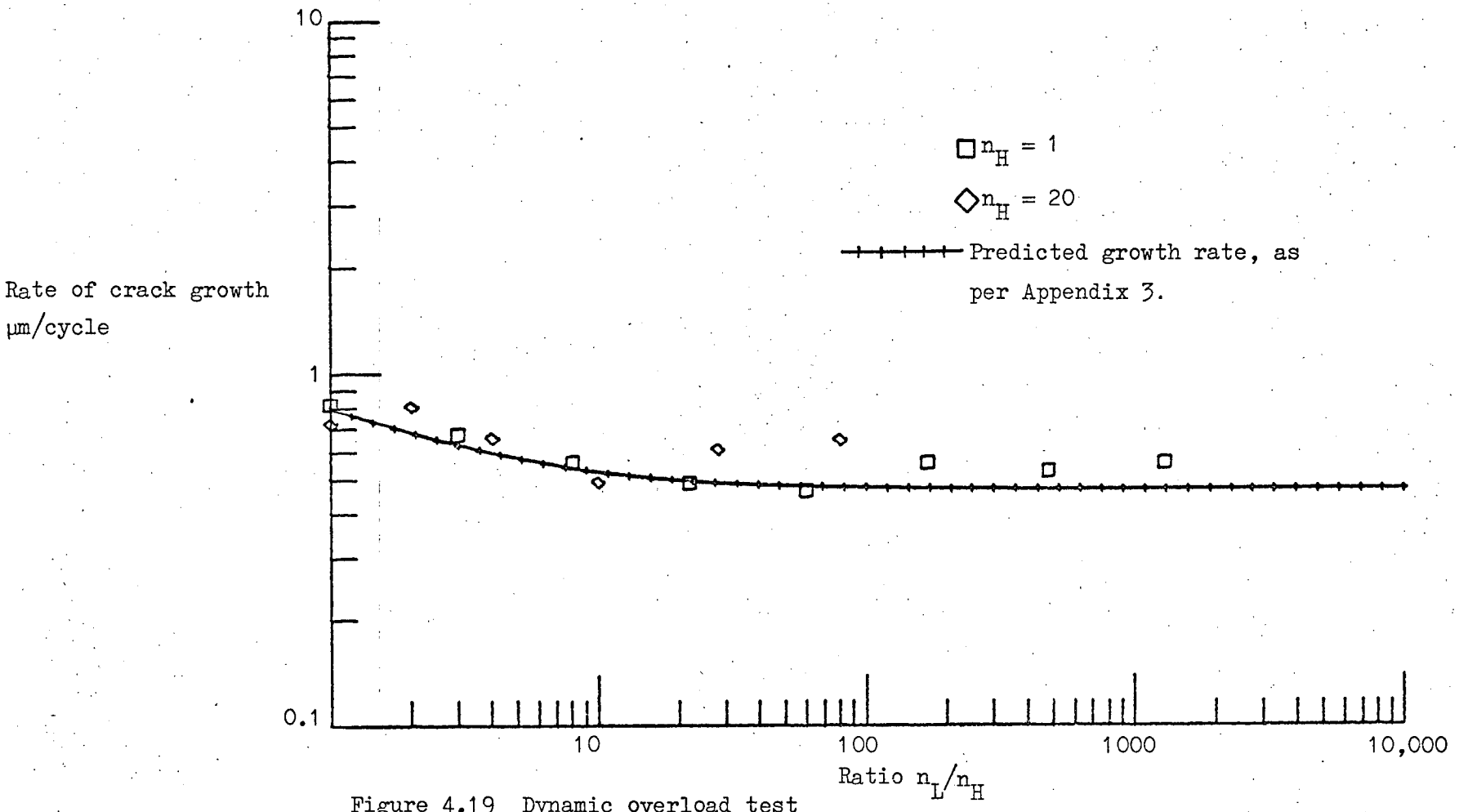

Figure 4.19 Dynamic overload test

$\bar{K} = 100$, $\Delta K_L = 50$, $\Delta K_H = 70$ $MNm^{-3/2}$

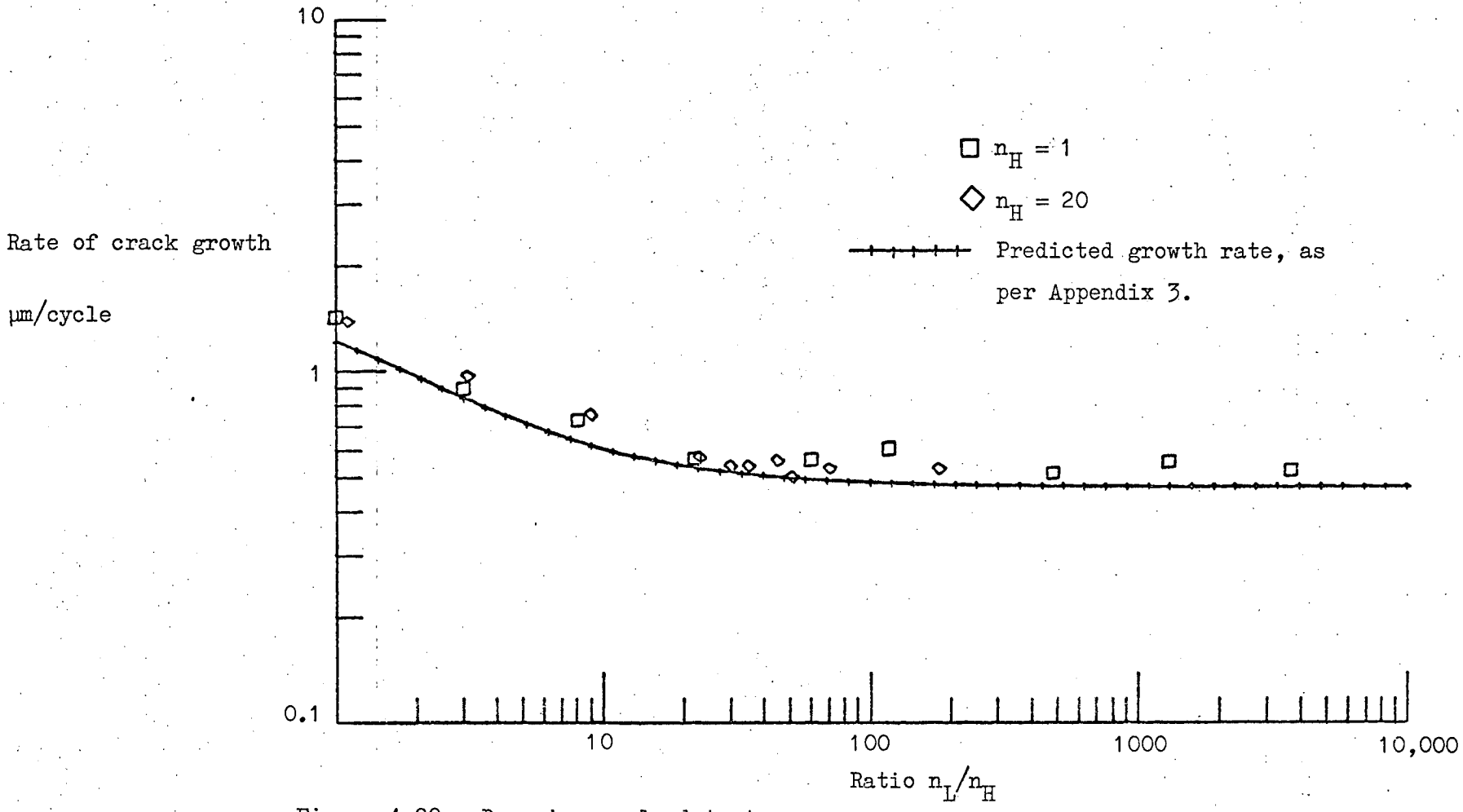

Figure 4.20 Dynamic overload test

$\overline{K} = 100, \quad \Delta K_L = 50, \quad \Delta K_H = 90$ $MNm^{-3/2}$

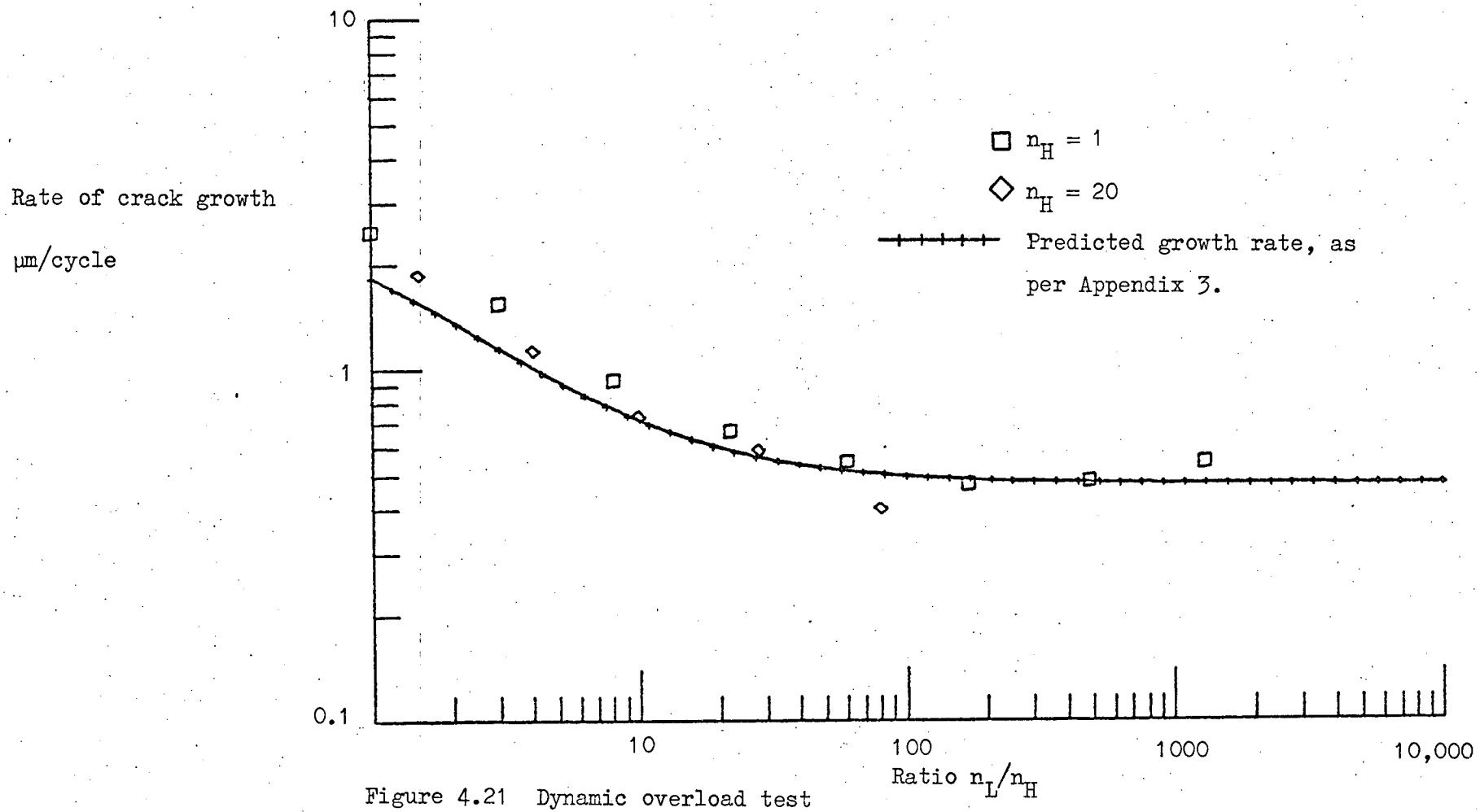

Figure 4.21 Dynamic overload test

$\overline{K} = 100, \quad \Delta K_L = 50, \quad \Delta K_H = 110$ MNm$^{-3/2}$

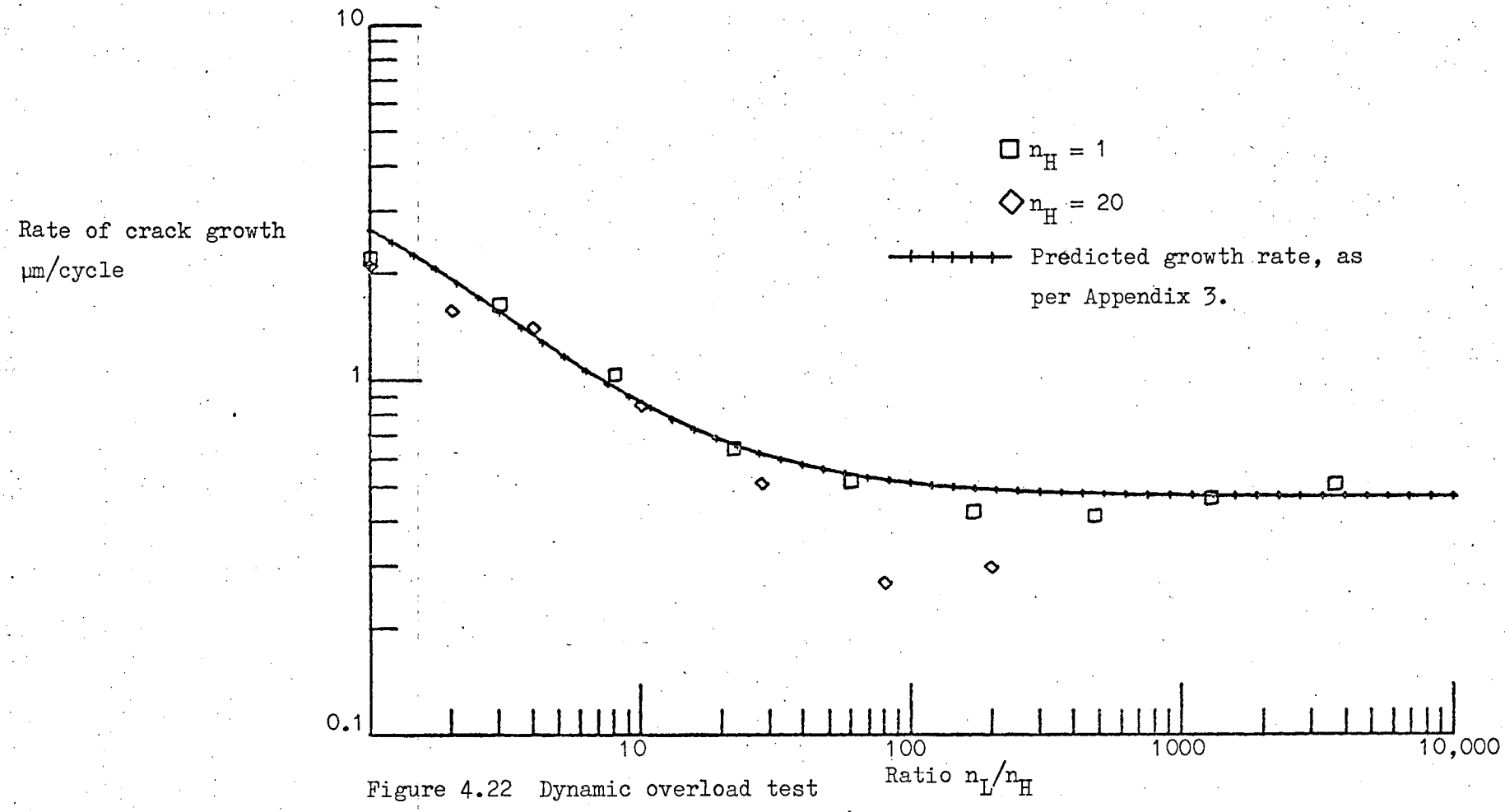

Figure 4.22 Dynamic overload test

$\overline{K} = 100$, $\Delta K_L = 50$, $\Delta K_H = 130$ $MNm^{-3/2}$

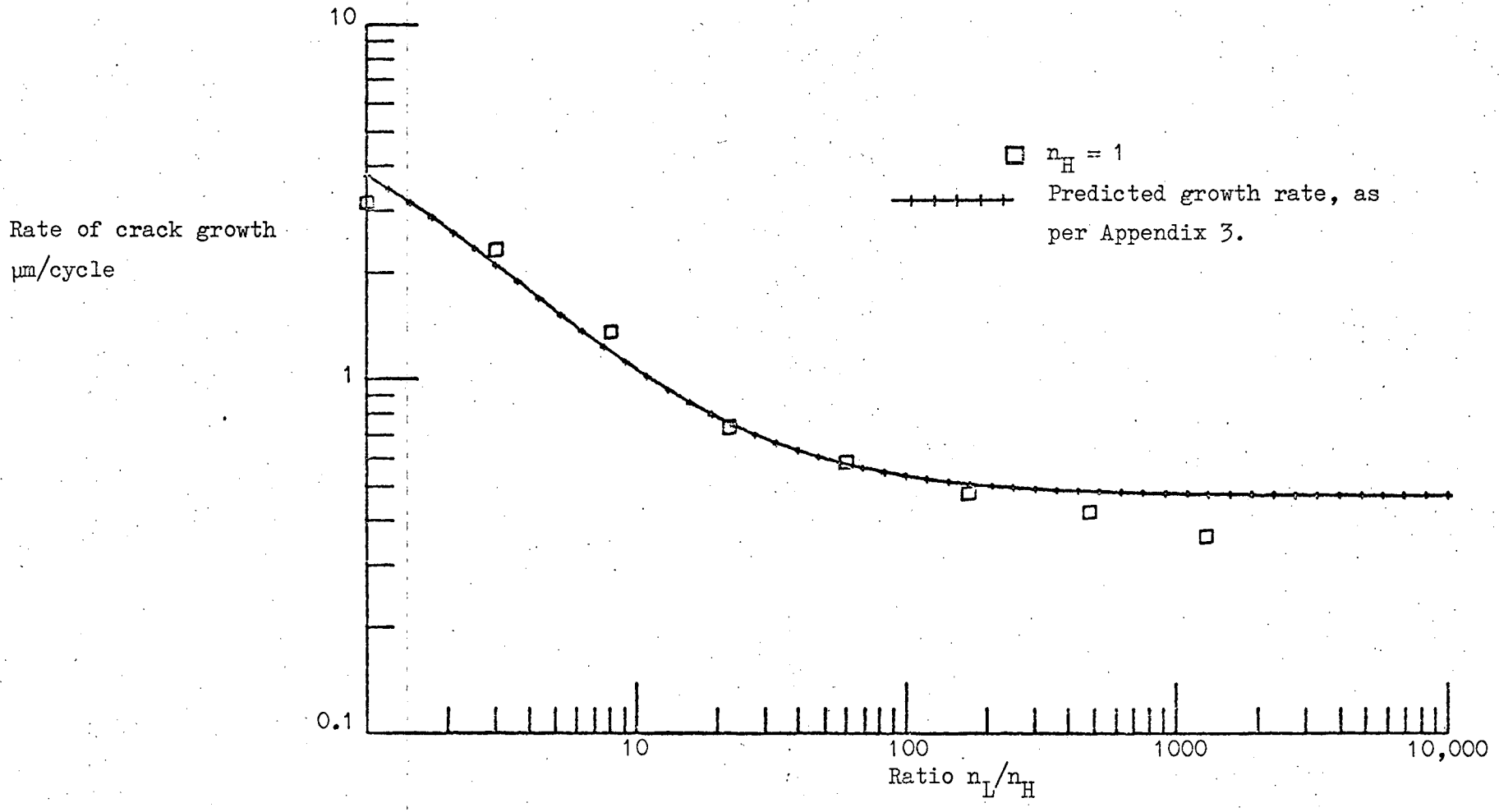

Figure 4.23 Dynamic overload test

$\overline{K} = 100$, $\Delta K_L = 50$, $\Delta K_H = 150$ $MNm^{-3/2}$

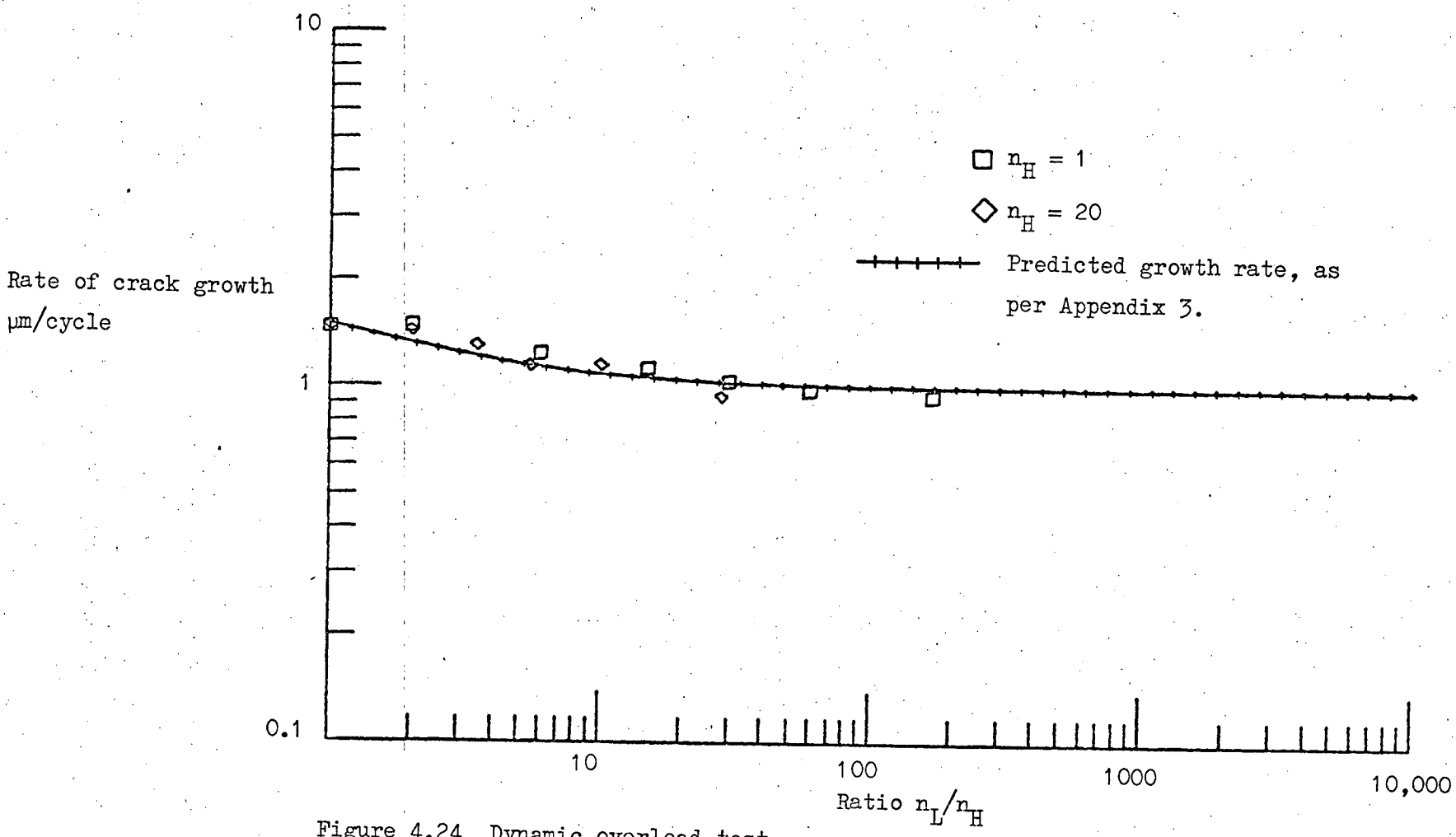

Figure 4.24 Dynamic overload test

$\overline{K} = 100$, $\Delta K_L = 70$, $\Delta K_H = 90$ $MNm^{-3/2}$

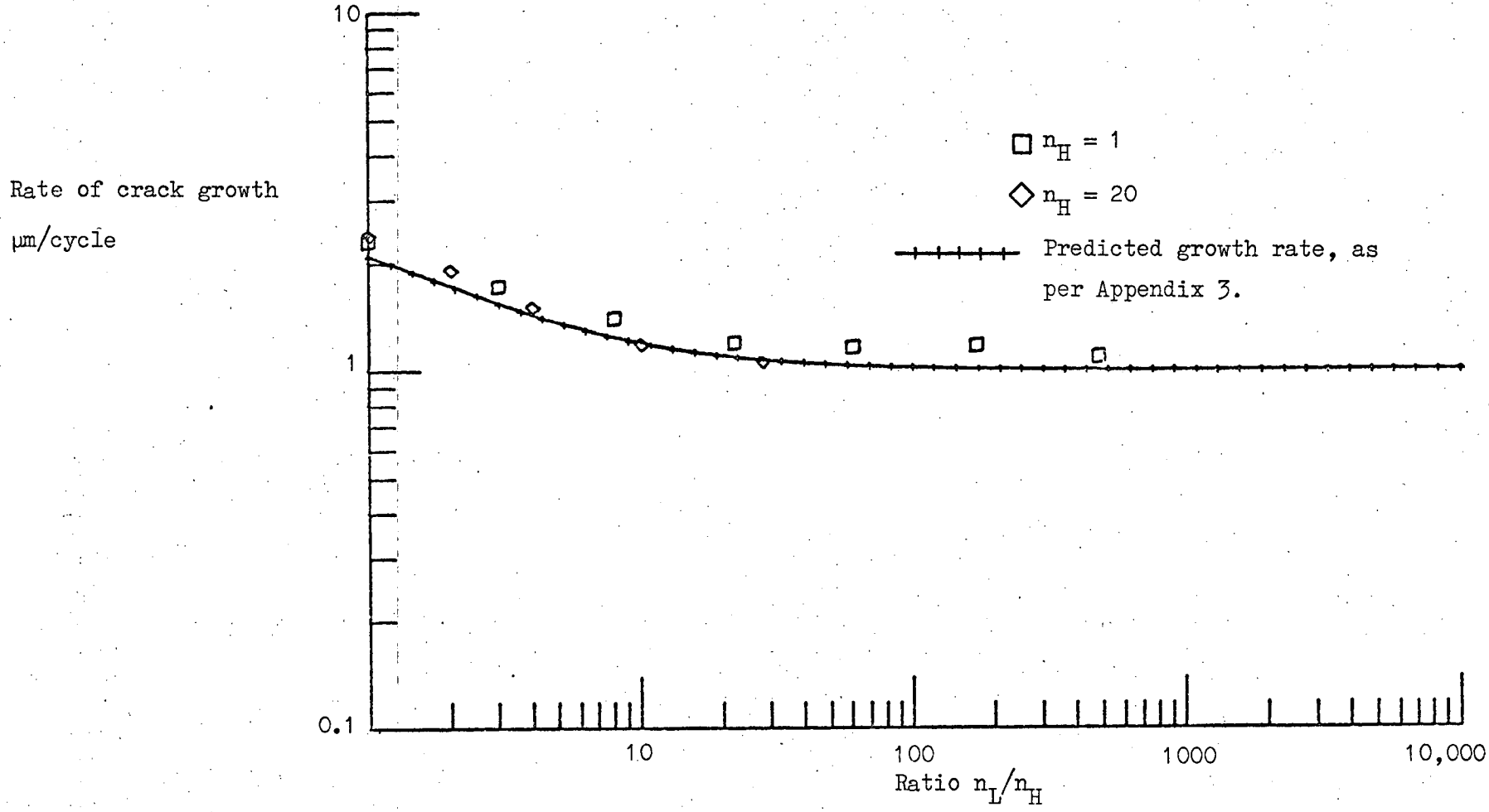

Figure 4.25 Dynamic overload test

$\overline{K}$ = 100, ΔK_L = 70, ΔK_H = 110 $MNm^{-3/2}$

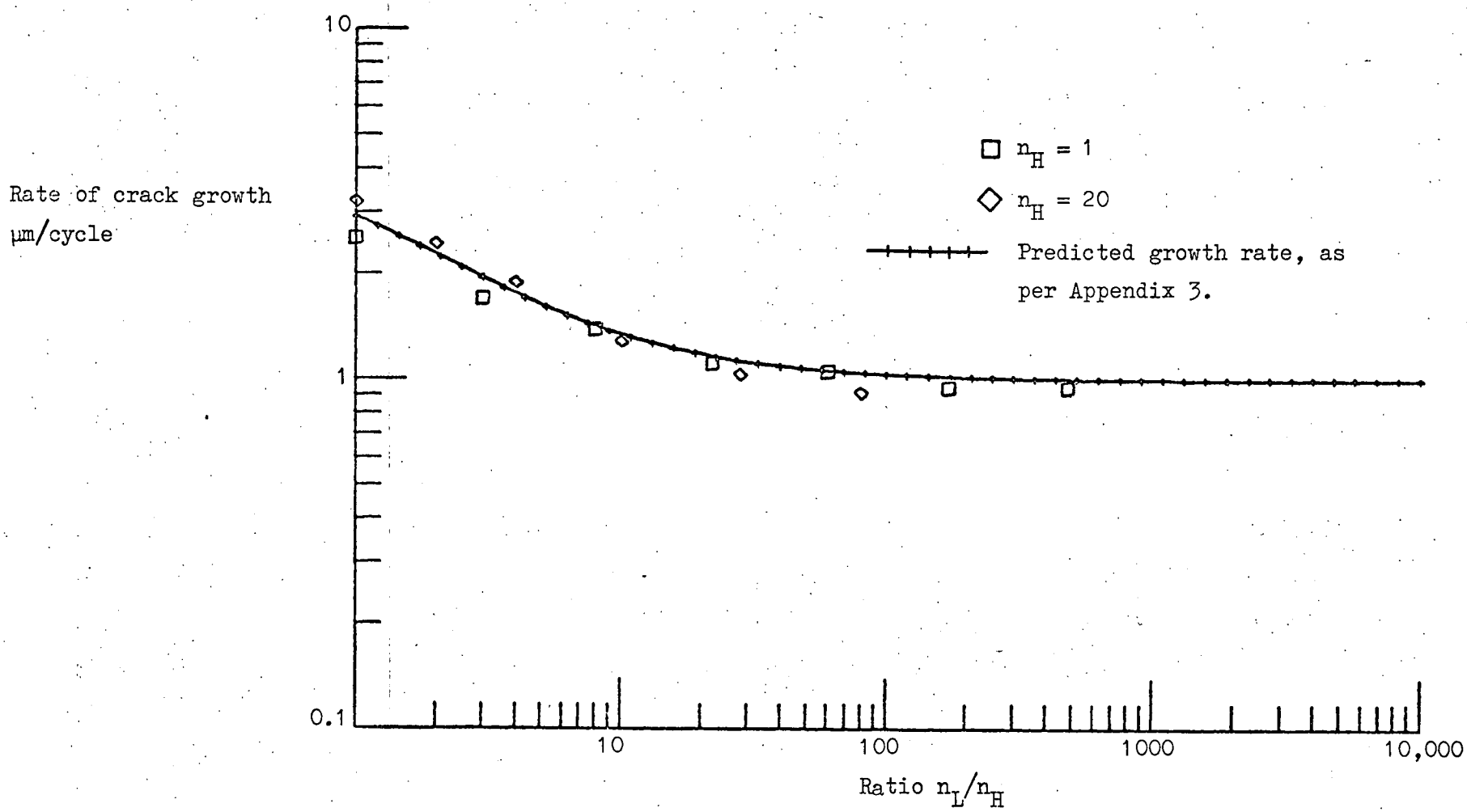

Figure 4.26 Dynamic overload test

$\overline{K}$ = 100, ΔK_L = 70, ΔK_H = 130 $MNm^{-3/2}$

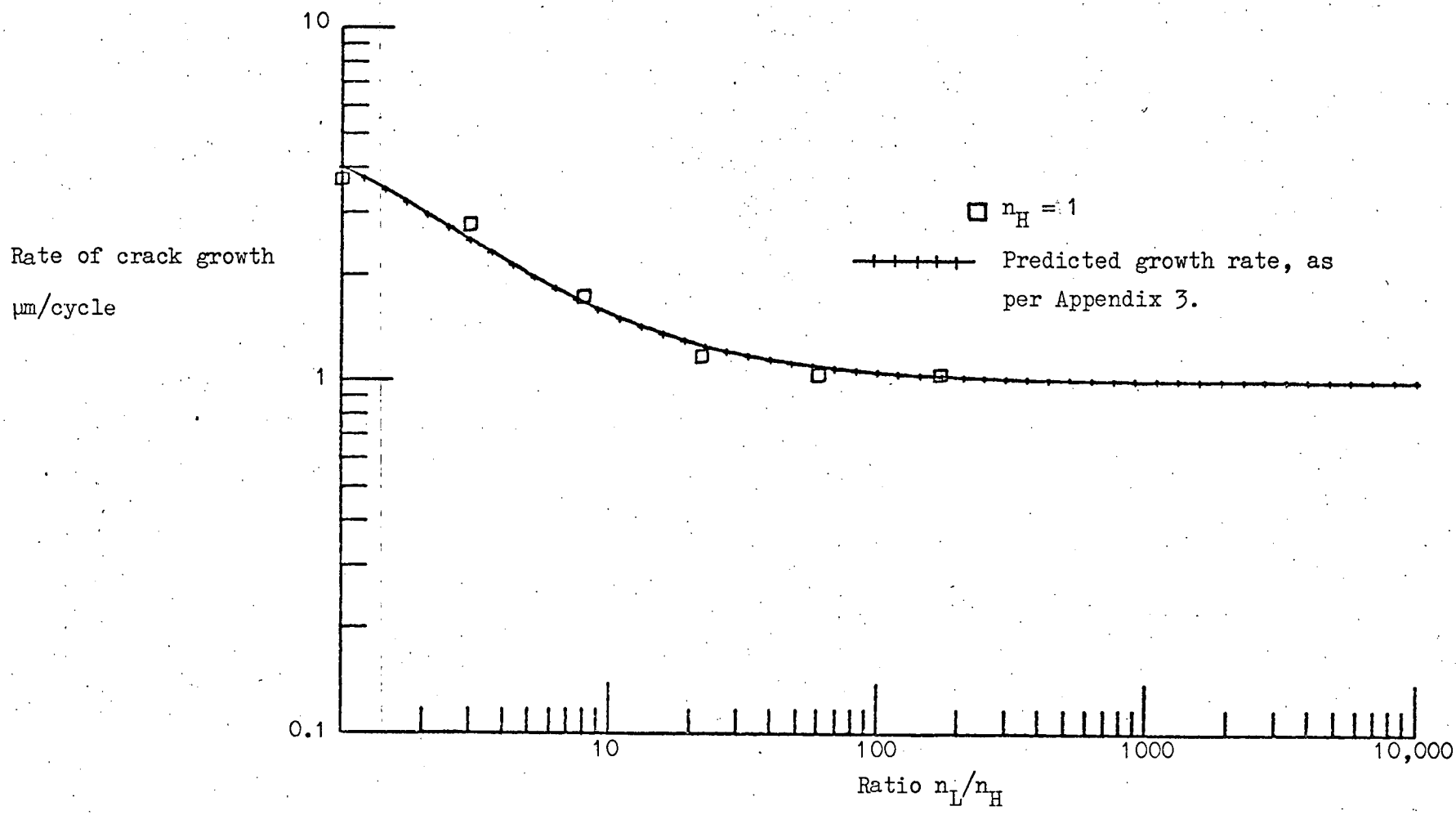

Figure 4.27 Dynamic overload test

$\overline{K} = 100$, $\Delta K_L = 70$, $\Delta K_H = 150$ $MNm^{-3/2}$

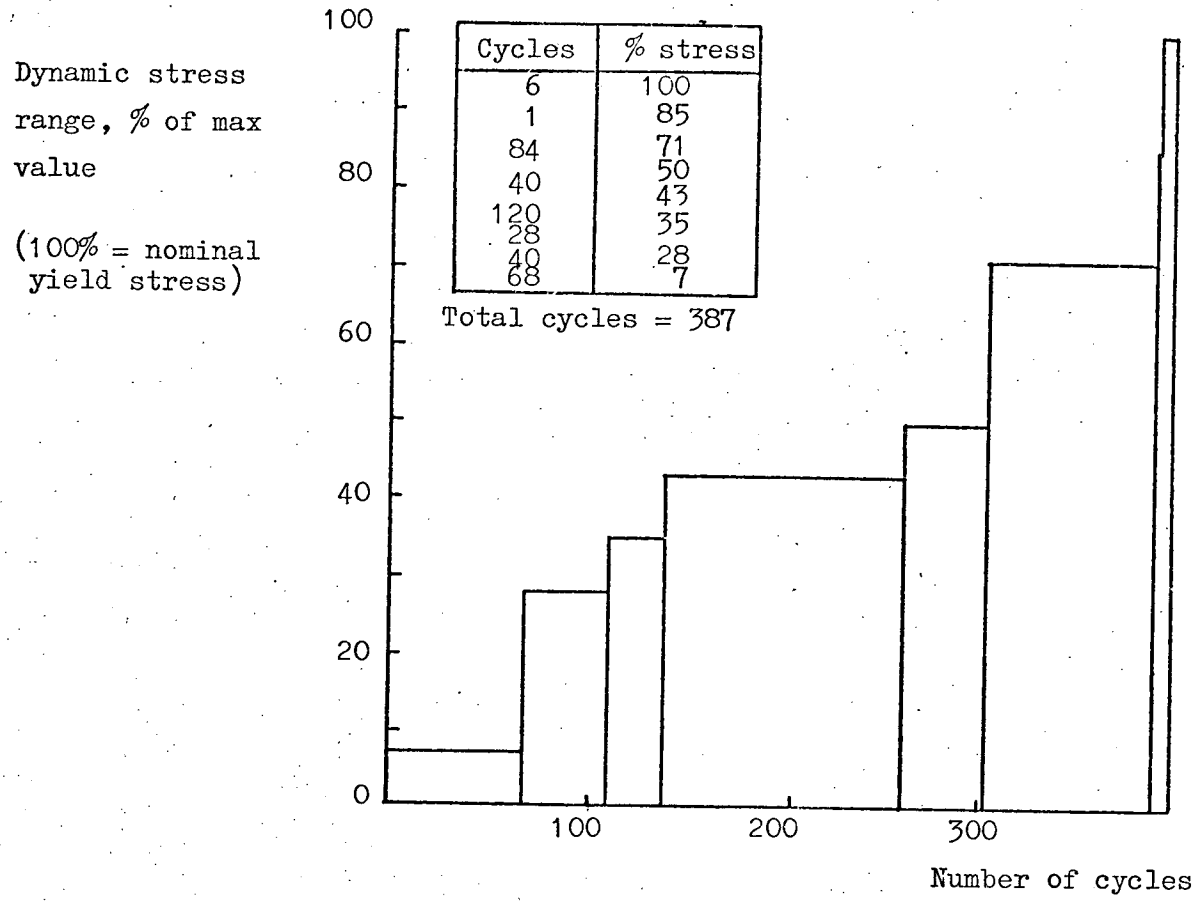

a) 8 Level test sequence proposed by NCRE

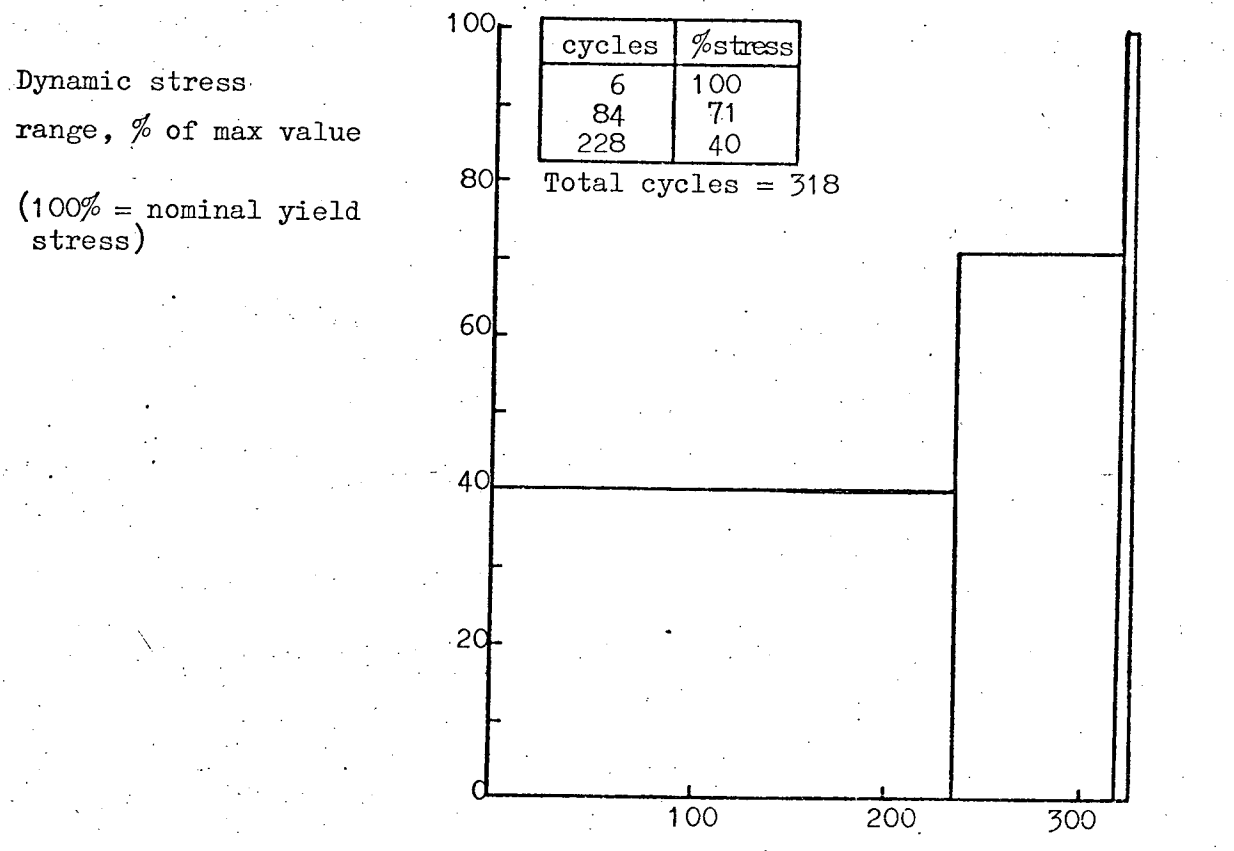

b) 3 level test sequence evolved from (a) above.

Figure 4.28 Dynamic "stress" ranges used in block loading tests.

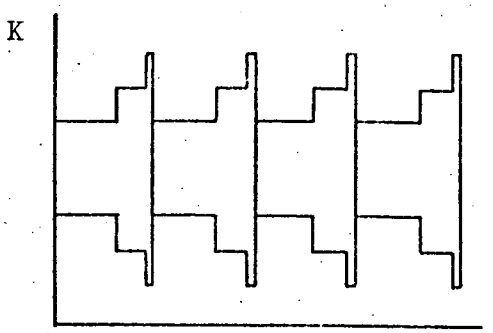

a) $\overline{K}$ = constant, low-high

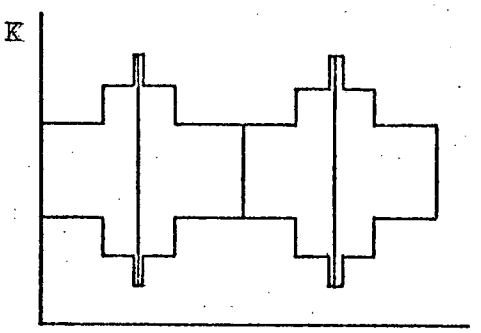

b) $\overline{K}$ = constant, low-high-low

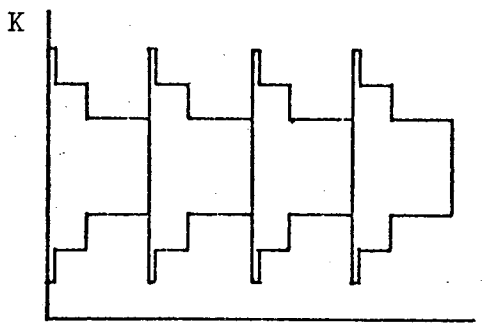

c) $\overline{K}$ = constant, high-low

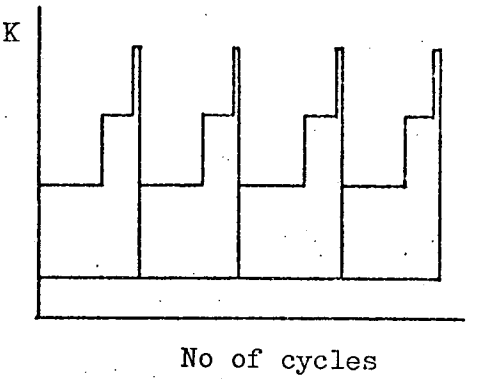

d) K_{min} = constant, low-high

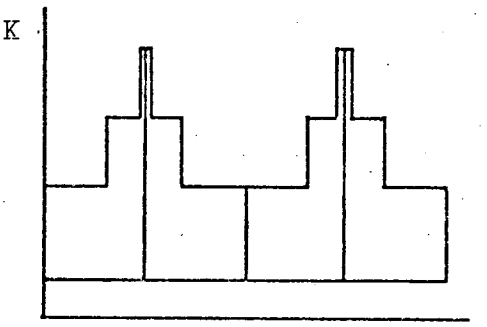

e) K_{min} = constant, low-high-low

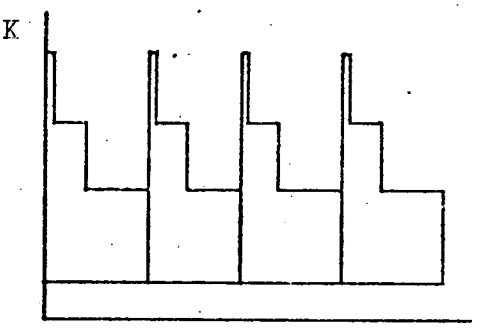

f) K_{min} = constant, high-low

Figure 4.29 Schematic representation of the six, three level, block loading sequences used. Details of stress intensity levels and number of cycles per block are given in Figure 4.28(b).

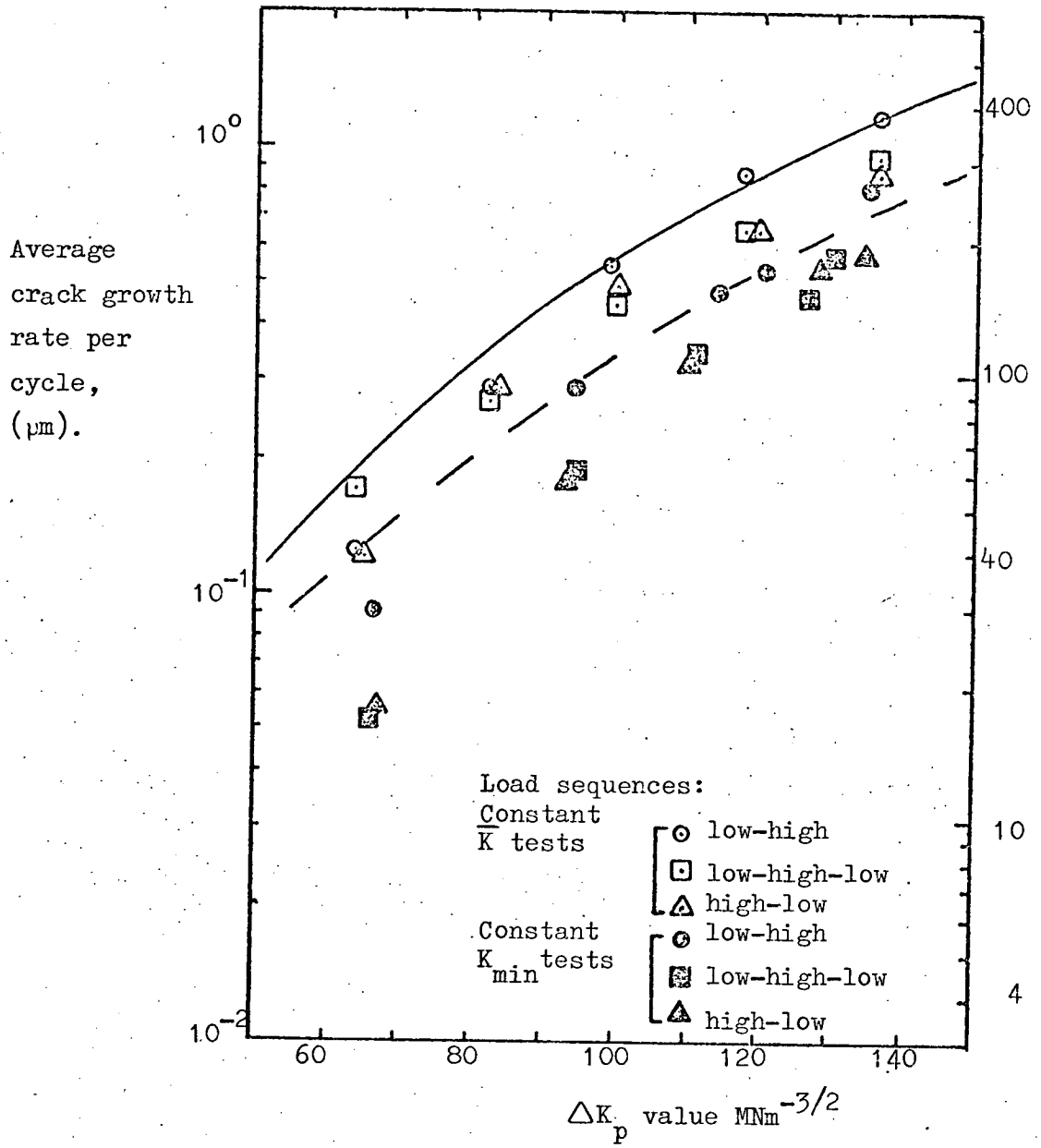

Continuous line: Growth rate predicted by linear summation of equilibrium rates for all blocks.

Broken line: Growth rate predicted by linear summation of equilibrium rates for two highest load blocks only.

Figure 4.30 Crack growth rates measured under 3 level block loading conditions. Details of the load sequences are given in Figure 4.29.

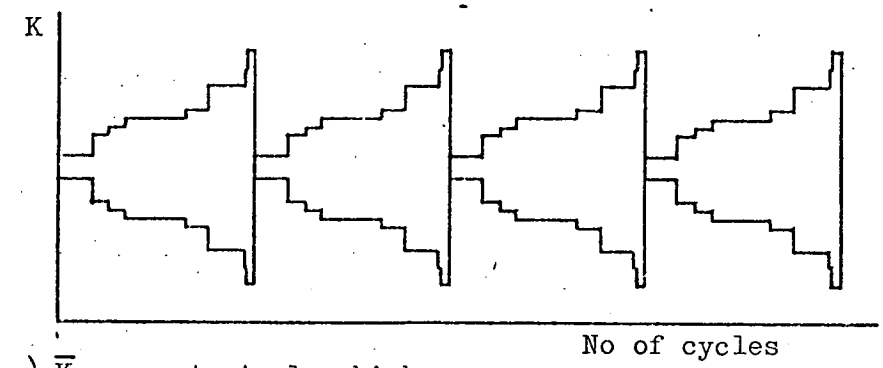

a) $\overline{K}$ = constant, low-high

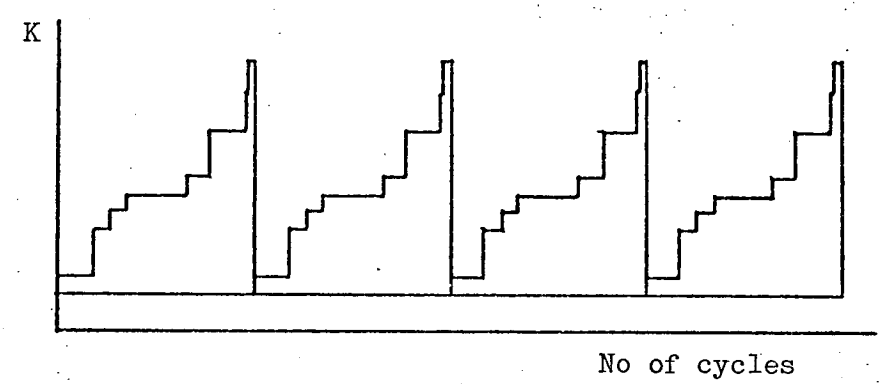

b) K_{min} = constant, low-high

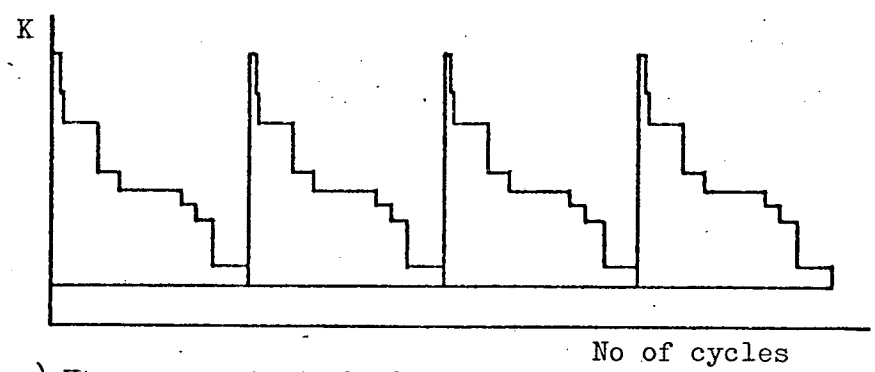

c) K_{min} = constant, high-low

Figure 4.31 Schematic representation of the three eight level, block loading sequences used. Details of stress intensity levels and number of cycles per block are given in Figure 4.28a.

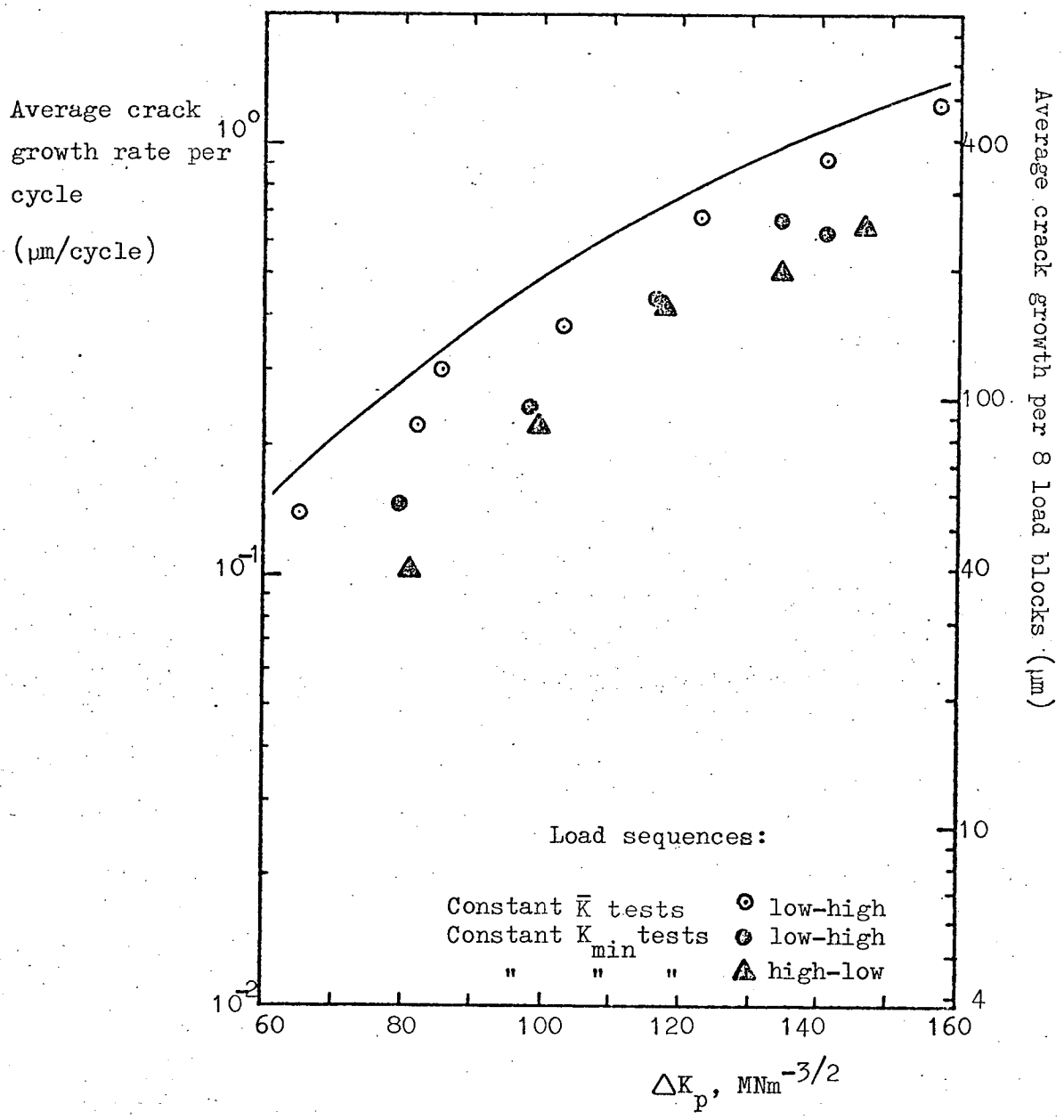

Continuous line: Growth rate predicted by linear summation of equilibrium rates for all blocks.

Figure 4.32 Crack growth rates measured under 8 level block loading conditions. Details of the load sequences are given in Figure 4.31.

CHAPTER 5

METALLOGRAPHY AND FRACTOGRAPHY

5.1 Preamble

The results presented in this chapter are all of a photographic nature. Conventional optical micrographs of polished and etched sections of Q1(N) are presented first, these are followed by a series of optical macro-photographs of typical fatigue fracture surfaces. The final part of the chapter presents a sequence of micrographs of fracture surfaces obtained from the scanning electron microscope. The conventional format of the various optical photographs makes their interpretation straight forward. Specific details relating to individual figures are given in both the main text and in the captions. The SEM fractographs are less readily understood. It has become apparent that readers who are not familiar with the appearance of fatigue fracture surfaces in Q1(N) may initially experience considerable difficulty in distinguishing "features" that are readily apparent after more prolonged study. An attempt has been made to mitigate this difficulty by prefacing the detailed description of the SEM fractographs with a brief explanatory section which is intended to give an overall view of the results that are subsequently, individually described in greater detail. The relevant section, which is designated 5.4.1, may be omitted advantageously by readers who have experience of SEM fractography of Q1(N).

5.2 Microstructure of Q1(N)

As part of a general survey of the basic properties of Q1(N) a brief investigation was made of its microstructural characteristics. Structures were examined from the same six samples that were subjected to hardness investigations. Specimens were cut from the CKS samples to permit examination of three mutually perpendicular faces, each one lying parallel to one of the original plate surfaces. Apart from the carbide banding mentioned below no significant variation was detected between the differently oriented material. The specimens were examined for structural variation through the plate thickness. No major inhomogeneities were detected. However both the transverse surfaces* did exhibit very slight carbide segregation in the form of "banding". The effect was most readily detected at the plate mid thickness, but even there it was not uniformly present. Where the "bands" could be distinguished their separation was approximately 200μm. No "banding" was observed on surfaces lying parallel to the rolling plane of the plate.

Typical microstructures are shown in Figures 5.1 and 5.2. In each case the near surface and plate mid thickness structures are shown for two of the orientations examined. A trivial, and representative, example of "banding" can just be detected in the lower right hand corner of Figure 5.1(b). This apart, the figures demonstrate the noteable uniformity of the Q1(N) microstructure.

5.3 Optical Fractography

The surface roughness of Q1(N) fatigue fracture surfaces prohibits optical examination at high magnifications. However some information can be gained from low magnification work. Figure 5.3 shows how both mean and dynamic stress intensity conditions effect the fracture surface appearance. In each case ΔK was maintained constant whilst

*i.e. The surfaces lying perpendicular to the short transverse and

periodic "step-like" increases in $\overline{K}$ were applied. Thirteen different levels of mean stress intensity are shown in each photograph. The points at which $\overline{K}$ was increased are not clearly visible except in the lower part of Figure 5.3a where clearly defined "steps" are seen. Careful examination of the other photographs reveals similar, but less distinctive, features. It is seen that surface roughness increases with both $\overline{K}$ and ΔK.

It was stated in section 4.2.3 that under constant dynamic stress intensity conditions a reduction of $\overline{K}$ resulted in crack tip tunelling. This change in crack front profile is readily confirmed by optical examination of the fracture surface. Figures 5.4(a) and (b) show the effect under a variety of conditions. The points of mean stress reduction, marked in each photograph, are seen to be followed by a "smooth" region in which the centre of the crack front clearly tunnels ahead of the edges. The "rougher" region that follows results from returning the mean stress intensity to its original value. Under these conditions the crack front is seen to straighten to its original shape. The duration of the tests was insufficient to determine how long the curved profile would have persisted at the lower value of $\overline{K}$.

Fracture surfaces produced by the dynamic overload tests reported in Section 4.2.4 varied considerably in appearance. At high values of n_L/n_H both single and twenty cycle overloads create a visible "step" on the surface. These features are most readily seen when the difference between ΔK_L and ΔK_H is large. At lower values of n_L/n_H the fracture surface assumes a more uniform appearance as a result of the frequent overloads. When n_L/n_H is less than 50 the surface cannot be distinguished from that produced by uninterrupted loading at the ΔK_H level. Figure 5.5 shows full width fracture surfaces resulting from different dynamic overload conditions applied when $\Delta K_L = 30$ MNm$^{-3/2}$. The "smooth" fracture surface associated with this dynamic stress intensity optimises the visibility of features created by the overloads. Figure 5.6 shows

the surface produced when $\Delta K_L = 50 MNm^{-3/2}$ and $\Delta K_H = 130\ MNm^{-3/2}$. The difference, $\Delta K_H - \Delta K_L$, is the same as for the surface shown in Figure 5.5(b). The increased relief associated with the higher value of ΔK_L is seen to reduce the clarity of the overload features; this apart, the two surfaces are seen to be generally similar. At higher values of ΔK_L the influence of overloads becomes even less distinct, Figure 5.7 shows the effect of two overload conditions applied when $\Delta K_L = 70 MNm^{-3/2}$. The resulting features are seen to be less clear than in the previous figures as a result of the general increase in surface roughness associated with the prevailing value of ΔK_L. The trend is for the facture surfaces to assume a more uniform appearance as the value of ΔK_L is increased.

Optical examination of the fracture surfaces produced under 3 and 8 level block loading conditions was not very rewarding. Figure 5.8 shows the fracture surfaces produced by the different three level sequences detailed in section 4.2.5. Parts (a), (b) and (c) of the figure present the surfaces created under constant mean stress intensity conditions. As one would expect the longer repetition period of the low-high-low sequence is seen to produce a more distinctly marked surface than those created by the other two regimes. For tests under conditions of constant K_{min} the different load regimes were applied sequentially at the same ΔK_p value. Figure 5.8(d) shows the surface that resulted; the various loading conditions are detailed at the edge of the photograph. It is possible to identify some of the low-high-low sequences from the more pronounced markings on the fracture surface. This apart, the surface produced under constant K_{min} conditions is notable only for its uniformity.

Very little difference is detectable between the fracture surfaces produced under 3 and 8 level block loading conditions. Figure 5.9 shows the results of 8 block tests performed under conditions of both constant $\overline{K}$ (5.9(a)) and constant K_{min} (5.9(b)). Details of the loading

conditions are given adjacent to the photographs. As with the 3 block tests the principal feature of these fracture surfaces is their uniform appearance.

5.4 Scanning Electron Microscope Fractography

5.4.1 Explanatory introduction to the appearance of SEM fractographs

All the photographs presented were taken when the specimen was tilted at 45° to the electron beam. Magnifications given are therefore nominal, being accurate only for the central part of the micrograph. In most photographs the direction of crack propagation was from left to right, however, different orientations occur in Figures 5.10 and 5.19. In every case the prevailing direction of crack growth has been indicated by an arrow placed beneath the photograph. A general impression of the features that are of importance in the detailed description of the fractographs may be gained from the abbreviated review that follows.

Consider first the characteristic tensile failure shown in Figure 5.20. Part (c) of the figure shows the "dimpled" appearance that is typical of ductile failure in a "clean" steel. Fatigue fracture surfaces created under high dynamic load conditions are shown in Figure 5.10(i) and (j). The dimples seen in the tensile failure are seen to have been replaced by "striations" which are normal to the direction of crack growth. For constant amplitude loading each striation corresponds to a single dynamic load cycle. The irregular or broken nature of the surface in Q1(N) can be seen from Figure 5.10(i). More complicated load sequences which have a repeated, or periodic, nature sometimes produce additional regularly spaced features. Figure 5.13(a) shows such an effect resulting from the application of periodic dynamic "overload" conditions. The "gross" features associated with the overloads are superimposed on a fracture surface that

is characteristic of the prevailing ΔK_L^- conditions.

The block loading conditions used in the present study also had a repetative nature. The periodicity of the load sequence can sometimes be distinguished in the scanning electron microscope. When actually operating the instrument the observer has the advantage of being able to continuously vary the magnification used, thus micro-features, such as individual striations, can be correlated with the macro-appearance of the fracture surface. Figures 5.16(a) and (b) exemplify this procedure. Consider first the general appearance of part (a) of the figure. A distinct "dark" vertical band approximately 3mm wide is seen a quarter of the way across the photograph from the left. Similar but less well defined bands can be seen at the centre and three quarters right positions. Do these represent the load periodicity? The problem was resolved by higher magnification studies of the bands. Part (b) of the figure shows one of the bands at higher magnification. At the top left is a small region of particularly clear striations, indicated "S", which stop abruptly at a definite vertical break line. The striations, which are typical of high dynamic loading conditions, can be seen both above and below the indicated area. The region ("L") immediately to the right of the line has no apparent striations, (confirmed at even higher magnification), and is generally typical of crack growth under low dynamic loads. Thus, with the prior knowledge that the region was formed under a "low-high" three level block loading sequence, the vertical break line in Figure 5.16(b) can be positively identified as the high/low load discontinuity. Examination of several such regions positively identifies the "bands" seen in part (a) of the figure as the product of the lowest load block of the three level sequence. Thus the periodicity of the sequence may be measured from the micrograph and compared with the growth rate deduced from ultrasonic macro-growth measurements.

The eight level block load sequences investigated posed similar problems of identification. The test sequence meant that the prevailing loading conditions had in part to be deduced from the fractographs. Figure 5.18 shows a case where this was successfully achieved. Part (c) of the figure is outwardly uniform in appearance. However, closer examination reveals a possible "break" line at the centre; striations may be seen to the left and right but not in the central section. Part (d) of the figure shows the left hand half of the previous photograph at a higher magnification. A clear sequence of increasingly distinct striations can be seen leading up to a "break" line at the extreme right of the photograph. Thus the 8 level load sequence can be positively identified as being of the "low-high" type.

The above constitutes a brief introduction to the SEM examination of Q1(N) fracture surfaces. A detailed description of the influence of different load sequences is given in the sections that follow.

5.4.2 Fracture surfaces created by simple loading conditions

A brief survey was made of the fracture surfaces created under conditions of constant dynamic stress intensity. Figure 5.10 shows typical micrographs of surfaces produced at five different values of ΔK. The pairs (a)/(b), (c)/(d), (e)/(f) of the figure show that the topography was much less influenced by mean stress intensity than by the dynamic loading conditions. The extremely "broken" appearance of the fracture surfaces shown in the figure is typical of those examined by the author. It is important to appreciate that where striations existed as very clear features, e.g. Figure 5.10(j), the regularity was localised, the overall picture was more confused, e.g. 5.10(i). Fatigue striations were readily identified on fracture surfaces produced at the higher ΔK values investigated. Under lower dynamic stress intensity conditions the surfaces were more broken and showed fewer regions of clearly defined markings. Measurements of

striation spacings indicated a "one to one" correspondence with the applied load cycles. The fracture surface created at a dynamic stress intensity of $25MNm^{-3/2}$, the lowest value of ΔK investigated, exhibited no characteristic fatigue features; instead poorly defined markings lying parallel to the direction of crack growth were observed; (see Figure 5.10(a)).

SEM examination of fracture surfaces produced by dynamic overload conditions has been concentrated principally on those tests in which ΔK_L was $30MNm^{-3/2}$. The tests were conducted at a constant mean stress intensity of $100MNm^{-3/2}$. The fracture surface associated with these conditions, in the absence of any overloads, is shown in Figure 5.11. It has a generally broken and irregular appearance having no significant areas of clear striations or other markings. The effect of a single overload cycle is shown in Figure 5.12(a) and (b), whilst part (c) of the same figure shows the result of a 20 cycle overload sequence. For both overload conditions ΔK_H was $110MNm^{-3/2}$; these are the same conditions that produced the surface shown in Figure 5.5(b) where both single and multiple overloads were seen to produce optically resolvable "steps" at high values of n_L/n_H. The marked difference between the two overload steps is clearly seen from the SEM micrographs. The 20 cycle regime results in a clearly striated zone in which a pronounced secondary crack is located. It is interesting to note that the well defined "step" that results from a single overload cycle is not seenat the start of the region damaged by the 20 cycle sequence. Approximate measurement of the different features shows that the "damage area" associated with the 20 cycle condition extends only 3 to 4 times the distance of that resulting from the single cycle. The extent of the "damage area" produced by the single cycle is in good agreement with the predicted cyclic crack growth increment under the overload conditions applied. No features were observed to distinguish the post-overload fracture surface from the

equilibrium appearance shown in Figure 5.11.

Figure 5.13 shows the fracture surface that results from multiple repetition of a single overload cycle. The sequence shows how the surface appearance changes as the interval between overloads is reduced. Where the overloads are isolated they produce the features shown in Figure 5.13(a) and (b); the surface in between the overloads being typical of that produced under equilibrium ΔK_L conditions. As the interval between overloads is reduced the low load growth region is progressively diminished until it cannot be detected at all. Figure 5.13(d) shows the surface when $n_L = 1$ and $n_H = 1$; even at higher magnifications no evidence of the alternate low load cycles is detectable. The appearance is typical of the surface produced under equilibrium ΔK_H conditions, c.f. Figure 5.10(h). Figure 5.14 comprises a similar sequence of micrographs for periodic 20 cycle overloads. Again the low load growth region becomes increasingly indestinct as the ratio n_L/n_H is reduced. The final micrograph, (d), shows the surface created when $n_L = 20$, $n_H = 20$; the appearance is indistinguishable from that produced by constant amplitude loading at $\Delta K = \Delta K_H$.

Limited studies have been made of fracture surfaces created when dynamic overloads were applied to higher values of ΔK_L. The smaller difference between ΔK_L and ΔK_H together with the increased "roughness" of surfaces makes the features associated with the overloads more difficult to identify. Parts (a) and (b) of Figure 5.15 show the influence of a single cycle overload when $\Delta K_L = 70 MNm^{-3/2}$ and $\Delta K_H = 130 MNm^{-3/2}$. Parts (c), (d) and (e) of the same figure show similar micrographs for 20 cycle overload conditions. At these load levels single cycle overloads can be located at low magnifications when there is extensive growth between cycles, e.g. Figure 5.15(a). However, at higher magnifications or lower values of

n_L/n_H the point of overload application can no longer be detected. The 20 cycle overload sequence is more readily located at high values of n_L/n_H, however, it is seen from Figure 5.15(e) that the features can not be positively identified at low values of n_L/n_H. Broadly speaking the overload features produced at high values of ΔK_L are similar to, but much less pronounced than those created at the lowest ΔK_L value used in this work.

5.4.3 Fracture surfaces created under block loading conditions

Fracture surfaces produced under block loading conditions were difficult to study as a consequence of their extremely irregular appearance. The few features that did exist were most clearly seen at the lowest values of ΔK_p employed. Figure 5.16 shows typical fracture surfaces produced under 3 level, constant mean stress intensity conditions. Under "low-high" and "low-high-low" regimes the periodicity of the 3 block sequence can be seen at low magnifications, e.g. Figure 5.16(a) and (c). At higher magnifications the different load levels can sometimes be identified but it is not possible to accurately determine where the load changes occur. The "high-low" load sequence, Figure 5.16(e) and (f), produced a more "broken" surface than the other two regimes. Neither the periodicity of the regime nor the effect of the different load levels could be detected.

Testing under constant K_{min} conditions produced surfaces similar to those discussed above. Figure 5.17 shows typical surfaces for each of the load sequences employed. None of the regimes produced a clear "periodicity" at low magnifications, at higher magnifications the effects of the different load levels could sometimes be identified. As with the constant mean stress intensity tests the extremely broken nature of the fracture surface prevented quantitative measurement of the crack extension occurring at each individual load level.

The fracture surfaces produced by eight level block test sequences closely resemble those described above for three level tests. Figure 5.18 shows the surface created by the application of the "low-high" load sequence at constant mean stress intensity. The "break line" that corresponds to the high-low load discontinuity can be seen quite clearly at the left of part (b) of the figure. (Striations are seen to give way to features lying parallel to the direction of propagation). Despite the ease with which this feature was located the surface did not exhibit a clear periodicity at lower magnifications. The fracture surfaces resulting from the two eight block constant K_{min} test sequences were very similar in appearance. Figures 5.18(c) and (d) show a particularly clearly marked region that was identified as corresponding to the "low-high" load sequence. In general, identification of individual regions was not possible; no"high-low" regions were positively located.

5.4.4 Fracture surfaces created by monotonic failure

An SEM examination was made of the surface of the sample used for the fracture toughness tests reported in section 4.1.4. Figure 5.19 shows the fracture surface at the point corresponding to test number 3, (see Table 4.2). The test load sequence was: zero $\rightarrow$ P_{max} $\rightarrow$ zero; this fully reversed condition produced a "step-like" surface feature similar to that caused by a single dynamic overload, c.f. Figure 5.12(b). It is interesting to compare the stretch zone produced under these two loading conditions with the appearance of a typical tensile failure produced by monotonically loading Q1(N) to failure. Figure 5.20 shows the surface that results from loading to failure a CKS specimen previously fatigue cracked to an a/W value of 0.7. The crosshead displacement rate was 1mm per second. Figure 5.20(a) shows the zone of transition from fatigue to monotonic tensile failure; details of

the tensile region are shown in parts (b) and (c) of the figure. The highly "dimpled" appearance of this section of the fracture surface is in sharp contrast to the featureless stretch zones produced by single cycle overloads and the fracture toughness tests.

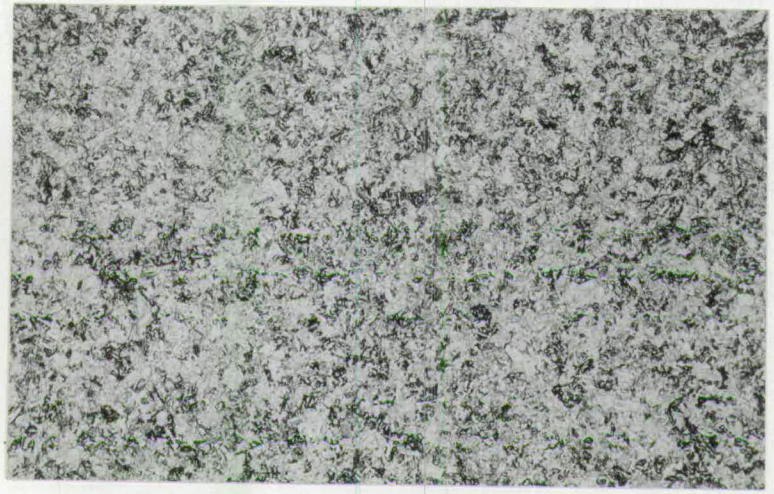

a) x55. Near surface, ↑ Short transverse Long transverse →

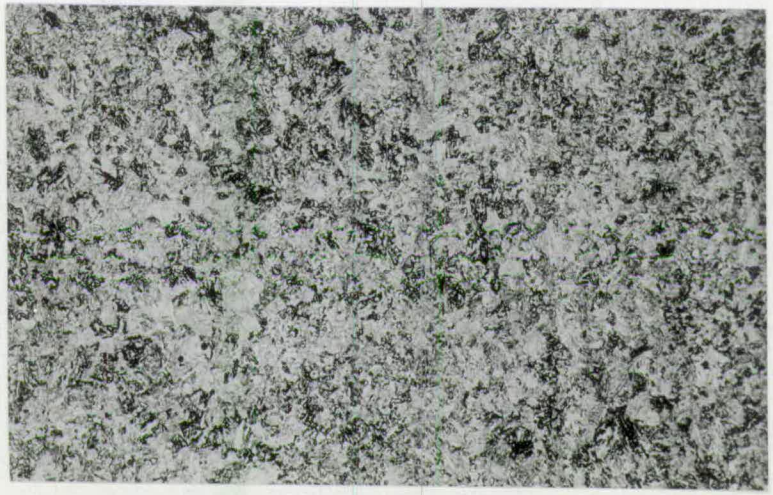

b) x55. Plate mid thickness, orientation as per (a).

c) x55. Near surface, ↑ Long transverse Rolling direction →

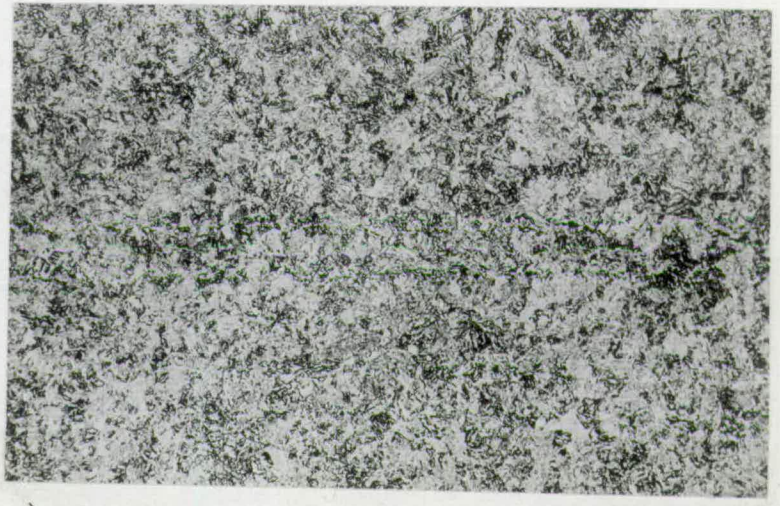

d) x55. Plate mid thickness, orientation as per (c).

Figure 5.1 Low magnification Q1(N) microstructures, (sample 12). Namasci interference. Etch: 3% HNO_3 in glycerol.

a) x563. Near surface ↑ Short transverse Long transverse →

b) x563. Plate mid thickness, orientation as per (a)

c) x563. Near surface ↑ Long transverse Rolling direction →

d) x563. Plate mid thickness, orientation as per (c).

Figure 5.2 Higher magnification studies of the areas shown in Figure 5.1. Etch 3% NHO_3 in glycerol. Namasci interference.

Figure 5.3 The influence of mean and dynamic stress intensity on the optical appearance of the fracture surface.

The fracture surface shown in each photograph was created under conditions of constant dynamic stress intensity. In each case the mean stress intensity was periodically increased as the crack advanced. The horizontal lines in the lower part of (a) indicate the points at which $\overline{K}$ was increased. Similar, less well defined, "steps" can be seen in the other photographs. Thirteen different values of $\overline{K}$ were applied to create the surfaces shown in each photograph.

Mean stress intensity values are given adjacent to the photographs. All photographs show the full fracture surface width.

Magnification: All x 2.5

Dynamic stress intensity values: a) 25 $MNm^{-3/2}$

b) 51 $MNm^{-3/2}$

c) 80 $MNm^{-3/2}$

NOTE

Heavy arrows below photographs indicate the direction of crack growth

5.3(a)

5.3(b)

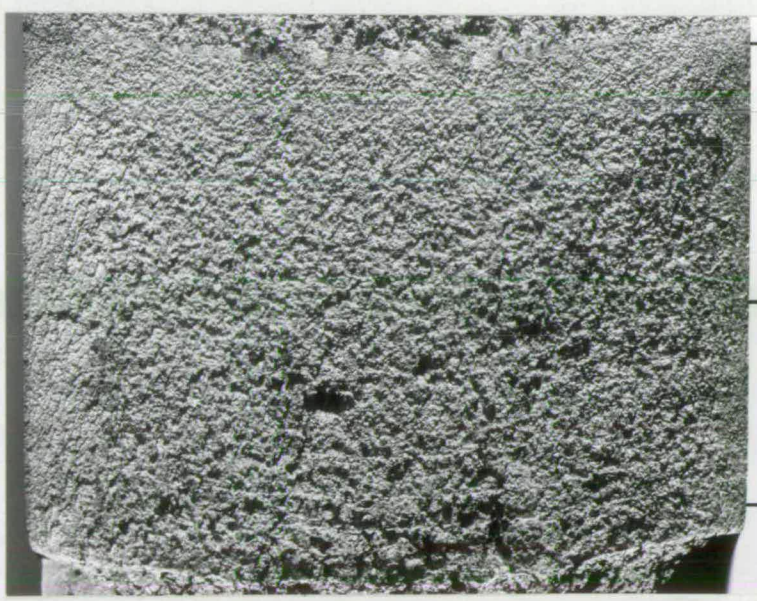

5.3(c)

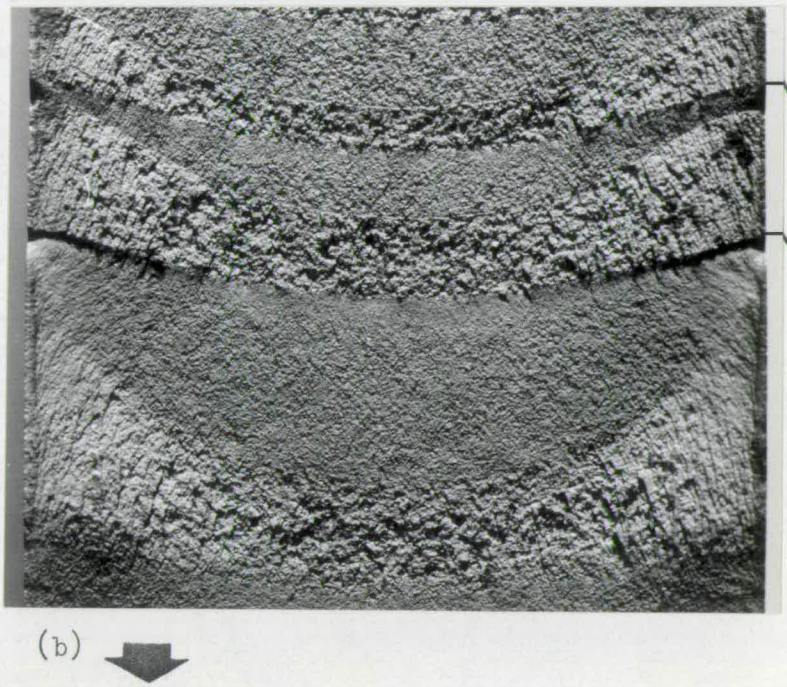

Figure 5.4 Examples of the "tunnelling" effect associated with reductions of the mean stress intensity.

Optical photographs of the full fracture surface width.
Magnification: Both x2.5.

Figure 5.5 Three examples of the effect of dynamic overloads on the fracture surface appearance.

Optical photographs of the full fracture surface width.

Magnification: All x2.5

Each photograph shows a crack growth interval during which ΔK_L and ΔK_H were maintained constant. n_L and n_H were varied; values are given to the right of the photographs where it was possible to identify the corresponding area of the fracture surface. The surfaces were created during the two level tests which were reported in Section 4.2.4.

Loading Conditions:

For all photographs: $\overline{K} = 100\ MNm^{-3/2}$, $\Delta K_L = 30\ MNm^{-3/2}$

a) $\Delta K_H = 70\ MNm^{-3/2}$ At top $n_H = 1$

At bottom $n_H = 20$

b) $\Delta K_H = 110\ MNm^{-3/2}$ At top $n_H = 1$

At bottom $n_H = 20$

c) $\Delta K_H = 150\ MNm^{-3/2}$ $n_H = 1$


n_L/n_H = 1300/1
480/1
1/1
1600/20
4000/20
560/20
200/20
20/20
Constant ΔK_L

5.5(a)

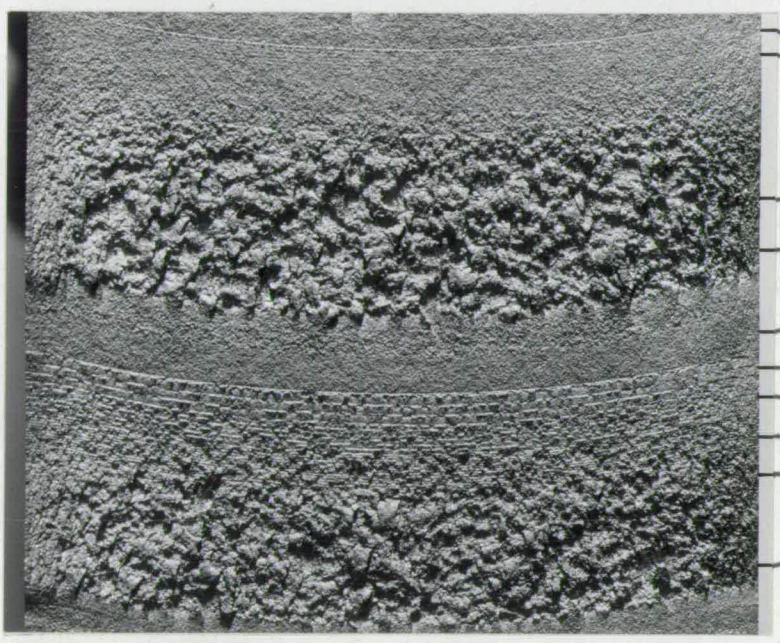
n_L/n_H = 1300/1
480/1
1/1
Constant ΔK_H
Constant ΔK_L
n_L/n_H = 4000/20
1600/20
560/20
200/20
20/20

5.5(b)

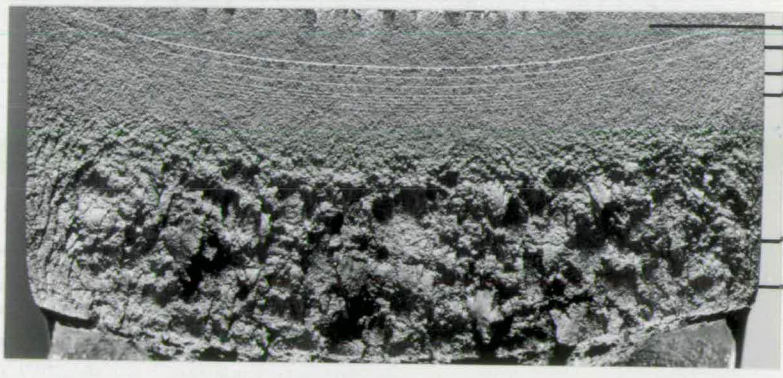
Constant ΔK_L
n_L/n_H = 3700/1
1300/1
480/1
1/1
Constant ΔK_H

5.5(c)

Figure 5.6 The effect of dynamic overloads on the appearance of the fracture surface when $\Delta K_L = 50\ MNm^{-3/2}$.

Optical photograph of the full fracture surface width.

Magnification: x2.5.

As per figure 5.5 the values of n_L and n_H are indicated wherever it was possible to identify the corresponding area of the fracture surface.

Loading conditions:

$\overline{K} = 100\ MNm^{-3/2}$, $\Delta K_L = 50\ MNm^{-3/2}$, $\Delta K_H = 130\ MNm^{-3/2}$

At top $n_H = 1$; at bottom $n_H = 20$.

Figure 5.7 The effect of dynamic overloads on the appearance of the fracture surface when $\Delta K_L = 70\ MNm^{-3/2}$.

Optical photograph of the full fracture surface width.

Magnification: Both x2.5.

As per Figure 5.5 the values of n_L and n_H are indicated wherever it was possible to identify the corresponding area of the fracture surface.

Loading conditions:

For both photographs: $\overline{K} = 100\ MNm^{-3/2}$, $\Delta K_L = 70\ MNm^{-3/2}$

a) $\Delta K_H = 110\ MNm^{-3/2}$ At top $n_H = 1$

At bottom $n_H = 20$

b) $\Delta K_H = 150\ MNm^{-3/2}$ $n_H = 1$

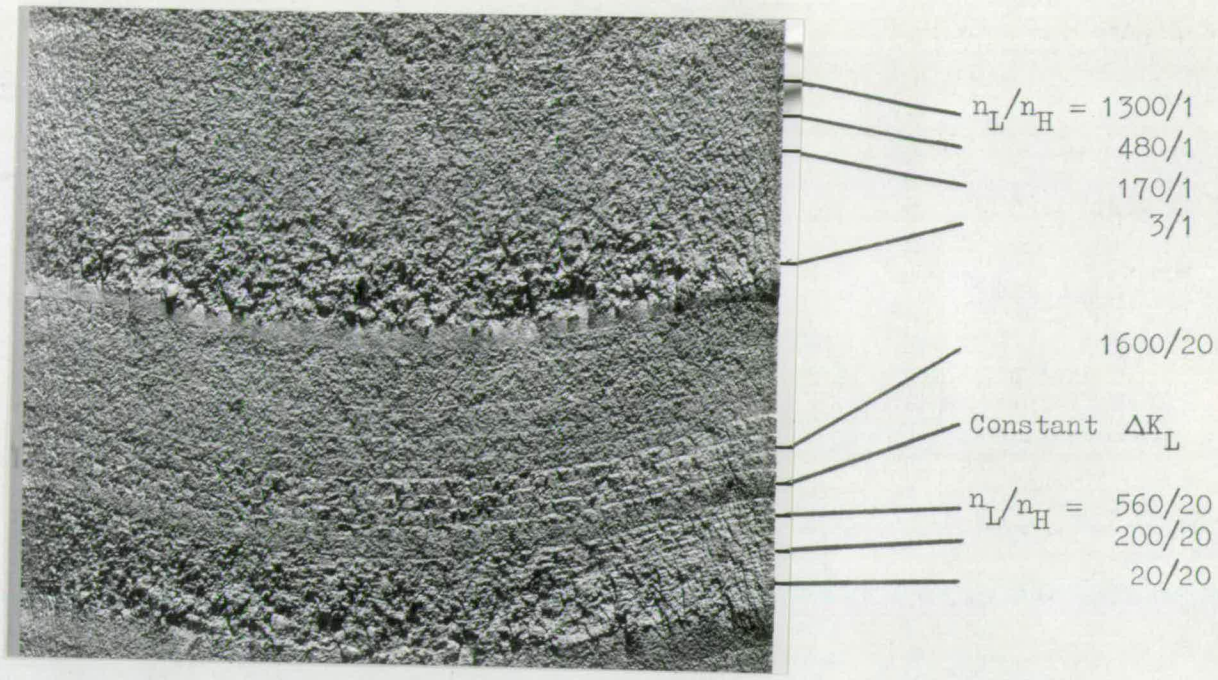
n_L/n_H = 1300/1
480/1
170/1
3/1
1600/20
Constant ΔK_L
n_L/n_H = 560/20
200/20
20/20

5.6

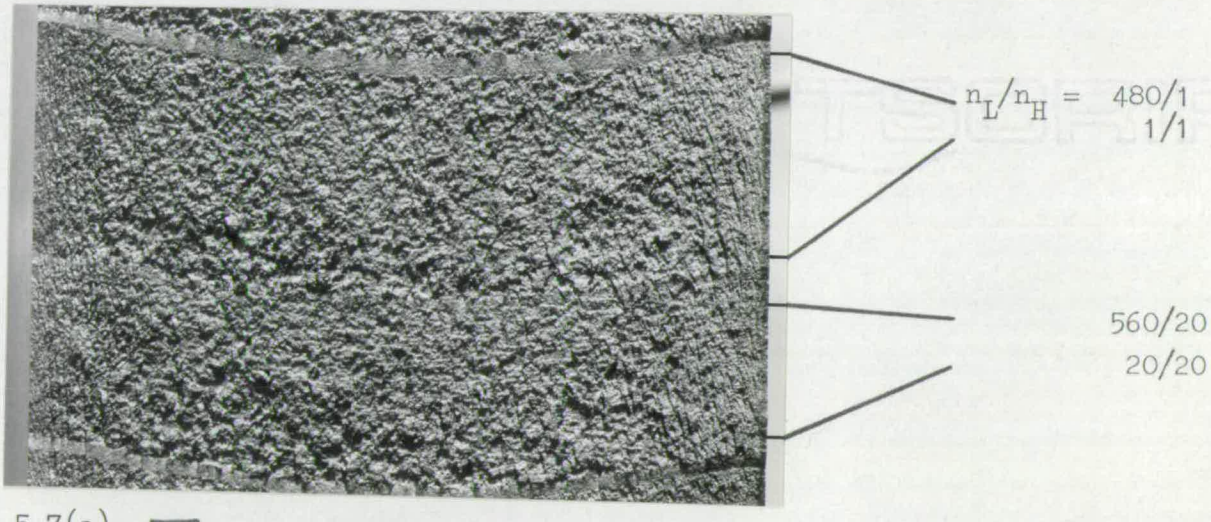
n_L/n_H = 480/1
1/1
560/20
20/20

5.7(a)


n_L/n_H = 170/1
1/1

5.7(b)

Figure 5.8 Appearance of fracture surfaces created by 3 level block loading regimes

Optical photographs of full fracture surface width.

Magnification: All x2.5.

See Figure 4.29 for the load sequences and notation.

a) "Low-high" sequence. $\overline{K}$ constant at 100 $MNm^{-3/2}$. Four values of ΔK_p as indicated at the right of the photograph.

b) "Low-high-low" sequence. $\overline{K}$ constant at 100 $MNm^{-3/2}$. Five values of ΔK_p as indicated at the right of the photograph.

c) "High-low" sequence. $\overline{K}$ constant at 100 $MNm^{-3/2}$. Five values of ΔK_p as indicated at the right of the photograph.

d) 3 block tests at constant K_{min}. K_{min} = 20 $MNm^{-3/2}$. 3 load sequences were used, see Figure 4.29 At each value of ΔK_p the sequences were applied successively; ΔK_p was then increased and each sequence was re-applied. The fracture surface is too uniform to permit identification of the area of growth corresponding to each loading condition. Those areas which have been identified are indicated at the right of the photograph.

5.8(a)

5.8(b)

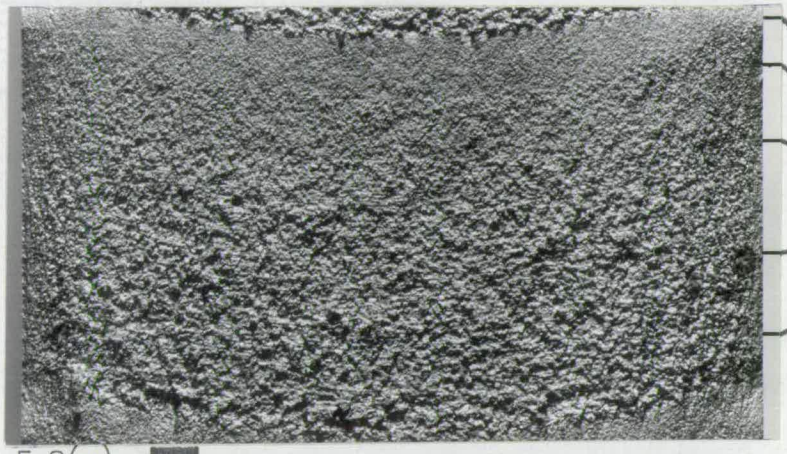

5.8(c)

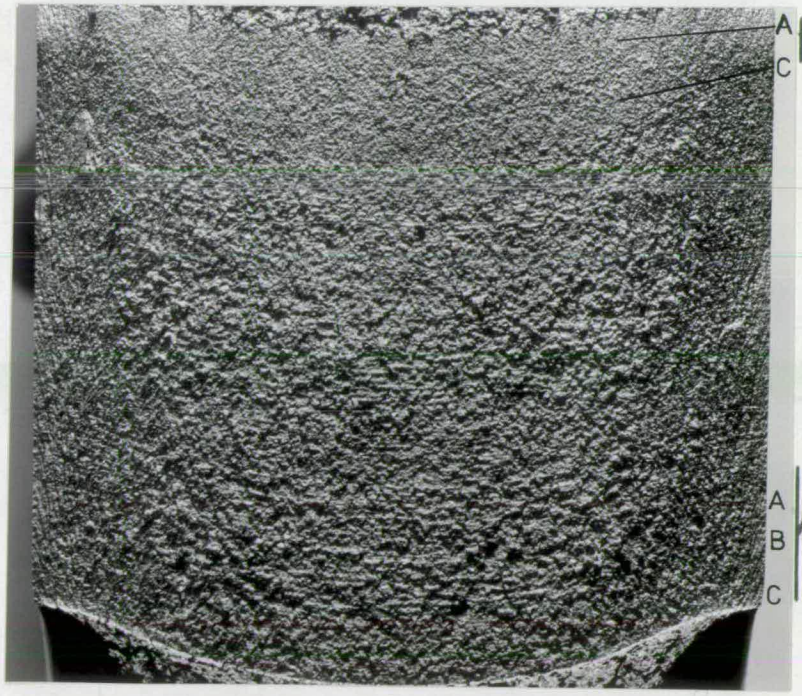

5.8(d)

Figure 5.9 Appearance of fracture surfaces created by 8 level block loading regimes

Optical photographs of full fracture surface width.

Magnification: Both x2.5.

See Figure 4.3i for the load sequences and notation.

a) "Low-high" sequence. $\overline{K}$ constant at 100 $MNm^{-3/2}$. This was the only sequence investigated under 8 level, constant $\overline{K}$ conditions. 7 values of ΔK_p were investigated in order of increasing magnitude; the corresponding areas are indicated, as far as possible, to the right of the photograph.

b) "Low-high" and "high-low" sequences at constant K_{min}.
K_{min} = 20 $MNm^{-3/2}$.
5 levels of ΔK_p were investigated in order of increasing magnitude. The two block load sequences were successively applied at each level. It is not generally possible to identify the growth area corresponding to each loading condition. Those areas which have been identified are indicated to the right of the photograph.

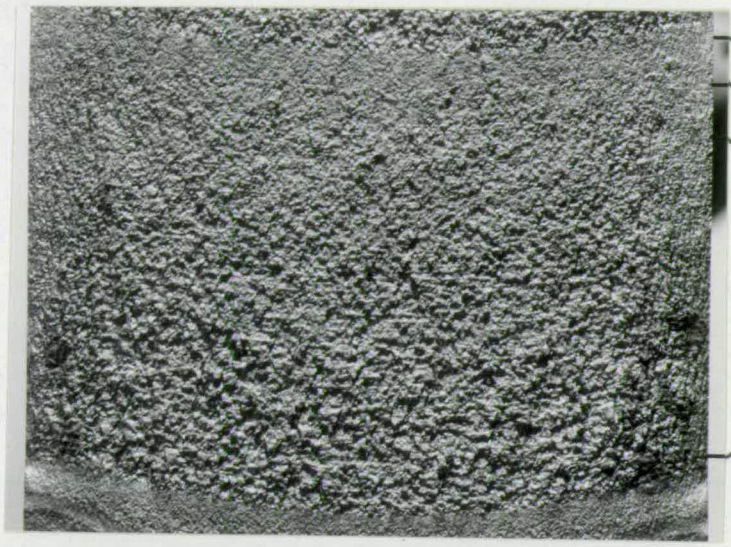
ΔK_p values $MNm^{-3/2}$
68
85
103
158

5.9(a)


C
A
A
C
C
A
81
99
117
143
Load Sequences
A = low-high
C = high-low

5.9(b)

Figure 5.10 Ten SEM fractographs showing the effect of $\overline{K}$ and ΔK on fracture surface appearance.

Magnifications are given below the individual micrographs.

Loading Conditions:

a) $\Delta K = 25$, $\overline{K} = 14$ $MNm^{-3/2}$

b) $\Delta K = 25$, $\overline{K} = 150$ $MNm^{-3/2}$

c) $\Delta K = 56$, $\overline{K} = 53$ $MNm^{-3/2}$

d) $\Delta K = 56$, $\overline{K} = 150$ $MNm^{-3/2}$

e) $\Delta K = 80$, $\overline{K} = 85$ $MNm^{-3/2}$

f) $\Delta K = 80$, $\overline{K} = 180$ $MNm^{-3/2}$

NOTE

Heavy arrows below photographs indicate the direction of crack growth.

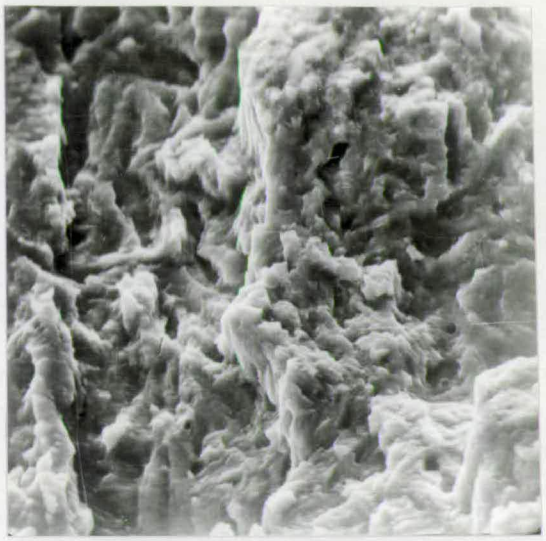

5.10(a) x1580

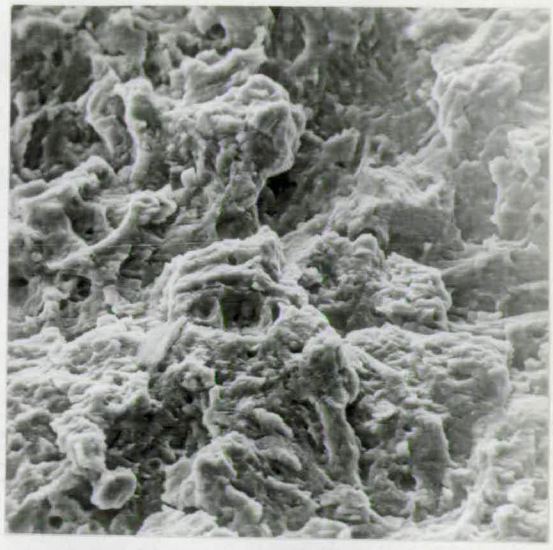

5.10(b) x770

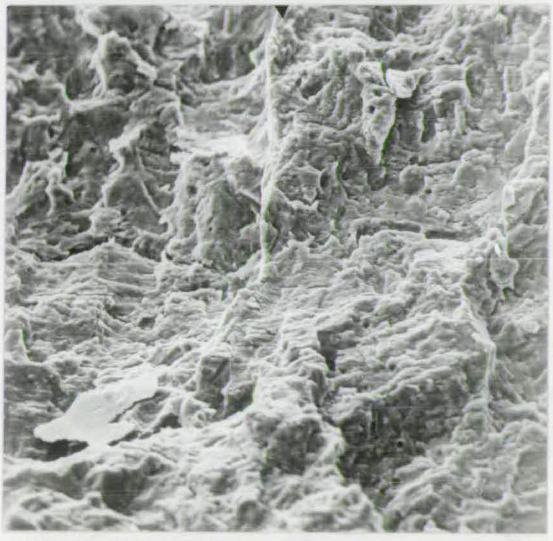

5.10(c) x440

5.10(d) x826

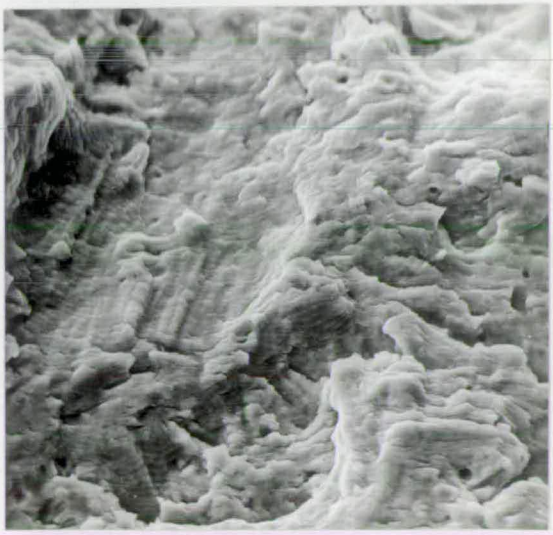

5.10(e) x950

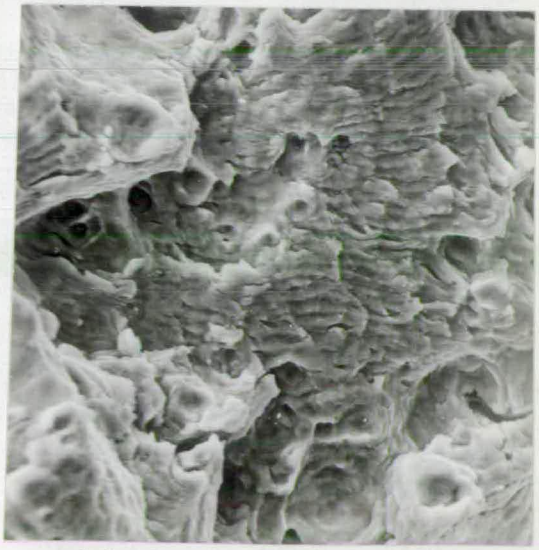

5.10(f) x966

Figure 5.10 (continued)

Loading conditions:

g) $\Delta K = 110, \quad \overline{K} = 100 \text{ MNm}^{-3/2}$

h) Detail from (g) at higher magnification

i) $\Delta K = 150, \quad \overline{K} = 100 \text{ MNm}^{-3/2}$

j) $\Delta K = 150, \quad \overline{K} = 100 \text{ MNm}^{-3/2}$

Figure 5.11 Fracture surface appearance at $\Delta K = 30, \quad \overline{K} = 100 \text{ MNm}^{-3/2}$. These are the ΔK_L conditions applied in the dynamic overload tests whose fracture surfaces are shown in the figures that follow.

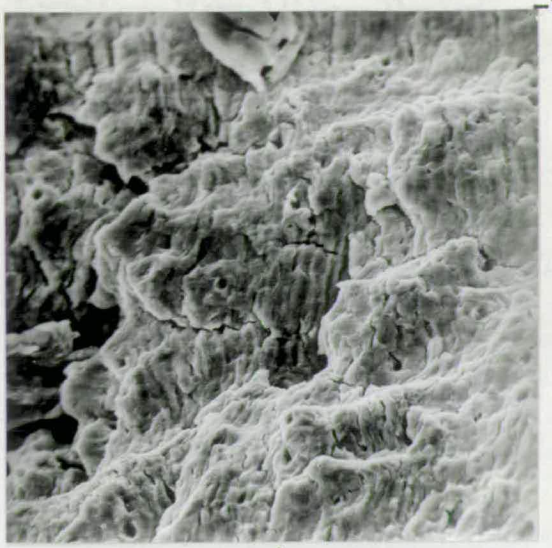

5.10(g) x840

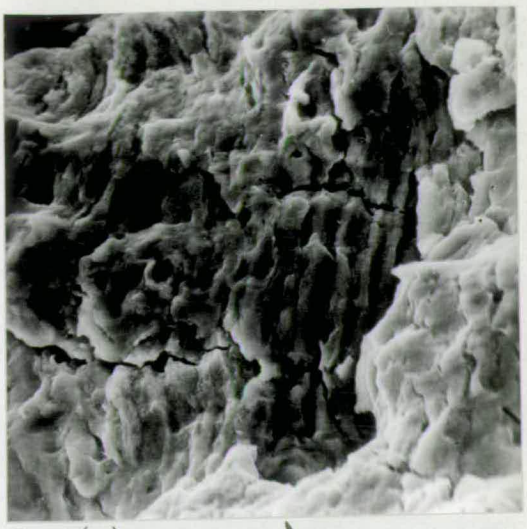

5.10(h) x1580

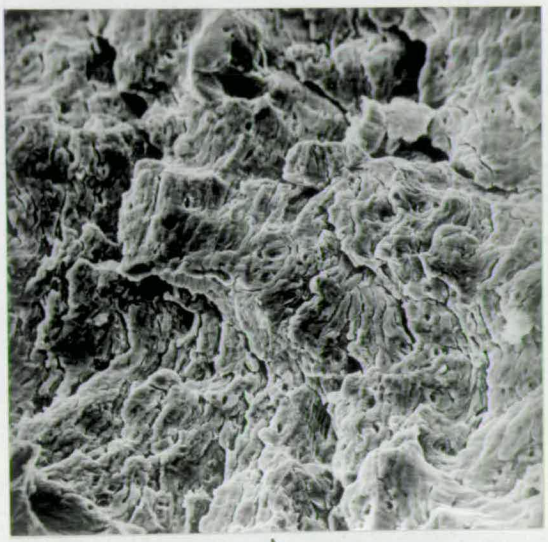

5.10(i) x434

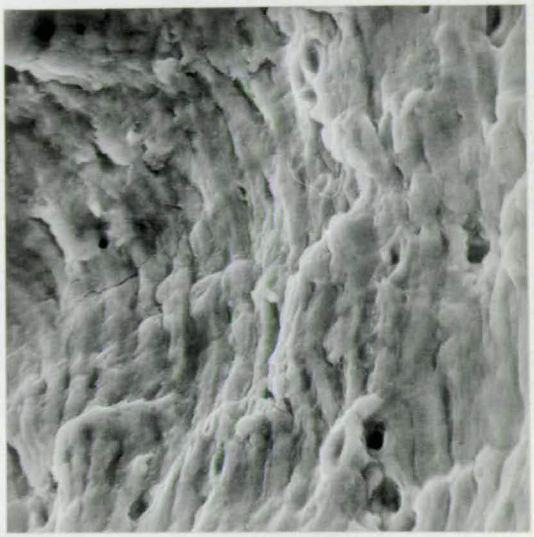

5.10(j) x1660

5.11(a) x400

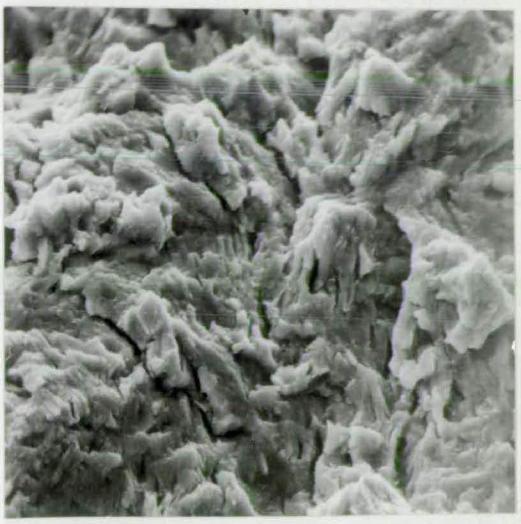

5.11(b) x1570

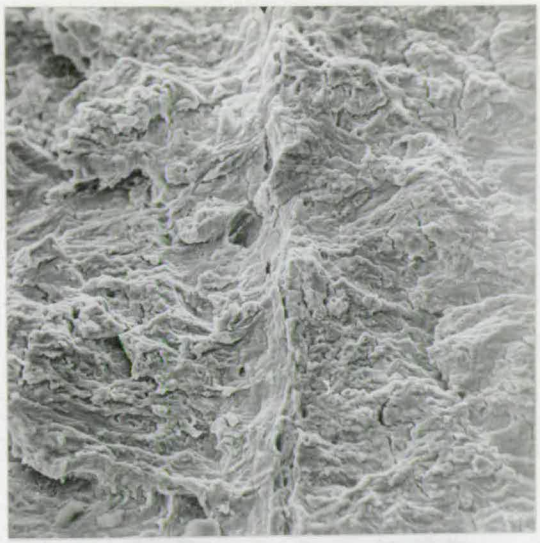

(a) x380

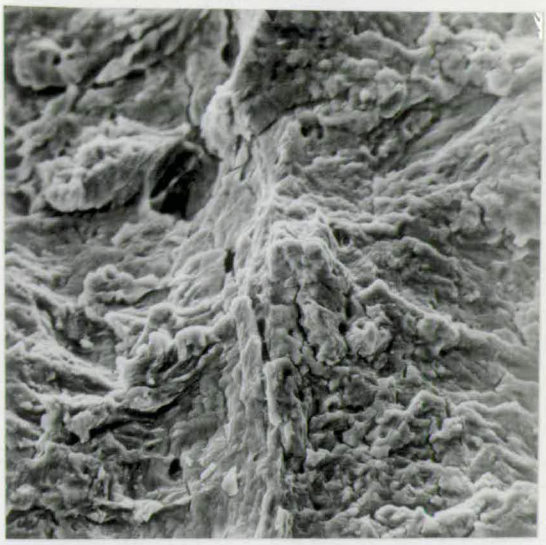

(b) x756

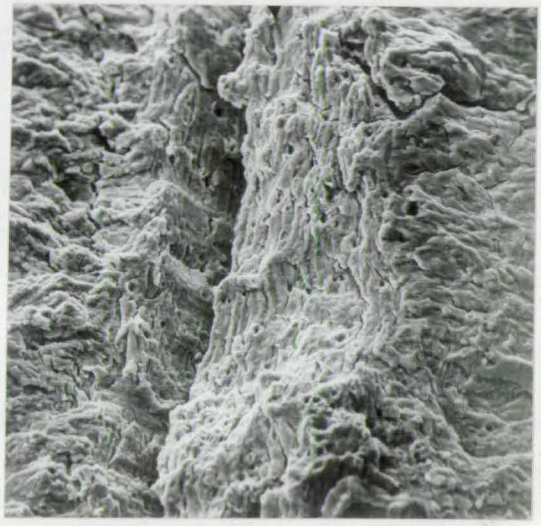

(c) x420

Figure 5.12 Dynamic overload tests. Fracture surfaces resulting from the tests reported in Section 4.2.4.

Loading conditions:

$\overline{K} = 100$, $\Delta K_L = 30$, $\Delta K_H = 110$ $MNm^{-3/2}$

a) $n_H = 1$; b) Detail from (a) at higher magnification

c) $n_H = 20$, note the striations similar to Figure 5.10h and the apparent bifurcation of the crack.

(a) x76

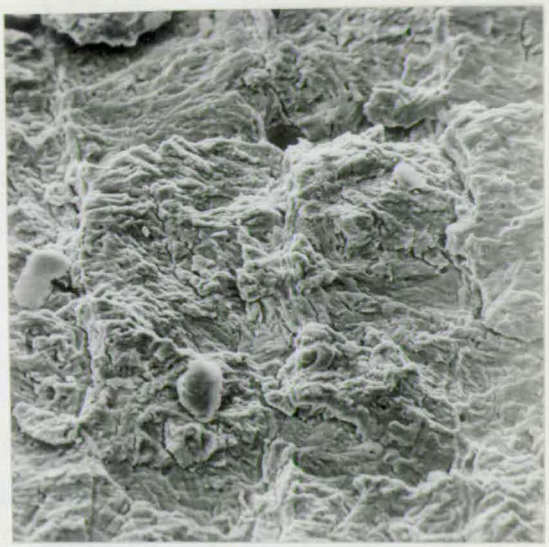

(b) x380

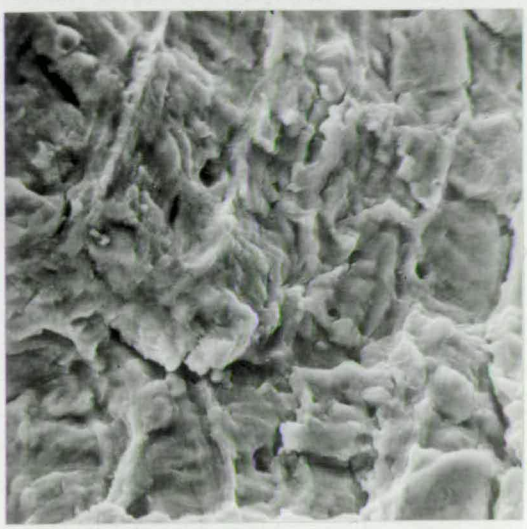

(c) x1500

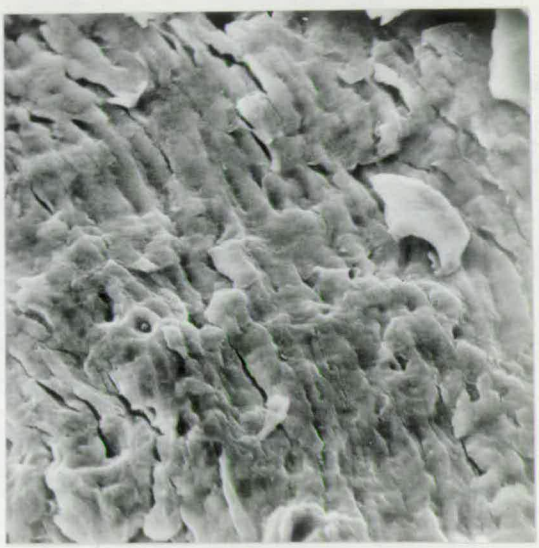

(d) x1550

Figure 5.13 The fracture surface resulting from the repetitive application of a single dynamic overload cycle, (n_H=1).

A sequence of fractographs is shown for different values of n_L/n_H. As the ratio is reduced the features produced by the overload became less distinct.

Loading conditions for all micrographs:

$\overline{K}$ = 100, ΔK_L = 30, ΔK_H = 110 $MNm^{-3/2}$ n_H = 1

a) n_L = 1300, b) n_L = 480, c) n_L = 60, d) n_L = 1

(a) x40

(b) x440

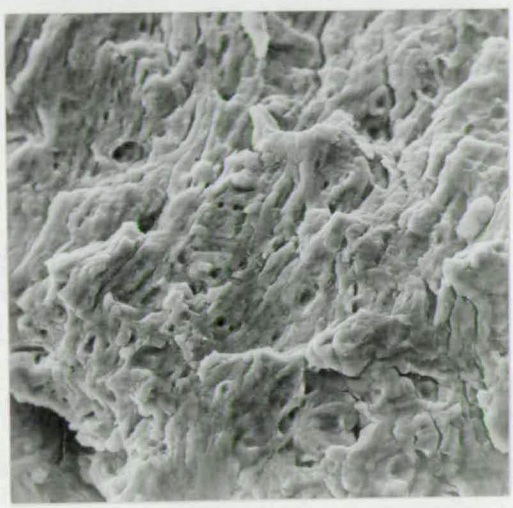

(c) x850

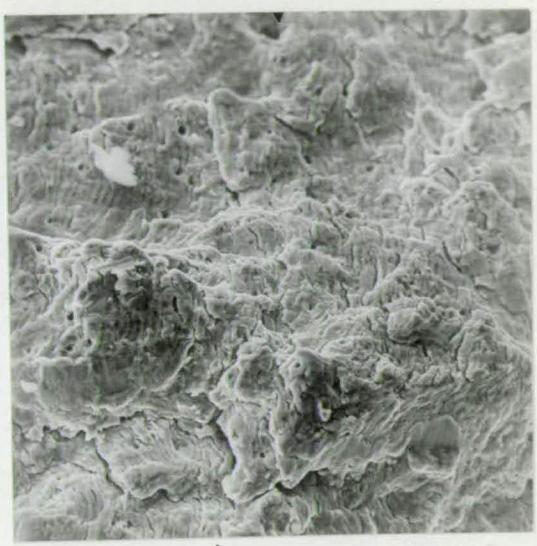

(d) x430

Figure 5.14 The fracture surface resulting from 20 cycle dynamic overload conditions.

A sequence of fractographs is shown for different values of n_L/n_H. As the ratio is reduced the features produced by the overload cycles become less clear.

Loading conditions for all micrographs:

$\overline{K} = 100$, $\Delta K_L = 30$ $MNm^{-3/2}$, $n_H = 20$

a) $\Delta K_H = 90$ $MNm^{-3/2}$; From the left the intervals (n_L) between overloads are 3200, 2650, 2200, 1800, 1500 and 1250 cycles.

b) $\Delta K_H = 90$ $MNm^{-3/2}$, $n_L = 420$.

c) $\Delta K_H = 110$ $MNm^{-3/2}$, $n_L = 80$.

d) $\Delta K_H = 110$ $MNm^{-3/2}$, $n_L = 20$.

Figure 5.15 Fracture surfaces produced by dynamic overload tests when $\Delta K_L = 70\ MNm^{-3/2}$

Loading conditions for all micrographs:

$\overline{K} = 100,\ \Delta K_L = 70,\ \Delta K_H = 130\ MNm^{-3/2}$.

a) $n_L = 480,\ n_H = 1$

The overload features are just resolvable at this magnification. (The heavy line at the right is a scribe line).

b) Part of (a) at higher magnification.
The overload features could not be identified at this and higher magnifications.

c) $n_L = 1600,\ n_H = 20$

Features produced by 20 cycle overloads are seen distinctly at intervals of approximately 17mm in the micrograph.

d) Part of (c) at higher magnification.
Shows a single overload "step" at the centre.

e) $n_L = 80,\ n_H = 20$.
Macro crack growth measurements indicate that the load sequence is repeated approximately every 180μm, this is equivalent to 15mm on the micrograph. Some but not all of the overload regions can be distinguished. It is noticable that the overload sequence does not result in a "step" of the type seen in (c) and (d).

NOTE

Heavy arrows below the photographs indicate the direction of crack growth.

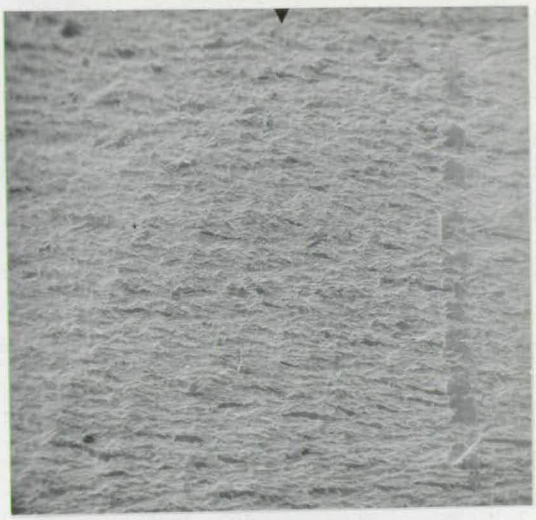

5.15(a) x17

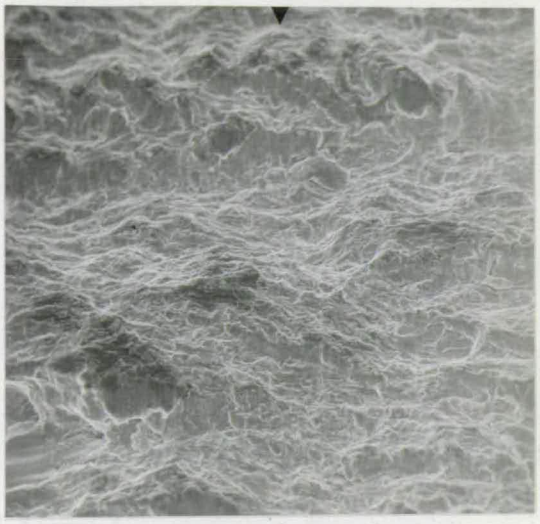

5.15(b) x175

5.15(c) x17

5.15(d) x84

5.15(e) x165

Figure 5.16 Fracture surfaces resulting from three level constant $\overline{K}$, block loading

See Figure 4.29 for load sequences and notation.

a)* "Low-high" sequence. $\overline{K} = 100$, $\Delta K_p = 82$ $MNm^{-3/2}$. The "periodicity"** of the load sequence is clearly seen (arrowed) at intervals of approximately 15mm in the micrograph, this is equivalent to 100μm on the fracture surface.

b)* Load as per (a).
The "period" of the load sequence is equivalent to approximately 40mm in the micrograph. A high to low change is visible to the left of centre.

c) "Low-high-low" sequence $\overline{K} = 100$, $\Delta K_p = 82$ $MNm^{-3/2}$.
The "periodicity" of the load sequence can be seen at intervals of approximately 15mm in the micrograph, this is equivalent to 180μm on the fracture surface. (See note below re "periodicity".)

d) Load as per (c).
The period of the load sequence is equivalent to approximately 75mm at this magnification.

e) "High-low" sequence. $\overline{K} = 100$, $\Delta K_p = 82$ $MNm^{-3/2}$.
This load sequence results in the least distinct marking of the fracture surface. The periodicity of the sequence is 6mm in the micrograph, this is equivalent to 78μm on the fracture surface.

f) Load as per (e)
The "period" of the load sequence is 30mm in the micrograph.
The fracture surface is again seen to have no distinctive features.

Notes: * The symbols in parts (a) and (b) of the figure are referred to in the explanatory part of the text, Section 5.4.1.

** "Periodicity" has been used above to describe the interval over which the load sequence repeats itself. Reference to Figure 4.29 shows that this is three load blocks for the "low-high" and "high-low" regimes. The "low-high-low" sequence has a periodicity of six load blocks, i.e. twice that of the other regimes.

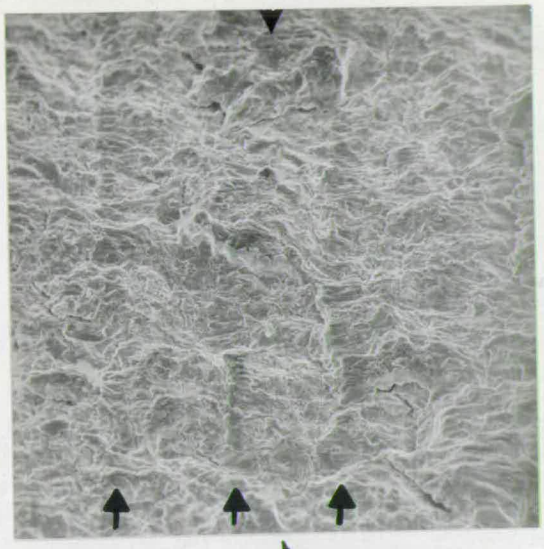

5.16(a) x147

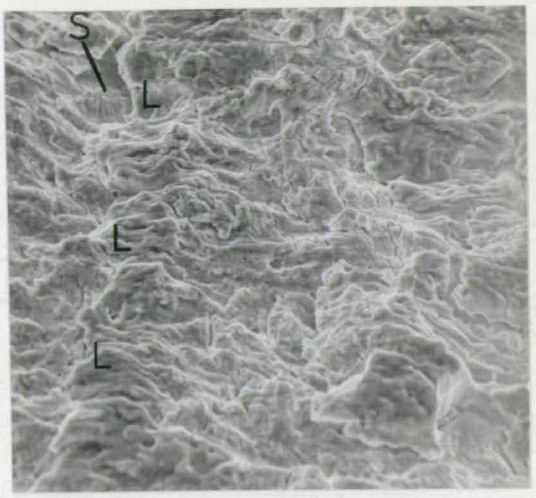

5.16(b) x378

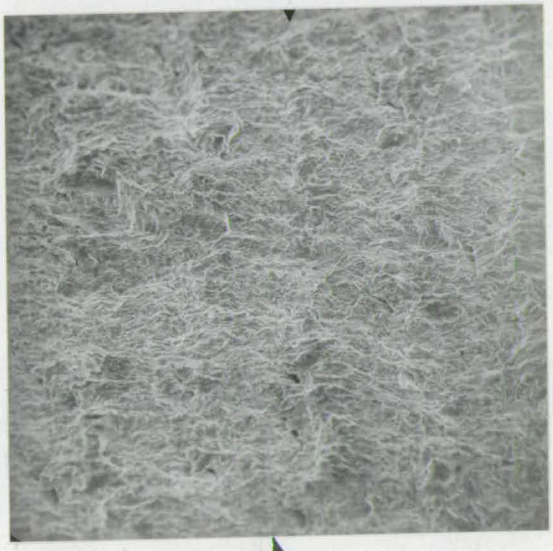

5.16(c) x84

5.16(d) x420

5.16(e) x77

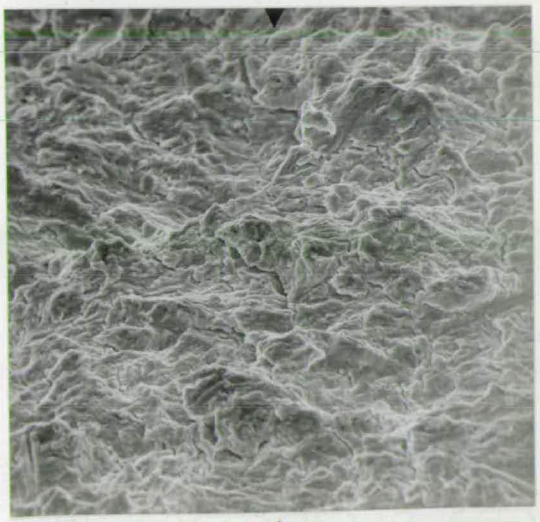

5.16(f) x385

Figure 5.17 Fracture surfaces resulting from 3 level, constant K_{min}, block loading

See Figure 4.29 for load sequences and notation.

a) "Low-high" sequence. $K_{min} = 20$, $\Delta K_p = 121$ $MNm^{-3/2}$. The periodicity of the sequence can be seen at intervals of 30 mm in the micrograph, this is equivalent to 180 μm on the fracture surface.

b) Load as per (a).
Shows a typical area at higher magnification. The period of the load sequence is approximately 75mm at this magnification.

c) "Low-high-low" sequence. $K_{min} = 20$, $\Delta K_p = 133$ $MNm^{-3/2}$.
This load sequence results in a distinctly marked fracture surface. The "periodicity" is seen to be approximately 50mm in the micrograph, this is equivalent to 300μm on the fracture surface.

d) Load as per (c).
Shows part of (c) at higher magnification. The surface to the left was created under the lowest dynamic stress intensity ($\Delta K_1 = 53$ $MNm^{-3/2}$), the striations to the right were formed at the intermediate level of ΔK,($\Delta K_2 = 94$ $MNm^{-3/2}$).

e) "High-low" sequence. $K_{min} = 20$, $\Delta K_p = 130$ $MNm^{-3/2}$.
The surface created at ΔK_p can be seen on either side of the centre line of the micrograph. The period is seen to be approximately 30mm, this is equivalent to 195μm on the fracture surface.

f) Load as per (e).
The load sequence can be distinguished in this micrograph. The low to high change can be seen to the right of centre.

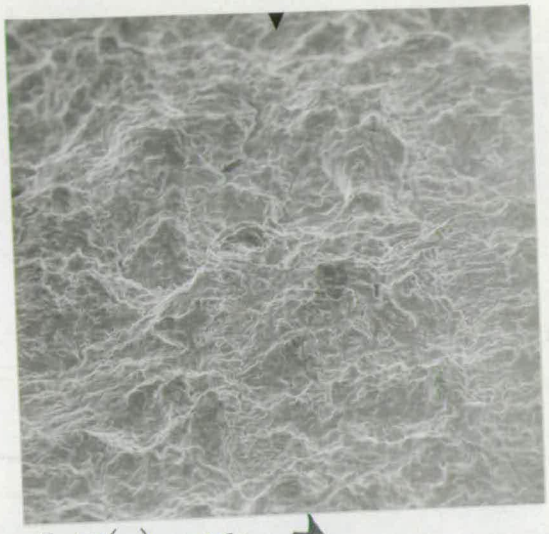

5.17(a) x164

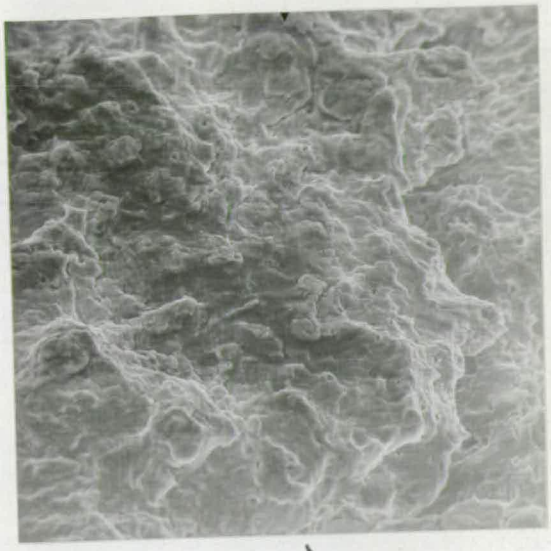

5.17(b) x413

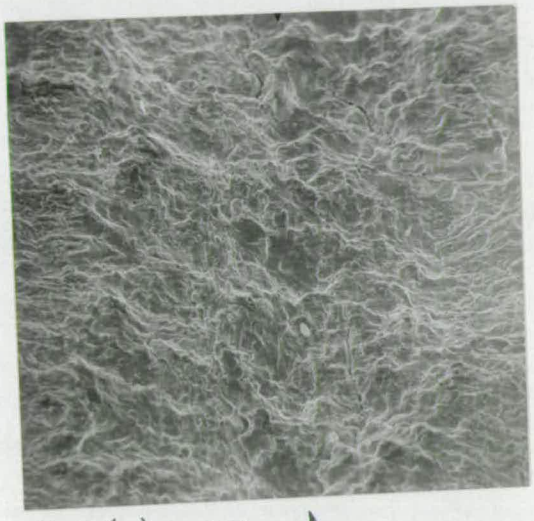

5.17(c) x164

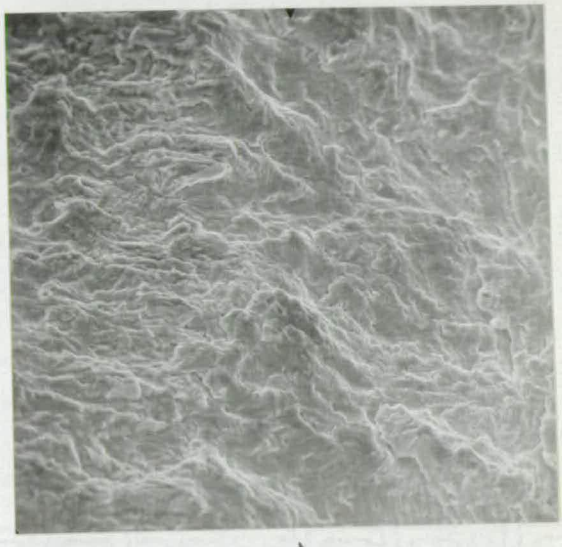

5.17(d) x400

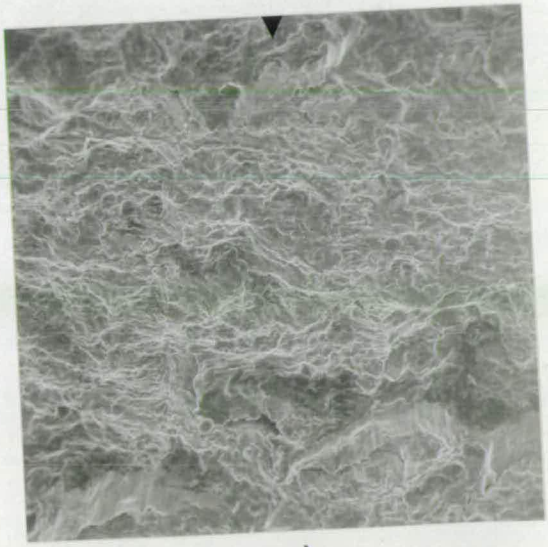

5.17(e) x154

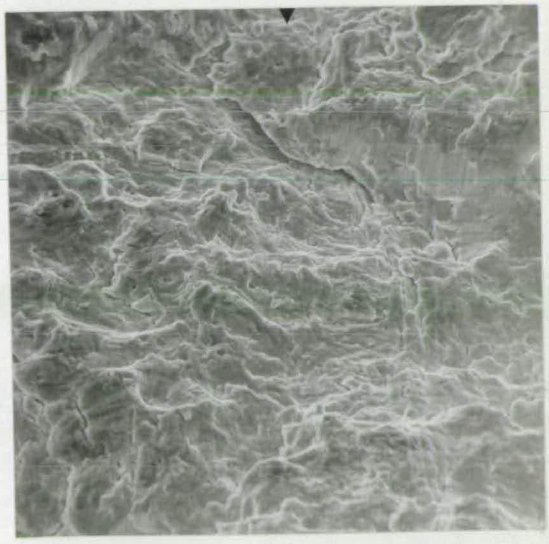

5.17(f) x385

Figure 5.18 Fracture surfaces resulting from 8 level block loading

See Figure 4.31 for load sequences and notation.

a) Constant $\overline{K}$; "low-high" sequence. $\overline{K} = 100$, $\Delta K_p = 103$ $MNm^{-3/2}$
Macro crack growth measurements predict a period of approximately 120μm for these loading conditions. This is equivalent to 20mm in the micrograph. Features consistent with this interval can be seen, through the points at which changes in ΔK occurred are not readily distinguished.

b) Load as per (a).
Part of (a) at higher magnification. Parts of the load sequence can be distinguished in this region. The "periodicity" at this magnification is approximately 50mm.

c) Constant K_{min}. "Low-high" sequence. $K_{min} = 25$, $\Delta K_p = 140$ $MNm^{-3/2}$.
The periodicity predicted from macro-growth measurements is approximately 250μm which is equivalent to 21mm in the micrograph. The extent of the "band" seen at the centre agrees well with this interval; however elsewhere the periodicity of this surface was not readily determined.

d) Load as per (c).
Part of (c) at higher magnification. The "periodicity" at this magnification is approximately 106mm. Striations of different spacing are seen but it is not generally possible to identify the points at which ΔK was changed.

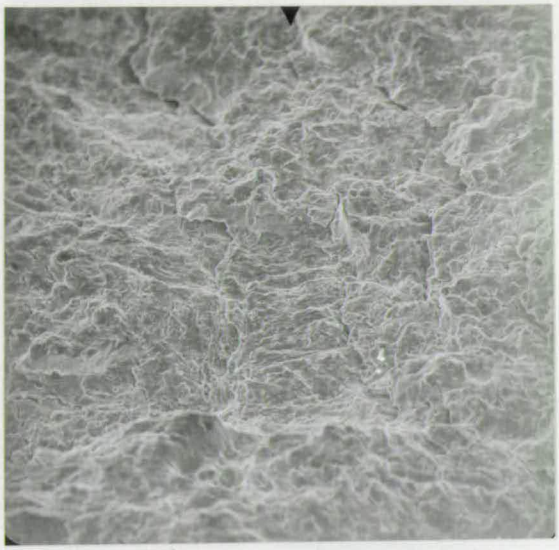

5.18(a) x172

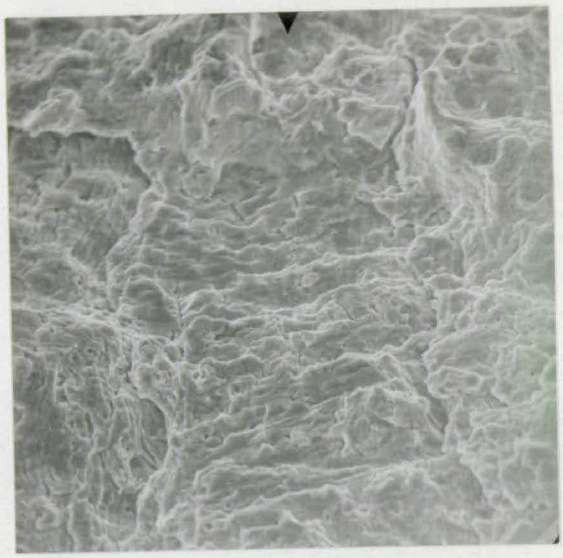

5.18(b) x427

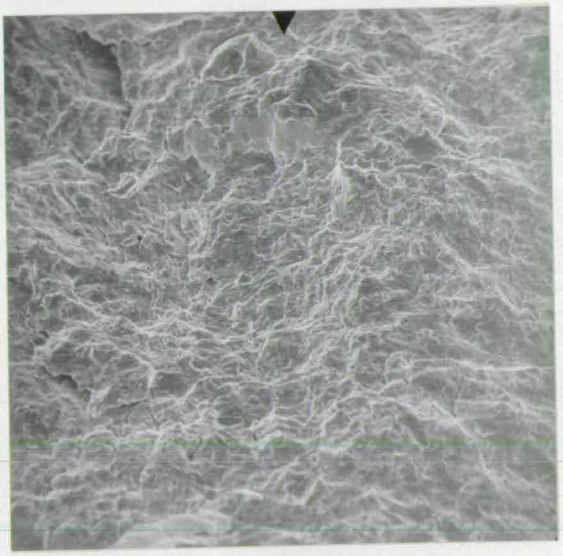

5.18(c) x84

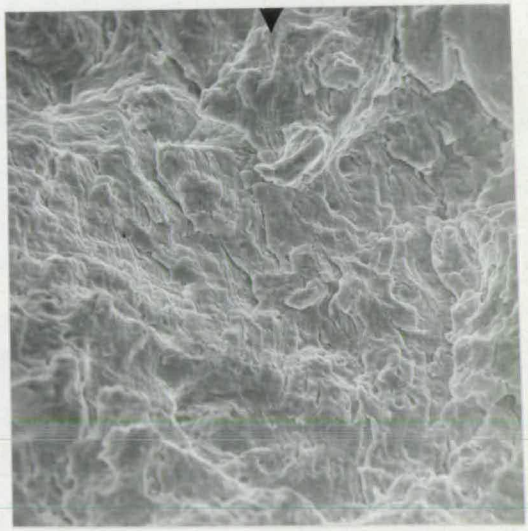

5.18(d) x424

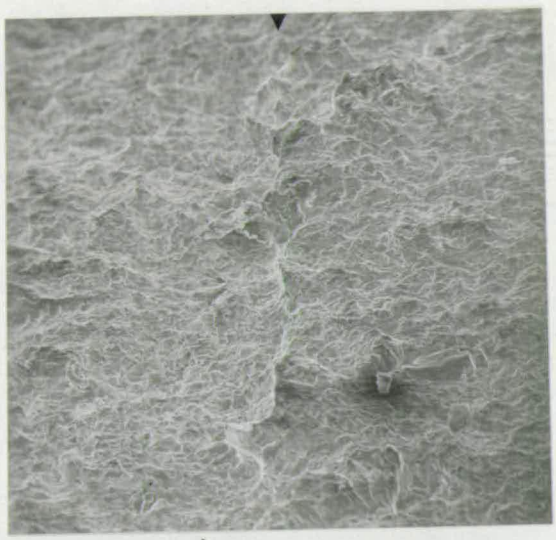

(a) x90

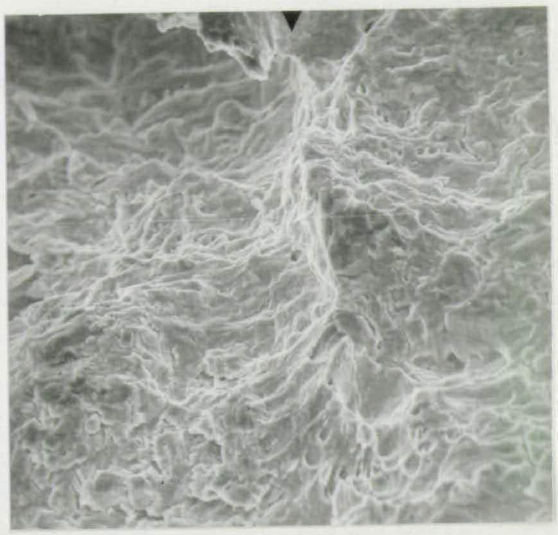

(b) x450

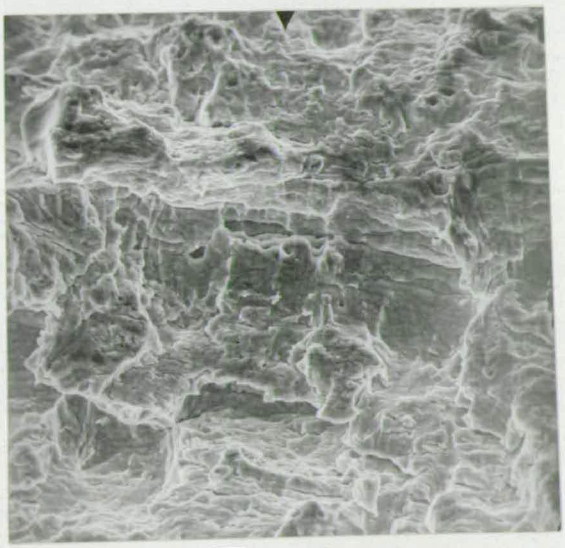

(c) x470

Figure 5.19 Fracture toughness tests.

Three views of the "stretch zone" produced by test 3, see Table 4.2.

(a) x42 Fatigue crack surface at left of centre, "stretch" zone and dimpled tensile failure at right.

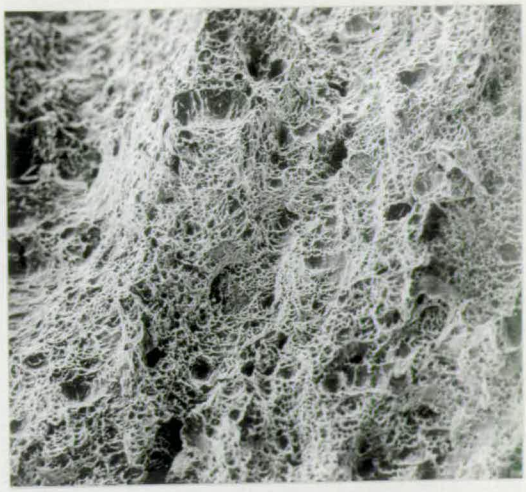

(b) x87 Stretch zone at left, tensile failure to right.

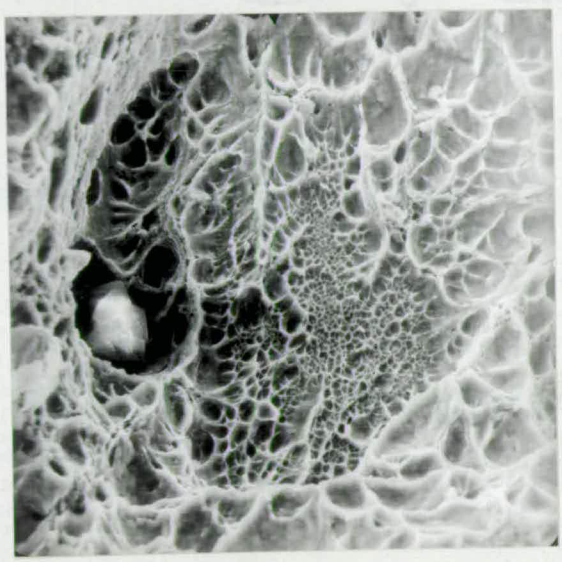

(c) x860. Part of (b) at higher magnification, shows the complex "dimple" pattern typical of tensile failure.

Figure 5.20 The micrographs show the distinctive appearance of the Q1(N) fracture surface when tensile failure occurs under monotonic loading. The surface shown was obtained by loading a precracked sample to failure.

CHAPTER 6

DISCUSSION

6.1 The Application of Fracture Mechanics to Q1(N)

6.1.1 Preamble

All crack growth rates determined in the present study have been correlated against the prevailing crack tip stress intensity conditions. This is consistent with the current trend in published literature. The overall significance of this and other work is therefore critically influenced by the validity of using the stress intensity parameter under cyclic loading conditions. It is particularly notable that no "validity" criteria, equivalent to those employed in fracture toughness testing, are imposed on the fracture mechanics analyses of fatigue test conditions. The applicability of the stress intensity parameter to crack growth in Q1(N) will therefore be considered before the detailed results of the author's work are discussed.

The potential restrictions on the use of the stress intensity parameter are a direct consequence of the modifications that are necessarily made to Irwin's linear elastic analysis in order to accommodate the reality of crack tip yielding. The development of the "small scale yielding" solution for crack tip stress intensity was outlined in Chapter 2. It is the extent to which the approximations involved remain acceptably accurate that is crucial to establishing the validity of using the stress intensity parameter for the analysis

of crack tip conditions in relatively tough materials. Theoretical consideration of the conditions under which the small scale yielding analysis becomes invalid are, at best, semi-quantitative. No precise model of crack tip stress distributions is available for comparison with the predictions of the fracture mechanics analyses. Rice's [22] work concerning plasticity under mode III crack opening conditions was reviewed in Section 2.2.3. His results indicated that the approximations inherent in the "small scale yielding" approach were acceptable whilst the nett section stress remained below $0.4\sigma_{YS}$ for monotonic loading; this limit was extended to $0.8\sigma_{YS}$ for cyclic loading conditions. As these limits are not applicable to mode I opening and no equivalent values are available it has been necessary to make empirical assessments of the stress intensity parameter's suitability for use in both fracture toughness testing and fatigue crack growth studies.

6.1.2 General limitations of fracture mechanics when applied to statically loaded cracks

The recent development of standard procedures for plane strain fracture toughness testing in both Britain [111] and the USA [112] has resulted in extensive experimental investigation of the loading conditions for which the stress intensity parameter, K_I, and its critical value K_{Ic}, are valid. Extensive restrictions regarding specimen geometry and load application have necessarily been formulated for fracture toughness testing in order to ensure that K_{Ic} determinations represent a genuine material property. The experimental procedures are dominated by the necessity to achieve nominal plane strain conditions during testing. The requirement results from the complicated way in which the fracture toughness of a given material varies with the specimen thickness. Figure 6.1 shows a toughness characteristic determined for 7075 Al alloy. It

is seen that in order to obtain a "thickness independent" value for the fracture toughness it is necessary to test sections whose thickness lies to the right of the figure. A lower limit of the allowable test piece thickness has been evolved from practical investigations of its effect on K_{Ic} in a wide range of alloys [113,114]. In both the British and ASTM standards the requirement is that:

$$B > 2.5 \left(\frac{K_Q}{\sigma_{YS}}\right)^2 \tag{6.1}$$

It is important to emphasise that this restriction is justified on a purely empirical basis, it simply represents a minimum thickness above which the fracture toughness is generally found to be independent of B. The criterion has no analytical significance with regard to the state of stress at the crack tip. Before the above discussion is extended to cyclic loading conditions it is worth considering the restrictions that are placed on net section stresses in the standard fracture toughness tests.

Although the standard K_{Ic} test procedures do not specifically define an upper limit for the allowable maximum, nominal ligament stress the various geometrical restrictions implicitly control this parameter. For the CKS sample the analysis outlined by Katcher [115] may be used to relate the nominal stress conditions in the uncracked ligament to the applied stress intensity. Referring to Figure 6.2 the nominal stress at the crack tip is given by:

$$\sigma_{max} = \frac{P}{A} + \frac{Mc}{I} \tag{6.2}$$

where A, I and c pertain to the uncracked ligament. Appropriate substitution and rearrangement yields:

$$\sigma_{max} = \frac{K_I W^{\frac{1}{2}}}{Y(W-a)} \left[1 + \frac{3(W+a)}{(W-a)}\right]. \tag{6.3}$$

Using this approach it may be shown that, in the case of CKS samples, the standard test procedures limit the value of σ_{max} to approximately 95% of the material's yield strength. A similar calculation for the three point bend specimen indicates that the limit is lower; the value is approximately 74% of σ_{YS}. The geometrical restrictions that define the above limits have been determined by the same empirical approach from which the thickness requirement was evolved.

Scrutiny of the various factors that influenced the formulation of these restrictions indicates that the nominal ligament stress at the crack tip was not a primary influence; other considerations were dominant. Thus the maximum ligament stress attainable at the crack tip during standard K_{Ic} testing does not represent the point at which the stress intensity parameter ceases to be applicable. The present author is not aware of any investigations which have sought to define such a limit. One interesting result can be deduced from the data presented by Brown and Srawley [116]. They examined the influence of the uncracked ligament length on the apparent fracture toughness of a maraging steel tested in pure bending. A summary of their results is presented in Figure 6.3; the nominal crack tip ligament stresses, as calculated by the present author, are also shown. The data points at the right of the figure correspond to tests that were "valid" by the criteria of the standard procedure. It can be seen that the tests performed on samples having very much smaller ligaments yielded identical values of the apparent fracture toughness. It is particularly notable that the nominal crack tip ligament stress was nearly $1.5\sigma_{YS}$ for the data points at the left of Figure 6.3. The authors' remarks, regarding the linearity of the load/COD record, confirm that the gross yielding predicted for these loading conditions did indeed occur.

The interesting point about the reanalysis of this series of tests is that the apparent fracture toughness determined under gross

yielding conditions was identical to that obtained from "valid" standard K_{Ic} tests. Although only a very limited amount of data is involved the observations do throw considerable doubt on the normally held view that for the stress intensity parameter to be applicable it is necessary to prevent the net section stress exceeding the material's yield stress. It is reasoned that if this restriction is not applied there is no effective constraint placed upon the crack tip plastic zone, the consequent gross plasticity invalidates the assumptions of small scale yielding fracture mechanics, with the result that the use of the stress intensity parameter is inappropriate. This argument is easily supported for loading configurations in which the nominal net section stress is uniform. However it would appear from the above discussion that when the uncracked ligament is subjected to bending or as with the CKS sample a combination of bending and tension, higher nominal crack tip stresses may be tolerated. It is reasonable to suggest that under these conditions the tension/compression gradient of the nominal stress ahead of the crack tip imposes an additional constraint on the development of the plastic zone. Certainly, purely elastic conditions will prevail in the central section of the ligament. It may be that under these conditions the stress intensity parameter is genuinely applicable at nominal crack tip stresses in excess of those that may be permitted when the ligament is subjected to "uniform" loading.

The foregoing discussion may be summarised as follows. From a theoretical standpoint use of the stress intensity parameter is only correct when the inherent assumptions of the "small scale yielding" model are not invalidated by extensive, unrestrained crack tip yielding. There are two distinct factors that influence the extent of crack tip plasticity. These are; firstly, the through thickness constraint that gives rise to the distinction between plane

strain and plane stress; and secondly, the influence of the prevailing ligament stress in preventing the plastic zone extending excessively ahead of the crack tip. In practice the first mentioned effect is found to have the more critical influence on the fracture toughness of a given material. Standard fracture toughness tests have therefore of necessity been limited to nominal plane strain conditions.

6.1.3 General limitations of fracture mechanics when applied to cyclically loaded cracks

The foregoing discussion provides valuable guide lines for assessing the applicability of fracture mechanics to the analysis of fatigue crack propagation. Validity criteria, similar to those applied in fracture toughness testing, are required for fatigue tests in order to ensure that the crack propagation characteristics determined in any investigation are truly representative of the material properties and not simply a product of the specimen geometry and the loading configuration adopted. The argument is as follows. Flaw growth under fatigue loading is considered to be primarily influenced by the prevailing crack tip strain conditions [117]. These conditions are directly related to the existing stress state which in theory may be most adequately defined by the stress intensity approach of fracture mechanics. The generality of this approach has been well demonstrated by Frost et al [38]. In realistic materials use of the stress intensity parameter will be invalidated when excessive crack tip plasticity occurs. From the point of view of the present study it is important to determine whether or not the tests that have been performed were sufficiently independent of geometrical influences to be considered "valid". As no formal criteria exist which are comparable to those embodied in the standard K_{Ic} test procedures, it is necessary to make a fundamental assessment of the acceptable fatigue test conditions. The initial discussion

may be generalised advantageously; specific details concerning Q1(N) will follow later.

Consideration of crack tip yielding under cyclic loading conditions is complicated by the dual nature of the deformation that occurs. The distinction between monotonic and cyclic yielding at the tip of a fatigue crack was made in Chapter 2. To a first approximation it is considered that material that has yielded monotonically thereafter behaves elastically. Thus cyclic deformation is limited to the relatively smaller reversed zone at the crack tip. The benefit of this situation is reflected by Rice's consideration of mode III loading [22], he showed that under cyclic loading net section stresses could rise to twice the acceptable monotonic level without invalidating the use of the dynamic stress intensity parameter (ΔK). However it is generally not possible to make theoretical predictions of "valid" conditions for the application of fracture mechanics to fatigue. Thus, as with fracture toughness testing, empirical criteria must be invoked. Furthermore the same two effects that were critical for monotonic loading will again be of importance; these are the influence of the through thickness constraint and the net section stress.

Thickness effects in fatigue are not clearly defined. There are two influences to be considered. Firstly it is observed that growing cracks may be inclined to the principal applied stress. A typical condition is shown schematically in Figure 6.4. Although a crack may be initiated perpendicular to the prevailing principal stress there is a tendency for the plane of fracture to rotate as shown in the figure. The cause of the reorientation is not clearly understood, however it would seem to be a complex interrelation of thickness and the loading conditions [118,119]. In the inclined condition the mode of crack opening is mixed and it is probable

that in thin materials some localised buckling occurs at the crack tip [120]. Theoretically the mode I stress intensity parameter is not applicable to a crack growing in this complex manner. However in practice the transition is often ignored and crack growth rates for both flat and shear mode failures are presented in terms of the mode I parameter. It is not clear if crack growth rates are influenced by the change in fracture plane geometry. The results of several investigations of the effect are inconclusive [118,119,121]. Crack growth transition has been empirically associated with accelerated damage in a wide range of materials [38]. However, it has been suggested that the increased rate of crack growth was principally influenced by the net section stress; this possibility will be considered later. Meanwhile the point to be noted is that as a direct result of its influence on crack plane geometry the specimen thickness may indirectly determine the equilibrium growth rate at a given value of ΔK.

Specimen thickness may also influence the micro-mechanisms of crack extension. This matter has been well reviewed by Richards and Lindley [122]. It is clear that certain mechanisms are favoured by the existence of a highly triaxial stress field. There are two manifestations of the effect. Firstly a change in the through thickness dimension may cause a change in the operative mechanisms of crack extension, this may be either a change in the relative importance of two competing mechanisms [54] or a wholesale change from one growth process to another [122]. The second possibility is that the basic process by which crack extension occurs may be sensitive to the triaxiality of the applied stress condition, thus a change in thickness causes a change in the growth rate without involving a simultaneous change in the mechanism of growth. Richards and Lindley have considered the influence of thickness on the commonly observed growth mechanisms. They conclude that cracks growing by

mode I striation formation are generally not sensitive to the prevailing specimen thickness. Other growth mechanisms, e.g. micro-cleavage, void coelescence and intergranular separation are more sensitive to the prevailing stress conditions and may not therefore be considered to yield growth rates that are independent of the sample thickness. It is not clear what particular feature of the striation mechanism results in the anomolous thickness independence of the associated growth rates.

Turning now to the effect of net section stress; the value of this parameter that invalidates the use of the stress intensity approach in fatigue is not clearly defined. In principle the factors to be considered are the same as those previously discussed with respect to monotonic loading. The problem is to determine the level of net section stress at which the elastic field ahead of the crack is no longer adequately defined by K, or in the case of fatigue ΔK. As in the case of monotonic loading, extensive crack tip plasticity is expected to invalidate the stress intensity analysis. The theoretical approach to plastic deformation under cyclic loading was reviewed in Chapter 2. The important conclusion reached was that material that yields monotonically will thereafter behave elastically unless the local stress range exceeds $2\sigma_{YS}$*. Thus it was concluded that under fatigue conditions the nominal crack tip stress may approach $2\sigma_{YS}$ before extensive cyclic plasticity is expected. Furthermore it will be remembered that when the uncracked ligament was subjected to bending, meaningful values of K_{Ic} were obtained at nominal crack tip stresses in excess of σ_{YS}. It was suggested that this was a consequence of crack tip plasticity being

*More accurately the value is twice the cyclic yield stress, the distinction has been ignored for the sake of simplicity.

restricted by the stress distribution associated with bending. If a similar benefit is obtained under fatigue conditions it is possible that the nominal cyclic ligament stress may, in the case of bend specimens, exceed $2\sigma_{YS}$ without invalidating the use of the stress intensity parameter. A further implication of the suggestion is that specimens in which the nominal ligament stress is uniformly tensile would be subject to a lower acceptable limit of $\Delta\sigma_{net}$.

From the practical point of view no satisfactory limits have been established to define stress levels in the uncracked ligament which are compatible with fracture mechanics analyses. Nominal crack tip stress conditions are normally not reported when crack growth rates are presented as a function of the applied stress intensity. Although some workers [38, 115] have regarded nominal stress levels in excess of $0.8\sigma_{YS}$ as potentially invalidating the stress intensity analysis, the work of Richards and Lindley [122] indicates that higher values of σ_{max} are generally acceptable. It is possible that some misunderstanding of the influence of monotonic yielding occurred during the early development of the application of fracture mechanics to fatigue studies. In the extensive tests performed on centre cracked sheets of thin (< 5mm) materials "accelerated" crack growth was frequently observed at the higher crack lengths which coincided with the approach of σ_{max} to σ_{YS}. It was also under these conditions that the crack plane was likely to rotate from mode I opening to a 45° shear configuration, with the result that the K_I parameter was no longer strictly applicable. These difficulties were compounded into a general suspicion of crack growth rates determined under conditions which involved monotonic yielding in the net section. More recent considerations [122] indicate that a less severe limitation on crack tip stress conditions is probably acceptable, though the present author is unaware of any systematic study of the influence the nominal ligament stress on cracks

propagating under constant stress intensity conditions. Until such an investigation is completed the present difficulties with regard to the influence of net section stress will persist.

In summary it may be stated that it is not clear at what level of nominal crack tip stress the stress intensity parameter is invalidated for the correlation of fatigue crack growth rate data. "Accelerated" growth rates have been reported for conditions where σ_{max} approaches σ_{YS}. However, it is not clear if this effect results from a material property or if it is a manifestation of "invalid" use of the stress intensity concept. The distinction is complicated by the possible influences of crack plane rotation, and the different specimen geometries that have been employed.

6.1.4 Assessment of the validity of employing fracture mechanics in the present study

With regard to the present investigation it is not necessary to justify the general reasons for presenting fatigue crack growth rate data in terms of fracture mechanics parameters. These matters are well reviewed by Johnson and Paris [123], further support for the approach may be inferred for the widespread use of the stress intensity parameter in current fatigue literature. What is not self evident is if any of the particular conditions pertaining to the present study invalidate the use of fracture mechanics. A formalised approach to this problem has been proposed by Katcher [115] who placed restrictions on the crack tip stress conditions in terms of a minimum specimen thickness and a maximum permissible value of the nominal stress. The latter restriction simply limited σ_{max}, in his CKS specimens, to values below $0.8\sigma_{YS}$. This condition, developed at North American Rockwell, is even more restrictive than the requirements of the standard K_{Ic} test procedures. With regard to thickness the intention was to ensure that "plane strain" conditions

prevailed at the crack tip. The ASTM thickness requirement for plane strain fracture toughness testing was therefore modified from

$$B > 2.5\left(\frac{K_Q}{\sigma_{YS}}\right)^2 \qquad (6.1) \text{ restated}$$

to yield a maximum permissible stress intensity condition, viz:

$$K_{max} < \sigma_{YS}\sqrt{B/2.5} \qquad (6.4)$$

The assumptions of this transformation are clearly erroneous. The final condition implies that for a given sample plane strain conditions prevail up to a critical value of K, K_{max}, which is a function of the thickness, B. In practice the proportionate nature of an elastic stress field is such that at a given thickness the balance between "plane stress" and "plane strain" will be independent of the prevailing value of K. If the original, and more correct, ASTM criteria is applied to Katcher's tests two of the four materials tested are found to have been too thin. However, the empirical nature of the ASTM thickness criteria has already been emphasised; there is not direct justification for its use under fatigue conditions.

The difficulties associated with formalising validity criteria are thus well demonstrated. The restrictions of the above approach are particularly acute in the case of tough materials having a low value of the ratio K_Q/σ_{YS}. For Q1(N) a more flexible approach is required. Consider first the thickness requirement. Preliminary tests performed by Evans and Taylor at NPL [55] indicated that crack growth rates were independent of thickness over the range 13 to 25mm. Furthermore Figure 4.6 demonstrates the excellent agreement between their results on 13mm thick samples and those from the present author's 35mm thick material. Thus it would appear

that specimen thickness is not a primary variable under the conditions of the present investigation. This conclusion is supported by consideration of the crack growth mechanism. The appearance of Q1(N) fracture surfaces examined at NPL was characteristic of crack growth by a striation forming mechanism. Furthermore all the present author's tests yielded fracture surfaces that were consistent with this failure mechanism. Reference to the work of Richards and Lindley [122] indicates that this type of fracture surface is associated with thickness independent growth rates. The final point to be made with regard to the thickness concerns the orientation of the fracture surface to the principal stress direction. In all the Edinburgh tests the crack plane remained essentially normal to the load axis. From this it may be inferred that the specimen thickness did not lie in a "sensitive region" as crack plane rotation, giving growth by mixed modes, is associated with critical values of the applied load and specimen thickness [118, 119]. More obviously it may be stated that as the crack plane was consistently normal to the load axis use of the mode I stress intensity parameter was at no time invalidated by the occurrence of mixed mode crack tip deformation.

The above discussion establishes that the crack growth rates determined in the present study were substantially independent of the prevailing specimen thickness. The potential problems associated with the maximum ligament stress are less readily resolved. Reference has already been made to the possibility of crack growth rates being influenced by static yielding of the uncracked ligament. Some insight into this problem can be gained from the present author's study of mean stress effects. It is possible to separate the data originally presented in Figure 4.4 into three catagories, according to the nominal stress conditions in the uncracked ligament. The different categories are defined by the uppermost pair of data

lines in Figure 6.5. In each case the stress intensity characteristic of the 254mm, Edinburgh CKS sample has been plotted as a function of crack length for a particular stress condition in the ligament. The lower line, designated "A", defines the loading conditions under which nominal tensile yielding occurs at the crack tip, i.e. $\sigma_{max} = \sigma_{YS}$. The upper line ("B") defines the more severe conditions under which yielding is also expected in the compressive extremity of the ligament*. Thus three conditions are defined:

1) Stress intensity levels below which no nominal yielding occurs. (Below "A").

2) Stress intensity levels at which yielding is nominally confined to the crack tip region. (Between "A" and "B").

3) Stress intensity levels at which tensile and compressive yielding occur on opposite sides of the uncracked ligament. (Above "B").

The mean stress intensity results, originally presented in Figure 4.4, have been represented in Figure 6.6 in a form which permits the data points to be identified in accordance with the above categories. Referring to the figure the "open" symbols refer to category (1), the "shaded" symbols to category (2) and the "double" symbols to category (3). Interpretation of the data with regard to the influence of yielding in the uncracked ligament is complicated by the simultaneous variation of the mean stress intensity. However it may reasonably be suggested that under equilibrium conditions the crack growth rate will not decline as the value of $\overline{K}$ increased. If

*The values given are only approximate in that prior tensile yielding at the crack tip will influence the value of K at which compressive yielding occurrs. A "lower bound" solution in which crack tip yielding was treated indicated that the "elastically" derived values given in Figure 6.5 are adequate for the purpose of the present discussion.

this is accepted it is then apparent that neither the onset, nor the degree of nominal monotonic yielding in the ligament significantly influences the rate of crack growth.

If, as suggested above, monotonic yielding in the uncracked ligament may be discounted as a factor that influences the crack growth rate, it is logical to extend the discussion to consider crack propagation under loading conditions which cause gross cyclic yielding. No specific investigation of such conditions has been undertaken, however it is possible to infer certain information from a comparison of the present author's results with those obtained by Evans and Taylor at NPL [55]. In both cases CKS type specimens of Q1(N) were tested, but the overall dimensions of the test pieces differed dramatically as shown in Figure 6.7. The size difference resulted in the individual samples having distinctive "stress intensity/nominal ligament stress" characteristics. Furthermore the standardised nature of the NPL tests makes it possible to calculate the prevailing stress intensity conditions at any given value of crack length. The relevant data is presented in the lower part of Figure 6.5. The lines rising from left to right detail the stress intensity conditions of the NPL tests; a constant load ($\overline{P} + \Delta P$) was applied, the increasing K_{max} and ΔK characteristics simply reflect the form of the compliance function (Y) for the CKS sample. The two intersecting lines with negative gradients represent nominal crack tip stress conditions. The lower of the two details the static stress intensity that corresponds to the condition $\sigma_{max} = \sigma_{YS}$. Thus the point of intersection of this curve with the K_{max} characteristic defines the point at which nominal monotonic yielding occurred at the crack tip. It is seen that all tests conducted at ΔK values in excess of 48 $MNm^{-3/2}$ would have satisfied this condition for yielding. The onset of gross cyclic yielding is less easily predicted. However an approximate estimate

may be based on the cyclic stress/strain data presented in Figure 4.2. It is apparent that the cyclic yield stress is about $0.8\sigma_{YS}$. Thus nominal cyclic plasticity would be expected when $\Delta\sigma_{max} > 1.6\sigma_{YS}$. The dynamic stress intensity values corresponding to this condition are plotted in Figure 6.5. The point of intersection of this curve with the ΔK test characteristic indicates the level at which gross cyclic plasticity is expected. It is seen that for the NPL tests nominal cyclic yielding is predicted when ΔK exceeds 71 $MNm^{-3/2}$.

A similar consideration of the equilibrium crack growth data determined at Edinburgh is complicated by the less standardised test procedure. However certain generalisations may be made. Firstly none of the data presented in Figure 4.6 satisfies the above condition for nominal cyclic yielding. The data point at the extreme top right of the figure corresponds to the condition $\Delta\sigma_{max} = 1.3\sigma_{YS}$, the adjacent point below this extreme value corresponds to a $\Delta\sigma_{max}$ value of $0.86\sigma_{YS}$. The other data points all represent even lower values of $\Delta\sigma_{max}$ which at no time approaches the "critical" value of $1.6\sigma_{YS}$. On the other hand nominal monotonic yielding of the crack tip is possible at any value of ΔK in excess of $32MNm^{-3/2}$. In practice test sequences were such that such yielding was mostly confined to tests in which ΔK exceeded 80 $MNm^{-3/2}$. This point is not critical to the current discussion. The situation may be summarised as follows.

1) The NPL test conditions were such that the nominal conditions for both monotonic and cyclic yielding were satisfied.
2) Only monotonic yielding is predicted for the Edinburgh tests.
3) Monotonic yielding has already been discounted as a principal influence on the crack growth rate in Q1(N). Thus any systematic differences in the crack growth rates determined

by the different workers may prove informative with respect to the influence of gross cyclic plasticity.

When compared, as in Figure 4.6, the two sets of results are seen to divide into three distinct regions. At dynamic stress intensities below $25 MNm^{-3/2}$ a significant discrepancy exists. This is considered to be a mean stress effect and as such will be discussed later. At intermediate values of $\Delta K (25\text{-}60 MNm^{-3/2})$ agreement between the different workers is seen to be excellent. In this region nominal monotonic yielding is predicted for both test configurations but neither system would be expected to exhibit gross cyclic plasticity. At the highest values of ΔK investigated there is a suggestion that the NPL growth rates tend to exceed the Edinburgh values. It is extremely interesting to note that the onset of this trend is consistent with the dynamic stress intensity level ($71 MNm^{-3/2}$) at which gross cyclic plasticity was predicted for the NPL tests. The significance of this observation should not be overrated at this stage; some further work is necessary to test the possible influence of gross cyclic plasticity on the rate of fatigue crack growth. With regard to the present study the important point is that the rate of fatigue crack growth in Q1(N) is not significantly influenced by the prevailing net section stress when $\Delta\sigma_{max}$ is less than $1.6\ \sigma_{YS}$. This limit was not approached in the Edinburgh tests.

The aim at the outset of this chapter was to examine the validity of using the stress intensity parameter for the correlation of fatigue crack growth rates in the present study. The relevant loading conditions have been critically examined from a fundamental viewpoint. It has been confirmed that fracture mechanics concepts are appropriate for application to crack growth in Q1(N). Empirical reasoning has been used to demonstrate that the loading configuration employed has not had an adverse "geometrical" influence on the observed

crack growth rates. In themselves these conclusions are an essential pre-requisite for the evaluation of the author's experimental programme. A further benefit derived from the foregoing discussion has been the identification of several areas in which further research would help to resolve some of the difficulties currently associated with the application of the stress intensity parameter to low and medium strength steels. These matters will be summarised in Chapter 8. Before evaluating the results of the fatigue crack propagation studies it is logical to consider the general properties of Q1(N) as revealed by the tests reported in Section 4.1.

6.2 Basic Properties of Q1(N)

6.2.1 Hardness and microstructure

Investigations of the through thickness hardness and microstructural properties of Q1(N) have been reported in Sections 4.1.1 and 5.1. The dual aims of the work were to assess the homogeneity of individual samples and the variation that existed between samples. In both respects Q1(N) was found to be extremely uniform. The CKS samples received from NCRE were not identified with regard to their source locations in the "as rolled" plate. In this respect the hardness and microstructional examinations do not represent a systematic study of properties at different plate locations but constitute a randomised survey of approximately one third of the total number of samples tested.

The impressive uniformity of the properties is a direct consequence of the very slow transformation rates that prevail during both the quenching and tempering of Q1. The as quenched uniformity of the alloy is further aided by the relatively high M_s and M_f temperatures that govern the formation of martensite. From the partial TTT diagram shown in Figure 6.8 the M_s temperature

is seen to be in excess of 370°C; the M_f temperature has been reported as 340°C [124]. Although both the chemical composition and the austenitizing temperature influence the precise values of the transformation temperatures it is apparent that a very high degree of martensite uniformity should be attainable in quenched 35mm thick plate. Martensite decomposition during tempering is sufficiently slow to permit very extended treatments to be employed without producing undue softening. The treatment specified by the ASTM commercial standard [104] is $\frac{1}{2}$ hr above 593°C per 12mm of section. For 35mm plate the holding time is therefore 1.5 hrs. The benefit of the long treatment times is that consistent properties may be achieved through the plate thickness as evidenced by both the hardness determinations and microstructural observations reported in earlier chapters.

Neal and Doig [125] have observed severe micro-segregation of carbides in a trial cast of Q2 which is chemically essentially identical to Q1*. This defect, commonly referred to as "banding", arises from chemical segregation in the ingot. It is normally observed to be most severe at the section mid thickness and plate centre, these positions correspond to the central, slow cooled,

---

* Q2 is the British made equivalent of the alloy which is designated HY-100 in the USA, (σ_{YS} = 100 ksi = 690MNm^{-2}). The permitted composition range overlaps the Q1 specification, the commercial heat treatments are also identical. The ASTM specification [104] distinguishes Q1 and Q2 as classes 1 and 2 respectively of the same alloy.

section of the ingot. As mentioned in Section 5.1 the Q1(N) used in the present study sometimes exhibited very light banding but the severity was such that it was not reliably detected. Certainly the effect was more prevalent at the section mid thickness, but as the point of origin of the samples in the as rolled plate was unknown, it was not possible to determine if there was a variation in the severity across the long transverse direction. It should be emphasised that the degree of "banding" observed was trivial, the Q1(N) microstructures were notable principally for their uniformity.

6.2.2 Monotonic and cyclic stress/strain characteristics

The monotonic and cyclic stress/strain response of Q1(N) was reported in Sections 4.1.2 and 4.1.3. The monotonic characteristic is notable for the low value of the "UTS/proof stress" ratio. From the results given in Table 4.1 this parameter has a value of 1.17, (= 1/0.85). Landgraf [126], in his review of cyclic properties, reports that alloys having a value of this ratio less than 1.2 are expected to exhibit cyclic softening. Q1(N) conformed to this prediction as shown in Figure 4.2. Alternatively the tendency to cyclically harden or soften may be deduced from the monotonic strain hardening exponent, (m') where

$$\sigma = A\varepsilon^{m'}.$$

The data from Figure 4.2 has been replotted on logarithmic axes in Figure 6.9, it is seen to yield a value of 0.089 for the exponent. Replotted in the same figure is the cyclic data from Figure 4.2. The cyclic strain hardening exponent (m''), as given by

$$\sigma = A\left(\frac{\Delta\varepsilon_p}{2}\right)^{m''},$$

was evaluated at 0.115. The values taken by both these exponents are consistent with the generalisations made by Landgraf; viz: if m' is less than 0.1 the material is expected to cyclically soften and that, for most metals, cyclic hardening exponents are found to lie between 0.1 and 0.2.

From the point of view of fatigue crack propagation the importance of a material's cyclic stress/strain characteristic is well appreciated. However, to date, none of the more successful crack growth rate expressions have incorporated data derived from cyclic tests. Thus, at the present, both monotonic and cyclic stress/strain data are of limited utility in the prediction of crack growth rates; however, they do contribute important background information which is essential to a general understanding of the deformation processes associated with crack extension.

6.2.3 Fracture toughness tests

The fracture toughness test reported in Section 4.1.4 constituted a logical extension of the use of the stress intensity parameter previously adopted for correlating fatigue crack growth rates. The specimen thickness criteria embodied in both British [111] and American [112] standards made it quite clear that a valid K_{Ic} value could not be obtained from 35mm thick samples of Q1(N). However it was considered that it would be informative to determine a K_c value for the fatigue test configuration. In the absence of a recommended procedure for K_c testing it was considered logical to follow the standard plane strain procedures as far as possible. Specimen dimensions apart, the principal violation of the standard test procedure was the implementation of multiple tests on a single sample. It is important to examine the possible consequences of this action.

The most obvious consequence of a multiple test sequence is that residual stresses, from previous tests, may affect subsequently determined values of K_c. For residual stresses to exist plastic flow must have occurred during an earlier test. In a CKS sample tensile yielding occurs at the crack tip whilst compressive yielding may be induced at the opposite side of the ligament. The effect of the latter deformation is to "prop" the crack open thus maintaining the stress singularity. Had "macro" crack closure occurred the singularity would have been destroyed with the result that the applied load would not have been proportional to the crack tip stress intensity conditions until a sufficient force was applied to physically separate the crack faces and thus restore the singularity. The effect of tensile yielding and the resultant compressive residual stress at the crack tip is more complex. After each test the crack was grown under fatigue conditions for at least 10mm in order to "resharpen" the crack tip and to eliminate the prevailing compressive residual stresses. It is impossible to determine to what extent this procedure was successful, however in all cases fatigue crack growth was observed to occur at the "equilibrium" rate during the latter part of the growth interval. In contrast high values of dynamic stress intensity were required to recommence propagation after each test. These facts suggest that the crack tip damage inflicted by the tests was largely eliminated by the subsequent growth interval.

Section 4.1.4 details two additional points on which the author's tests failed to satisfy the requirements of the standard plain strain fracture toughness tests. The limited range of a/W specified for standard tests is not of prime importance. The influence of ligament width has already been extensively discussed with regard to the results presented by Srawley and Brown [116]. The same authors indicate that the principal reason for restricting the permitted a/W

range is to avoid performing tests at high crack lengths in the region where the K calibration curve rises steeply with the measured value of crack length. The nature of the present tests was such that this accuracy consideration was not of prime importance. The other test condition that conflicted with the requirements of the standard procedure for K_{Ic} determination concerned the level of K_{max} during fatigue pre-cracking. In fact there is some disagreement between the British and American authorities as to what the limitation should be. The BISRA standard proposal [106] requires that K_{max} be less than 0.5 K_Q, this was also the original ASTM limit, though this body has now raised the limit to $0.6K_Q$. Kaufman and Schilling [127] have recently obtained additional evidence to show that the limit might reasonably be extended to 0.8 K_Q for aluminium alloys. May [128] has reported that an even higher limit would be acceptable for maraging steels. It would seem that the level of $0.5K_Q$ is unnecessarily conservative and that the 10% by which the precracking conditions used in the present work exceeded the limit is unlikely to have had a critical influence on the values of K_c obtained.

Before summarising the overall importance of the tests it is important to consider the extent to which the concept of fracture toughness is applicable to a material as ductile as Q1(N). When a material exhibits obvious "pop-in" under fracture toughness test conditions the K_c value is clearly of importance in that it defines a lower limit to the stress conditions at which catastrophic component failure may be expected. For ductile materials the situation is not so clear. The test records shown in Figure 4.3 are typical of a ductile material which exhibits progressive, as opposed to discontinuous, failure. Knott [129] has considered the implications of such load/COD test records. He draws attention to the difficulties associated with the validity check applied at $0.8P_Q$. The current series of tests just satisfied this criterion

whose purpose is to discriminate against tests in which gross crack tip plasticity occurs. However the SEM fractographs presented in Figure 5.19 show that the tests caused very little observable crack extension; the extent to which the apparent damage was shared between true crack extension and exaggerated yielding remains in doubt.

Knott recommends that the fracture characteristics of materials that do not exhibit pop-in should be assessed by full R-curve analyses. An alternative approach has been proposed by Egan [130] who has considered the equivalence of fracture criteria as expressed by K_c, J_c and COD_{crit}. He concludes that although the individual approaches yield different values for the critical fracture condition, the similarities between the tests are sufficient to make any one of them meaningful in a practical fracture control excercise. To perform R-curve analyses in the context of the present investigation was not only impractical but also irrelevant with regard to the aims of the tests. The intention was not to evaluate a material property but to identify the loading conditions under which crack tip damage became excessive. It was important that these conditions be expressed in terms of the same loading parameter that was employed for the correlation of crack growth rate data. Thus although there remains considerable doubt as to the absolute significance of a fracture toughness test conducted on Q1(N), the determination of a K_c value for the CKS fatigue sample provided valuable guidance as to the upper limit of stress intensity that should be used during fatigue testing.

The results of the individual tests, as given in Table 4.2, indicate a notable consistency of the K_c values obtained. Consideration of K_{Ic} data from various sources [113, 114] indicates that variations of $\pm 10\%$ are common. The scatter associated with the present author's K_c determinations is marginally superior to this value. It is

particularly unfortunate that the first test performed did not yield a result as it would have provided some indication of whether the multiple test procedure adversely influenced the values of K_c obtained. Tests on further samples would have provided some insight into this problem, however, as the principal aim of the fracture toughness tests had been satisfactorily achieved experimental effort was subsequently directed at the crack propagation studies that are discussed in the sections that follow.

6.3 Fatigue Crack Propagation in Q1(N)

6.3.1 Crack growth under constant amplitude loading

Fatigue crack propagation under constant amplitude loading conditions is known to be influenced by a wide range of variables. In the present study it was necessary to determine "equilibrium" crack growth rates for simple loading conditions in order to provide basic data against which propagation rates resulting from complex load sequences could be compared. Considerable care was therefore taken to perform tests under conditions in which only the amplitude of the applied load was critical in determining the crack growth rate. The influence of test frequency and the atmospheric conditions prevailing at the crack tip were considered in Chapter 2, both were discounted as being of primary importance in the context of the author's work. The discussion in the early part of this chapter established the independence of the measured growth rates from geometrical influences of the test piece configuration. Furthermore the stress intensity parameter was demonstrated to be the most appropriate load variable for the correlation of growth rate data. Thus it has been established that, in the present study, crack growth rates were principally determined by the prevailing loading conditions. Under simple loading conditions the dynamic stress intensity range (ΔK) is acknowledged as the dominant variable in determining the rate of

crack extension. However, in certain circumstances, the prevailing value of mean stress intensity ($\bar{K}$) is also critical; an early evaluation of the mutual interdependence of these parameters in $Q1(N)$ was therefore necessary. The results of the author's investigation of mean stress intensity were presented in section 4.2.1.

There are two distinct ways in which mean stress conditions may influence equilibrium crack growth rates. At low R values ($K_{min} \lesssim 0$, $R < 0.1$) growth retardation may be caused by crack closure effects of the type proposed by Elber [63, 65]; (see section 2.7.7). At higher values of R crack closure is eliminated but the growth rate may be influenced by mechanistic considerations of the type advanced by Richards and Lindley [122] and Ritchie [54]. It was unfortunate that in the present study the test facility employed generally restricted R to values in excess of 0.2. Thus it was not possible to investigate crack growth under conditions at which closure effects were likely to be significant. However, it was important to investigate the effect of practically attainable levels of mean stress intensity. To this end the extensive series of tests reported in Figure 4.4 was undertaken; the range of $\bar{K}$ employed was determined by the practical limitations of the test facility. The growth rates were originally reported as a function of the applied mean stress intensity as this was the parameter that was most directly applicable to the selection of suitable conditions for subsequent tests. Furthermore, the format adopted facilitated the location of the $K_{max} = K_c$ condition which, it was originally thought, might influence the crack growth rate. Some workers prefer to present mean stress sensitivity as a function of the prevailing R value, with this in mind the data from Figure 4.4 has been reanalysed and is presented in terms of R in Figure 6.10. The nature of the transformation is such that no fundamental reassessment of the data is necessary.

Fractographic studies clearly indicated that a striation forming mechanism was operative at all values of $\bar{K}$, there was no evidence to suggest that an alternative growth process was favoured at high values of mean stress intensity. In this respect the present author's data is consistent with the generalised conclusions of Richards and Lindley concerning the mean stress insensitivity of striation forming crack growth mechanisms. It is interesting to note that the macro-growth rates were uninfluenced by crack tip conditions that might reasonably have been expected to result in accelerated growth. Reference has already been made in Section 6.1 to the fact that the onset of monotonic yielding in the uncracked ligament had no detectable influence on the rate of crack extension. This point was important in establishing the validity of employing the stress intensity parameter for the cross-correlation of growth rates measured in geometrically different samples. From the point of view of material properties it is perhaps more significant to note that the growth rate was not accelerated when K_{max} approached K_c; the critical condition, $K_{max} = K_c$, was indicated for each value of ΔK in Figure 4.4. This insensitivity castsfurther doubt on the significance of fracture toughness testing in Q1(N). Clearly the critical stress intensity that produces "crack extension" under monotonic loading is in no way indicative of the loading conditions that will result in catastrophic component failure.

The insensitivity of crack growth rates to the applied mean stress intensity made possible the presentation of a single equilibrium growth rate curve as given in Figure 4.5. The range of R over which the data is applicable may be deduced from Figure 6.10. For values of ΔK in excess of $33 MNm^{-3/2}$ the crack growth rates are independent of the applied mean stress intensity at values of R in excess of 0.3. The data obtained at the lowest value of

ΔK investigated, indicates that the threshold value of R below which growth retardation occurs may increase as ΔK is reduced. This postulate is supported by the comparative presentation of the present author's results with the equilibrium growth rates reported by workers at NPL [55]. Figure 4.6 indicated a significant divergence of the data sets at values of ΔK below $30 MNm^{-3/2}$. In the NPL tests R was equal to 0.1, in contrast the minimum value for the relevant Edinburgh tests was 0.6. It would seem probable that the discrepancy between the two sets of results at low values of ΔK is principally a manifestation of crack closure effects producing slower growth rates in the NPL samples tested at R = 0.1. There is clearly scope for further work to evaluate an appropriate equilibrium growth rate equation for Q1(N) in this mean stress sensitive region.

Crack growth rates which are solely dependent on the magnitude of the applied dynamic stress intensity are normally found to be adequately described by the original Paris equation* which has the form

$$\frac{da}{dN} = C(\Delta K)^m \qquad (6.5)$$

A linear characteristic is therefore predicted when the data is presented in log-log format. Figure 4.5 reveals that Q1(N) exhibits linearity over a crack growth rate interval of about one order of magnitude. In this region the exponent m takes the value 2.31. It is interesting to compare this value with the data presented by Ritchie [54]. He suggests that materials of low fracture toughness have both a high value of m and a sensitivity to mean stress resulting from the occurrence of "brittle" failure mechanisms at the crack tip. Figure 6.11 compares the values of K_c and m obtained for Q1(N) with the experimental results collated

*See section 2.3 for details

by Ritchie. The comparison is fundamentally invalid in the sense that the K_{Ic} value for Q1(N) would be expected to be less than the K_c value shown in the figure. It is none the less clear that Q1(N) conforms to the basic trend of Ritchie's data, i.e. it has a high fracture toughness, a low value of m and crack growth rates are entirely independent of the applied mean stress intensity at levels which preclude crack closure.

The final point to be made with regard to the equilibrium crack growth rates in Q1(N) is that the values obtained in the present study are in good agreement with the general observations of other workers. Figure 6.12 compares the data from Figure 4.5 with published "master curves". In particular it is seen that the growth characteristic of Q1(N) falls accurately into the region that is characteristic of growth by striation forming mechanisms. In this sense the crack propagation characteristics of Q1(N) are unremarkable.

6.3.2 The influence of simple load sequences on crack growth rates

Crack growth under service load conditions is critically influenced by a complex sequence of changes in the principal loading parameters. A series of tests was therefore undertaken to provide information concerning the individual effect of the different variables. The influence of mean stress changes on crack growth under constant dynamic loading conditions was reported in Section 4.2.3. Although both positive and negative values of $\Delta(\bar{K})$ were investigated the results were dominated by the growth retardation that followed a reduction of the applied mean stress intensity. The difficulties experienced in quantitising the delay effects have been previously discussed. Undoubtedly the concept of a "zero growth" interval, that was adopted for the purpose of analysis, should not be regarded as an accurate description of the true growth sequence.

Although temporary arrest certainly occurs at the specimen free surfaces it is not clear if the crack behaves in the same way in the interior. Experimental evidence indicates quite clearly that retardation is less severe at the specimen mid-thickness, any arrest that does occur in this region must consequently be of shorter duration. The fractographs presented in Figure 5.4 indicate dramatic differences in the growth rates prevailing at the free surfaces and in the more constrained specimen interior. For practical reasons the tests could not be continued for a sufficient time to re-establish the original equilibrium crack front profile. It was consequently not possible to evaluate the physical interval over which growth retardation occurred. Furthermore it was not possible to establish if total crack arrest could be induced by a reduction of $\bar{K}$ as the duration of appropriate tests would have been prohibitive.

Despite the above reservations ultrasonic determinations of the "zero-growth" interval have provided a valuable assessement of the relative influence of the way in which mean stress reductions affect crack growth rates. Retarded growth is almost certainly a consequence of crack closure effects reducing the effective range of the dynamic stress intensity. The interaction of the applied load and the residual stress field at the crack tip produces an effective value of $\bar{K}$ which is sufficiently low to cause significant crack closure effects. In this context it is interesting to note that large scale attrition of the fracture surfaces has not been observed. The closure effects apparently occur on a "micro" scale; unfortunately it has not been possible to determine if fracture surface attrition is detectable in the scanning electron microscope as no SEM examination of the surfaces shown in Figure 5.4 has been undertaken.

Mention was made in Section 4.2.3 of the apparent logarithmic relationship that existed between the zero growth interval (N_d) and the magnitude of the change in $\bar{K}$. The interdependence was detailed in equation 4.4. Further experimental work is required if the generality of the proposal is to be established. The through thickness variation of the retardation indicates that crack arrest is a complex pheomenon. Very much more detailed information is required if quantitative predictions of crack growth rates are to become possible; the number of parameters involved is truely daunting.

In contrast to the above discussion increases in $\bar{K}$ were found to have a very much less significant influence on the net crack growth rate. The investigation of mean stress effects on equilibrium growth rates, reported in Section 4.2.1, involved the application of increases in $\bar{K}$ to cracks growing under equilibrium conditions. Although the magnitude of $\Delta(\bar{K})$ was usually low ($\simeq 10 MNm^{-3/2}$) it was clear that damage was restricted to a "stretch zone" created by the increase. No subsequently acceleration of the growth rate was observed. For cracks exhibiting a non-equilibrium profile, i.e. following a reduction in $\bar{K}$, the effect was more complex. However it was concluded in Section 4.2.3 that no significant acceleration of growth occured at the most advanced part of the crack front. It may therefore be predicted that under complex loading conditions the net influence of a sequence of positive and negative changes in mean stress intensity will be to retard the overall rate or propagation relative to the rate expected at a constant value of $\bar{K}$.

The influence of periodic dynamic overload sequences on equilibrium crack growth rates was reported in Section 4.2.4. The

various alternative overload conditions were detailed in Figure 2.8. Referring to this figure* the signal generator used was only capable of applying the type (b) sequence; that is a purely dynamic, positive start overload. The conclusion drawn from the extensive series of tests, summarised in Figures 4.13 to 4.27, is that the overall crack growth rate shows no significant deviation from the rates predicted on the basis of a linear summation of the equilibrium damage rates. Fractographic studies indicate that single cycle overloads produce a "stretch" zone on the fracture surface, the multiple overload sequences created clearly striated regions that were typical of equilibrium growth under the overload conditions. Other workers have successfully determined growth rates occurring during overload sequences by measurement of individual striation spacings. It is extremely doubtful that the approach could be successfully applied to Q1(N). The general definition of features on the fracture surface is poor and dimensions are far from regular. For example an overload "band", such as that shown in Figure 5.12(c), may vary in width by $\pm 50\%$. Furthermore it is only under particularly favourable loading conditions that individual surface features may be satisfactorily correlated with the applied load sequence. Q1(N) is therefore an unsatisfactory material for providing micro-growth data for comparison with the various

---

* Overloads as per Figure 2.8:

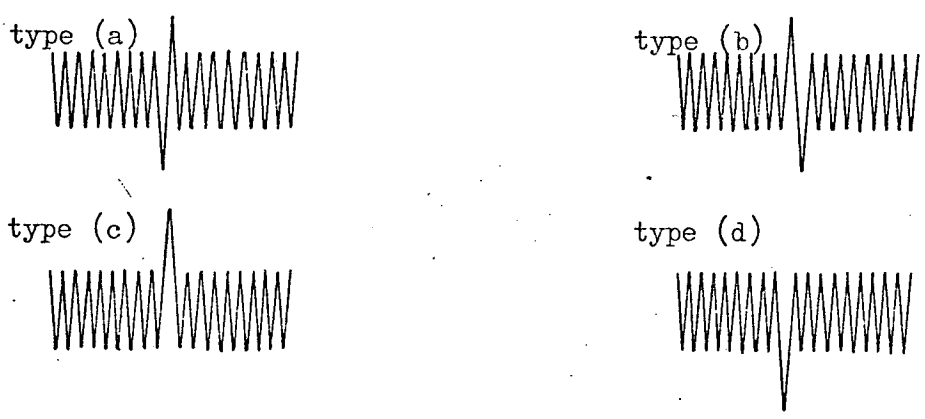

retardation models reviewed in Chapter 2. The average macro-growth rates determined by the author are not suitable for such purposes.

Although it was only possible to investigate the effect of one type of overload sequence it is possible to make reasoned predictions as to the influence of the other sequences on crack propagation in Q1(N). The critical factor is the materials response to changes in the net* mean stress at the crack tip. Referring to Figure 2.8 the effects of the type (c) and (d) sequences, that involved changes in mean stress, are readily evaluated. Consider the compressive overload (d). The load sequence is essentially that used by the present author to investigate the effect of changes in mean stress intensity. The only complication is that the dynamic stress is increased at the same time that $\overline{K}$ is reduced. However, relative to equilibrium growth, the damage rate during the "overload" phase will undoubtedly be retarded as a result of the reduced value of $\overline{K}$. The subsequent increase of $\overline{K}$, and simultaneous reduction of ΔK, to the original level is not expected to result in any significant acceleration of crack growth in Q1(N). Thus, depending on the frequency with which the "overload" sequence is applied, the overall growth rate will either be equal to or less than the value predicted by a summation of the equilibrium growth rates. Similar reasoning applies to the tensile overload shown as (c) in Figure 2.8. Trebules et al [79] have investigated this type of sequence in 2024-T3 aluminium alloy. Relative to the

*i.e. applied mean stress plus residual mean stress.

equilibrium growth rates they reported accelerated damage during the overload phase and subsequent retardation on return to the lower dynamic load conditions. Both effects were considered to be manifestations of a mean stress sensitivity. In Q1(N) acceleration during the overload phase will be minimal, on the other hand growth retardation is expected at the lower dynamic load level. The residual stress field, and hence the degree of retardation, may depend on the number of overload cycles applied for the reasons discussed by Trebules et al. However, once again, the qualitative conclusion is that, in practice, the rate of crack extension will not exceed the value obtained from a summation of the equilibrium growth rates. Only overloads of the type shown in Figure 2.8(a) remain to be considered. It has been demonstrated that in aluminium alloys type (b) sequences may produce sequential periods of accelerated and retarded growth rates after the overload conditions are removed [77]. The causes were considered in Section 2.5.4. Similar reasoning may be applied to type (a) overloads and Schijve [77] presents results which demonstrate that such sequences may either increase or reduce a component's net life. However sequences of types (a) and (b) are in essence each a combination of types (c) and (d) which, it has been argued, cannot individually produce an overall increase of the crack growth rate in Q1(N). Thus the mutual opposition of (c) and (d) overloads in a type (a) sequence is confidently expected to result in an overall damage rate that does not exceed the predicted value obtained by summing the equilibrium growth rates.

It is argued above that under no circumstances will crack growth rates in Q1(N) exceed predicted values obtained from consideration of equilibrium growth rates. This conclusion is based on the demonstrated insensitivity of Q1(N) to increases in the applied mean stress conditions. Whilst crack growth retardation may

occur as a consequence of closure effects, no load sequences are expected to result in damage rates that exceed the mean stress independent, "equilibrium" values given in Figure 4.5. The nature of the Q1(N) fracture surface has prohibited determination of micro-growth rates by striation measurement techniques, it has therefore not been possible to evaluate the various quantitative growth retardation models reviewed in Chapter 2. Changes in crack front profile, following reductions in mean stress intensity, indicate that retardation effects are influenced by the prevailing specimen thickness. This factor not only complicates growth rate predictions but also indicates that the established thickness independence of equilibrium crack growth rates may not hold for damage resulting from complex load sequences. The influences of the more complex sequences involved in block loading are discussed in the next section.

6.3.3 Crack propagation resulting from block load sequences

The investigation of crack growth rates under block loading sequences confirmed the general predictions of the simpler tests discussed above. The results of both 3 and 8 level tests were reported in Section 4.2. The test performed under constant mean stress intensity conditions constituted a logical extension of the earlier investigation of crack growth occurring under two level dynamic overload conditions. Whereas the two level tests indicated no significant growth retardation, damage caused by constant $\overline{K}$ block loading was generally about 20% below the rates predicted from equilibrium considerations. This result is not unreasonable in view of the tensile overloads that the block regimes impose; it is perhaps more surprising that no retardation was detected in any of the simpler two level dynamic overload tests. Macro-growth rate considerations and fractographic evidence indicated that crack

extension occurred during each block of the 3 level, constant $\overline{K}$ tests. Tests conducted with a constant K_{min} restriction yielded very much reduced growth rates. Again it was shown that crack extension occurred at each of the three dynamic load levels. The three level tests indicate that a distinct load history effect is operative under constant K_{min} conditions; growth occurred more rapidly under the "low-high" regime than under either of the other sequences. The trend is consistent with the observations of Hardrath [91,92] which were summarised in Figure 2.17. However whereas he established that the damage rate increased in the order:

"high-low","low-high-low", "low-high"

the present study revealed no differences in the influence of the "high-low" and "low-high-low" regimes. Figure 4.30 suggests that a similar load history effect may exist under constant $\overline{K}$ conditions; insufficient data is available to support a definite conclusion. The same limitation prevents the assessment of sequence effects assosicated with 8 level regimes, however it is notable that the results presented in Figure 4.32 do not conflict with the generalities of the foregoing discussion.

The limitations of block loading sequences for evaluating crack growth rates under service load conditions were discussed in Chapter 2. In the case of $Q1(N)$ it is growth retardation effects that determine the average rate of crack extension under complex load sequences. It is expected that in situations in which retardation occurs the absolute rate of crack extension, at any moment, will be a function of the number of cycles applied since a load discontinuity occurred. For block load tests this effect would be detectable as

a sensitivity, of the crack growth rate, to the number of cycles in the periodically repeated sequence. Figure 2.16 summarises the results of block length tests conducted on 2024-T3 aluminium. It is expected that Q1(N) will exhibit a comparable sensitivity to block length when significant retardation effects prevail. Thus it is anticipated that crack growth rates in Q1(N), tested at a constant value of $\overline{K}$, will be only slightly influenced by the prevailing block length as retardation effects under these conditions are minimal. In contrast retardation effects are more severe when K_{min} is maintained constant; a greater sensitivity would therefore be expected to changes in the applied block length. In practice service load sequences will involve frequent and essentially random changes in the loading conditions experienced by a given component. Consequently, as retardation effects are expected to be influenced by the precise nature of the load sequence, the crack growth rate at any moment will be uniquely determined by the prevailing load sequence. It is therefore expected that block load regimes, derived from service load data, will not generally be satisfactory for assessing the "in service" rate of fatigue damage.

A further point which may prove important in service load simulations concerns the specimen geometry. It has been shown that growth retardation effects are probably influenced by the thickness of the test piece. As, in Q1(N), growth rates under complex load sequences are principally influenced by retardation effects it is probable that the prevailing specimen thickness will have some effect on the overall growth rate associated with any given load sequence. The consideration of this possibility should constitute a rider to the conclusion of Richards and Lindley [122] concerning the thickness independence of striation forming crack growth mechanisms.

6.4 The Wider Implications of the Established Fatigue Properties of Q1(N)

The present study has been exclusively concerned with fatigue crack growth in Q1(N) parent plate material. It has been established that the equilibrium crack growth rates in the alloy are in excellent agreement with the published properties of other ductile steels. Furthermore it has been shown that in Q1(N) mode I crack growth occurs solely by a striation forming mechanism. Such mechanisms are generally found to be associated with equilibrium growth rates that are independent of both the specimen thickness and the applied mean stress intensity. Q1(N) is consistent with this trend. Under complex load sequences, non-equilibrium growth rates may prevail as a consequence of the retarding effects caused by the occurrence of "crack closure"; load history effects are not expected to result in accelerated rates of fatigue damage. With regard to the static strength of Q1(N) it has been demonstrated that the fracture toughness approach does not accurately predict the loading conditions under which catastrophic failure occurs. However, it has been shown that an acceptably reproducible value of K_c is obtainable and that the parameter has considerable value in defining dynamic loading conditions under which fatigue damage is extremely severe.

In the context of the structural integrity of Q1(N) the above generalisations are reassuring. The resistance of notched parent plate to damage under both static and dynamic loading conditions is essentially identical to that of more traditional structural steels. With particular reference to naval construction the very low inclusion content of Q1(N) makes the alloy superior to its immediate predecessor, QT35. Thus, as far as the parent plate is concerned, it is anticipated that only minimal changes in established design procedures are necessary. Procedures, that have in the past,

proved successful in defining a satisfactory balance between the static and fatigue strengths of a structure will remain valid for application to Q1(N). It is none the less important to appreciate that, relative to more traditional materials, the improvement obtained in the unnotched static strength of Q1(N) has not been matched by a similar improvement in its resistance to fatigue. Thus the potential benefits of the higher strength material may, in part, be discounted by the need to contain the unchanged susceptibility to damage by fatigue.

A further practical complication arises from the use of Q1(N) in the fabrication of large welded structures. In such applications the welded joints are found to have the greatest susceptibility to fatigue damage. A total appraisal of the alloy must therefore include studies of crack propagation in the "as welded" material. With regard to design procedures it is critical to establish that the fatigue properties of as welded Q1(N) are not inferior to those of its historical precursors in pressure vessel construction. Some comparisons of crack propagation in "as welded" specimens of QT35 and and Q1(N) have been made by Evans et al [55]. Their results indicated little difference in the equilibrium crack growth rates of the two "as welded" alloys when R was equal to 0.1. Significantly they did not investigate the influence of mean stress intensity on crack propagation rates in the welded joints. Results published by Griffiths et al [131] indicate that the applied mean stress intensity can have a critical influence on the rate of crack growth in ferritic weld metals. Figure 6.13 summarises their results which quite clearly demonstrate that the loading conditions may determine the crack growth mechanism which in turn may influence the rate of crack growth. Thus the change from striation formation to a void coalescence mechanism causes the "equilibrium" growth rates to become extremely sensitive to the level of the applied mean stress

intensity. The data presented in Figure 6.13 was obtained from tests on stress relieved welds; such a treatment is not practically applicable in the case of pressure vessel construction. The result is that cracks growing in the "as welded" material are subjected to the simultaneous influence of the retained stress field and the applied structural load. Thus, as retained stresses in excess of the nominal yield value are commonly encountered, the overall damage rate may be unfavourably accelerated if the crack growth rate in the "as welded" material is mean stress sensitive. It is important to bear this point in mind when assessing the suitablility of different materials for pressure vessel construction.

In the case of Q1(N) it is particularly important to establish that the "as welded" alloy is not inferior to its predecessor, QT35. The tests performed at NPL [55] established that welded samples of the two alloys had similar fatigue resistance at low values of mean stress intensity, R = 0.1. The relative mean stress sensitivity of crack growth in the "as welded" alloys was not investigated, it is considered that a full appraisal of the two materials should include consideration of this property. A series of tests, similar to those reported in Section 4.2.1 of the present study, would reveal if there were any significant differences in the properties of the "as welded" alloys. The present design and inspection procedures for pressure vessels may be endorsed as satisfactory so long as Q1(N) proves less mean stress sensitive than QT35; however if the reverse is true it will be necessary to reassess certain aspects of Q1(N)'s utilisation.

In the introduction to this thesis mention was made of the designers problem of ensuring that established principles of pressure hull construction provide the correct balance of static strength and fatigue resistance when a "new" material, such as Q1(N), is adopted. The present study has shown that the crack growth resistence

of Q1(N) parent plate is in no way inferior to that of other low alloy steels. Furthermore it has been established that load history effects will not result in accelerated damage rates; crack growth retardation, on the other hand, is to be expected under most complex load regimes. Thus design criteria established for materials such as QT35 are applicable to Q1(N) parent plate so long as it is appreciated that the relative increase in tensile strength is not associated with a similar increase in fatigue resistance; fatigue properties of the two alloys are basically identical. From the structural point of view the fatigue susceptibility of the welded joints is critical. Provided it is established that mean stress effects do not have a deleterious influence on crack growth rates in "as welded" Q1(N), it will be possible to reaffirm existing pressure vessel design and inspection procedures as satisfactory for application to structures fabricated from Q1(N).

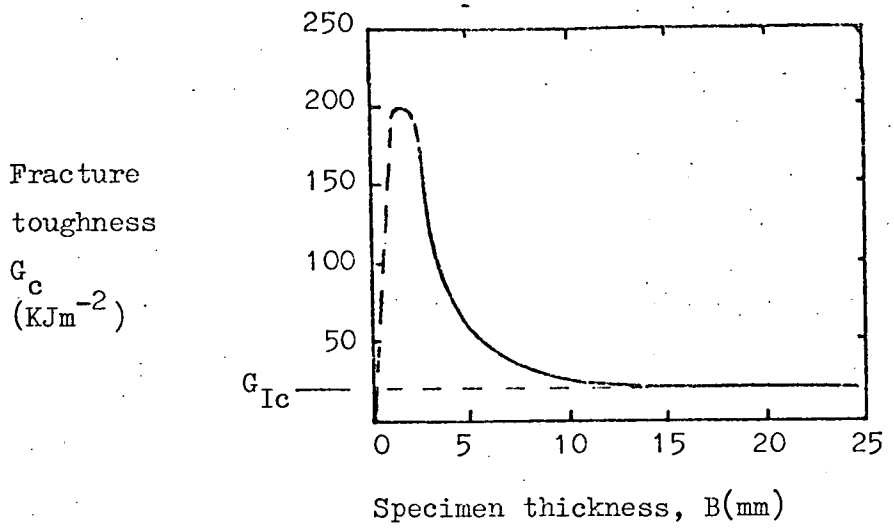

Figure 6.1 The variation of fracture toughness with specimen thickness in 7075-T6 aluminium alloy. (After Knott [4]). $G = K^2/E$.

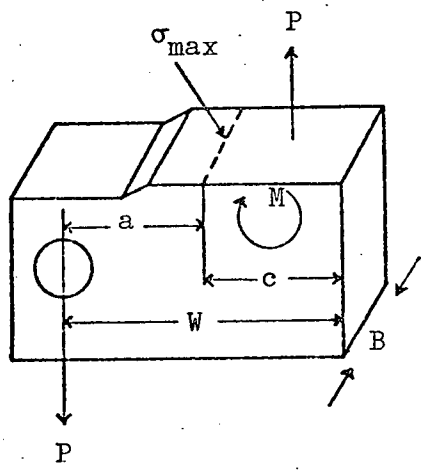

Figure 6.2 Free body diagram for CKS sample.
(After Katcher [115]).

$$\sigma_{max} = \frac{P}{A} + \frac{Mc}{I}$$

A = Area of uncracked ligament.

I = Second moment of area of uncracked ligament about its centre line.

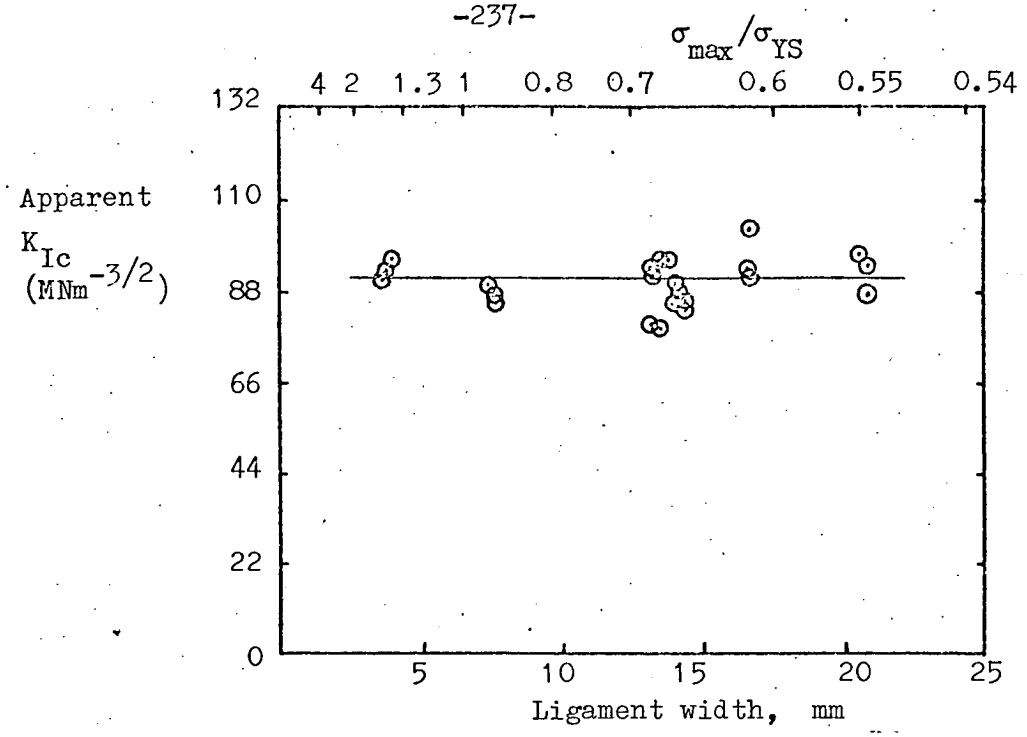

Figure 6.3 Data from Brown and Srawley [116] that demonstrates the possibility of determining K_{Ic} when $\sigma_{max} > \sigma_{YS}$ (Maraging steel, $\sigma_{YS} = 1670 MNm^{-2}$)

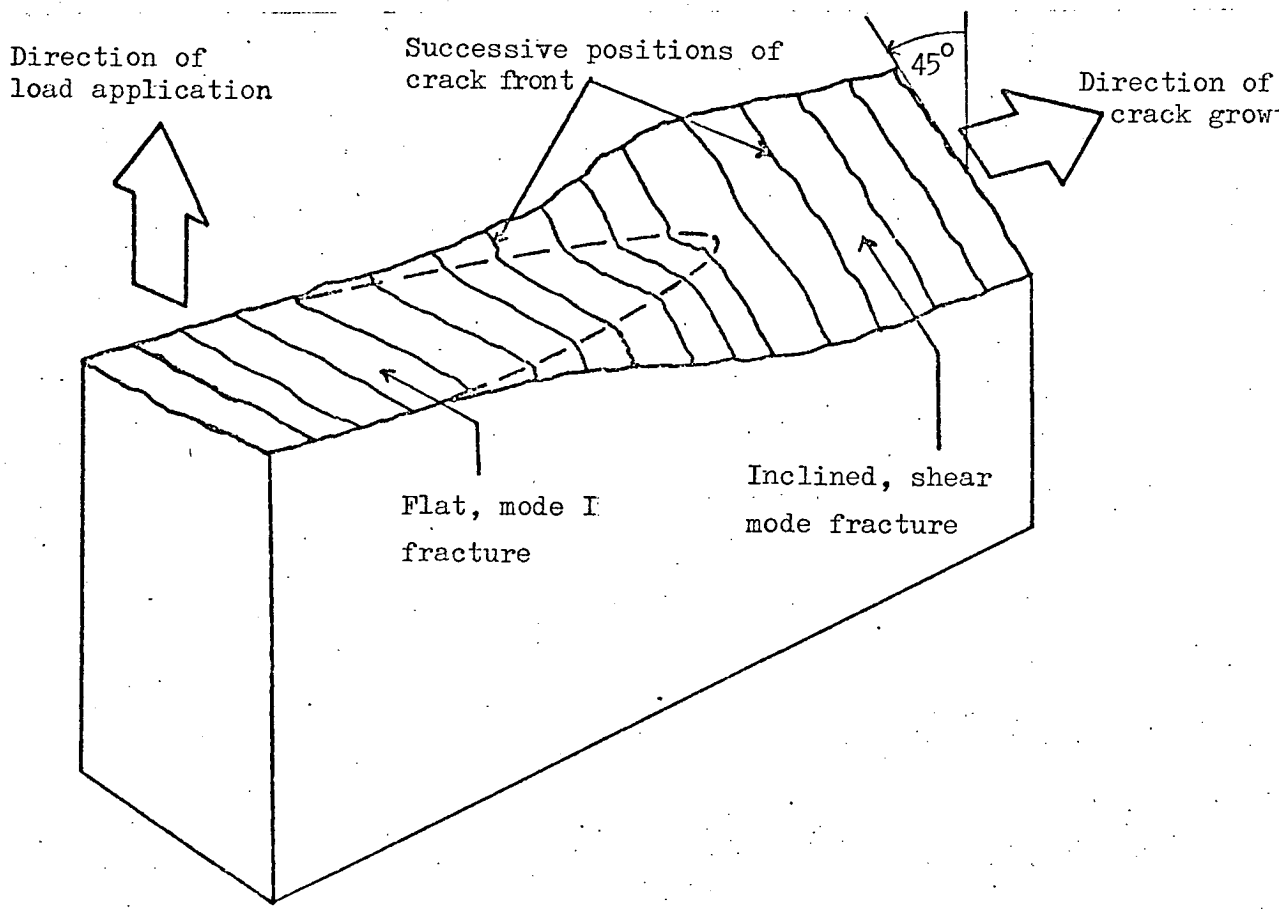

Figure 6.4 Schematic of fatigue fracture surface transitional behaviour in sheet materials. (After Schijve [77]).

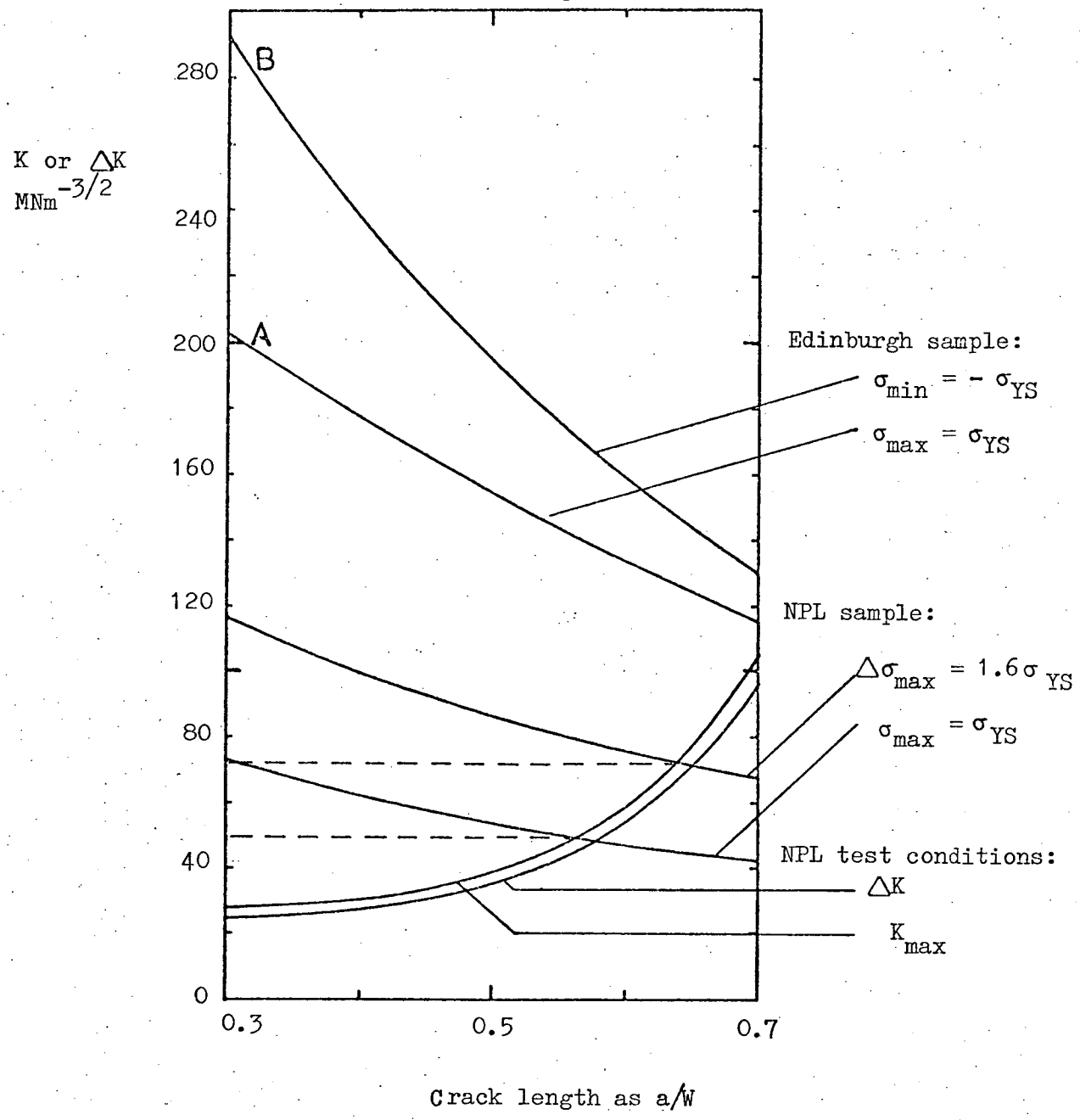

Figure 6.5 Nominal ligament yielding conditions for Edinburgh and NPL [55] samples. Also shown are ΔK and K_{max} for standard NPL tests.

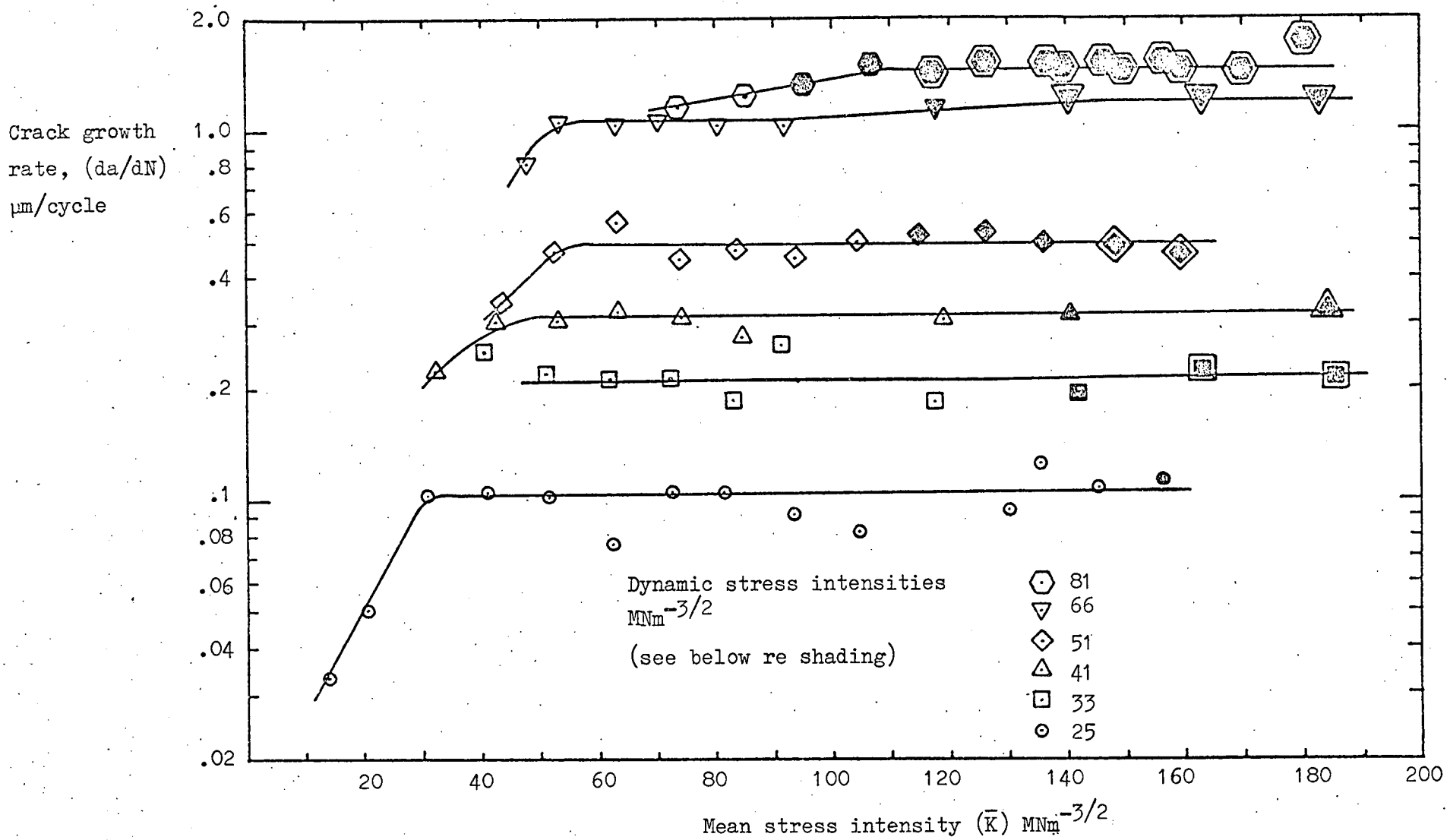

Figure 6.6 The influence of mean stress intensity and nominal yielding in the uncracked ligament on crack growth rates in Q1(N). (Data from Figure 4.4).

Symbols: "open" $\sigma_{max} < \sigma_{YS}$, i.e. no nominal yielding;
"shaded", $\sigma_{max} > \sigma_{YS}$ and $\sigma_{min} > -\sigma_{YS}$, i.e. nominal yielding at crack tip only;
"double", $\sigma_{max} > \sigma_{YS}$ and $\sigma_{min} < -\sigma_{YS}$, i.e. tensile and compressive yielding in ligament.

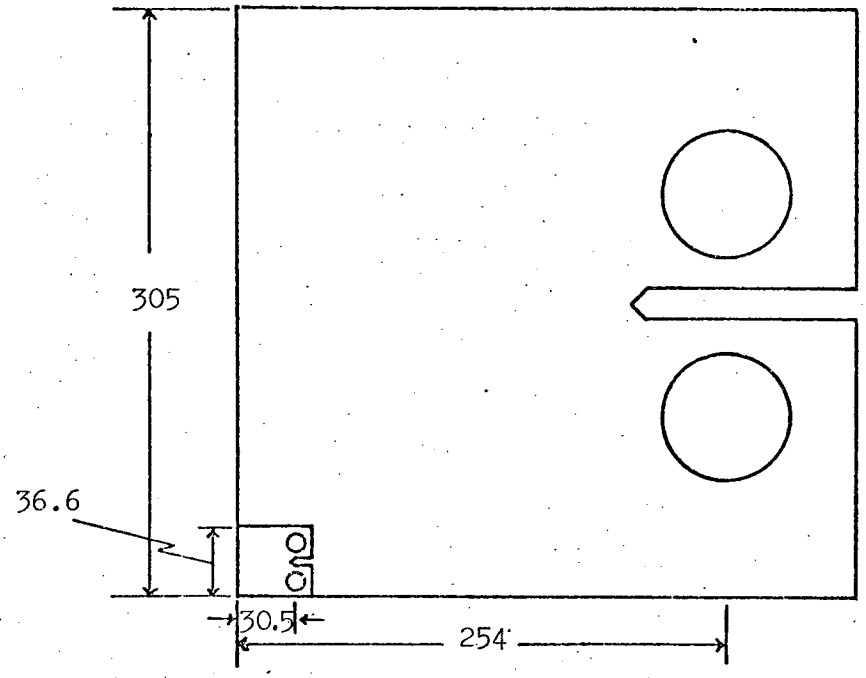

Figure 6.7 $\frac{1}{4}$ scale comparison of the author's CKS sample with the smaller NPL test piece.
Thickness: Edinburgh 35mm, NPL 14mm
Dimensions in mm.

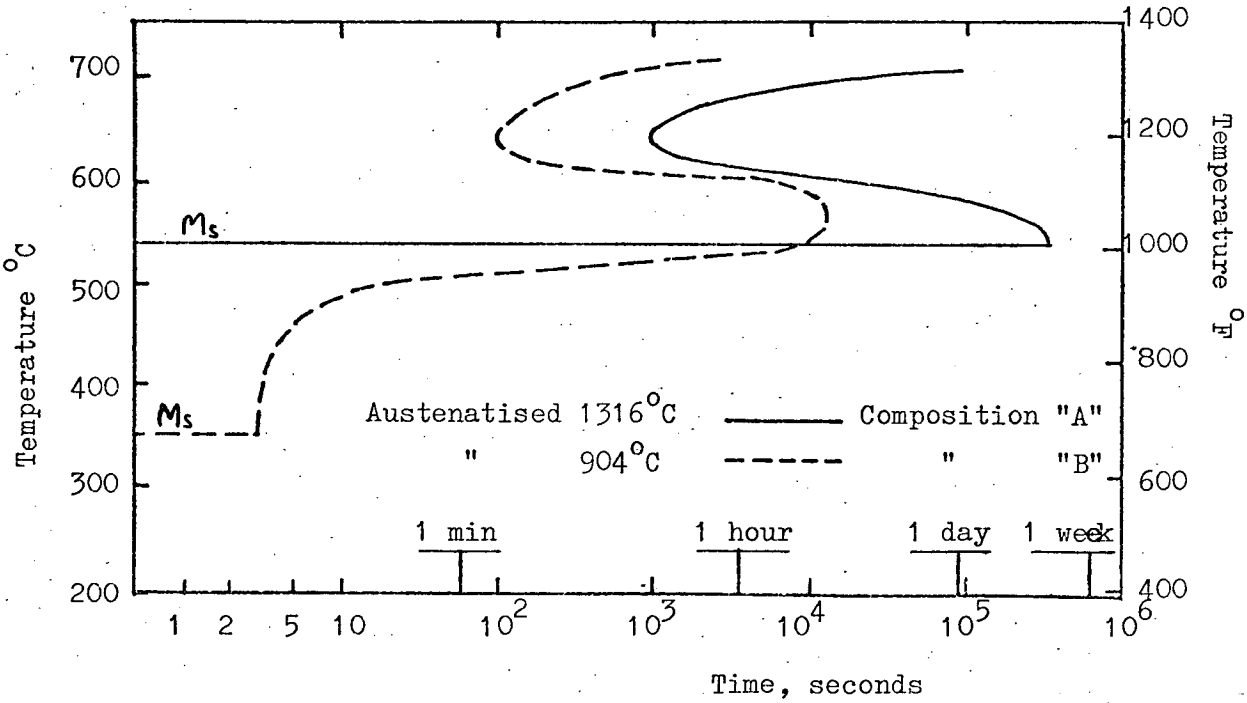

Figure 6.8 Partial TTT diagram for HY-80 from Emmanuel et al [124]

Analyses:	C	Mn	P	S	Si	Ni	Cr	Mo
A	.16	.34	.014	.024	.25	2.87	1.52	.41
B	.13	.16	.009	.013	.10	3.08	1.76	.49

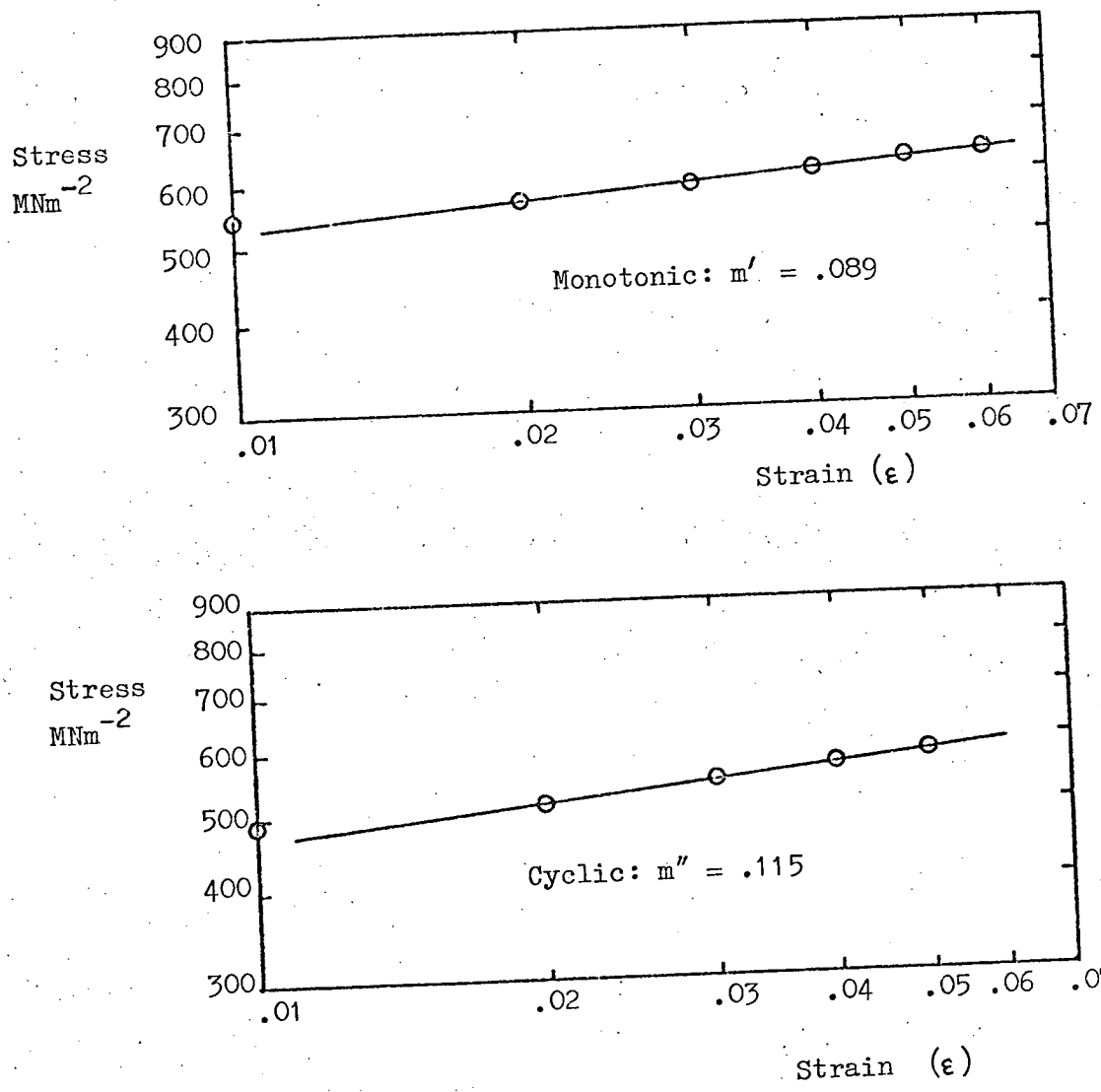

Figure 6.9 Monotonic and cyclic strain hardening exponents for Q1(N). Data taken from Figure 4.2.

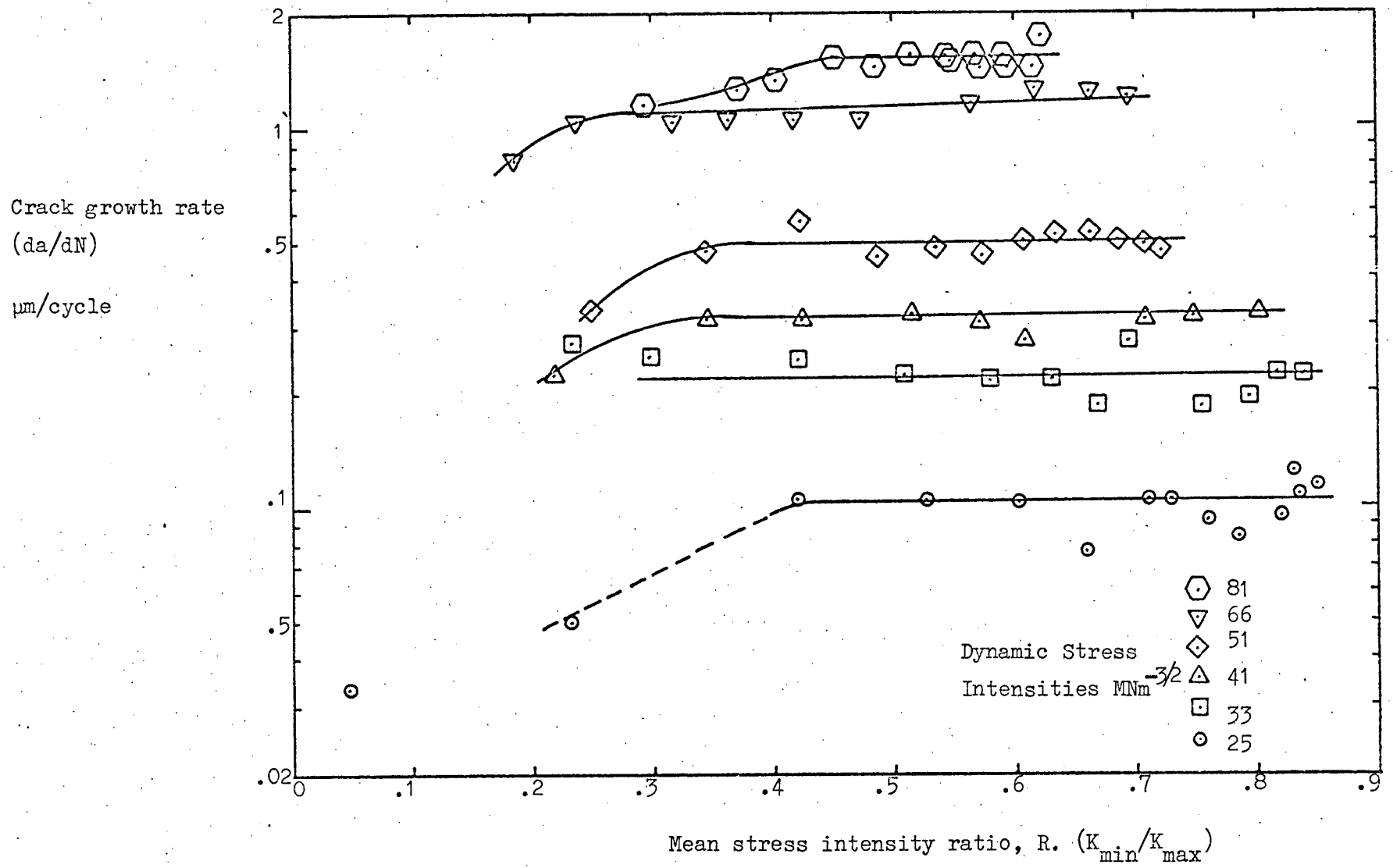

Figure 6.10 Mean stress intensity data presented as a function of the stress ratio R.
(Data from Figure 4.4)

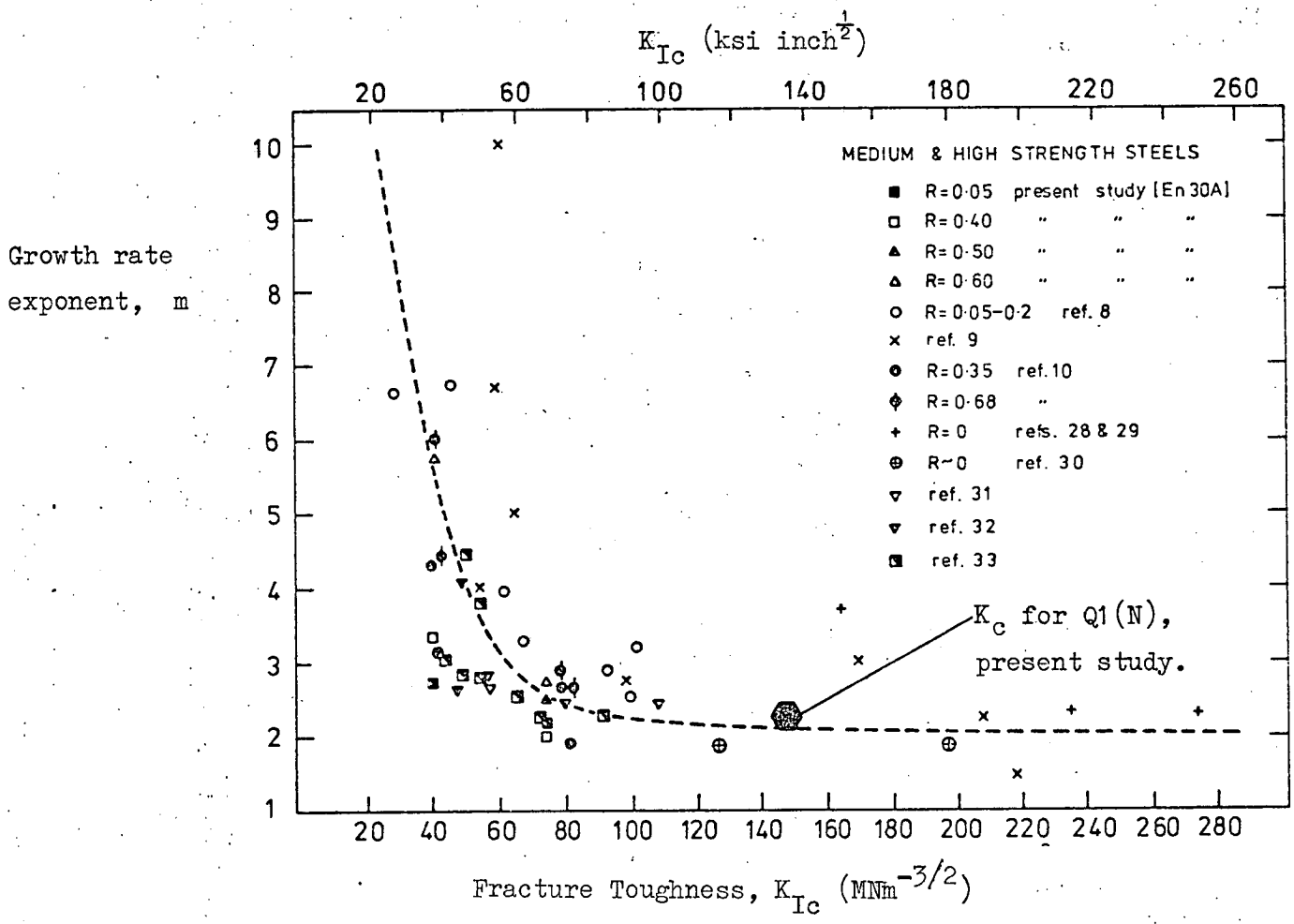

Figure 6.11 Correlation of fracture toughness values and the growth rate exponent m from the Paris equation, equation 6.5.
Basic data from Ritchie [54]. Reference numbers in legend are as given in [54].

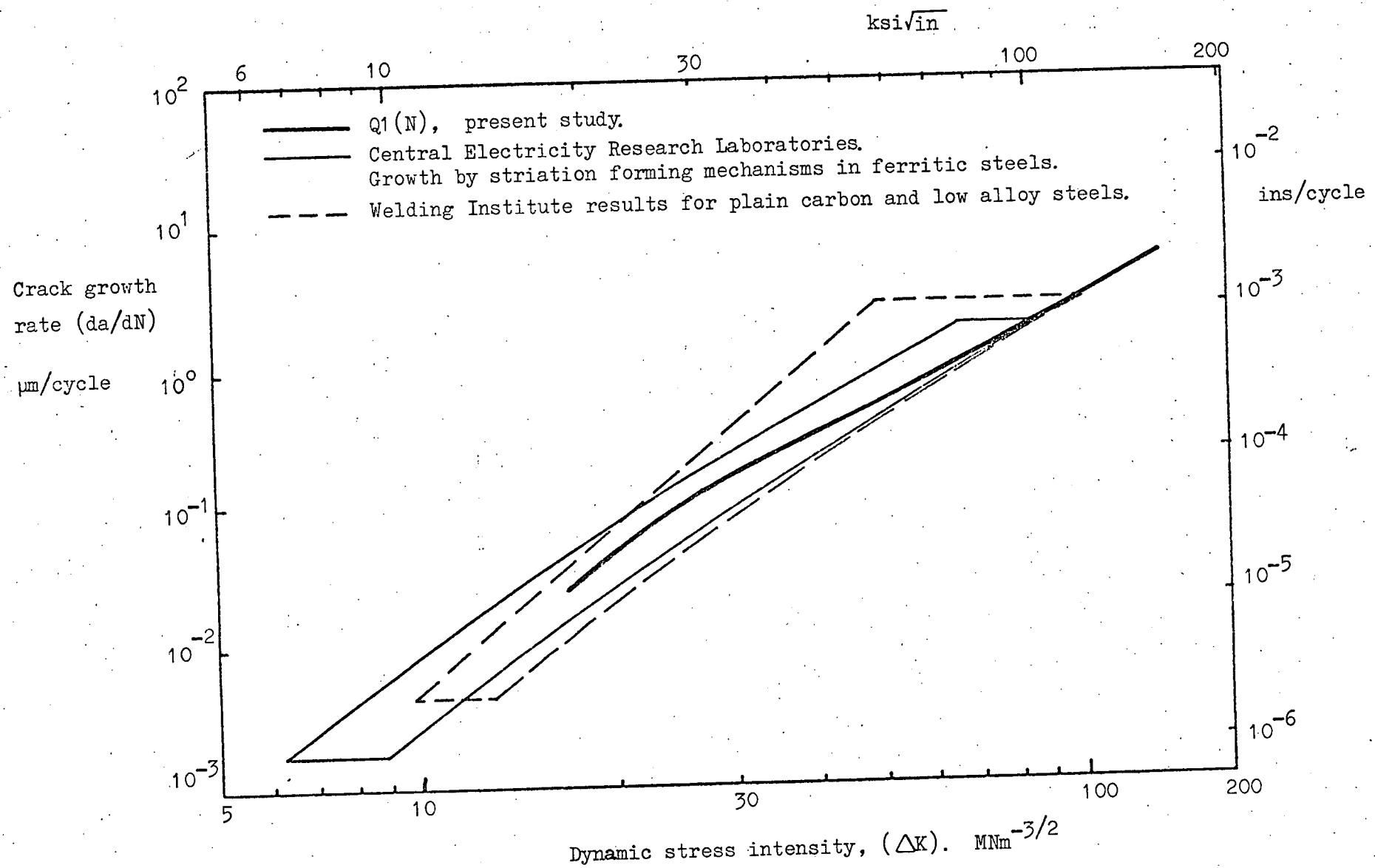

Figure 6.12 Comparison of equilibrium growth rates in Q1(N) with "master-curves" of other workers. (After [122]).

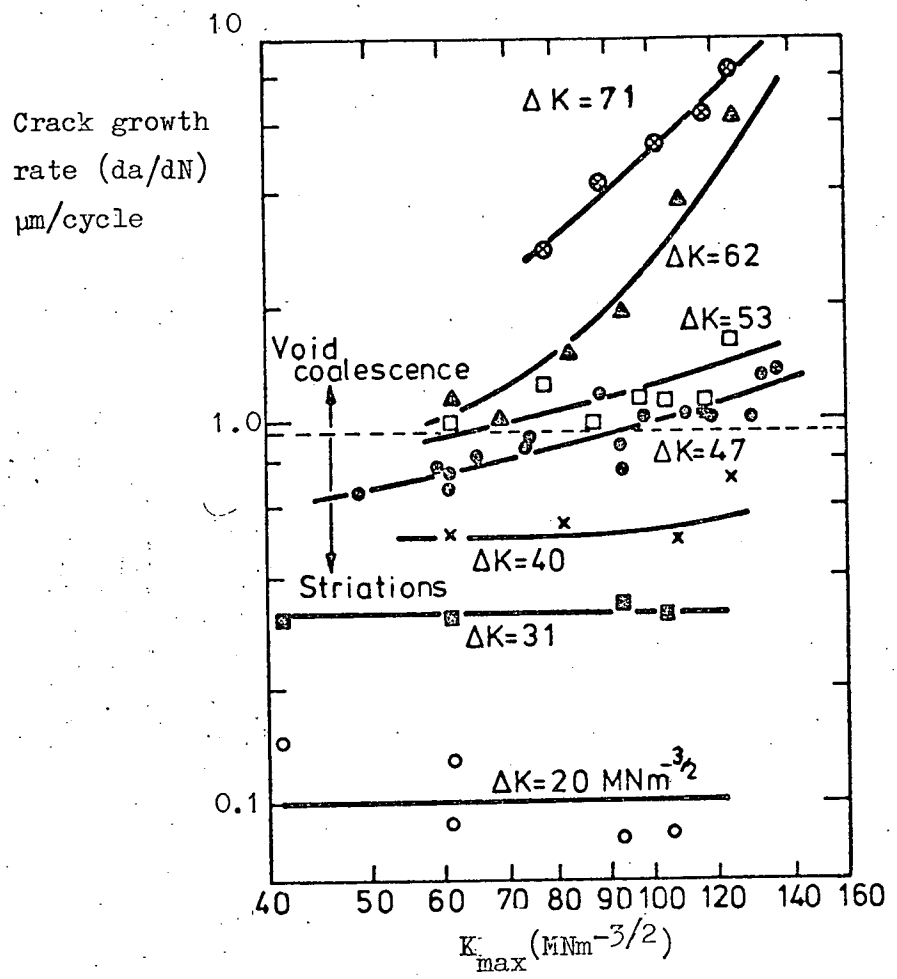

Figure 6.13 The effect of K_{max} on fatigue crack propagation rates in ferritic weld metal. (After Ritchie [54]).

These results, originally published by Griffith et al [131], demonstrate how the mean stress sensitivity of cracks propagating in ferritic weld metal may be influenced by a change in the growth mechanism.

CHAPTER 7

CONCLUSIONS

Basic Properties of Q1(N)

1) The mechanical and structural properties of the Q1(N) parent plate employed in the present investigation were found to be extremely uniform. The through thickness hardness was consistent to HV_{30} 248 ± 10; the yield stress was evaluated at 646 MNm^{-2}.

2) Cyclic stress/strain tests indicated that Q1(N) cyclically softened. This behaviour was consistent with predictions which may be made from consideration of either the ratio: σ_{YS}/σ_{UTS}, or the value of m', the monotonic strain hardening exponent [126].

3) Fracture toughness tests indicated that consistent values of K_c may be obtained from multiple tests performed on a single sample. K_c was evaluated at 146 ± 12 $MNm^{-3/2}$ for the 35 mm thick CKS fatigue sample. 35mm thick Q1(N) plate material is not suitable for determining the material's plane strain fracture toughness according to either British [111] or ASTM [112] standard procedures.

4) For Q1(N) the K_c value was found not to predict the loading conditions at which catastrophic component failure was imminent. Both static and cyclic loads could be supported

when K_{max} was considerably in excess of K_c. Fractographic studies indicated that static loading to K_c produced a "stretch zone" on the fracture surface but that there was no tendency for failure to occur by brittle fracture mechanisms. Despite its inapplicability to static failure in Q1(N), the K_c value was found to be a valuable indication of the fatigue loading conditions ($\Delta K = K_c$) which resulted in extremely rapid crack growth rates, ($da/dN \simeq 10\mu m/cycle$).

Equilibrium crack propagation in Q1(N)

5) The equilibrium fatigue crack growth rates determined in the present study have been shown to be substantially independent of the CKS specimen geometry. It has also been established that the stress intensity parameter may be meaningfully employed to correlate crack growth rate data. Only growth resulting from mode I crack opening has been investigated.

6) In Q1(N) equilibrium crack growth rates are independent of the applied mean stress intensity except at low values (<0.1) of the stress ratio R at which growth retardation may result from crack closure effects. It is particularly significant that neither monotonic yielding of the uncracked ligament nor values of K_{max} in excess of K_c result in accelerated crack growth. Mode I growth was observed to occur by striation forming mechanisms under all loading conditions, no alternative growth processes were detected.

7) It has not been possible to determine crack growth rates at low values of the stress ratio, R. It is expected that growth retardation, by crack closure, will become increasingly important as R is reduced below 0.1. A considerable amount of further work is required to define the equilibrium crack growth rates for conditions that involve crack closure.

8) At mean stress intensities above the levels that cause crack closure the equilibrium crack growth rate, for Q1(N) in air, may be expressed as a function of the applied dynamic stress intensity alone. For growth rates between 0.1 and 1 μm/cycle, the basic Paris expression [32] may be used in the form:

$$\frac{da}{dN} = C(\Delta K)^m \qquad (7.1)$$

where $C = 6.17 \times 10^{-5}$ and $m = 2.31$ when ΔK is expressed as $MNm^{-3/2}$ and da/dN as μm/cycle. Outwith the limits given the log-log da/dN/ΔK characteristic was found to be non-linear. An empirically determined polynomial may be used to define the growth rates over a wider range of da/dN. The expression

$$\log\left(\frac{da}{dN}\right) = -150.1 + 88.84\log(\Delta K) - 17.95(\log(\Delta K))^2 + 1.240(\log(\Delta K))^3 \qquad (7.2)$$

is applicable between the limits

$$.02 < \frac{da}{dN} < 4 \qquad (7.3)$$

when ΔK and da/dN are expressed as $kNm^{-3/2}$ and μm/cycle respectively.

9) The equilibrium $da/dN/\Delta K$ characteristic for Q1(N) was found to be in good agreement with the generalised "master curves", reported by other workers, for fatigue crack propagation in plain carbon and low alloy steels.

The influence of load sequence effects on crack propagation in Q1(N)

10) Simple load sequences have been used to investigate the influence of changes in mean stress intensity on crack growth rates. Reductions in $\overline{K}$ were found to result in crack closure effects which caused growth retardation. The degree of retardation varied through the specimen thickness, the effect was most severe at the free surfaces. Increases in $\overline{K}$ were found to have no significant influence on the macro-growth rate.

11) Simple, two level, dynamic overload sequences were found to produce crack growth rates that agreed with the values predicted from a summation of equilibrium growth rates. More complicated 3 and 8 level sequences applied at a constant value of $\overline{K}$ were found to result in some growth retardation relative to the equilibrium predictions.

12) Crack growth rates resulting from 3 and 8 level block load sequences applied at a constant value of K_{min} were found to be significantly retarded relative to both the predicted equilibrium damage and the damage produced by the same sequences when applied at a constant value of $\overline{K}$. The observed growth retardation is considered to be a manifestation of crack closure effects.

13) The three level, constant K_{min}, block load tests revealed that the overall damage rate was influenced by the sequence

of load application; the "low-high" regime was found to give significantly faster crack growth than the other two sequences. It is expected, but not proven, that growth rates in Q1(N) will also be sensitive to the repetition interval of block load sequences.

14) Consideration of the various experimental results indicates that, relative to the established equilibrium growth rates, Q1(N) will not exhibit accelerated growth rates as a consequence of load sequence effects. It is anticipated that service load sequences will, in all cases, result in a relative retardation of the overall damage rate. The exact crack growth rate in any situation will be principally influenced by the applied load sequence. It is expected that the geometry of the component may have a secondary influence, as growth retardation was found to be affected by the test piece thickness. Both these points should be borne in mind for simulations of "in service" damage rates.

15) Q1(N) has been found unsuitable for the application of striation measurement techniques to the evaluation of micro-growth rates following changes in the loading conditions. It has therefore been impossible to assess the accuracy with which existing retardation models describe micro-growth rates in the alloy.

Implications of the present work with regard to Q1(N) structures

16) Q1(N) shows no tendency to fail by brittle fracture mechanisms when subjected to static or cyclic loading at ambient temperature. The integrity of the notched parent plate material is no worse than that of more traditional structural steels, indeed the metallurgical cleanliness of

the alloy makes it in some ways superior to its immediate naval predecessor, QT35.

17) From the constructors' point of view it is important to appreciate that although the yield strength of Q1(N) is superior to that of its precursors, the various alloys have essentially the same susceptibility to fatigue damage. Thus the constructional advantages of the improved static strength may be partially discounted by the unchanged fatigue properties.

18) In practice the fatigue resistance of welded joints in Q1(N) is of critical importance. A full assessment of the relative merits of alternative alloys should include testing of the "as welded" material. It is particularly important to determine if residual welding stresses can accelerate fatigue damage rates. It is considered that an assessment of the influence of mean stress on crack growth rates in "as welded" Q1(N) should be undertaken.

Fatigue testing of Q1(N)

19) The circumstances in which fracture mechanics analyses may be correctly applied to fatigue testing are currently not satisfactorily defined. With regard to Q1(N) it has been established that static yielding of the uncracked ligament does not influence the crack growth rate, however the onset of gross cyclic yielding should be considered as undesirable until proved otherwise. Specimen thickness, in the range 13-35mm, has no significant effect on equilibrium crack growth rates; but the parameter may influence growth rates resulting from complex load sequences as a consequence of the thickness dependence of the growth

retardation mechanism. No simple thickness criterion, similar to that applied to standard fracture toughness tests, is applicable to fatigue testing of Q1(N).

CHAPTER 8

PROPOSALS FOR FURTHER WORK

The present study has revealed several problems which might advantageously be subjected to further attention. The recommendations that follow are divided into two categories: those that pertain to Q1(N) are given first; more general proposals regarding fatigue testing and the applications of fracture mechanics follow.

Proposals for further studies of Q1(N)

1) It is clear that crack growth rates in Q1(N) are affected by the applied mean stress intensity at low R values. A full definition of the equilibrium crack growth rates requires investigation of damage occurring at lower R values than were attainable in this work. A relatively simple series of tests could be undertaken to determine crack growth rates at levels of mean stress intensity below those used in the present investigation. Such a study would enable the equilibrium crack growth rates for Q1(N) to be fully defined in terms of both ΔK and $\overline{K}$. The work would require a test facility with a reversed load capability; furthermore, as considerably "retarded" growth rates are expected at low values of R, a high test frequency would be desirable.

2) It has been suggested that specimen thickness will influence crack growth rates when growth retardation occurs. If "in service" damage rates are to be simulated by laboratory tests it will be important to understand the influence of this parameter. An investigation of the thickness effect should therefore constitute a preliminary requisite of future studies of crack growth rates resulting from complex load sequences.

3) The fatigue properties of "as welded" Q1(N) have been considered by workers at NPL [55]. It is however, considered that a more extensive series of tests is required to ensure that the alloy is in no way inferior to its predecessor, QT35. It is particularly recommended that a relative study be made of the influence of mean stress intensity on crack growth rates in "as welded" specimens of the two materials. In this way it may be established whether or not fatigue damage is accelerated by residual stresses present in the welded joints of the alloys. From the design point of view it is important to establish that, in this respect, Q1(N) is no more susceptible to fatigue damage than QT35.

Proposals concerning the application of fracture mechanics

4) Standard procedures for plane strain fracture toughness testing place extremely restrictive limitations on the allowable test piece geometry. Any justifiable relaxation of the requirements would be welcome. It would appear from the discussion in Section 6.1 that the current restrictions on the uncracked ligament size could be relaxed. It is suggested that a test program be directed at determining less restrictive limits for the allowable crack

length and ligament size. In particular, it will be necessary to evolve a satisfactory means of detecting crack extension when gross yielding occurs in the uncracked ligament. There is no reason to believe that the current thickness criterion may be relaxed but if the other specimen dimensions could be reduced the following benefits would accrue:

(a) Routine testing could be conducted on smaller samples. Test facilities could be sympathetically reduced with a consequent saving in expense.

(b) K_{Ic} testing could be extended to certain materials that are currently precluded for geometrical reasons. In the case of plate materials such as Q1(N) tests are currently only possible if the plate thickness is sufficient to satisfy the thickness requirement of the K_{Ic} test. If the existing crack length and ligament restrictions could be significantly relaxed it is possible that fracture toughness specimens could be cut in such a way that the test piece thickness lay in the rolling plane of the plate. Samples cut in this way would permit a limited extension of the materials for which K_{Ic} values were obtainable.

(c) A more accurate definition of the geometrical conditions for which K_{Ic} is a meaningful failure criterion would be of assistance in assessing the significance of structural flaws. It is apparent the K_{Ic} is applicable under conditions that cause gross static yielding in bend specimens; it would be valuable to define these limits more accurately for these and other specimen configurations.

(d) Significant reductions in the width and height of fracture

toughness test pieces would make them geometrically similar to impact specimens. Considerable advantage in the understanding of the interrelationship of fracture toughness and impact properties could result from the ability to use a common specimen for both types of test.

5) Following from the above it would be valuable to have a recommended procedure established for K_c testing. The difficulties of standardising tests of this nature are formidable. It would, however, be valuable to have some relative measure of fracture toughness, as defined by K_c, for materials which cannot satisfy the thickness requirements of the standard plane strain tests.

6) There is a widespread need to establish formalised guide lines to indicate the conditions under which fracture mechanics analyses may be correctly applied to the correlation of fatigue data. Although Richards and Lindley [122] have given extensive consideration to the influence of specimen thickness on crack growth rates, there is no detailed knowledge of the significance of the stress conditions in the uncracked ligament. It is suggested that crack growth rates, at nominally identical values of applied stress intensity, be investigated for influences of both specimen size and the general specimen geometry. The identification of unacceptable specimen configurations would be of great assistance to future workers who seek to optimise their specimen size without invalidating the approach of fracture mechanics.

APPENDIX I

DESIGN AND CONSTRUCTION OF THE ULTRASONIC CRACK MONITOR

A1.1 Introduction

A satisfactory means of measuring crack length is a pre-requisite of any experimental study of fatigue crack propagation. It was apparent from the outset of this work that a comprehensive investigation of the fatigue properties of Q1(N), of the type proposed, would entail the collection of a great deal of crack growth rate data. The low frequency of the fatigue tests installation (2Hz) meant that individual tests could take many hours. Crack length determination by traditional "manual" techniques would have required constant operator supervision of all tests. For the author to do this unaided was both impractical and unsatisfactory. Attention was therefore given to the various techniques that could be used for automatic crack length measurement.

The most common and simplest method of crack monitoring is by manual, optical measurement of the surface crack length. The technique may be readily automated by the provision of a remotely triggered camera to record the crack length at preset intervals. An alternative approach [132] is to attach a multi-ligament foil gauge ahead of the crack tip. The crack growth rate is determined from the timed intervals between successive ligament failures. Eddy current techniques have been successfully used by Swanson et al [118]. A sensing head mounted on an elaborate double axis traverse gear followed the crack tip in a servo controlled manner. As with optical measurements of crack

length, both the foil gauge and the eddy current techniques can only determine the position of the crack tip at the specimen surface. This limitation also applies to the ultrasonic monitor described by Buck [133]. He used surface waves to measure the length of a crack in a single edge notch specimen; the signal intensity was attenuated as the crack extended, thus a continuous record of the surface crack length was obtained. Clark and Ceschini [134] have made more conventional use of ultrasonic techniques. They used a 90^{o} surface contact probe to follow the crack in a WOL specimen. They monitored the sonic reflection from the surface of the fatigue crack; as the crack extended the ultrasonic probe was advanced to maintain a constant signal intensity. The probe was advanced in increments of 250μm by a stepper motor, smaller increments of crack growth were determined from changes in the reflected signal intensity. An accuracy of $\pm$ 250μm was claimed for crack length determinations. This method has the advantage that the crack length is measured in the interior of the specimen instead of at the surface. The same is true of the electric potential method which has been used for studies of both crack growth [135, 136] and crack closure [64] during fatigue. The technique has been described in detail by Ritchie [136] who reports a sensitivity to crack growth of $\pm$10μm for small specimens. The method is certainly attractive in terms of cost and appears to be satisfactory in operation. However as extreme stability is demanded of both the power supply and the potential measuring equipment great care must be taken to eliminate all possible sources of error. Stray thermal e.m.fs. represent a major problem, elaborate environmental control is therefore necessary for the critical components.

The above techniques have all been used in practical investigations of fatigue crack propagation. Two further methods of crack length measurement have been proposed but not widely adopted. Dover [137]

has considered the possibility of using COD measurements to determine the length of a fatigue crack. Although this parameter is satisfactory for detecting crack extension in fracture toughness tests there are considerable difficulties in applying it to the continuous measurement of fatigue crack length. Eisenstadt and Fuller [138] have described a technique for "marking" a fatigue fracture surface by periodically applying a block of load cycles that causes no significant crack extension. This approach offers the possibility of determining crack growth characteristics from traditional rotating bending specimens.

Consideration was given to determining which of the above techniques was best suited for use in the author's test program. As 35mm thick specimens were to be used, it was desirable to measure the crack length in the interior of the material rather than on the surface. This indicated that either the electrical potential method or an ultrasonic system, similar to that of Clark and Ceschini [134], should be adopted. The final descision was influenced by circumstances: on the one hand the electrical potential method was discounted by the lack of environmental control on the test site and the insufficient technical expertise to build the equipment; on the other hand provision had been made to purchase an ultrasonic flaw detector, which could be used as the principal component of an automated crack monitor. Consequently it was decided to construct a device that utilised ultrasonic flaw detection. The basic operational requirements of such a system are considered in the next section.

A1.2 Ultrasonic Considerations

The final geometry of the fatigue sample to be used was settled at the same time that the crack monitor was being designed. Initially there was considerable mutual influence of these matters, one upon

the other. However, once it had been decided to use an ultrasonic measuring system on a CKS specimen there were certain fundamental decisions to be taken with regard to the crack monitoring device.

Consideration was given to the problem of how best to detect the advancing fatigue crack. The alternatives are shown schematically in Figure A1.1. One can monitor the reflection from the crack surface by use of the sonic path PAP; as the crack extends the reflecting area is increased. Alternatively "the back wall echo", path PDP, can be monitored; in this case the reflecting area is reduced when crack growth occurs. In either case the probe is driven forward to maintain a constant reflected signal intensity. The crack length at any time is indicated by the physical position of the probe. Although Clark and Ceschini [134] successfully used the reflection from the crack surface to control their device, the present author favoured using the "back wall echo" for the following reason. The roughness, and hence the acoustic reflectivity, of a fatigue fracture surface is dependent on the loading conditions under which it was formed. Thus tests involving complex load sequences would be expected to produce fracture surfaces whose acoustic reflectivity varied. The intensity of the signal reflected from the crack surface would therefore be affected by both the crack's length and its surface quality. The back wall echo should be independent of the latter parameter.

Figure A1.2 compares the back wall echo from an uncracked sample (broken line), with the signal reflected from a typical fracture surface, (continuous line). It is seen that the reflection from the back wall exhibits a more uniform intensity and is thus the better suited for use as the control signal. A possible complication is contributed by the symmetry of the CKS sample. It is seen from Figure A1.1 that the "second reflection" from the crack surface, path

PABCP, has the same path length as the back wall echo. For control purposes a compound signal created by the super imposition of these signals would be inferior to the pure back wall reflection. In practice, to utilise the back wall echo, the probe was positioned slightly ahead of the crack tip with the result that the unwanted reflection from the fracture surface was effectively eliminated.

The foregoing discussion of signal uniformity has assumed the ability to inject into the sample a signal of constant intensity. This is no easy matter. Acoustic transfer across an interface may be expressed as the ratio:

$$\frac{\text{reflected signal intensity, (R)}}{\text{transmitted signal intensity, (I)}} .$$

For transfer from a medium, whose thickness is in excess of one wavelength, the ratio R/I is given by

$$\frac{R}{I} = \frac{(\rho_1 u_1 - \rho_2 u_2)^2}{(\rho_1 u_1 + \rho_2 u_2)^2} \quad , \quad t_1 > \lambda_1 \qquad \text{(A1.1)}$$

where u_1 and u_2 are the velocities of sound in the two materials. Under close contact conditions the thickness of the interface becomes critical; R/I becomes

$$\frac{R}{I} = \frac{(\rho_1 u_1/\rho_2 u_2 - \rho_2 u_2/\rho_1 u_1)^2}{-4\cot^2(2\pi t_1/\lambda_1) + (\rho_1 u_1/\rho_2 u_2 + \rho_2 u_2/\rho_1 u_1)^2} \quad , \quad t_1 < \lambda_1 \qquad \text{(A1.2)}$$

where t_1 is the thickness of the medium in which the wave is travelling before encountering the interface. The latter expression governs the transfer of a signal from a surface contact probe to a test piece. It is essential to have an acoustic couplant such as grease or water between the probe and the sample in order to obtain a favourable value of the ratio ρ_1/ρ_2. However, the thickness of this layer is critical.

Table A1.1 lists values of R/I calculated for acoustic transfer from water to steel for different thicknesses of the water layer. Similar transfer ratios would apply to the signal passing from a surface contact probe through a liquid couplant into a test piece, the reflected signal would also be affected when crossing the interface in the reverse direction. Clearly if it is required to inject a signal of constant intensity from a surface contact probe into a test piece elaborate control of the interface conditions is required.

Acoustic transfer between the probe and the specimen can be made independent of the thickness of the couplant by the use of immersion testing techniques. A remotely located probe is acoustically coupled to the test piece by a suitable liquid, usually water. The acoustic transfer across the various interfaces is governed by equation A1.1 and is thus independent of the thickness of the couplant layer. An additional advantage of the technique is that no probe contact pressure is involved, thus the mechanical traverse gear required to drive the probe can be made considerably less complex than the equipment that is required to locate and move a surface contact probe. For these reasons it was decided to employ a water immersion probe whose position was controlled by the intensity of the back wall echo. The mechanical construction adopted to accommodate such a system is detailed in the next section.

A1.3 Mechanical Design

The accommodation of a tank, probe, drive gear and measuring equipment on a 35mm wide sample required a series of design compromises. The principal limitations were the available width and height. The general construction of the device is shown in Figures A1.1, A1.3 and A1.4. A one litre brass tank, provided with a demountable perspex front panel, was bolted directly to the top surface of the CKS sample.

The base was cut away, as shown in Figure A1.4, to allow the couplant to make direct contact with the test piece. A 3mm rubber gasket was used to seal the interface between the tank and the sample. Water was used as the ultrasonic couplant, a 5% addition of commercial "antifreeze" was made to eliminate corrosion of the steel surface. It was found necessary to control the temperature of the liquid as the ultrasonic signal intensity was affected by both the probe temperature and thermal stratification of the couplant. An external reservoir, of 5 litres capacity, was provided in which the temperature of the water was controlled at $30^{\circ}C \pm 0.1^{\circ}C$. The water was circulated to the test tank at a rate of 2 litres per minute by a simple impeller. This pump had a tendency to generate bubbles which could adversely effect the ultrasonic signal by settling on the underside of the probe. The problem was eliminated by the introduction of a simple bubble trap in the test tank inlet line and by the daily replacement of the liquid with a freshly boiled (degassed) solution.

The ultrasonic probe was mounted on a carriage which ran on lateral guide rails. The carriage traversed beneath a 15.9mm (5/8in) micrometer threaded, drive shaft which ran in bearings located in the end plates of the tank. In order to minimise physical disturbance of the probe, by the drive mechanism, the probe carriage was "sprung" against the guide rails and driven through a pin joint from an isolated nut running on the micrometer shaft. The shaft was turned by a reversible AC motor, a gearbox provided two speed options: 2.5 r.p.m. for crack monitoring and 12.5 r.p.m. for rewinding. At 12.5 r.p.m. the torque supplied to the shaft was approximately 0.6Nm. A ganged pair of helically wound 10 turn potentiometers was driven from the main shaft through a 20:1 reduction gear box. The lower unit was used to control the applied load as described in Section A1.6. The

upper potentiometer was used to measure the position of the probe over a range of 127mm (5 ins). A resolution of ± 12μm was achieved. The method by which the probe drive system was controlled is detailed in the next section.

A1.4 Probe Drive Control

A Phillips PA1020 ultrasonic flaw detector was used to control the position of the 5MHz probe. The instrument had two independent signal monitors that could be switched to "gate" any desired part of the time base trace. Each monitor was internally linked to a relay which "switched" as the selected signal passed through a preset intensity level. Thus the probe was simply controlled: as the crack extended the "gated" reflection from the back wall was reduced and the relay contacts reversed. This activated the motor which drove the probe forward until the preset signal intensity was re-established. As supplied, the monitor gates had a significant hysterisis effect between the "ON" and "OFF" functions; this feature was eliminated to make the switching more sensitive. The motor was driven indirectly through a time delay device which permitted the physical increment of advance to be controlled. At a shaft speed of 2.5 r.p.m. drive for 1sec. resulted in 25μm of probe advance; this was the increment that was normally employed.

The apparent crack length, as determined ultrasonically, appears to increase with the applied load. This effect is partly due to crack tip opening but also due to a change in the angle between the top and bottom surfaces of the specimen. To eliminate the latter factor the ultrasonic signal should ideally be monitored at a constant value of the applied load. In practice, under constant amplitude dynamic loading conditions, it proved satisfactory to monitor the signal continuously; this is equivalent to determining the crack length at the moment of maximum load application. When complex load

sequences were employed the apparent craek length varied with the loading conditions. It was therefore necessary to prevent the probe driving forward to a non-equilibrium position as a result of overload cycles. This was achieved by linking the block load programmer into the probe drive system in such a way that the probe was automatically deactivated during selected blocks. Consequently the crack growth records obtained under complex loading conditions contain exaggerated growth "steps" which result from the probe advancing to its equilibrium position following the conclusion of a load block during which it was deactivated. The determination of crack growth rates under such conditions is considered in the next section.

A1.5 Accuracy of Crack Length Measurement

There are three aspects to the "accuracy" of a device such as that described above.

a) The measurement of absolute crack length.

b) The determination of "macro" crack growth rates by continuous measurement of crack extension over distances in excess of 1mm.

c) The detection of "micro" growth resulting, for example, from a limited number of overload cycles.

Throughout the author's work absolute crack lengths have been determined by optical methods. No attempt has been made to use the crack monitor for such measurements; its accuracy in this respect therefore remains unknown.

For the determination of "macro" growth rates the performance of the monitor was investigated by comparing optical measurements of surface crack lengths with simultaneously obtained ultrasonic measurements.

Four tests were performed at different crack lengths and different stress intensity levels. The procedure was as follows. An equilibrium crack front profile was obtained by applying the stress intensity conditions required for the test for 5mm of crack growth before measurements were taken. Optical crack length determinations were then made on both faces of the sample at growth intervals of approximately 0.4mm. Simultaneously determined ultrasonic values were taken from the chart recorder which continuously monitored the probe position. Figure A1.5 shows the result of a test performed as the crack length approached its maximum permitted value. A consistent discrepancy of approximately 0.3mm was obtained between the optical crack length measurements from the two faces as a result of a zero error in the measuring system. The figure demonstrates an excellent agreement between the optically and ultrasonically determined growth rates. The four calibration tests all yielded similar results to those presented in Figure A1.5, the individual results are summarised in table A1.2. It is seen that the greatest discrepancy in the growth rates determined by the different methods is 2.2%. This accuracy was considered satisfactory for crack growth rate studies.

The sensitivity of the monitor to growth increments in the "μm" range is not readily determined. The circulating water in the test tank causes the intensity of the ultrasonic signal, associated with a stationary crack, to vary over a short period between two accurately maintained limits. Thus if the crack is extended by, for example, an overload sequence, there may be an interval of up to a minute before the probe moves to its new position. The nature of this delay is statistical, a point that must be born in mind when examining a record in which discontinuous growth is expected. Tests have been performed in which crack arrest occurred. Under these conditions the ultrasonically determined length was stable to within 25μm per

hour. Figure A1.6 shows two crack growth records taken directly from the chart recorder. The lower trace represents growth under constant dynamic stress intensity conditions. The stepped appearance of the trace results from the incremental nature of the probe advance. Under these conditions growth increments of between 50 and 100μm can be detected. The upper record in the figure shows the monitor output when a periodic 20 cycle dynamic overload was introduced into the load sequence. (The probe was deactivated for the duration of the overload.) Clearly under these conditions the details of the trace should not be considered to represent the actual crack growth history. However, optical crack length measurements do confirm that the overall gradient of such traces does accurately represent the average crack growth rate.

It is concluded that under favourable conditions growth increment of less than 100μm can be detected, but under complex loading conditions only the overall gradient of the crack growth record is significant. In general the monitor is suited to determining "macro" crack growth rates over an interval of not less than 1mm. Under certain loading conditions it may be necessary to continue the tests for several millimetres in order to obtain a satisfactory value for the overall gradient of the growth record.

A1.6 Load Control for Constant Stress Intensity Testing

A general feature of the more commonly used fracture toughness type specimens is that, under constant loading conditions, the crack tip stress intensity increases as the crack grows. The determination of crack growth rates under these conditions is complicated by the non-linear characteristic of the growth record. It was considered that this effect would be particularly unwelcome in the analysis of crack propagation rates resulting from complex load sequences. A means was therefore sought to maintain constant crack tip stress

intensity conditions over extended growth increments. For the CKS sample used the crack tip stress intensity is given by [107]

$$K_I = \frac{PY}{BW^{\frac{1}{2}}} \qquad \text{(A1.3)}$$

where

$$Y = 29.6\left(\frac{a}{W}\right)^{1/2} - 18.5\left(\frac{a}{W}\right)^{3/2} + 655.7\left(\frac{a}{W}\right)^{5/2} - 1017\left(\frac{a}{W}\right)^{7/2} + 6[illegible]\left(\frac{a}{W}\right)^{9/2} \qquad \text{(A1.4)}$$

when $$0.3 < \frac{a}{W} < 0.7$$

For constant loading conditions

$$K \propto Y \qquad \text{(A1.5)}$$

and the stress intensity increases with crack length in the manner shown in Figure A1.7. To maintain a constant crack tip stress intensity it is necessary to control the load such that

$$P \propto 1/Y \qquad \text{(A1.6)}$$

It is seen from equation A1.4 that, for a given specimen geometry, Y is solely dependent on the crack length a. Consideration of the 1/Y characteristic, Figure A1.8, shows it to be an approximately linear function of the crack length. This suggests that the necessary load control may be simply affected by the use of the output from the ultrasonic crack monitor.

In practice a multitap potentiometer was used as a potential divider to attenuate the servo amplifier load demand signal. An 11 tap, helically wound potentiometer was ganged to the position measuring potentiometer on the ultrasonic crack monitor. The taps were "shunted" to modify the linear attenuation characteristic to the

1/Y function shown in Figure A1.8. The load demand signal from the digitally controlled block programmer was passed to the servo amplifier by way of the potential divider. The nature of the attenuation function required that the potential divider be set to correspond to the absolute crack length. This was achieved by calibrating the probe position signal against the crack length and by making provision to turn the common potentiometer shaft independently of the probe position. At the start of a test, with the probe in its equilibrium position at the crack tip, the position signal was manually set to correspond to the optically determined crack length. The ganged potential divider was thus set to provide the appropriate load signal attenuation.

This semi-automatic control of the load signal considerably simplified the procedure for setting up the block load programmer to achieve any given crack tip stress intensity conditions. All loads were set on the programmer according to the expression

$$P = 3.015 \times 10^{-3} K_I \qquad (A1.7)$$

where K_I was expressed in units of $MNm^{-3/2}$. In a 35mm thick specimen this expression gives the load requirement for $a/W = 0.3$, this is the shortest crack length at which the stress intensity function is applicable. Appropriate attenuation of the signal to suit the prevailing crack length was achieved by setting the monitor position signal in the manner previously described. In this way complex stress intensity sequences could be quickly set by reference to a table of prepared values.

A1.7 Experimental Procedure for the Determination of Crack Growth Rates

To determine crack growth rates experimentally it was first necessary to locate the ultrasonic probe in its equilibrium position

at the crack tip. Normally during a sequence of related tests the probe would not need repositioning between each test. However it was necessary to adjust the ultrasonic equipment before the first test on any day and at times when major changes were made in the loading conditions. The probe was located as follows. The appropriate loading conditions were applied to the sample at a frequency of 0.5Hz. The manual override controls of the crack monitor were then used to determine the ultrasonic "profile" of the crack tip. This comprised an x/y plotter record of the ultrasonic signal intensity as a function of the probe position. A typical profile, with explanatory comments, is shown in Figure A1.9. The sensitivity of the signal monitor gate in the ultrasonic flaw detector was adjusted to provide automatic control of the probe at the point at which the back wall echo showed the greatest rate of change, see Figure A1.9. The probe was then allowed to find its equilibrium position under automatic control at the normal test frequency of 2Hz. Finally the probe position signal was compared with the optically determined crack length and if necessary adjusted as detailed in Section A1.6.

Crack growth rate measurements could at this stage be undertaken. A two pen Honeywell y/t recorder was used to monitor the probe position and the duration of each block in the loading sequence. As displayed a pen deflection of 94mm was equivalent to 1mm of crack growth. The rate of chart advance was selected to yield a crack growth record with a gradient of between 0.5 and 1.2. The lower limit was principally to prevent excessive consumption of chart paper, the upper limit was imposed in consideration of the errors involved in determining the crack growth rate. For a trace of inclination θ the principal error term is proportional to $\sec^2\theta$. This term increases at an unfavourable rate for gradients in excess of 1.2, ($\theta \simeq 50^{\circ}$).

During the early stages of experimentation crack growth rates were determined by the use of a computerised curve fitting technique.

A Ferranti "Freescan" Digitiser was used to convert the analogue crack growth records to a digital form. A least squares routine was then employed to fit a "best straight line" to the data. Analysis by this method was discontinued as a result of the severe operating difficulties which were experience with the digitiser. The growth rate data presented in this thesis was all determined by manual interpretation of the analogue output obtained from the Honeywell chart recorder. For each test the apparent best straight line was constructed on the chart recorder output; the gradient was then measured to yield an average growth rate. Any attempt to make a definitive statement of the accuracy of this procedure is complicated by the variable appearance of the growth records. However, consideration of a cross section of the chart records indicates that the measured gradient was within $\pm$ 5% of the "true" value for any trace. It was found that the natural scatter of the fatigue results was more severe than the potential errors associated with manual interpretation of growth rate data.

The measured growth rates were correlated against the prevailing crack tip stress intensity conditions. These latter data was derived from periodic measurements of the applied load and the simultaneous optical crack length.

A1.8 Possibilities for Further Development of the Crack Monitor

The ultrasonic crack length monitor described in this appendix was developed only as far as was necessary for the satisfactory completion of the fatigue tests that constituted the principal aim of the author's research contract. It is anticipated that future development of the device would further extend its capabilities. The most immediate requirement is to make provision to determine crack growth rates under truly random loading conditions. At present the dependence of the ultrasonically determined crack length on the load applied to the sample, limits the monitor to use under conditions

of block load programming. It is considered that satisfactory performance under more complex loading conditions could be achieved by monitoring the ultrasonic control signal at a constant value of the applied stress intensity, or a similar parameter. By this means the measured crack length would be rendered independent of the instantaneous loading conditions permitting the device to be used for continuous monitoring of growth under truly random sequences.

The possibility of using a mini-computer to perform the various control functions necessary for complex fatigue tests has been considered. The computer would be used to generate an analogue load signal that was comparable with the servo amplifier input. The output from the ultrasonic crack monitor would be recorded in digital form and examined to detect preprogrammed conditions. With this control facility the requirement for operator supervision could be reduced to the absolute minimum; a significant improvement in the utilisation of the test facility could therefore be achieved. Such a system would make on-line analysis of crack growth rate data possible. This would constitute a major reduction in the operator's committments.

Proposed improvements in the departmental fatigue test facilities will permit further development of the ultrasonic crack monitor. A 400 kN double acting hydraulic actuator is currently awaiting the construction of a suitable test frame. When commissioned the new facility will eliminate the current dependence on the sample to sustain a sufficient load to return the actuator to its "zero" position during the unloading stroke of each load cycle. It will therefore be possible to select the specimen size to optimise the performance of the crack monitor. It is not currently clear if a change in the ultrasonic path length of the control signal would favour more accurate detection of crack growth. This matter may be investigated by testing differently sized samples in the more veratile test facility that is planned for the future.

Finally it is worth noting that a very similar system to that described above can be based on the application of ultrasonic surface waves. Surface wave probes can be placed on the machined faces of the notch such that the ultrasonic signal travels from the probe, along the fracture surface, around the crack tip and back along the adjacent fracture surface to a second, receiving probe. Using this configuration the crack length is proportional to the time interval between transmission and reception of the ultrasonic pulses. Preliminary investigations indicate that sufficient signal power is available from standard flaw detectors, however some detailed modification of the signal analysis equipment would be required to provide the necessary control functions. The principal attraction of the system is that the fixed nature of the probes eliminates the requirement for an elaborate traverse gear, thus permitting a neater specimen configuration to be adopted. The possibility of using smaller samples on the new double acting hydraulic actuator should prompt serious reconsideration of the surface wave approach to crack length determination.

Governing equation for close contact acoustic transfer:

$$\frac{R}{I} = \frac{\left(\rho_1 u_1/\rho_2 u_2 - \rho_2 u_2/\rho_1 u_1\right)^2}{4\cot^2(2\pi t_1/\lambda_1) + \left(\rho_1 u_1/\rho_2 u_2 + \rho_2 u_2/\rho_1 u_1\right)^2} \quad \text{Equation A1.2}$$

Thickness, t, of medium 1. (μm)	Acoustic transfer coefficient R/I
1	3×10^{-5}
5	8×10^{-4}
10	3×10^{-3}
50	7×10^{-2}
100	5×10^{-1}

Table A1.1 Typical values for acoustic transfer under close contact conditions. Medium 1 = water, medium 2 = steel. Calculated for 5MHz probe at 20°C.

Sample No	$\overline{K}$ $MNm^{-3/2}$	ΔK $MNm^{-3/2}$	Crack length (mm)		Discrepancy between optical and ultrasonic values of da/dN (%)[1]
			Start	Finish	
11	92	66	60.5	66.0	-2.2
11	110	29	71.5	77.0	-1.1
12	59	49	14.0	20.0	-0.8
14	110	56	104.5	109.5	+1.1[2]

Notes: 1 Expressed as percentage of optically determined growth rate; + ve value indicates ultrasonic rate exceeds optical value.

2 Shown in Figure A1.5.

Table A1.2 Summary of tests performed to calibrate the ultrasonic monitor against optically determined crack growth rates.

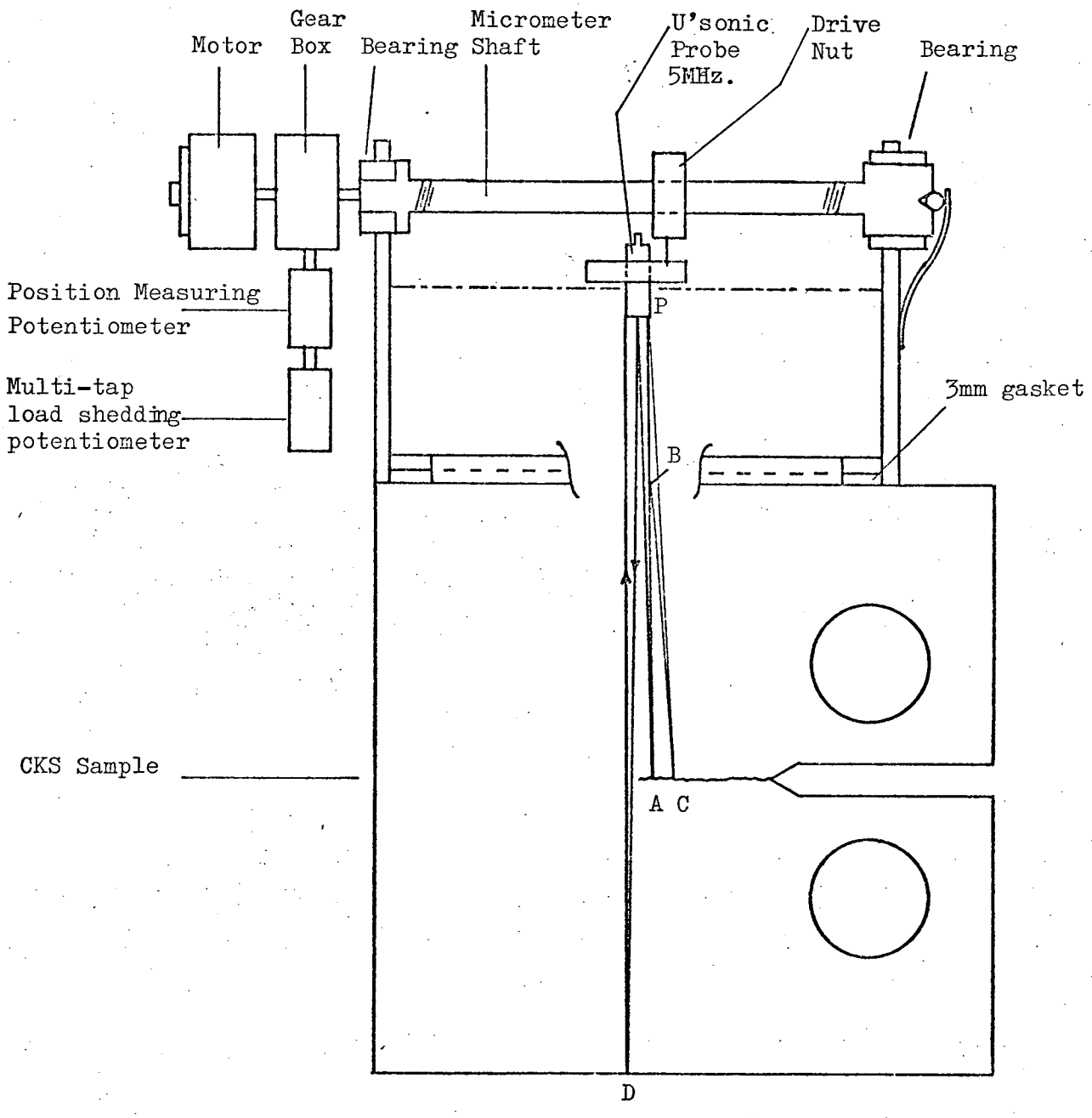

Figure A1.1 Schematic diagram showing construction of the ultrasonic crack monitor and the sonic paths of the alternative control signals.

Scale: x 1/3.4

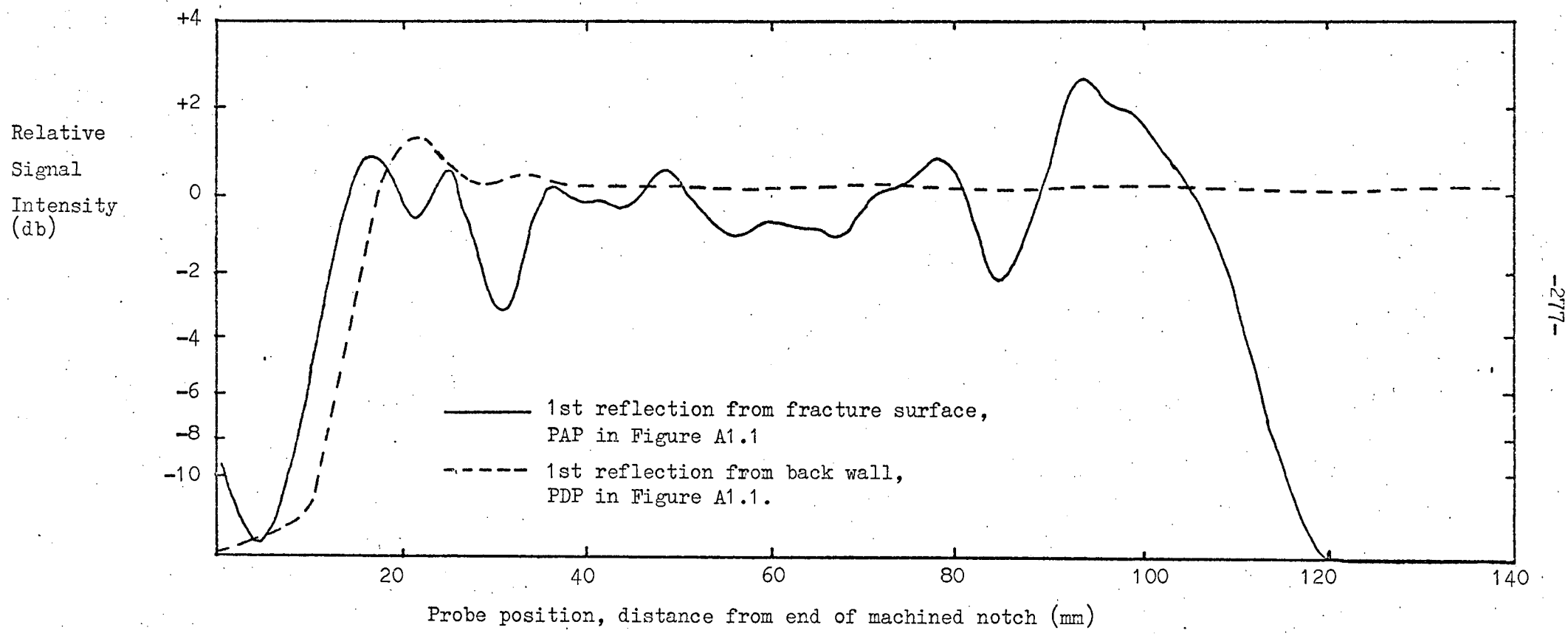

Figure A1.2 Comparison of intensities of alternative ultrasonic signals.

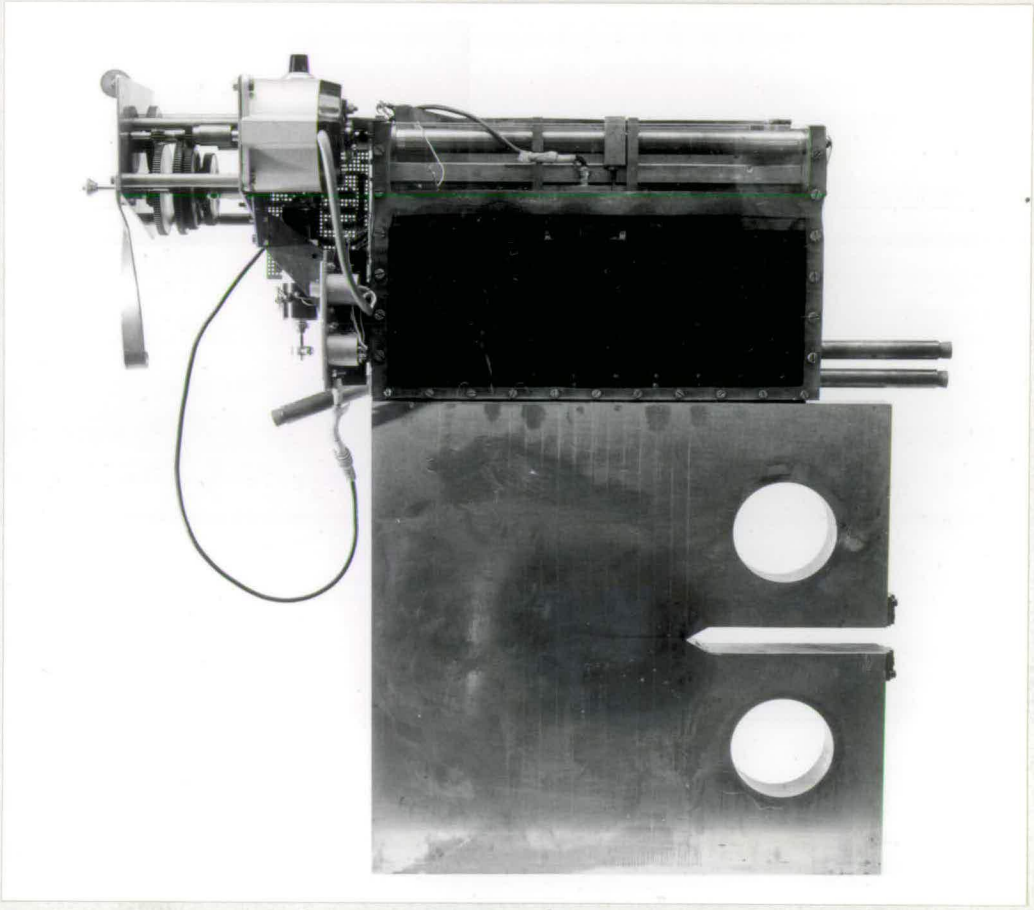

Figure A1.3 Crack monitor mounted on 305mm high CKS sample.

Magnification: x1/5

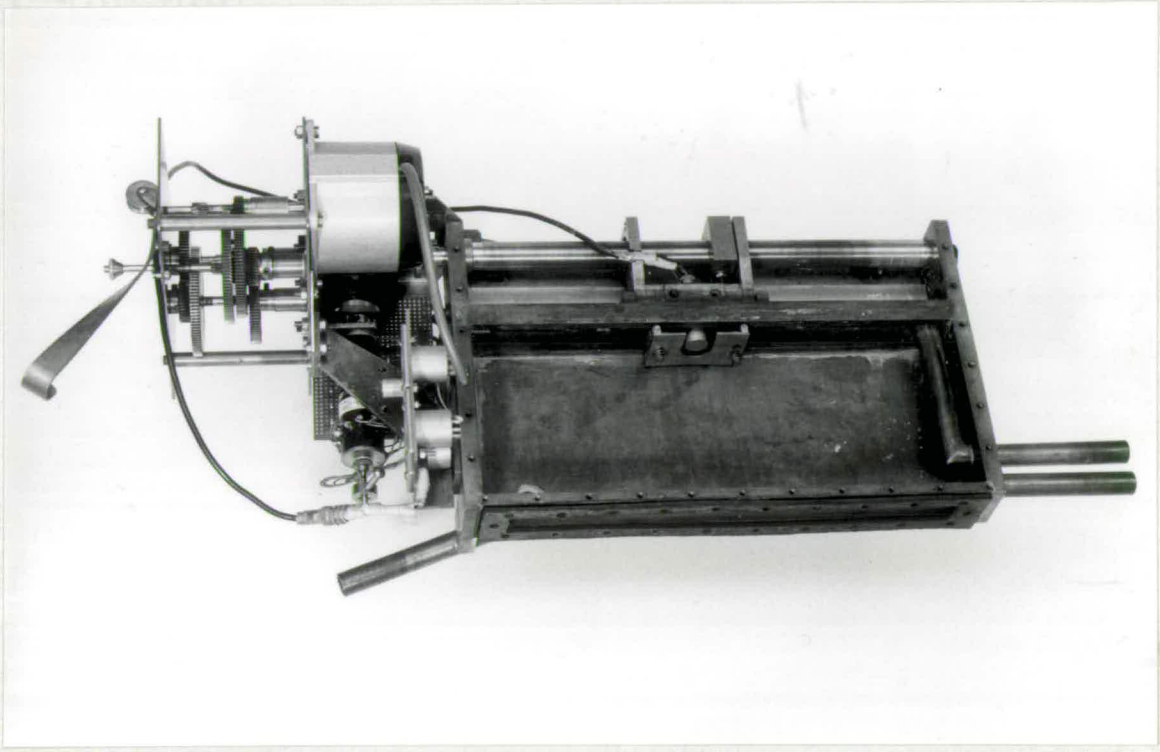

Figure A1.4 Photograph showing the general construction of the crack monitor.

Magnification: x1/3

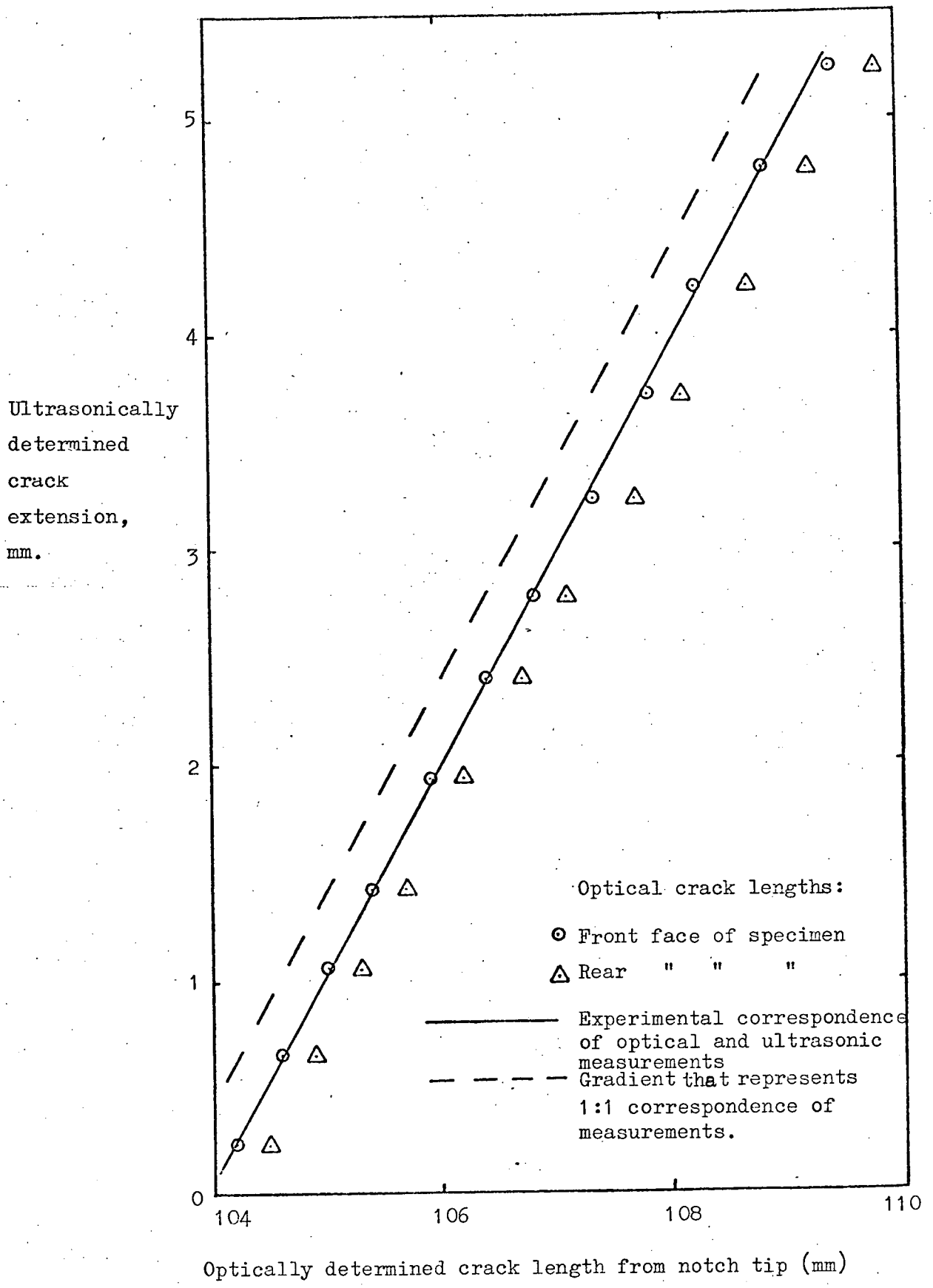

Figure A1.5 Crack monitor accuracy test record.

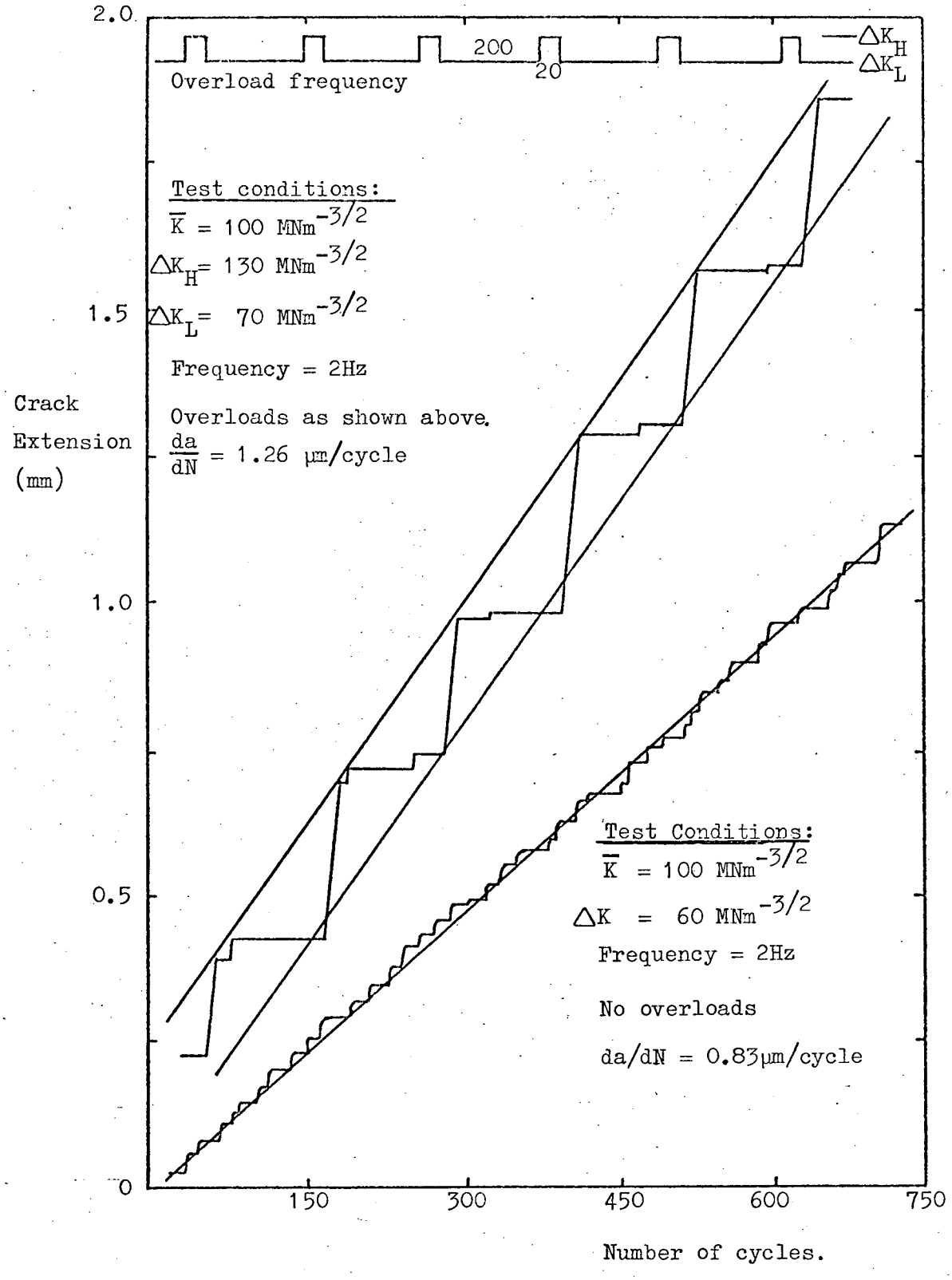

Figure A1.6 Typical crack growth records. The lower record is for constant dynamic stress intensity conditions; the upper shows the trace obtained when periodic dynamic overloads are applied.

(Reproduced at original size).

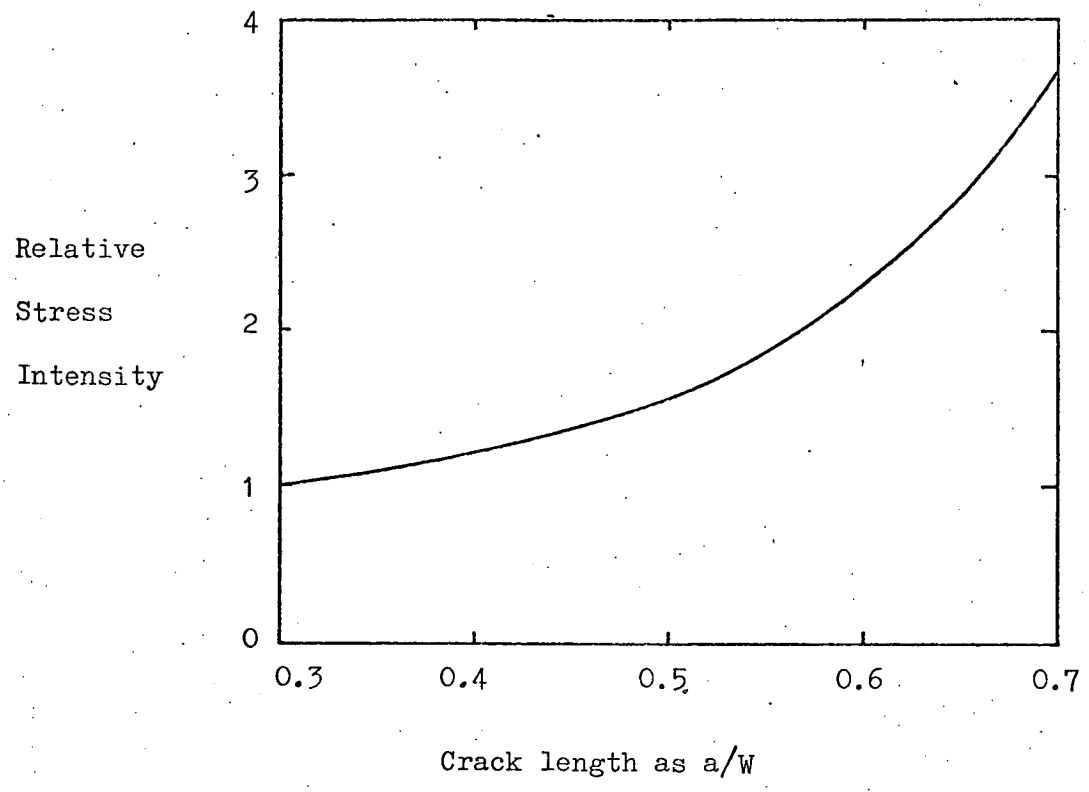

Figure A1.7 Crack tip stress intensity conditions for a CKS sample subjected to constant loading conditions.

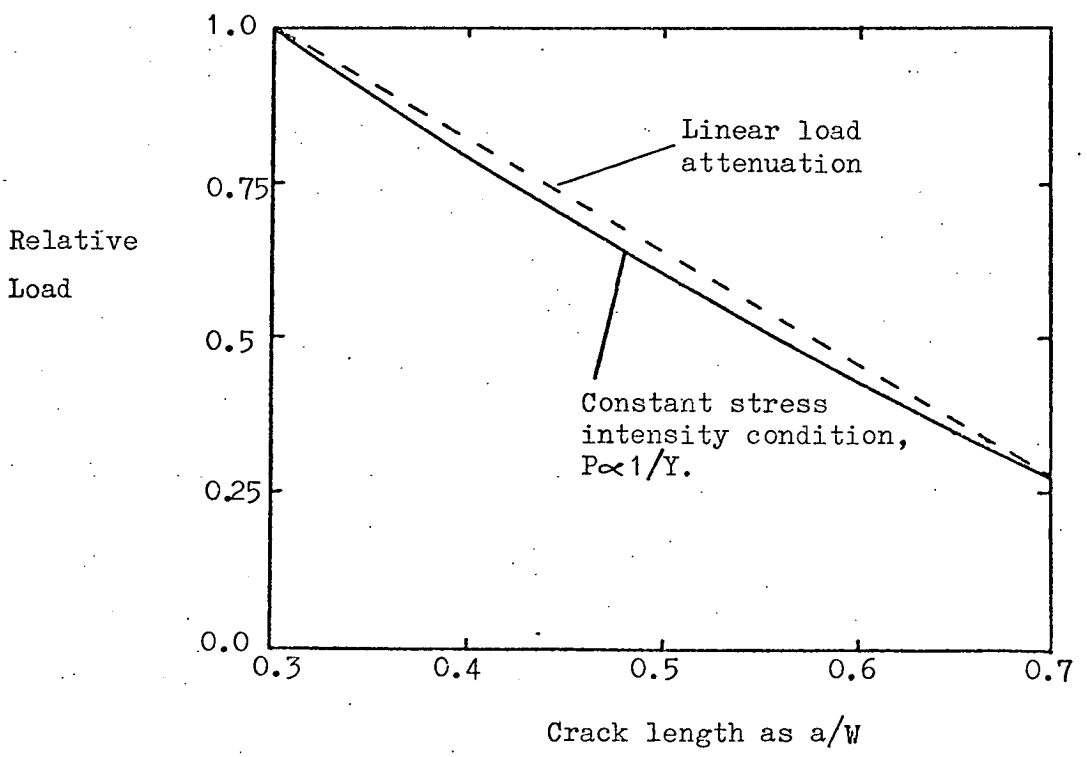

Figure A1.8 Load characteristic required to maintain constant stress intensity conditions at the tip of a crack growing in a CKS sample.

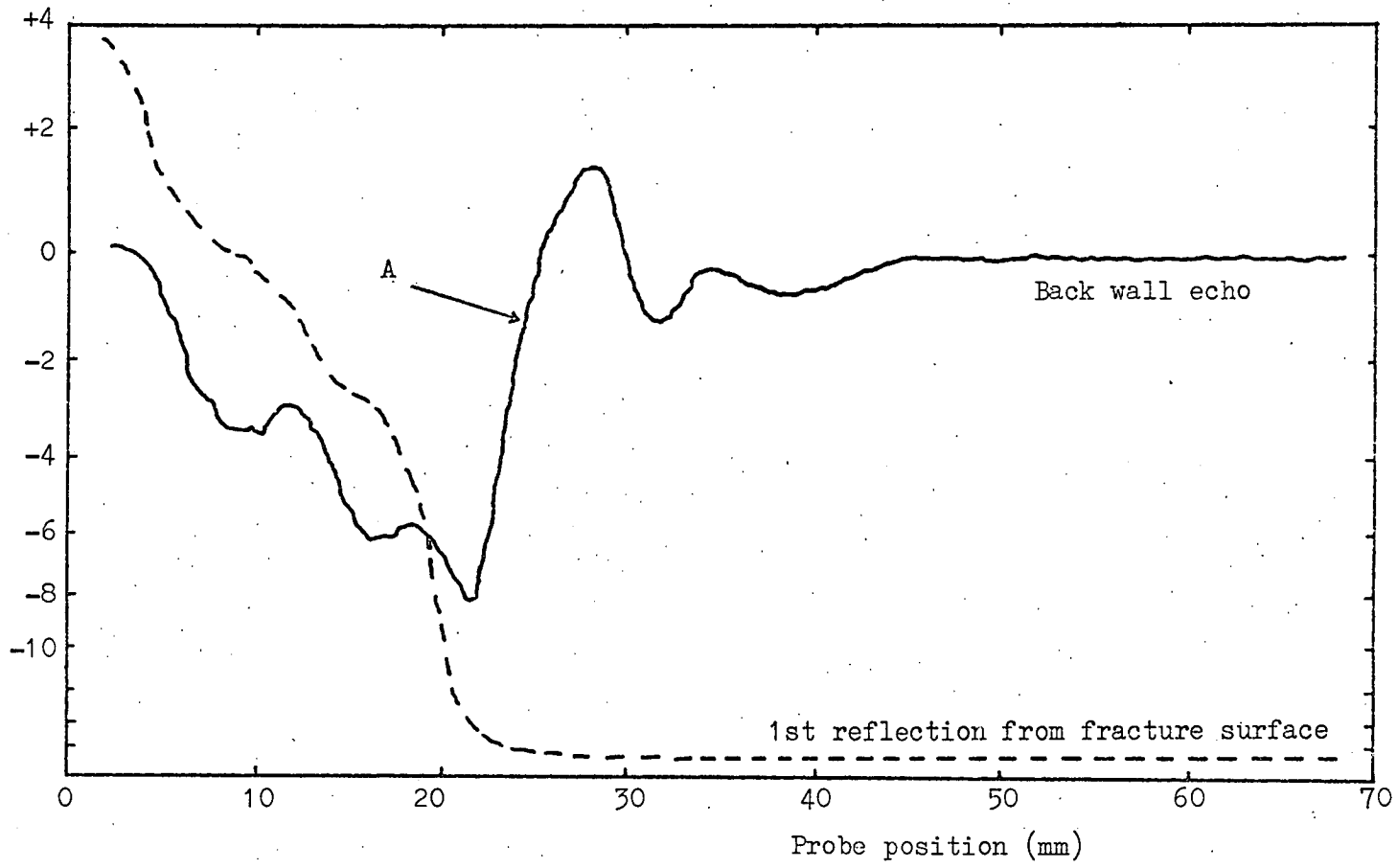

Figure A1.9 A typical ultrasonic "profile" obtained by running the probe over the crack tip region. The monitor was adjusted to control at the level indicated by "A". Note the insignificance of the fracture surface reflection at this point.

APPENDIX 2

CONSIDERATION OF LOADING CONFIGURATION FOR CKS SAMPLE

A2.1 Pin Friction Effects

Pook [108] has drawn attention to the significance of pin friction effects in the loading of single edge notch tension specimens. Crack opening in the CKS sample will result in similar effects as a consequence of the relative movement of the sample and the loading yokes. The form of the analysis that follows is that suggested by Pook [139].

Consider the specimen shown in Figure A2.1. Crack opening results in the creation of a frictional force, μP, at the pin/sample interface. The stress in the uncracked ligament results from the tensile force P and bending moment M. The influence of pin friction is to reduce the bending moment M.

Frictionless condition: $M = xP$

With pin friction: $M \Rightarrow M' = xP - r\mu P$

To a first approximation the bending moment reduction associated with pin friction can be equated to a notional displacement of the loading centre towards the uncracked ligament. Thus for the displaced loading centre with no frictional effects

$$M \Rightarrow M'' = (x - \delta_x)P$$

Equating M' and M''

$$\delta_x = r\mu.$$

To examine the influence of this displacement on the crack tip stress intensity it is necessary to evaluate the compliance function Y. This is expressed as a function of a/W, thus δ_x must be translated to these dimensionless units. Referring to Figure A2.1

$$\frac{a}{W} \Rightarrow \frac{a'}{W'} = \frac{a-\delta_x}{W-\delta_x}$$

Y is given by [107] as

$$Y = 29.6\left(\frac{a}{W}\right)^{\frac{1}{2}} - 185.5\left(\frac{a}{W}\right)^{3/2} + 655.7\left(\frac{a}{W}\right)^{5/2}$$
$$- 1017\left(\frac{a}{W}\right)^{7/2} + 638.9\left(\frac{a}{W}\right)^{9/2}$$

Values for Y' are obtained by substituting the appropriate value of a'/W' in place of a/W. Table A2.1 shows how for the CKS sample used in this work, Y and Y' depend on crack length for an assumed value of the coefficient of friction of 0.2. This is the same value taken by Pook, as representative of metal to metal contact, in his analysis of the single edge notched specimen. It will be noted that these severe frictional conditions result in a maximum error of -4%. In practice care was taken to preserve "lubricated" conditions for which the coefficient of friction is typically 0.1. Such a value would half the error values given in Table A2.1.

The above analysis ignores the increase in the ratio H/W that occurs if the loading centre is displaced in the manner discussed. A change in this ratio also influences the value of the compliance

function in a second order manner. Values given by Brown and Srawley [140] indicate that for the loading centre displacements associated with a coefficient of friction of 0.2, ΔY is reduced by a further 0.5% at $a/W = 0.3$ as a consequence of the implied change in the ratio H/W. This value, which is of less significance at higher crack lenghts, should be added to to the error term given in the final row of figures in Table A2.1. However as the additional error is small compared to the uncertainties of an assumed value of μ, it has not been included in the Table.

The above analysis indicates that stress intensity values determined for the CKS sample used in this work are not unreasonably influenced by pin friction effects. The potential percentage errors in stress intensity values are equal to the ΔY terms given in Table A2.1.

A2.2 Specimen alignment

Accurate specimen alignment is critical to the correct determination of the loading conditions. The Mohr and Frederhauf test frame provides for the alignment of test pieces by the inclusion of spherical "seats" in the loading system. This system, slightly modified, was maintained for the testing of CKS specimens. A standard Mohr and Frederhauf spherical seat was used above the sample, a specially purchased spherical bearing was incorporated in the lower part of the system. Figure 3.7 details the location of these components. No quantitative assessment of the success of this self aligning system has been made, however as the test frame manufacturers found their spherical seats satisfactory for calibration purposes it is reasonable to suggest the system adopted is adequate for test use.

The pin jointed nature of the loading links presents a further alignment problem. Figure A2.2 shows the two possible misalignment configurations. In both cases the system should be self-aligning, however the frictional effects at the loading pins prevent this action being completed. Samples were therefore manually positioned prior to testing by laying a straight edge along the machined faces of the loading links. Consideration of the possible geometries indicates that the maximum value of θ (Figure A2.2) obtained during this procedure was 1^{o}. Both configurations shown in Figure A2.2 result in the stress distribution in the sample being modified by pin friction effects of the type discussed in Section A2.1. Misalignment can also result in the creation of a shear force in the x direction of the uncracked ligament. In theory this would produce an element of mode II crack opening, however the precautions taken in positioning the sample make such an effect insignificant.

It is concluded that specimen misalignment is a direct consequence of pin friction effects and that, given careful manual positioning of the sample prior to testing, loading inaccuracies are limited to those evaluated in Section A2.1.

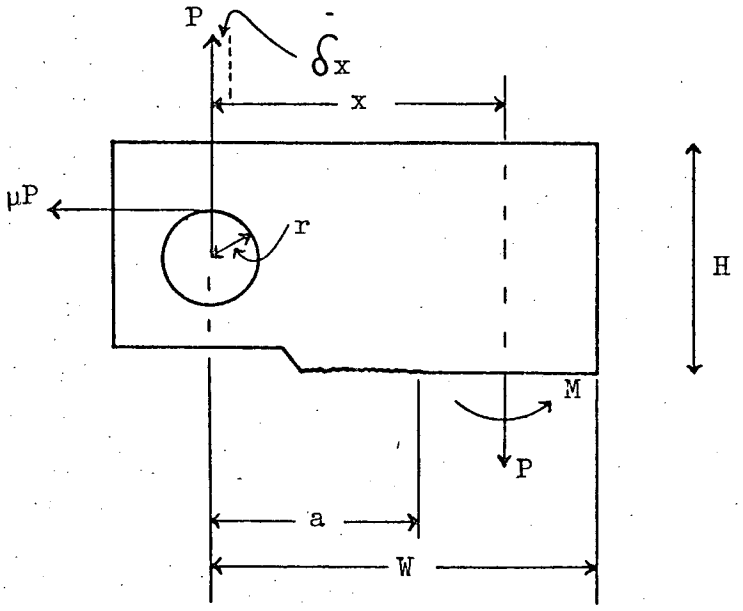

Figure A2.1 Free body diagram of half CKS sample showing force resulting from pin friction.

a/W	.32	.40	.50	.60	.70
Y	6.09	7.32	9.60	13.54	21.43
Y′	5.87	7.05	9.24	13.01	20.60
ΔY%	-3.53	-3.69	-3.75	-3.91	-3.87

Table A2.1 Percentage change in compliance function (Y) caused by pin friction ($\mu = 0.2$).

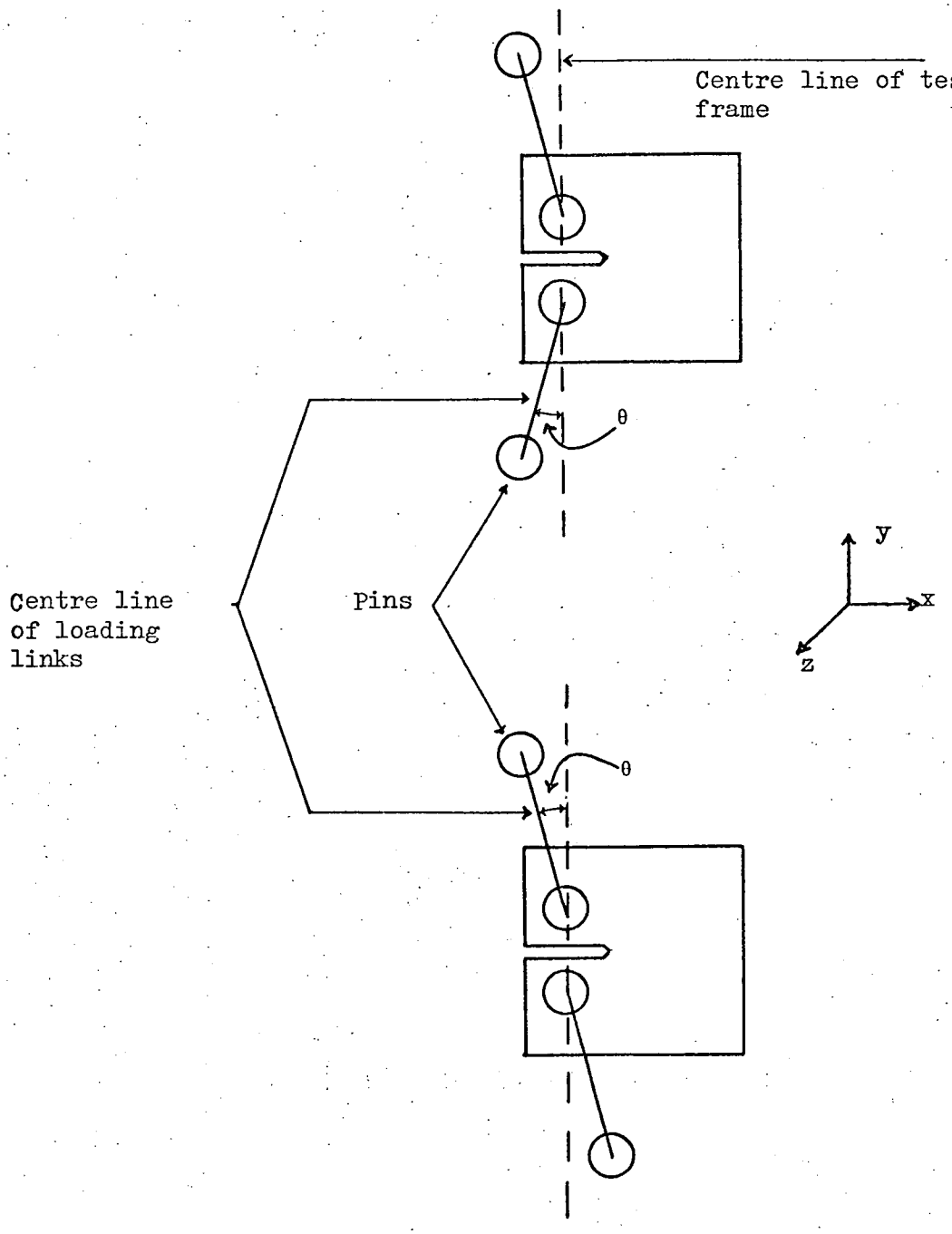

Figure A2.2 Misalignment configurations for CKS sample.

APPENDIX 3

THE EVALUATION OF "EQUILIBRIUM" GROWTH RATES FOR COMPLEX LOAD SEQUENCES

The cumulative damage law proposed by Miner [96] in 1945 has been much attacked for its demonstrated inadequacies under many loading conditions. However it does provide a simple criterion against which experimentally determined cumulative damage effects may be gauged. Miner originally stated his hypothesis as

$$\sum \frac{n_i}{N_i} = 1 \qquad \text{(A3.1)}$$

where n_i and N_i refer respectively to the number of cycles applied, and the fatigue life at any given load level. The above expression may be modified to express fatigue damage in terms of crack growth rates instead of the life fraction, n_i/N_i, used by Miner. Assuming that growth rates may be expressed as a function of the applied stress intensity in the general form:

$$\frac{da}{dN} = f(K) \qquad \text{(A3.2)}$$

then over any interval of a complex load sequence the average crack growth rate per cycle, $(\frac{da}{dN})_a$, is given by:

$$(\frac{da}{dN})_a = \sum (\frac{f(K_i).n_i}{\sum n_i}) \qquad \text{(A3.3)}$$

where n_i is the number of cycles applied at a stress intensity of

K_i. $\sum n_i$ is thus the total number of load cycles applied. For the two level, dynamic overload tests reported in Section 4.2.4, equation A3.3 reduces to:

$$\left(\frac{da}{dN}\right)_a = \frac{f(K_1).n_1}{n_1 + n_2} + \frac{f(K_2).n_2}{n_1 + n_2} \qquad (A3.4)$$

The above expression was used to predict "equilibrium" growth rates for the tests reported in Figures 4.13 to 4.27. The function $f(K_i)$, was deduced from the constant amplitude growth rate data presented in Figure 4.5; the empirically determined expression given as equation 4.2 was used to make quantitative predictions of $\left(\frac{da}{dN}\right)_i$. Equilibrium growth rates for the 3 and 8 load level tests reported in Chapter 4 were also obtained by the above procedure.

REFERENCES

[1] FORREST, P.G., "Fatigue of Metals", Pergamon, (1962).

[2] YOKOBORI, T., "Strength, Fracture and Fatigue of Materials", Noordhoff, (1965).

[3] BARNBY, J.T., "Fatigue", Mills and Boon, (1972).

[4] KNOTT, J.F., "Fundamentals of Fracture Mechanics", Butterworths, (1973).

[5] LIEBOWITZ, H., (editor), "Fracture, an Advanced Treatise", Academic Press (1968).

[6] FORSYTH, P.J.E., Proc. Cranfield Crack Propagation Symp., (1961) p76.

[7] PLUMBRIDGE, W.J. and RYDER, D.A., Metall. Rev. No. 136; Metals and Materials, (1969).

[8] SCHIJVE, J., NLR Report No: NLR-TR M.2122, (1964).

[9] WILLIAMS, H.D. and SMITH, G.C., Phil. Mag. 13(1966) p835.

[10] GOLLAND, D.I. and JAMES, P.L., Acta Met. 15(1967), p1889.

[11] LAIRD, C. and THOMAS, G., Ford Motor Co., Scientific Lab Report, (1967).

[12] LYNCH, S.P., Ph.D. Thesis, University of Manchester, (1969).

[13] FORSYTH, P.J.E. and RYDER, D.A., Aircraft Engineering, 32(1960) p96.

[14] GRIFFITH, A.A., Phil Trans. A221, (1920) p163.

[15] OROWAN, E., Proc. Symp. on Fatigue and Fracture of Metals; Wiley, New York, (1952) p139.

[16] KENNY, P. and CAMPBELL, J.D., Progress in Materials Sci., 13 (1968), p135.

[17] IRWIN, G.R., Trans. ASME, J. App. Mech., 24, (1957), p361.

[18] IRWIN, G.R., "Encyclopaedia of Physics", vol. 6, (1958), p551.

[19] BUECKNER, H.F., Trans. ASME, (1958) p1225.

[20] PARIS, P.C. and SIH, G.C., ASTM STP 381, (1965), p30.

[21] IRWIN, G.R., Proc. Seventh Sagamore Ordinance Materials Conf., Syracuse University. (1960) part IV, p63.

[22] RICE, J.R., ASTM STP 415, (1967), p247.

[23] McCLINTOCK, F.A. and IRWIN, G.R., ASTM STP 381, (1965) p84.

[24] HULT, J.A. and McCLINTOCK, F.A., Proc. 9th Int. Congress App. Mech., Brussels (1956) Vol. 8.

[25] RICE, J.R., Proc. Int. Conf. Fracture., Sendai, Japan, (1965).

[26] HOEPPNER, D.W. and KRUPP, W.E., Eng. Fract. Mech., 6(1974), p47.

[27] PARIS, P.C. and ERDOGEN, F., Trans ASME, J. Bas. Eng., (1963) p528.

[28] HEAD, A.K., Phil. Mag. 44, (1953) p925.

[29] FROST, N.E. and DUGDALE, D.S., J. Mech. and Phys. of Solids, 6, (1958), p92.

[30] LIU, H.W., Trans ASME, J. Bas. Eng., 85 (1963) p116.

[31] McEVILY, A.J. and ILLG, W., NASA Tech. Note 4394, (1958).

[32] PARIS, P.C., GOMEZ, M.P. and ANDERSON, W.E., Trend in Engineering, 13, (1961) p9.

[33] McCLINTOCK, F.A., "Fracture of Solids", (Eds. Drucker and Gilman), Interscience, (1963) p63.

[34] WEERTMAN, J., Int. J. Fract. Mech. 2, (1966), p460.

[35] WEERTMAN, J., Ibid, 5, (1969), p13.

[36] McEVILY, A.J. and JOHNSTON, T.L., Ibid 3, (1967) p45.

[37] TOMKINS, B., Phil. Mag. 18, (1968), p1041.

[38] FROST, N.E., Pook, L.P. and DENTON, K., Eng. Fract. Mech., 3, (1971), p109.

[39] FORMAN, R.G., KEARNEY, V.E. and ENGLE, R.M., Trans. ASME, J. Bas. Eng. 89, (1967) p459.

[40] DOVER, W.D. and HIBBERD, R.D., Dept. Mechanical Engineering, University College, London. Report ME 73/4, (1973).

[41] McMILLAN, J.C. and HERTZBERG, R.W., ASTM STP 436, (1968) p89.

[42] HERTZBERG, R.W., ASTM STP 415, (1967) p205.

[43] FORSYTH, P.J.F. and RYDER, D.A., Metallurgica, 63, (1961) 117.

[44] LAIRD, C., ASTM STP 415, (1967), p131.

[45] SCHIJVE, J., Ibid p533 (discussion).

[46] McMILLAN, J.C. and PELLOUX, R.M.N., Ibid p505.

[47] KLESNIL, M. and LUKAS, P., Proc. 2nd Int. Conf. on Fracture, Brighton, (1969), p725.

[48] TOMKINS, B. and BIGGS, W.D., J. Mat. Sci. 4, (1969), p532.

[49] SPITZIG, W.A., TALDA, P.M. and WEI, R.P., Eng. Fract. Mech. 1, (1968), p155.

[50] SCHIJVE, J., ASTM STP 415, (1967), p415.

[51] PLUMBRIDGE, W.J., J. Mat. Sci., 7, (1972) p939.

[52] KOTERAZAWA, R., MORI, M., MATSUI, T. and SHIMO, D., Trans. ASME, J. Eng. Materials and Technology. (1973), p202.

[53] POOK, L.P. and FROST, N.E., Int. J. Fract. Mech., 9, (1973), p53.

[54] RITCHIE, R.O., Proc. Conf. on Practical Implications of Fracture Mechanisms. Inst. of Metallurgists, (1973), p73.

[55] EVANS, P.R.V. and TAYLOR, L.H., NPL Report, DMA 119, (1972).

[56] PEARSON, S., Eng. Fract. Mech., 4 (1972), p9.

[57] WALKER, K., ASTM STP 462, (1970), p1.

[58] TOPPER, T.H. and SANDOR, B.I., Ibid, p93.

[59] BROEK, D. and SCHIJVE, J., NLR Report No. Tn.M2111, (1963).

[60] FROST, N.E., J. Mech. Engng. Sci. 4, (1962) p22.

[61] EVANS, P.R.V., OWEN, N.B. and McCARTNEY, L.N., Eng. Fract. Mech. 6, (1974), p183.

[62] FEDDERSEN, C.E., MOON, D.P. and HYLER, W.S., Metals and Ceramics Information Centre, Report No. MCIC-72-04, (1972).

[63] ELBER, W., Eng. Fract. Mech. 2, (1970), p37.

[64] SIH, T.T. and WEI, R.P., Eng. Fract. Mech., 6, (1974), p19.

[65] ELBER, W., ASTM STP 486, (1971), p230.

[66] RITCHIE, R.O. and KNOTT, J.F., Acta Met. 21 (1973), p639.

[67] KNOTT, J.F., "Fundamentals of Fracture Mechanics", Butterworths, (1973) p254.

[68] DOWLING, N.E., J. of Materials, JMLSA, 7, (1972), p71.

[69] JONES, R.E., Eng. Fract. Mech., 5, (1973), p585.

[70] SCHIJVE, J., BROCK, D. and de RIGLE, P., NLR Report No. M2094, (1962).

[71] HARDRATH, H.F. and McEVILY, A.T., Proc. Crack Propagation Symp., Cranfield, (1961), p231.

[72] JONDS, D. and WEI, R.P., Int. J. Fract. Mech., 7, (1971).

[73] von EWU, E., HERTZBERG, R. and ROBERTS, R., Nat. Symp. on Fracture Mechanics (USA), (1971).

[74] HUDSON, M.C., and RAJU, K.N., NASA TN D-5702, (1970).

[75] CORBLY, D.M. and PACKMAN, P.F., Eny. Fract. Mech. 5, (1973), p479.

[76] RICE, R.C. and STEPHENS, R.I., ASTM STP 536, (1973), p95.

[77] SCHIJVE, J., AGARDograph No. 157 (1972).

[78] PORTER, T.R., Eng. Fract. Mech. 4, (1972), p717.

[79] TREBULES, V.W., ROBERTS, R. and HERTZBERG, R.W., ASTM STP 536, (1973), p115.

[80] SCHIJVE, J., Eng. Fract. Mech., 5, (1973), p269.

[81] JACOBY, G.H., ASTM STP 462, (1970), p184.

[82] NAUMANN, E.G., NASA TN D-1584, (1964).

[83] HILLBERRY, B.M., ASTM STP 462, (1970), p.167.

[84] BUSSA, S.L., Ford Motor Co., Detroit, Report No. 900 21-1, (1967).

[85] HODDINOTT, D.S., Eng. Fract. Mech. 6, (1974), p163.

[86] JACOBY, G.H., Air Force Materials Laboratory, USA, Report AMFL-TR-67-215, (1967).

[87] SCHIJVE, J., Proc. Int. Committee on Aeronautic Fatigue, 11th Conf. Stockholm, (1969).

[88] WATSON, P., HODDINOTT, D.S. and NORMAN, J.P., ASTM STP 519, (1973), p271.

[89] GASSNER, E., Proc. Int. Conf. Fatigue of Aircraft Structures, (1956), p178.

[90] BARSOM, J.M., ASTM STP 536, (1973), p147.

[91] HARDRATH, H.F. and NAUMANN, E.C., ASTM STP 274, (1960), p125.

[92] NAUMANN, E.C., HARDRATH, H.F. and GUTHRIE, E.C., NASA TN D-212, (1959).

[93] KAWAMOTO, M., ISHIKAWA, H. and SHIBATA, T., Memoirs Faculty of Engineering, University of Kyoto, Japan, (1973), p29.

[94] TEDFORD, J.D., CARSE, A.M. and CROSSLAND, B., Eng. Fract. Mech. 5, (1973), p241.

[95] PALMGREN, A., Z.V.D.I., 68, (1924), p339.

[96] MINER, M.A., J. App. Mech., 12, (1945), pA159.

[97] BLAND, R.B. and PUTNAM, A.A., Ibid 13, (1946) pA169.

[98] SCHIJVE, J., Minutes 4th Conf. of the Int. Committee on Aero. Fatigue. Zürich, (1956), Appendix 2.

[99] CORTEN, H.T. and DOLAN, T.J., Proc. Int. Conf. Fatigue of Metals, Inst. of Mech. Engineers, (1956) p235.

[100] MANSON, S.S., FRECHE, J.C. and ENSIGN, C.R., ASTM STP 415, (1967), p384.

[101] ENGLE, R.M., Air Force Flight Dynamics Laboratory, USA, Report No. TR-70-107 (1970).

[102] WHEELER, O.E., ASME MetX, (1972).

[103] WILLENBORG, J., ENGLE, R.M. and WOOD, H.A., Air Force Flight Dynamics Laboratory, USA. Report No. TM-71-1-FBR, (1971).

[104] ASTM, Book of Standards (1965), p834. Specification A543-65.

[105] FLAX, R.W., KEITH, R.E., and RANDALL, M.D., ASTM STP 494, (1971), p8.

[106] Proposed British Standard for Plane Strain Fracture Toughness (K_{Ic}) Testing. BISRA Industry Report MG/EB/350/68, (1968).

[107] WALKER, E.F. and MAY, M.J., BISRA Report MG/E/307/67.

[108] POOK, L.P., Int. J. Fract. Mech., 4, (1968), p295.

[109] BROWN, W.F. and SRAWLEY, J.E., ASTM STP 410, (1969), Discussion, p73.

[110] RASKE, D.T. and MORROW, J., ASTM STP 465, (1969), p1.

[111] British Standard Draft for Development DD3. "Methods for Plane Strain Fracture Toughness Testing", (1974).

[112] ASTM Book of Standards, (1973), vol 31. Specification E399-72, "Method of Test for Plane Strain Fracture Toughness of Metallic Materials".

[113] ASTM STP 410 (1969).

[114] ASTM STP 463 (1970).

[115] KATCHER, M., Eng. Fract. Mech. 5(1973) p793.

[116] BROWN, W.F. and SRAWLEY, J.E., ASTM STP 410 (1969) p24.

[117] FROST, N.E. and DIXON, J.R., Int. J. Fract. Mech. 3, (1967), p301.

[118] SWANSON, S.R., CICCI, F. and HOPPE, E., ASTM STP 415, (1967), p132.

[119] WILHEM, D.P., ASTM STP 415 (1967) p363.

[120] KNOTT, J.F., "Fundamentals of Fracture Mechanics", Butterworths, (1973), p118.

[121] SCHIJVE, J., Eng. Fract. Mech. 6, (1974), p213.

[122] RICHARDS, C.E. and LINDLEY, T.C., Eng. Fract. Mech. 4, (1972), p951.

[123] JOHNSON, H.H. and PARIS, P.C., Eng. Fract. Mech., 1, (1968), p3.

[124] EMMANUEL, G.N., YOUNG, D.E. and SPAHR, G.L., Metals Eng. Quarterly, 1, (1961), p82.

[125] NEAL, B. and DOIG, A., Proc. Conf. on Practical Implications of Fracture Mechanisms; Institution of Metallurgists, (1973), p145.

[126] LANDGRAF, R.W., ASTM STP 467, (1970), p3.

[127] KAUFMAN, J.G. and SCHILLING, P.E., ASTM STP 536, (1973), p312.

[128] MAY, M.J., ASTM STP 463, (1970), p47.

[129] KNOTT, J.F., "Fundamentals of Fracture Mechanics", Butterworths, (1973), p142.

[130] EGAN, G.R., Eng. Fract. Mech., 5, (1973), p167.

[131] GRIFFITHS, J.R., MOGFORD, I.L. and RICHARDS, C.E., Metal Sci. J., 5, (1971) p150.

[132] ADAMS, N.J.I. and MUNRO, H.G., Strain 5, (1969), p68.

[133] BUCK, O., Int. J. Fract. Mech., 8, (1972), p121.

[134] CLARK, W.G. and CESCHINI, L.J., Materials Evaluation 27, (1969), p180.

[135] LOWES, J.M. and FEARNEHOUGH, G.D., Eng. Fract. Mech. 3, (1971), p103.

[136] RITCHIE, R.O., "Crack Growth Monitoring, Some Considerations on the Electrical Potential Method".

Internal report, Dept. of Metallurgy and Materials Science, University of Cambridge, (1972).

[137] DOVER, W.D., Eng. Fract. Mech. 5, (1973), p11.

[138] EISENSTADT, R. and FULLER, W.D., J. Basic Eng., (1970), p183.

[139] POOK, L.P., Private Communication, (1974).

[140] BROWN, W.F. and SRAWLEY, J.E., ASTM STP 410 (1969), p14.

ACKNOWLEDGEMENTS

The author wishes to express his gratitude to the many people who have made possible the work reported in this thesis. Specific thanks are extended to:

Dr. G.M.C. Lee for initiating the project and providing continued assistance and encouragement.

Professor J.L. King for the provision of laboratory facilities.

Mr. D. Pringle and his staff for the essential workshop support which they have provided.

The Ministry of Defence, Navy Department, for financing the work through NCRE, Rosyth.

Mr. P. Christopher and Mr. D. Crabbe of NCRE for the generous assistance which they have provided at all times.

Mrs. D. Davies for typing the manuscript.